

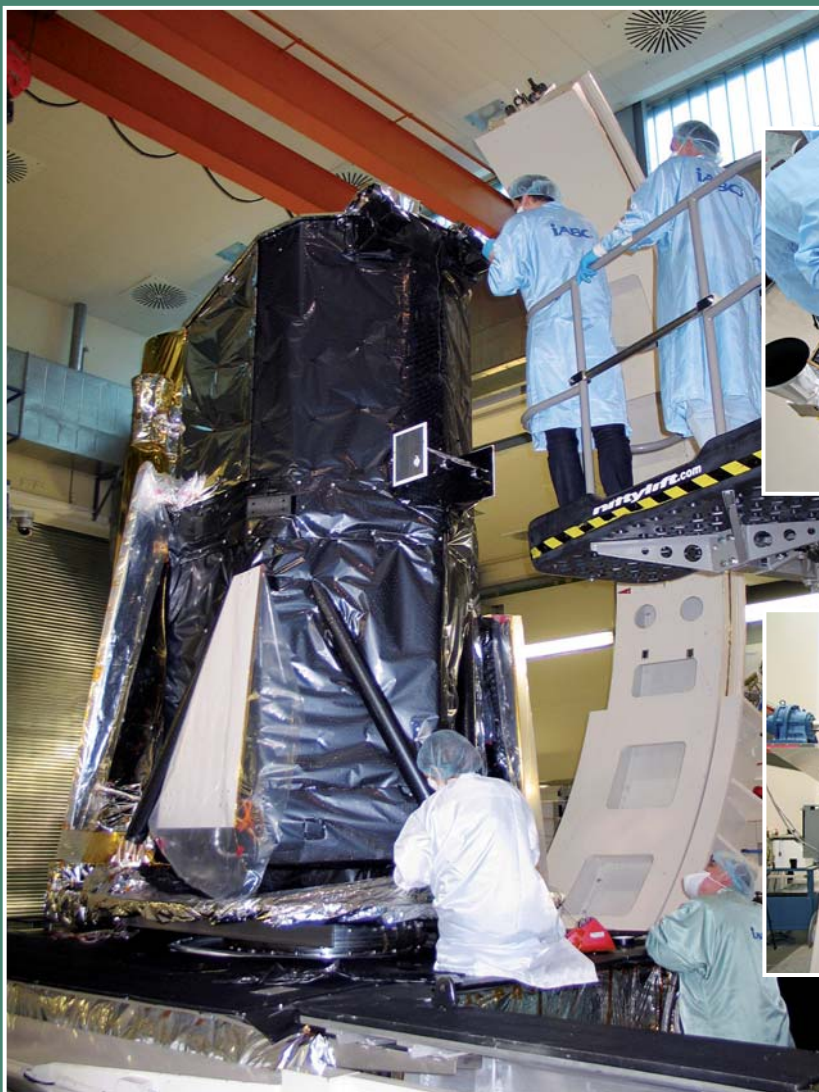


MAX-PLANCK-GESELLSCHAFT

Max-Planck-Institut für
extraterrestrische Physik
Garching



REPORT 2007-2012



Front Cover:

eROSITA will be the primary instrument on-board the Russian "Spectrum-Roentgen-Gamma" (SRG) satellite. It will perform the first imaging all-sky survey in the medium energy X-ray range up to 10 keV with an unprecedented spectral and angular resolution.

eROSITA underwent all qualification tests end of 2012. The images, taken at the test campaign, show the complete instrument (left), the front view with the seven mirror modules (upper right) and its very complicated focal plane instrumentation (lower left).

Back cover:

Important instruments for MPE scientists to pursue their research in multiwavelength astronomy and in fundamental physics.



Report 2007-2012

MPE Science Report

Imprint

Responsible for contents: R. Bender
Editors and Layout: W. Collmar, B. Niebisch and J. Zanker-Smith
Print: MPE Printshop (R. Hauner)

Text and Figure Contributions: MPE Science and Research Groups

Further Support: R. Mayr-Ihbe

1. Edition June 2013

Table of Contents

Preface	5
1 Research Areas and Institute Structure	9
2 Infrared and Submillimeter Astronomy	13
3 Optical and Interpretative Astronomy	53
4 High-Energy Astrophysics	95
5 Theory and Complex Plasmas	143
6 Independent Research Groups	169
7 The Institute	181

PREFACE

This report summarizes the scientific, experimental and project activities at the Max-Planck Institute for Extraterrestrial Physics (MPE) during the period 2007-2012 (including the first few months of 2013).

Following an introduction to the Institute in Chapter 1, Chapters 2-6 summarize the scientific research of the main research divisions and the independent research groups. Each chapter starts with a general overview followed by selected highlights of the last six years. Obviously, this structure cannot capture all of the many individual research projects and results at the MPE. For this purpose, we refer the readers to the 'Poster Booklet' that gives extended Abstracts of the individual activities. With the retirement of Gregor Morfill in July 2013, the activities of the 'Complex Plasma and Theory' division will come to an end at MPE (but will continue at an institute of the German Space Organisation DLR). Thus, Chapter 5 provides a broader account of the division's fantastic achievements, with spin-offs branching out into the field of medicine and hygiene. Chapter 7 presents an overview of our central technical and administrative groups, as well as our teaching activities, public outreach and social interactions.

The last six years have seen a further increase of MPE's scientific output and produced many outstanding results. In space, ESA's far-infrared space telescope HERSCHEL (equipped with MPE's PACS instrument) operated flawlessly until all helium was exhausted in April 2013. The Fermi satellite (again built with significant MPE contributions) provided data on γ -ray sources, while XMM-Newton and Chandra continued to be the key workhorses in X-ray astrophysics. The successful complex-plasma experiments continued in the laboratory and on the International Space Station (PK3-plus, PK4).

On the ground, the MPE-built SINFONI instrument at the ESO-VLT produced impressive results on high redshift galaxy evolution, the Galactic center and nearby black holes. The new KMOS multi-IFU IR spectrograph was commissioned successfully in November 2012 and will start regular observations in fall 2013. GROND provided efficient follow-up of γ -ray bursts with the ESO/MPI 2.2m telescope and the LUCI near-infrared camera and spectrometer started regular observations at the LBT. MPE has also entered the PanSTARRS1 and the SDSS-III surveys to analyse the large scale distribution of galaxies and constrain the nature of dark energy and dark matter.

We have also made good progress in preparing the next series of experiments and projects. eROSITA is currently assembled in the MPE clean room with launch foreseen at the end of 2014 or in 2015. The dark energy mission EUCLID was adopted by ESA in June 2012, with MPE being in charge of the design and procurement of the major optical elements for the NIR imaging spectrograph; launch of EUCLID is planned for 2020. The GRAVITY experiment for the ESO-VLT interferometer, the HETDEX multi-fiber spectrograph on the HET, the ARGOS wide-field adaptive optics system for the LBT, and the MICADO study of an astrometric camera for the E-ELT all have successfully gone through major project milestones. On the downside, ATHENA was not selected as ESA's first large mission (L1) in the Cosmic Vision program but will now compete for the L2 slot in 2028.

On the science part, we have seen spectacular new results with SINFONI on the Galactic Center (in particular on the disruption of an earth-mass molecular cloud by the black hole), on nearby massive black holes and on distant galaxy dynamics. HERSCHEL/PACS has delivered break-through results on cosmic star formation, the Milky Way, nearby external galaxies and very luminous distant galaxies. The IRAM Plateau de Bure interferometer has given exciting glimpses on the amount and properties of cold gas in forming massive galaxies at high redshift. GROND is discovering the most distant γ -ray bursters seen to date. The studies of the hot gas, stellar light and stellar dynamics in the intra-cluster medium have given important new insights on the structure and dynamical processes in massive galaxy clusters. The work on the cosmic evolution of galaxy clusters, as well as the large-scale distribution of galaxies has yielded new constraints on the nature of dark energy.

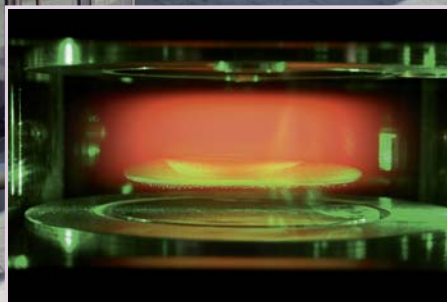
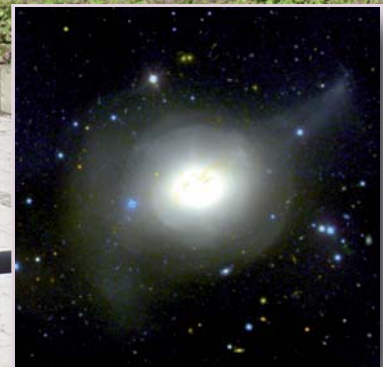
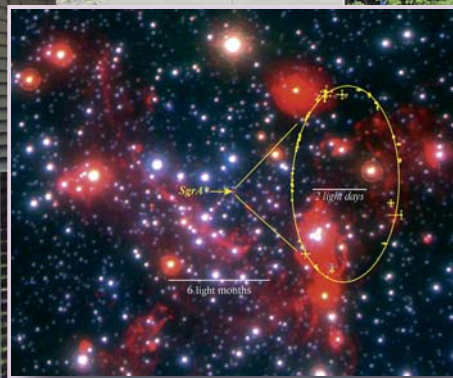
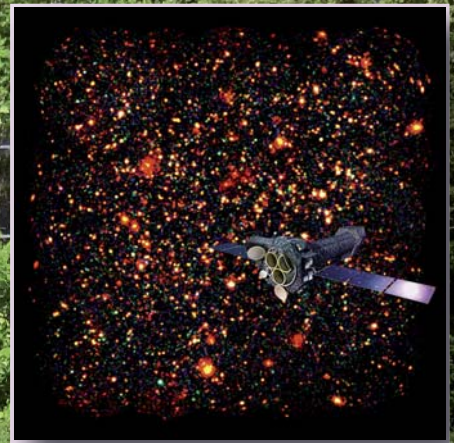
We are continuing to learn ever more about the properties of accreting massive black holes, their interaction with their host galaxies and beyond, with each other as a result of galaxy mergers, and their cosmic evolution. The work with Fermi, INTEGRAL and XMM has delivered new insights into the properties and evolution of magnetars, pulsars, neutron stars, stellar black holes and evolved binaries, as well as the ejection by massive stars of radioactive material into the interstellar medium of the Milky Way. The studies of complex plasmas under microgravity have uncovered a remarkable range of new phenomena, including bubbles and droplets, lane formation in penetrating streams and phonon/soliton excitations. We have also been able to gain important new insights into the microphysics of the melting of plasma-crystals. Last-not least, the spin-off technology of cold plasma therapy may open revolutionary new approaches to hygiene and wound treatments in medicine.

I am grateful to my colleagues at MPE for their contributions, help and input to this six-year report.

A handwritten signature in black ink, appearing to read 'Ralf Bender', with a stylized flourish at the end.

Ralf Bender
Managing Director of the
Max Planck Institute for Extraterrestrial Physics

1 Research Areas and Institute Structure



1. Research Areas and Institute Structure

The research at the Max Planck Institute for Extraterrestrial Physics (MPE, Fig. 1) addresses topics of astrophysics and plasma physics. We combine experiments and instrumental development with observations, data analysis and theoretical work. The main themes of our work during the period 2007-2013 were:

- Cosmology and Large-Scale Structure
- Galaxies and Galaxy Evolution
- Massive Black Holes and Active Galactic Nuclei
- Stellar Evolution and the Interstellar Medium
- Physics of the Solar system
- Complex Plasmas, Plasma Medicine and Complex Systems

Our experimental work in astrophysics during the last six years focused on a number of key questions with a variety of projects, spanning more than twelve decades of the electromagnetic spectrum from millimeter/sub-millimeter, infrared to optical, X- and γ -ray bands. For observations at high energies and most infrared wavelengths we used XMM-Newton, Chandra, Fermi, Herschel and other spacecrafts in order to “escape” from the atmospheric absorption. In the near infrared and optical bands we also have a very strong program of ground-based experiments/instruments (at VLT, LBT and other telescopes) and in the millimeter range we are a very active user of the telescopes of the Institute for Radio Astronomy in the Millimeter Range (IRAM), located in the Alps and in Spain. For the complex plasma experiments, microgravity conditions are very important, and a number of successful experiments on the International Space Station (ISS) have been carried out. Our field work is complemented by laboratory experiments, and analytical, numerical and observation-related interpretational research. The strong interaction between theoreticians, observers and experimentalists is a central element of our research style.

Our scientific activities are organised into four major research fields, each of which is supervised by one of the directors: (1) Infrared- and Submillimeter Astronomy (IR), (2) Optical and Interpretative Astronomy (OpInAs), (3) High-Energy Astrophysics (HE), (4) Theory and Complex Plasmas (CP). Within the main research areas of the MPE, research is often organized in integrated project groups, which include scientists, postdocs, students and staff from the Institute's central support divisions. These central divisions play a key role in the development of our ambitious space- and ground-based instruments/experi-

ments and primarily consist of mechanical and electronic engineering and their associated workshops. We are also engaged in the development of large software packages for the analysis of large amounts of primary data. For coordination of computer hardware and software activities a data-analysis team has been established with representatives from all institute branches. In addition, we are supported by an efficient administration and a technical and building services team (the latter team also services the neighbouring Max Planck Institute for Astrophysics). Key facilities of the Institute outside Garching, in particular for the High-Energy Astronomy Group, are an X-ray test facility (PANTER) located in Neuried near München (Fig. 2) and a semiconductor laboratory (Halbleiterlabor = HLL) on the ‘Siemens campus’ in München-Neuperlach (Fig. 3). Know-how transfer from our research into applications has been particularly important in two research areas at



Fig. 1: MPE building

MPE. The theory division has transferred know-how in the area of “analysis of complex systems” into applications in medicine, hygiene and engineering. The semiconductor laboratory is producing X-ray and particle detectors that find applications in other research institutes and in industry.

The implementation of most experimental projects cannot be envisaged without close cooperation with industry, both locally in the Munich area as well as all over Europe and world-wide. Our 50-year success record in experimental astrophysics and space research demonstrates the efficiency of such cooperations, primarily with space industry, speciality workshops and electronics companies. The challenging technological requirements of our experiments also often lead to technology transfer to industry.

In addition to the institutional support by the Max-Planck-Gesellschaft, which is the most important element of our



Fig. 2: Panter X-ray test facility in Neuried

funding of personnel and projects, our research is supported by government institutions such as the German Federal Ministries for Education and Research (BMBF) and for Economy (BMWi) and the German Space Organisation (DLR), international organisations such as the European Space Agency (ESA) and European Southern Observatory (ESO), as well as the European Community, with additional financial contributions from the German Science Foundation (DFG), the Alexander von Humboldt Gesellschaft (AvH) and the Dr. Johannes Heidenhain-Foundation.

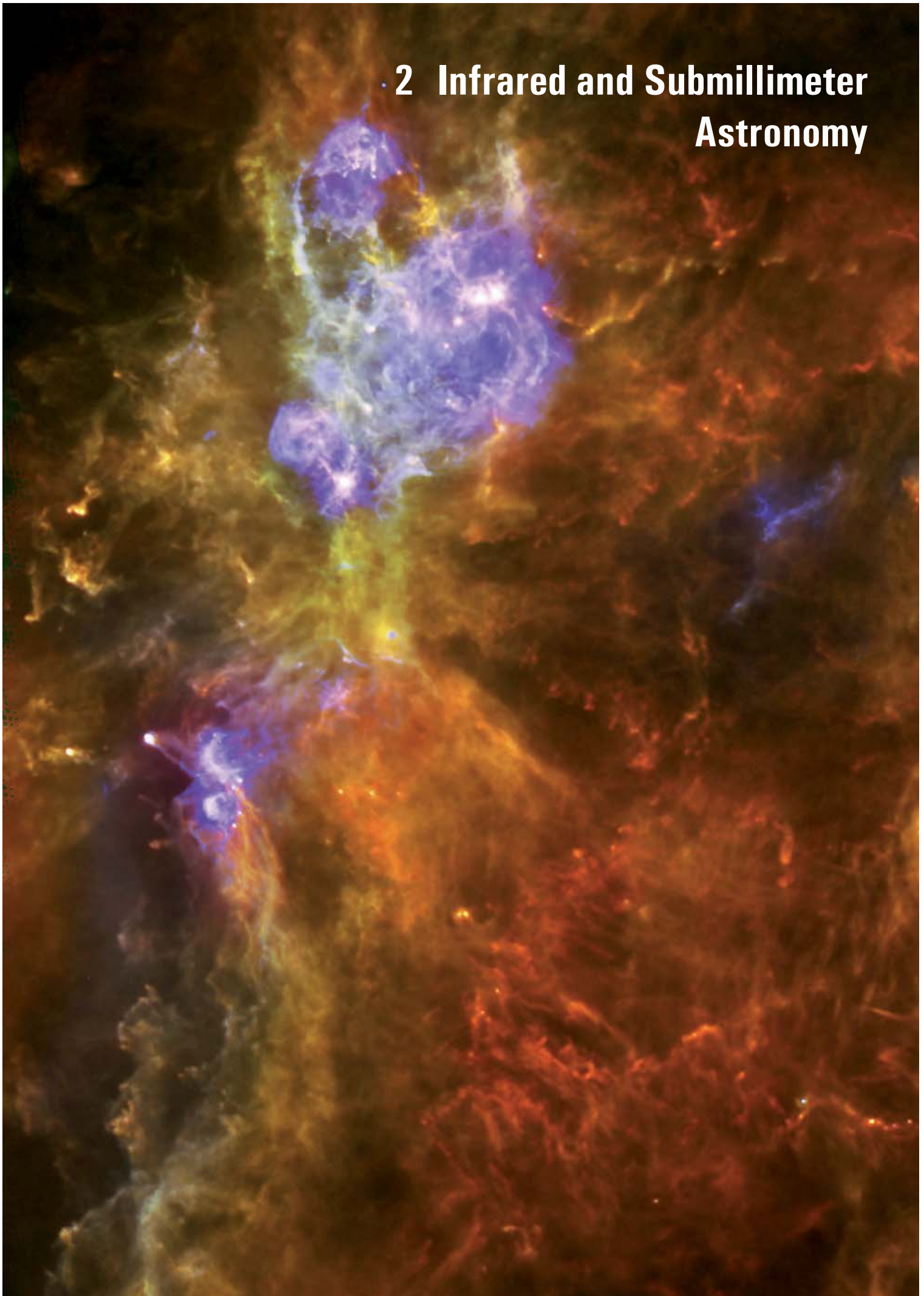
Our institute is strongly engaged in vocational and academic education: MPE researchers teach at several universities and supervise student research (Master, Ph.D.), mainly at both Munich universities, but also in other German universities, and as far away as the University of California (Berkeley). Seminars, workshops and conferences are held by the Institute in our own and adjacent research fields, often in cooperation with the universities. Our very successful “International Max-Planck Research School on Astrophysics” at the Ludwig-Maximilians-Universität München continues to attract a large number of motivated students to astrophysical research.



Fig. 3: Semiconductor laboratory building in München-Neuperlach

During the reporting period, MPE increased its efforts and professionalism in public outreach by creating a dedicated position for this task (together with MPA). This is the first such position in the history of the institute. One of the main aims is to supply information and other scientific public relations material to the local and national presse and a wider audience in general. In addition, our scientists are engaged in giving public talks in schools and planetaria, school classes visit MPE regularly, and we have an Open House day every other year.

2 Infrared and Submillimeter Astronomy



2. Infrared and Submillimeter Astronomy

2.1 Summary

The last six years (2007-2013) have seen a major peak of the science output of the MPE-Infrared Group (Fig. IR.1). This culmination resulted from the confluence of several unique observational and instrumental capabilities becoming operational (SINFONI@VLT, PACS@HERSCHEL, PdBI@IRAM, LUCI@LBT), as well as important scientific synergies emerging from these capabilities. Some of these instruments had been in development for more than a decade. MPE-authors published ~350 refereed papers in this time period, with more than 13,000 citations to date. Most of the highly cited papers in this harvest were led by an MPE-IR senior scientist, postdoc or student. Almost thirty papers captured more than 100 citations to date, and six more than 200, with the leader being the 2010 paper of Poglitsch et al. describing the MPE-led PACS instrument on the ESA Herschel space telescope (521 cites). The IR-group led 2007-2013 papers with more than 100 citations are listed in Table 1 at the end of this summary.

Fig. IR.1 summarizes the output of the past six years in pictorial form, along with nine of our science highlight results. Our aim has been to exploit our new instrumental/observational tools by focusing on two major science themes, which we briefly summarize below and expand on in the following pages. Often in collaboration with external colleagues, we combine the main observational efforts with interpretational/theoretical work.

A very positive development of the last decade has been the overall increase in the fraction of women in the group from about 24% to 34% (both in the total and technical staff). The female fraction is 38% for the (tenured) senior scientists and 60% for the students. About half of the group's scientists are German, the other half come from a dozen countries world-wide.

The IR group also hosts the research group "Star and Planet Formation" of Prof. Ewine van Dishoeck (External Scientific Member of MPE), whose results are discussed in section 2.6.

Theme 1: Massive black holes and their environment.

During the 2007-2013 period we were able to achieve further major progress in exploiting the Galactic Center 'laboratory' for precision tests of the black hole paradigm. We now have thirty-five well defined stellar orbits making a compelling case for a point mass gravitational potential centered on the compact radio source Sgr A* to a scale of <10 light hours (Fig. IR.1b). Combined with ever more constraining radio observations of its size and motion, our research, along with that of our colleagues at UCLA, demonstrates that Sgr A* must be a massive black hole, beyond any reasonable doubt, as long as General Relativity is valid.

We discuss in the next sections these precision measurements with NACO and SINFONI at the ESO VLT.

Star Cluster, G2 and GRAVITY. The Galactic Center studies also provide a wide range of unexpected insights into the stellar cluster surrounding the black hole, the star formation activity and stellar mass function in this cluster, and into the remarkably inefficient radiation from the black hole itself. The most recent excitement is a small gas cloud (G2, Fig. IR.1c) falling almost radially towards Sgr A*, getting tidally disrupted before our eyes, and providing us with a unique probe of the innermost accretion zone.

The next big step for our research in the Galactic Center will be GRAVITY, a very ambitious experiment to obtain 10- μ arcsecond-precision imaging astrometry of stars and gas very close to the event horizon, by combining interferometrically all four VLT unit telescopes. GRAVITY should be able to detect several of the effects predicted by General Relativity, such as prograde orbital precession, it may test the equivalence principle on curvature scales previously not accessible, and, if we are lucky, it may be able to determine the metric on a scale of a few Schwarzschild radii.

Active Galactic Nuclei. We have applied the power of our PACS spectrometer on the Herschel space telescope to study the far-infrared line emission in active galaxies in the Local Universe. Highlights were the discovery of powerful molecular outflows in AGN dominated luminous infrared galaxies (Fig. IR.1d), as well as highly excited molecular gas components towards the nuclei of nearby AGN. High resolution follow-up imaging observations with the IRAM Plateau de Bure millimeter interferometer (PdBI) show that these molecular outflows are spatially extended.

Theme 2: Evolution of massive star forming disks at the peak of galaxy formation.

Most of the IR-group's research during the past six years focused on in-situ observations of the physical, dynamical and gas properties of massive star forming galaxies near the peak of the cosmic galaxy formation epoch, about 10 billion years ago. With SINFONI in its adaptive optics mode, we have shown that at least half of these massive star forming galaxies are clumpy, thick and turbulent rotating disks, with a minority of mergers (Fig. IR.1f). SINFONI, HST and PACS observations show that more than 90% of the cosmic star formation activity between $z=2.5$ and $z=0$ occurs in a well-defined 'Main Sequence' (MS) of star forming disks in the stellar mass - star formation plane.

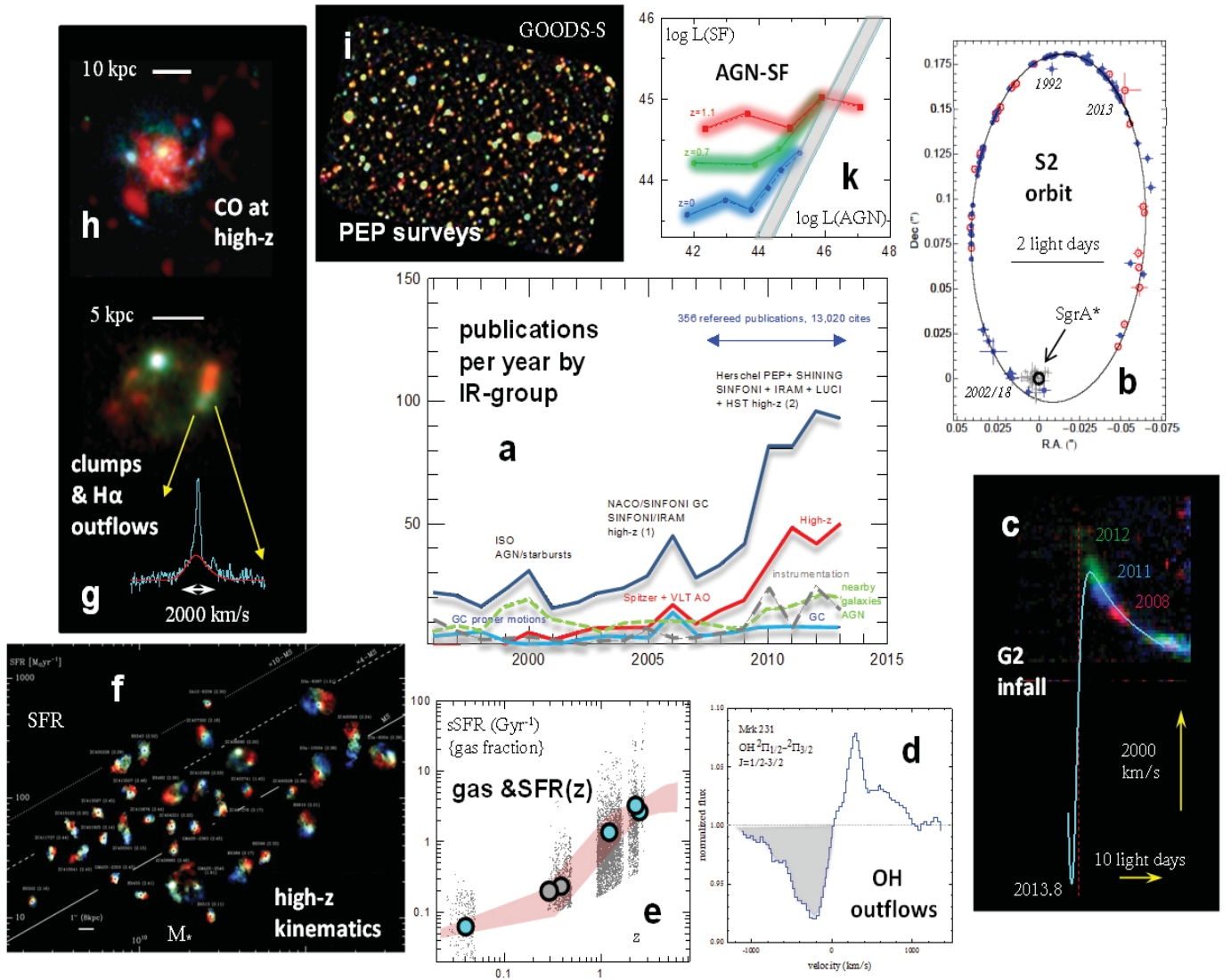


Fig. IR. 1: Publications and science highlights of the MPE-IR group in the period 2007 - 2013.

(a): Publications per year by the MPE-IR group, total (dark blue), as well as in different science areas (high- z (red), GC (light blue), AGN (green) and instrumentation (grey)). Over the past 6 years, ~ 350 MPE-IR refereed papers received 13,000 citations to date.

(b): Astrometric measurements of the star S2, moving on a highly eccentric 15.8 y orbit around the radio source Sgr A*, with a closest approach ~ 17 light hours from the black hole (in 2002, and again in 2018). Blue circles denote SHARP/NTT and NACO/VLT measurements, covering more than one revolution. For comparison the red points show the Keck measurements.

(c): Evolution of the Br γ line emission from the ionized gas cloud G2 in the plane spanned by radial velocity (up and down) and offset from Sgr A* (left-right). Red, blue and green shows the distribution in the three years 2008, 2011 and 2012 as observed with SINFONI+AO at the VLT, moving along the best fit, eccentricity ~ 0.96 orbit (cyan) and at the same time shearing along the orbit due to tidal disruption by the black hole. The cloud will reach the closest distance (~ 20 light hours) from Sgr A* in fall 2013.

(d): Profile of the $79\mu\text{m } ^2\Pi_{1/2} J=1/2 - ^2\Pi_{3/2} J=3/2$ transition of OH toward the ultraluminous infrared galaxy/QSO Mrk231, observed with the PACS spectrometer onboard HERSCHEL. The OH profile exhibits an inverse P-Cygni shape, indicative of a powerful molecular outflow with $v_{\text{out}} \sim 1000$ km/s.

(e): Evolution of molecular gas fraction with cosmological redshift, as observed in star forming galaxy samples in the IRAM PHIBSS ($z=1-2.5$) and COLDGASS ($z=0$) programs (large black circles with cyan filling), compared to the evolution of specific star formation rate in the parent galaxy samples (grey dots and red shaded). The specific star formation rate follows the evolution of the gas fractions suggesting that cosmic star formation is gas regulated.

(f): SINFONI+AO H α velocity fields in $z\sim 2$ star forming galaxies in the stellar mass (horizontal) –star formation rate (vertical) plane. Red and blue denote receding and approaching motions. More than 50% of these galaxies are supported by rotation.

(g): HST I-band (red) +H α line emission (green) of a clumpy ring galaxy at $z\sim 2$, exhibiting kpc-size giant star forming clumps, which drive high velocity outflows in ionized gas (cyan spectrum).

(h): HST I-band (blue) and IRAM-PdBI CO 3-2 line emission (red) in a $z\sim 1$ star forming galaxy.

(i): Deep 70/100/160 μm imaging of the GOODS-S field with PACS on HERSCHEL as part of the PEP cosmological survey, allowing for the first time the direct detection of the far-IR dust emission from distant star forming galaxies.

(k): Correlation between AGN-luminosity (horizontal, from X-rays) and far-infrared luminosity (from PACS) in X-ray selected samples in the GOODS and COSMOS fields, at redshift ~ 0.6 (shaded green line) and ~ 1.1 (shaded red line). The shaded blue line denotes a comparison $z\sim 0$ sample. While the observations in the two lower redshift bins exhibit an upswing of far-infrared luminosity (as a proxy to star formation rate) at the highest AGN-luminosities, the $z\sim 1.1$ bin does not show such a correlation. This may suggest a different, ‘secular’ mode of black hole growth near the peak of the cosmic galaxy formation.

Molecular gas in high- z MS galaxies. These early disks appear to have grown mainly by semi-continuous gas accretion from the cosmic web and minor mergers (Fig. IR.1 e), rather than in bursts triggered by major mergers. The ‘equilibrium growth’ of the MS galaxies is regulated by the replenishment of fresh gas on the one hand, and by consumption of the gas by star formation and powerful galactic winds on the other (Fig. IR.1g). Our millimeter observations with the IRAM PdBI and 30m telescopes have begun to trace the cosmic evolution of gas content directly (Fig. IR.1e, h). Our SINFONI data on ionized gas outflows (Fig. IR.1g), along with UV spectroscopy of ionized and atomic outflows by several other groups demonstrate the ubiquity and efficiency of mass outflows driven by massive stars, supernovae, and perhaps active galactic nuclei. If these outflows are effective in driving out a significant fraction of the cold interstellar gas of MS galaxies, as predicted by simulations, they should be detectable in molecular line emission in future NOEMA and ALMA measurements.

Star formation and AGNs. To test the possible role of accreting massive black holes (AGN) in galaxy evolution, especially for the ‘shutdown’ of star formation near the Schechter mass, we have been using PACS, SINFONI, HST and the PdBI (Fig. IR.1 h, i, k). It is clear that AGNs become increasingly common at high masses, where high- z MS galaxies also grow substantial central bulges. For high- z galaxies, and in contrast to the local Universe, our PACS-PEP survey indicates that AGN activity is not correlated with powerful starbursts, as expected for major mergers (Fig. IR.1k). We also have discovered that these massive bulge-disk systems frequently exhibit nuclear outflows, possibly driven by AGN activity.

Our scientific and experimental strategy for the future. While these observations, along with increasingly powerful simulations, give us a first direct glimpse of the key physical processes operating at the peak of galaxy formation, the next big step will be to cast the qualitative picture sketched above into an increasingly firm quantitative form.

This goal requires more comprehensive spectroscopic surveys of the star formation, gas reservoirs and metallicity evolution, in terms of numbers of galaxies, and the coverage in redshift and in the stellar mass-star formation plane. We are in the process of executing or proposing several next generation surveys, with up to 103 MS galaxies in the redshift range leading up to and dropping down from the $z\sim 1-2$ peak (Fig. IR.2). We have begun this next generation effort with the LUCI multi-slit unit on the Large Binocular Telescope (LBT), and are in the process of undertaking the first highly multiplexed integral field unit survey with KMOS-3D on the ESO VLT, taking advantage of the much increased surface density of reliable redshifts from the 3D-HST program. We have also just begun an equally ambitious effort with the IRAM facilities (PHIBSS2), as the ongoing expansion of the PdBI into NOEMA will increase the speed and sensitivity of the interferometer. The capabilities of NOEMA and ALMA will revolutionize spatially resolved follow-up studies of molecular gas on the scale of individual star forming regions in high- z galaxies.

Instrumentation efforts. On the instrumentation side, we discuss below several avenues we are pursuing for the future. In addition to GRAVITY (upper right in Fig. IR.2), we are in the process of equipping the LBT with a ground-layer, laser correction system (ARGOS). LUCI & ARGOS will provide $\sim 0.2''$ multiplexed spectroscopy across a field of several arcminutes, for both eyes of the LBT, ideal for spatially resolved follow-up of the spectroscopic surveys. With ESO we are engaging in a significant upgrade of the NACO+SINFONI instruments in a future combined system, ERIS, that will take advantage of the new adaptive secondary at UT4 and the next generation laser beacons, for improved Strehl ratio and sensitivity, again of great interest for spatially resolved follow-up of our spectroscopic surveys. Our most ambitious instrumentation project will be the leadership of the first light camera and spectrometer, MICADO, for the European Extremely Large Telescope (Fig. IR.2).

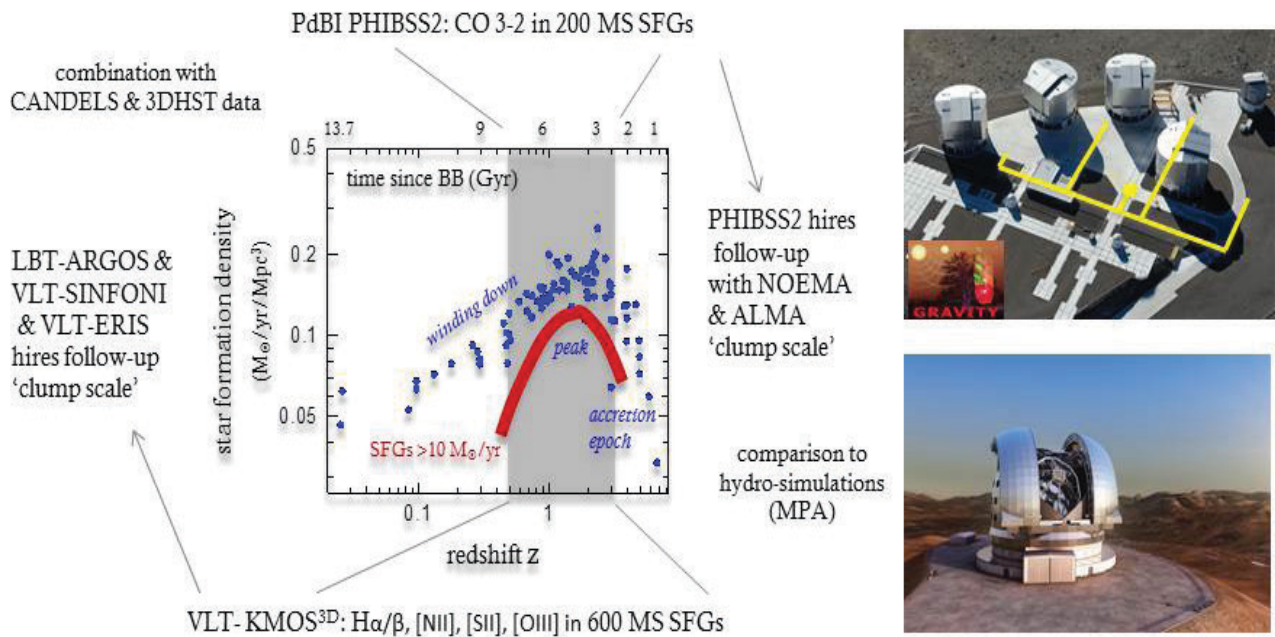


Fig. IR.2. The MPE-IR science/instrument strategy 2014-2020 at a single glance. Left: The next generation spectroscopic surveys and their follow-up (exploiting our next generation LBT, VLT and IRAM instruments, along with ALMA) will address the build-up, peak and winding down epochs of cosmic star formation from the aspects of gas, galaxy dynamics, metallicities, and intra-galactic star formation. The GRAVITY project (upper right) will make possible the big next step in studying the massive black hole in the Galactic Center, as well as nearby AGN. By the end of the decade we hopefully will move toward the completion of MICADO, the first light instrument for the EELT (bottom right).

Table 1: Papers > 100 Citations with IR-Group Lead from 2007 - 2013

- 1) Poglitsch et al. 2010 "The Photodetector Array Camera and Spectrometer (PACS) on the Herschel Space Observatory" A&A, 521 cites
- 2) Gillessen et al. 2009 "Monitoring Stellar Orbits Around the Massive Black Hole in the Galactic Center" ApJ, 394 cites
- 3) Tacconi et al. 2008 "SMGs at $z \sim 2$: Evidence for Major Mergers and Constraints on Lifetimes, IMF, and CO-H₂ Conversion Factor" ApJ, 316 cites
- 4) Förster Schreiber et al. 2009 "The SINS Survey: SINFONI Integral Field Spectroscopy of $z \sim 2$ Star-forming Galaxies", ApJ, 312 cites
- 5) Genzel et al. 2008 "From Rings to Bulges: Evidence for Rapid Secular Galaxy Evolution at $z \sim 2$ from Integral Field Spectroscopy in the SINS Survey" ApJ, 267 cites
- 6) Tacconi et al. 2010 "High molecular gas fractions in normal massive star-forming galaxies in the young Universe", Nature, 259 cites
- 7) Genzel et al. 2010 "A study of the gas-star formation relation over cosmic time" MNRAS, 189 cites
- 8) Davies et al. 2007 "A Close Look at Star Formation around Active Galactic Nuclei" ApJ, 168 cites
- 9) Bouché et al. 2007 "Dynamical Properties of $z \sim 2$ Star-forming Galaxies and a Universal Star Formation Relation" APJ, 141 cites
- 10) Veilleux et al. 2009 "Spitzer QSO-ULIRG Evolution Study QUEST, IV" ApJ 132 cites
- 11) Netzer et al. 2007 "Spitzer QSO-ULIRG Evolution Study QUEST, II" ApJ 131 cites
- 12) Shapiro et al. 2008 "Kinometry of SINS High-Redshift Star-Forming Galaxies: Distinguishing Rotation Disks from Major Mergers" ApJ, 117 cites
- 13) Bartko et al. 2010 "An Extremely Top-Heavy Initial Mass Function in the Galactic Center Stellar Disks", ApJ, 116 cites
- 14) Genzel, Eisenhauer & Gillessen 2010 "The Galactic Center Massive Black Hole & Nuclear Star Cluster" RvMP, 111 cite
- 15) Bouché et al. 2010 "The Impact of Cold Gas Accretion Above a Mass Floor on Galaxy Scaling Relations", ApJ, 110 cites
- 16) Genzel et al. 2011 "The Sins Survey of $z \sim 2$ Galaxy Kinematics: Properties of the Giant Star-forming Clumps", ApJ, 101 cites
- 17) Valiante et al. "A Mid-Infrared Spectroscopic Study of SMGs: Luminous Starbursts at High Redshift" ApJ, 101 cites



Reinhard Genzel

2.2 The Galactic Center: a Unique Astrophysical Laboratory

Located at a distance of a mere 8 kpc (26,000 light years), the Galactic Center is a unique astrophysical laboratory for testing the massive black hole (MBH) paradigm and for studying in unparalleled detail the properties and evolution of a dense star cluster around such a MBH (Genzel, Eisenhauer & Gillessen 2010) In the future we will probe to scales revealing the effects of General Relativity.

For more than 20 years our group has been pioneering infrared observations of the Galactic Center by employing novel, high-angular resolution techniques. The outstanding, fundamental result of our work is the proof of existence of an astrophysical massive black hole, beyond any reasonable doubt. The proof rests on straightforward, unambiguous evidence: We have observed individual, short-period stars on Keplerian orbits around the compact radio source Sgr A*, the mass of which can be measured from the data to a statistical uncertainty of 1.5% (Schödel et al. 2002, 2003, Gillessen et al. 2009a). In addition to the tests of the MBH paradigm, the two main topics of our Galactic Center research program are the interaction of the MBH with its surrounding dense stellar environment, and the radiation from the MBH itself. This research has led to a wealth of remarkable and largely unexpected insights and is a widely recognized success story:

- We have discovered and characterized the spectral, temporal and polarization properties of Sgr A*'s infrared emission (Genzel et al. 2003a, Dodds-Eden et al. 2009, 2010, 2011).
- We have measured the distance R_0 to the Galactic Center geometrically to an accuracy of 3% (Eisenhauer et al. 2003, Gillessen et al. 2009a, Gillessen et al. 2013b).
- We have determined more than 30 individual stellar orbits of the 'S-stars' in the immediate vicinity of Sgr A* (Schödel et al. 2002, Eisenhauer et al. 2005, Gillessen et al. 2009a).
- We have characterized the stellar cluster surrounding the massive black hole (Genzel et al. 2003b, Paumard et al. 2006, Bartko et al. 2009, 2010). The result is totally unexpected. There is no cusp of old stars centered on the hole. Instead there are at least two populations of young stars. About 120 massive O- and Wolf-Rayet stars reside in one or two disks located a few arcseconds from Sgr A* (Paumard et al. 2006, Martins et al. 2007, Bartko et al. 2009), with moderate eccentricities. These stars formed probably in-situ from a massive, infalling cloud \approx 6 Myr ago that was compressed and overcame the strong tidal forces from the black hole. Even more surprisingly, there are \sim 30 B stars orbiting the black hole on highly elliptical, randomly oriented orbits in the central arcsecond (<0.1 pc, Eisenhauer et al. 2005, Martins et al. 2008, Gillessen et al. 2009a). The presence of these young cusp stars is a 'paradox of youth' (Ghez et al. 2003).

The basis of this work is astrometric and spectroscopic monitoring at the diffraction limit of the ESO VLT with

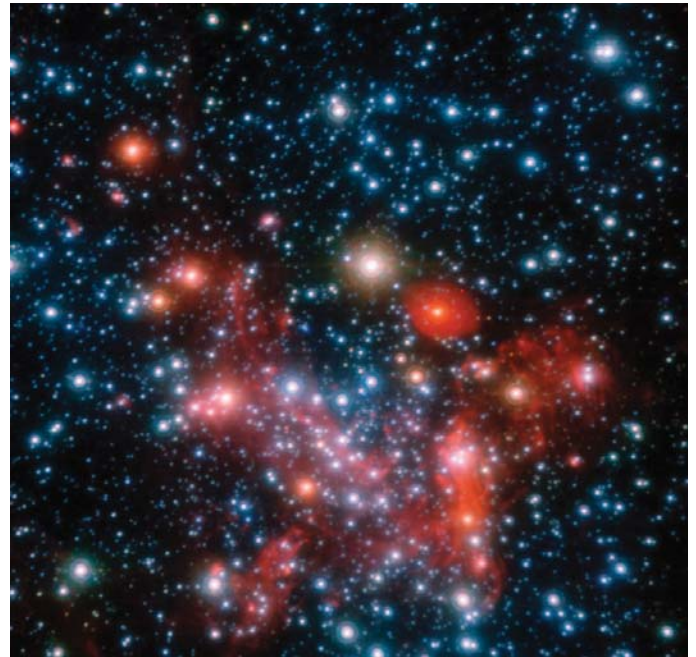


Fig. IR.3: Combined H- K- and L-band adaptive optics image of the Galactic Center obtained with NACO on the VLT. The image is 30" (1.2pc) across.

the two instruments SINFONI and NACO, whose developments our group has led and strongly contributed to, respectively. We now routinely achieve a positional accuracy of 300 μ s (Fritz et al. 2010) and a radial velocity accuracy of 15 km/s. We are aiming at soon opening up a new domain of precision astrometry (10 μ s) with near-infrared interferometry. Our group is leading a European consortium currently building the GRAVITY instrument for the VLT-Interferometer (see below), the design of which is precisely matched to the observing opportunities in the Galactic Center.

Paradox of youth: origin of the S-stars. The S-stars around Sgr A* have orbital periods spanning 12 to 103 years and have typical semi-major axes of $\sim 0.3''$ (0.01 pc). Most are young, main sequence B-type stars (Eisenhauer et al. 2005, Martins et al. 2008), with lifetimes one to two orders of magnitude shorter than the two-body relaxation time of the nuclear cluster. How did they then get to their current location so close to the MBH?

Due to the formidable tidal forces, it is implausible that the S-stars have formed near their current locations. They may have formed in the O/WR-star disk(s) 1-10" from the MBH. However, simulations suggest that there was not enough time for disk stars to sink inwards and at the same time acquire the current random and eccentric orbits characteristic of the S-stars. The most likely explanation invokes the 'Hills' capture mechanism (Hills 1988). The three-body interaction of a binary star on a near-radial orbit with the MBH can redistribute the energy such that one member gets captured on a tight orbit, while

the other gets ejected at several thousand kilometers per second from the system, in the end escaping as a hyper-velocity star into the halo of the Milky Way and beyond. The theoretical work of the last years suggests that there is a sufficient number of massive perturbers in the central 10 parsec to inject binaries on near-loss cone orbits and to account for the observed S-stars. Once captured, the highly eccentric original orbits can plausibly relax quickly through a combination of ‘resonant relaxation’, Lense-Thirring precession and interactions with stellar remnants in the cusp.

More significant measurements of the impact of General Relativity (such as the Lense-Thirring term due to the MBH’s spin) on the dynamics of stars (and gas) near the massive black hole require greater measurement accuracy, higher angular resolution and test particles yet closer to the center. Achieving these goals is the main driver for our current and future instrument developments. Together with ESO we will be building ERIS, the successor for NACO and SINFONI, with a second-generation adaptive optics system delivering higher Strehl ratio and sensitivity. MPE is the PI-Institute for the first-light camera MICADO at the European ELT, reaching five times higher resolution than the current VLT. But most notable are the 4 mas resolution and 10 μ as astrometry that we will achieve with GRAVITY (see below).

The next steps. The current level of precision of the stellar orbit work of our group and of our colleagues at the Keck telescope (Fig. IR.4, Ghez et al. 2008, Gillessen et al. 2009a,b) indicates that we will be able to detect deviations from the Keplerian motion in the next five years.

The relativistic corrections for the radial velocity of S2 during the next pericenter passage (2018) amount to ≈ 200 km/s. The relativistic precession due to the Schwarzschild correction yields a prograde rotation of the orbit in its plane of $\approx 0.2^\circ$ per revolution. Our current precision is $\approx 0.5^\circ$, and by 2018 a 3σ detection of the Schwarzschild precession of S2’s orbit should be possible.

Flares - emission from the immediate vicinity of the black hole. Since our discovery of the first infrared flares from Sgr A* (Genzel et al. 2003a) we have undertaken a large number of observations to study its radiative properties. The infrared emission is polarized synchrotron light of transiently heated electrons in the immediate vicinity of the black at hole at a few Schwarzschild radii (Dodds-Eden et al. 2009). Most probably the emission is magnetically powered (Dodds-Eden et al. 2010), similar to flares on the Sun. Fig. IR.5 shows that Sgr A* is a continuously variable source with large flux excursions. The distribution of fluxes can be described by a log-normal distribution plus possibly an excess at larger fluxes (Dodds-Eden et al. 2011). The excess is a hint that flares are events that occur in addition to the underlying variability process. That interpretation is supported by the strong linear polarization ($\leq 40\%$) in some flares (Eckart et al. 2006, 2008, Trippe et al. 2007). The underlying log-normal distribution can be naturally explained by a multiplicative, non-linear process. At any given time a single, causally connected region, such as a hot spot might dominate the emission. The size of such hot spots, perhaps triggered by local magnetic reconnections, would be a few to ten times the event horizon radius (10 μ as).

A measurement with GRAVITY of the orbital period and radius of such a spot would determine the metric and the MBH’s spin.

A gas cloud on its way toward

Sgr A*. Our most surprising recent discovery came in 2011, when we detected a gas cloud falling toward the MBH on a near radial orbit (Gillessen et al. 2012, 2013a). In our 2002 - 2012 adaptive optics L-band images (but not in the shorter wavelength bands K and H) a faint object, at projected distance of less than 200 mas from Sgr A*, has been moving at ≥ 2000 km/s along a curved trajectory toward Sgr A*. This object (nicknamed ‘G2’) is also visible in our 2004 - 2012 SINFONI data as a compact Br- γ , Pa- α and He-I recombination line emission source with a steadily increasing radial velocity. G2 is unlike any of the thousands of orbiting stars we have been following so far. Either it is an isolated dusty ionized gas cloud, or the gas/dust is associated with a cool and low mass (such as a T-Tau

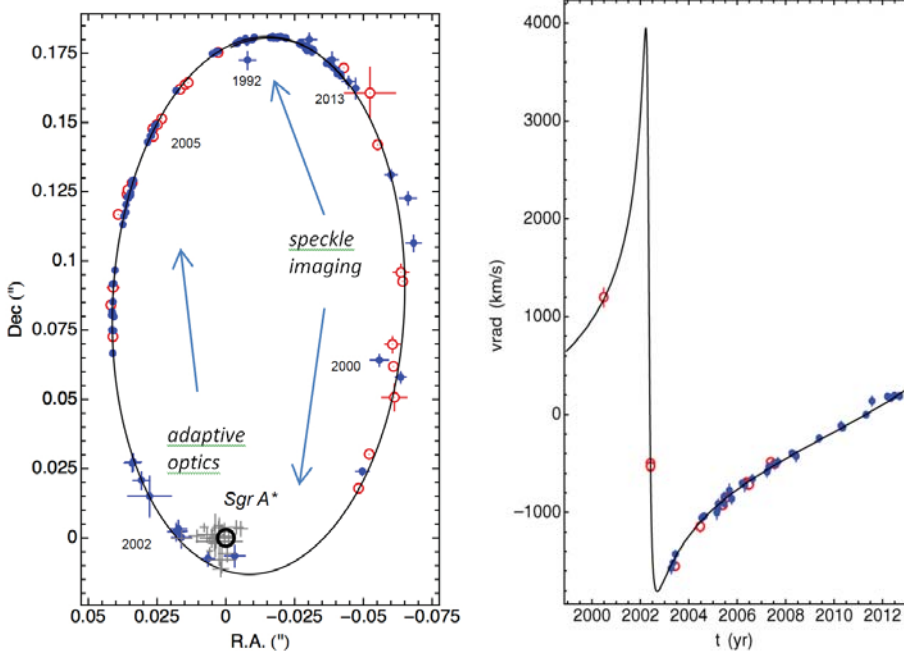


Fig. IR.4: The orbit of the star S2. Left: NTT/VLT (blue) and Keck measurements (red) of the positions of S2 from 1992 to 2013 show that the star is orbiting Sgr A* every 16 years on a Keplerian ellipse (best fit: black line). Right: The radial velocity data is fit simultaneously by the same orbit.

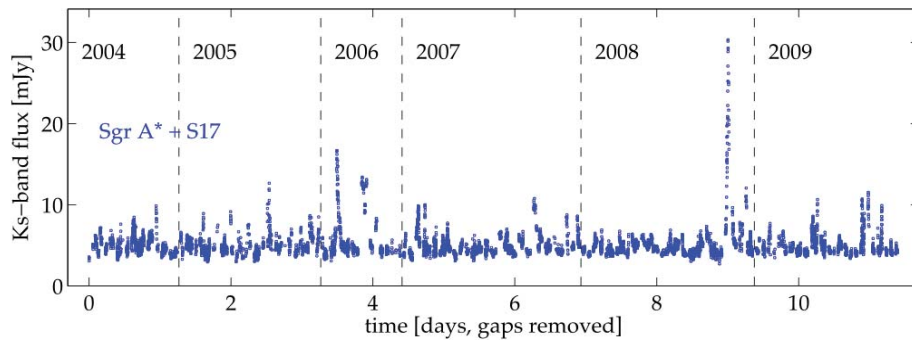


Fig. IR.5: Compilation of ≈ 10000 K-band flux measurements of Sgr A* collected over 6 years. Gaps in the data are removed. The flickering nature of Sgr A*'s emission is evident in this representation.

star), or a compact, hot object, so as to escape detection at H/K. G2 follows a highly eccentric ($e=0.97$) Keplerian orbit, coplanar with the clockwise stellar disk of young stars. The cloud will pass the pericenter of its orbit at a distance of 20 light hours (~ 1500 Schwarzschild radii, for comparison, the star S2 on a 16-year orbit passes at 17 light hours). The cloud was unresolved in 2004 and has developed a spatially resolved velocity gradient since then, with a Br- γ line width of 230 km/s in 2008, 370 km/s in 2011 and even 500 km/s in 2012. This evolution is fully consistent with tidal shearing (Fig. IR.6). From the Br- γ flux we estimate G2's mass to ≈ 3 Earth masses ($10^{-5} M_{\odot}$), which would double if the more diffuse 'tail' of Br γ emission is included.

The G2 encounter may be a unique opportunity to probe with a 'controlled experiment' the accretion zone around Sgr A* and observe the feeding of a MBH in real time. What might happen during the pericenter-passage will depend on the density structure of G2, and whether or not it was originally 'attached' to a central star (that is not detected by our measurements), as well as on the temperature and density profile of the accretion zone gas into which it plunges (Burkert et al. 2012, Schartmann et al. 2012). Depending on these, the cloud may either be tidally stretched but otherwise pass without much destruction, or alternatively, be disrupted by hydrodynamic instabilities, develop a shock front, circularize and accrete onto the MBH.

As a result the luminosity evolution of G2 is uncertain. It is likely that Sgr A* will brighten moderately over the next years (Gillissen et al. 2012, Schartmann et al. 2012). Probably the first signs of material arriving in the inner accretion zone will be that the rotation measure (as obtained with mm observatories) of Sgr A* changes. A bow shock should develop, potentially leading to detectable X-ray and radio emission (Gillissen et al. 2012). If the cloud is disrupted by the

interaction with the accretion zone gas, its further evolution depends sensitively the viscous time scale. Most current theoretical estimates indicate that this process may take decades.

The origin of G2 is unclear. Burkert et al. (2012) note that if G2 has formed close to apo-center of its orbit, in the stellar disk, one can easily explain that its orbit is coplanar with this disk, but not its compactness in 2004-2008. Tidal forces should have by that time stretched G2 to an almost linear

feature. G2 may instead have formed more recently, for instance by a cooling instability of a wind-wind collision close to Sgr A* (Cuadra et al. 2005), or by a Nova explosion in an orbiting cataclysmic binary (Meyer & Meyer-Hofmeister 2012). Models with a central star overcome the disadvantage of early disruption, at the cost of needing to explain how such a star can reach a high-eccentricity orbit. Murray-Clay & Loeb (2012) suggest that G2 is a disrupting protoplanetary disk, while Scoville & Burkert (2013) propose that G2 forms from the wind of a T-Tauri star. Observationally, the basic types of models will be easily differentiated relatively soon: The models with a stellar source should show a strong increasing Br- γ line flux towards pericenter, unlike for a pure cloud scenario. In the T-Tauri picture the gas emission of G2 will build up again after pericenter, while the protoplanetary disk once it is disrupted will not release any new gas.

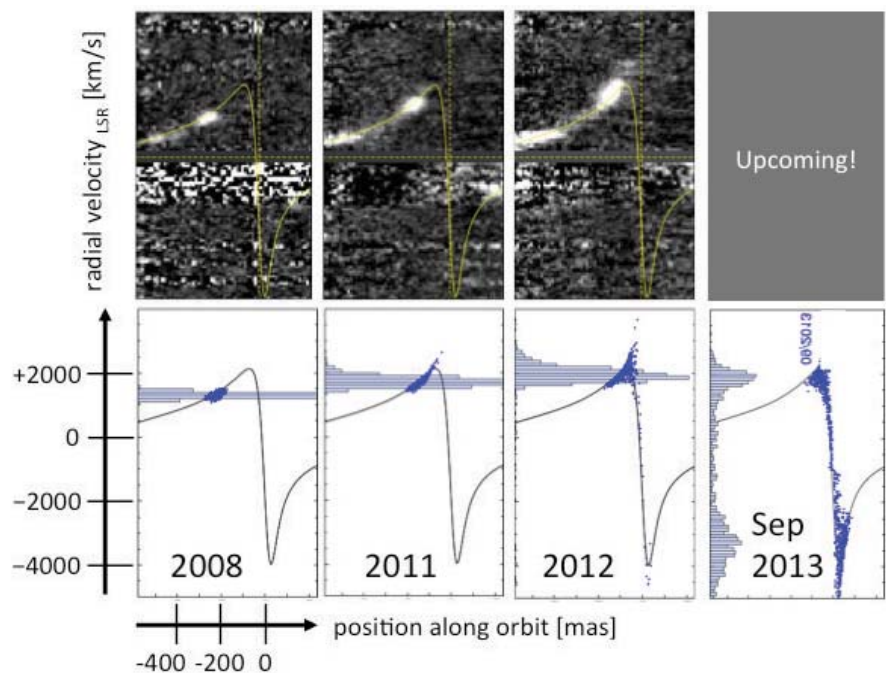


Fig. IR.6: Position-velocity-diagrams of G2 obtained from hydrogen and helium recombination lines observed in deep integral-field spectroscopy with SINFONI/VLT (top). As the cloud moves along the orbit (yellow line) it gets tidally more and more sheared in accordance with a test-particle simulation (bottom).



Fig. IR.7: The ESO VLT interferometer on Paranal (Chile) can coherently combine the light of the four 8m unit telescopes

GRAVITY - an imaging astrometry instrument for the VLTI. The second-generation VLT interferometer instrument GRAVITY will push resolution and astrometric accuracy in the near-infrared to their ultimate limits for the foreseeable future (Fig. IR.7, Eisenhauer et al. 2011), by employing a number of unique novel features (Fig. IR.8). Near-infrared wavefront sensors will be installed at each unit telescope, correcting atmospheric turbulence upfront. As the result GRAVITY should be able to detect faint (for interferometry: $K > 15..17$) sources. The light of each telescope is then routed through the VLTI delay lines toward the GRAVITY beam combiner in the underground VLTI laboratory. The beams are stabilized both in the field and in the pupil by means of additional light sources at the telescopes that are sensed inside the cryostat, where also the respective actuators are located.

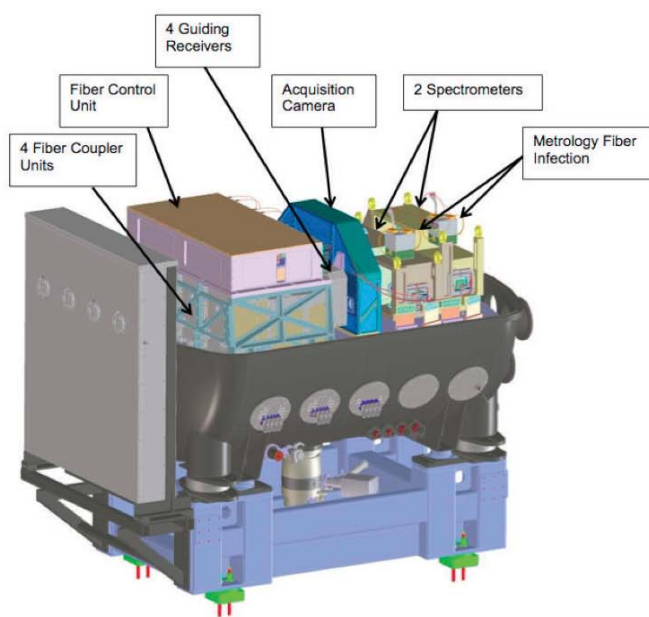
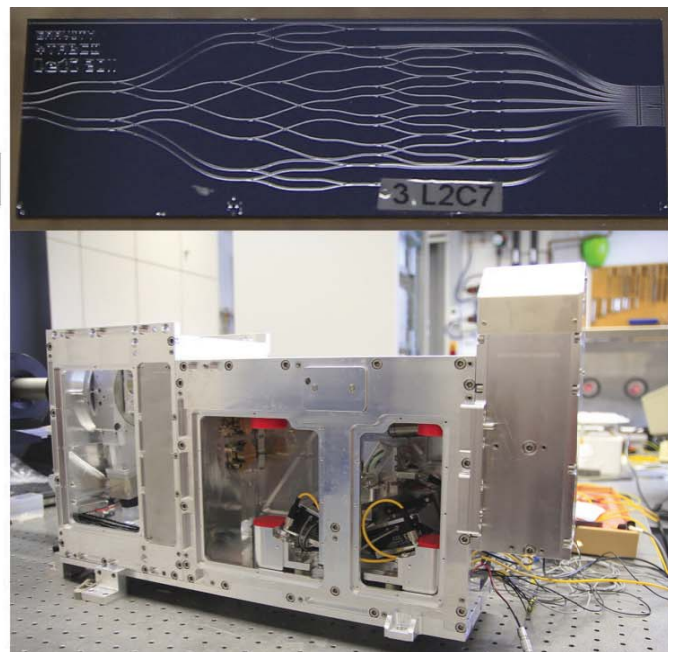


Fig. IR.8: Left: Design of the GRAVITY cryostat, hosting most of the GRAVITY hardware. The four light beams enter from the left and pass the fiber couplers (bottom right) and the fiber control unit before the actual beam combination is achieved by means of an integrated optics chips with waveguides realizing the 6 baselines and simultaneous fringe sampling (top right).

The science light is then coupled into single-mode fibers (one per star and telescope) for modal cleaning. Polarization and differential delay can be controlled at that stage by bending and stretching the fibers. The four fibers per star guide the light into an integrated optics beam combiner, a small piece of glass implementing simultaneous ABCD sampling of the fringes of all six baselines. The 24 output channels per star are then imaged with a classical spectrograph each, and the spectrally dispersed fringes are recorded. The internal optical paths are measured by means of a dedicated metrology system, the light of which propagates backward from the beam combiners up to the telescopes, where the beams originating from the two beam combiners interfere and form a fringe pattern. The latter is temporally sampled at kHz rate to monitor the optical path difference between the two stars towards each telescope. That ensures an optical link between the fringes of the two stars

and thus is crucial for obtaining the astrometric accuracy of $10 \mu\text{as}$. We are also undertaking the development of more sophisticated data analysis tools, largely funded by Stefan Gillessen's ERC starting grant.

The instrument has passed its final design review and is currently being manufactured. MPE is the PI institute of a European consortium, where LESIA (Paris-Meudon), IPAG (Grenoble), MPIA (Heidelberg), University of Cologne and SIM (Lisbon) and ESO are the other partners. GRAVITY will be shipped to Paranal in 2014/2015. We are very much looking forward to bringing to bear this new tool to study the massive black hole in the Galactic Center, with the ultimate goal of dynamically testing various aspects of General Relativity near a MBH.





Stefan Gillessen



Frank Eisenhauer

(Other MPE team members include Hendrik Bartko, Andreas Burkert, Leonard Burtscher, Katie Dodds-Eden, Tobias Fritz, Reinhard Genzel, Nico Hamaus, Marcus Haug, Annemieke Janssen, Stefan Kellner, Clemens Kister, Johannes Kolmeder, Magdalena Lippa, Fabrice Martins, Laura Mascetti, David Moch, Thomas Ott, Oliver Pfuhl, Sonja Rank, Marc Schartmann, Eckhard Sturm, Markus Thiel, Sascha Trippe, Ekkehard Wieprecht)

Selected References:

- Bartko, H.; Martins, F.; Fritz, T. K.; Genzel, R.; Levin, Y.; et al. 2009, *ApJ*, 697, 1741
 Bartko, H.; Martins, F.; Trippe, S.; Fritz, T. K.; Genzel, R.; et al. 2010, *ApJ*, 708, 834
 Burkert, A.; Schartmann, M.; Alig, C.; Gillessen, S.; Genzel, R.; et al. 2012 *ApJ* 750, 58
 Cuadra, J.; Nayakshin, S.; Springel, V.; Di Matteo, T. 2005 *MNRAS* 360, L55
 Dodds-Eden, K.; Porquet, D.; Trap, G.; Quataert, E.; Hauboix, X.; et al. 2009, *ApJ*, 698, 676
 Dodds-Eden, K.; Sharma, P.; Quataert, E.; Genzel, R.; Gillessen, S.; et al. 2010, *ApJ*, 725, 450
 Dodds-Eden, K.; Gillessen, S.; Fritz, T. K.; Eisenhauer, F.; Trippe, S.; 2011, *ApJ* 728, 37
 Eckart, A.; Schödel, R.; Meyer, L.; Trippe, S.; Ott, T.; Genzel, R. 2006, *A&A*, 455, 1
 Eckart, A.; Baganoff, F. K.; Zamaninasab, M.; Morris, M. R.; Schödel, R.; et al. 2008, *A&A* 479, 625
 Eisenhauer, F.; Schödel, R.; Genzel, R.; Ott, T.; Tecza, M.; et al. 2003, *ApJ*, 597, L121
 Eisenhauer, F.; Genzel, R.; Alexander, T.; Abuter, R.; Paumard, T.; et al. 2005, *ApJ*, 628, 246
 Eisenhauer, F.; Perrin, G.; Brandner, W.; Straubmeier, C.; Perraut, K.; et al. 2011, *The Messenger*, 143, 16
 Fritz, T. K.; Gillessen, S.; Dodds-Eden, K.; Martins, F.; Bartko, H. et al. 2010, *ApJ*, 721, 395
 Fritz, T. K.; Gillessen, S.; Dodds-Eden, K.; Lutz, D.; Genzel, R. et al. 2011, *ApJ*, 737, 73
 Genzel, R.; Schödel, R.; Ott, T.; Eisenhauer, F.; Hofmann, R.; et al. 2003, *ApJ*, 594, 812
 Genzel, R.; Schödel, R.; Ott, T.; Eckart, A.; Alexander, T.; et al. 2003a, *Nature* 425, 934
 Genzel, R.; Eisenhauer, F.; Gillessen, S. 2010 *Rev.Mod.Phys.* 82, 3121
 Ghez, A. M.; Duchêne, G.; Matthews, K.; Hornstein, S. D.; Tanner, A.; et al. 2003, *ApJ*, 586, L127
 Ghez, A. M.; Salim, S.; Weinberg, N. N.; Lu, J. R.; Do, T.; et al. 2008, *ApJ*, 689, 1044
 Gillessen, S.; Eisenhauer, F.; Fritz, T. K.; Bartko, H.; Dodds-Eden, K.; et al. 2009a, *ApJ* 707, L114
 Gillessen, S.; Eisenhauer, F.; Trippe, S.; Alexander, T.; Genzel, R.; et al. 2009b, *ApJ* 692, 1075
 Gillessen, S.; Genzel, R.; Fritz, T. K.; Quataert, E.; Alig, C.; et al. 2012, *Nature* 481, 51
 Gillessen, S.; Genzel, R.; Fritz, T. K.; Eisenhauer, F.; Pfuhl, O.; et al. 2013, *ApJ*, 763, 78
 Hamaus, N.; Paumard, T.; Müller, T.; Gillessen, S.; Eisenhauer, F. et al. 2009, *ApJ*, 692, 902
 Hills, J. G. 1988, *Nature*, 331, 68
 Maness, H.; Martins, F.; Trippe, S.; Genzel, R.; Graham, J. R. et al. 2007, *ApJ*, 669, 1024
 Martins, F.; Genzel, R.; Hillier, D. J.; Eisenhauer, F.; Paumard, T.; et al. 2007, *A&A*, 468, 233
 Martins, F.; Gillessen, S.; Eisenhauer, F.; Genzel, R.; Ott, T.; Trippe, S. 2008, *ApJ*, 672, L119
 Meyer, F.; Meyer-Hofmeister, E. 2012 *A&A*, 546, L2
 Murray-Clay, R.A.; Loeb, A. 2012, *Nature Comm.* 3, 1049
 Paumard, T.; Genzel, R.; Martins, F.; Nayakshin, S.; Beloborodov, A. M.; et al. 2006, *ApJ* 643, 1011
 Pfuhl, O.; Fritz, T. K.; Zilka, M.; Maness, H.; Eisenhauer, F. et al. 2011, *ApJ*, 741, 108
 Schartmann, M.; Burkert, A.; Alig, C.; Gillessen, S.; Genzel, R.; 2012, *ApJ*, 755, 155
 Schödel, R.; Ott, T.; Genzel, R.; Hofmann, R.; Lehnert, M.; et al. 2002 *Nature* 419, 694
 Schödel, R.; Ott, T.; Genzel, R.; Eckart, A.; Mouawad, N.; Alexander, T. 2003 *ApJ* 596, 1015
 Scoville, N., Burkert, A. 2013, *ApJ* 768, 108
 Trippe, S.; Paumard, T.; Ott, T.; Gillessen, S.; Eisenhauer, F.; et al. 2007, *MNRAS*, 375, 764
 Trippe, S.; Gillessen, S.; Gerhard, O. E.; Bartko, H.; Fritz, T.K. et al. 2008, *A&A*, 492, 419

2.3 Galaxy Evolution at the Peak Epoch of Cosmic Star Formation

The baryonic lifecycle of galaxies is determined by a balance between three rates: (1) the cosmological inflow rate of baryons through filaments of the cosmic web; (2) the rate at which stars form out of cooled gas; and (3) the outflow rate of material, blown out by AGN, supernovae, or radiation pressure from young stars. Any temporary imbalance between these three forces governing a galaxy's lifecycle is translated into a reduction or increase of its internal gas reservoir. As the galaxy and its halo accumulate more mass over time, newly accreting gas will settle in a rotating disk of larger scale length, which, when converted into stars, leads to structural growth of the stellar component. Eventually, bulges emerge as galaxies mature, and depart from their star-forming steady state to join the quiescent population. It is clear that the statistical census provided by deep look-back surveys has played an important role in establishing the broad scope of the above "equilibrium-growth-model" for galaxies. However, detailed studies of smaller subsets of galaxies, well sampled from the parent population, are critical in order to obtain a comprehensive understanding of the physical processes driving each facet of a galaxy's formation and growth history. This is the main objective of the research efforts within the IR/submm group at MPE: complementing large population studies with detailed multi-wavelength observations at high spectral and spatial resolution, together tracing the kinematics and structure of all baryonic components: from stars to dust to ionized and molecular gas. Many of these observations are performed with state-of-the-art instrumentation that was developed in-house.

It has long been known that the cosmic star formation rate density rises rapidly with look-back time, to peak at $z \sim 1 - 3$. Until recently, the associated prevalence of luminous and ultra-luminous infrared galaxies has been interpreted as major mergers driving galaxy evolution in the early universe. The increased fractions of galaxies with disturbed morphologies, as seen in the rest-UV imaging available was frequently invoked in support of this picture. Over the past few years, MPE led the way in bringing about a paradigm shift in galaxy evolution, from a merger-dominated early universe to one in which the bulk of galaxies live their lives in the aforementioned steady state. Three diverse yet synergetic observations were instrumental in laying the empirical foundation for this new framework:

- **Turbulent disks featuring vigorous outflows.** Our SINS and zC-SINF large programs with SINFONI at VLT demonstrated that the dynamical support of nearly half of all massive star-forming galaxies is dominated by ordered disk rotation, unlike what would be expected in the case of frequent major merging. However, high-redshift disks differ significantly from nearby spiral galaxies: large local random motions reveal a turbulent ISM. Early disks are far from closed boxes, as we find ubiquitous galactic-scale outflows.

- **High molecular gas mass fractions.** By targeting normal 'main sequence' (MS) star-forming galaxies at $1 < z < 3$, rather than rare star-bursting outliers, our PHIBSS survey with the Plateau de Bure Interferometer bridges the gap between conventional molecular gas studies and optical-to-infrared deep look-back surveys. PHIBSS revealed molecular gas mass fractions as high as 33% (47%) at $z \sim 1$ (2), quantified the integrated and resolved star formation law at high redshift, and established that the rapidly declining star formation rates since $z \sim 1$ are mainly controlled by a reduction of cold gas reservoirs.

- **Uniform MS galaxies, contrasted to a rare outlier population.** Throughout cosmic time, MS star forming galaxies produce new stars proportional to the amount of stellar mass they already assembled. Herschel/PACS deep imaging shows that $\sim 98\%$ of star forming galaxies reside on the MS at $z \sim 1-2$. Using Herschel and HST imaging, we mapped variations in galaxy structure, mode of star formation, dust temperature, and mid-to-far-infrared SED shapes across the MS, shedding light on the physical processes that can disturb galaxies from equilibrium.

In this chapter, we describe each of these observational findings, and the broader impact of the respective surveys in more depth. Furthermore, we lay out how we are building on past success through new surveys (KMOS^{3D}), and the development of instrumentation for high-resolution structural (ARGOS) and kinematic (ERIS) studies.



Stijn Wuyts

2.3.1 Probing the Processes Driving the Growth of Galaxies at $z \sim 2$

Spatially- and spectrally-resolved information of the rest-frame optical line and continuum emission is proving very powerful in exploring the baryonic mass assembly and star formation of distant galaxies. Our major near-IR imaging spectroscopic program of star-forming galaxies at $z \sim 1 - 3$ with SINFONI at ESO's Very Large Telescope (VLT), coupled with Hubble Space Telescope imaging surveys and multi-line spectroscopic observations with LUCI at the Large Binocular Telescope, have revealed the importance of internal galaxy dynamics in growing early disks and bulges, and the nature and energetics of feedback - pinning down for the first time details of physical processes driving and regulating early galaxy evolution in the emerging "equilibrium growth model". Our multi-year survey with the new KMOS instrument at the VLT will take the next step towards a comprehensive and unbiased view of the resolved properties of galaxies at the heyday of massive galaxy formation.

The SINS/zC-SINF survey with SINFONI and synergies with HST and LBT/LUCI surveys. "SINS/zC-SINF" is the first and largest survey of spatially-resolved ionized gas kinematics, star formation, and physical properties at $z \sim 2$, carried out with the near-IR integral field spectrometer SINFONI at the VLT. The survey was initiated as a major part of the MPE IR/Submm group Guaranteed Time Observations (GTO) for SPIFFI and PARSEC (the MPE-built spectrometer of SINFONI and the laser for the VLT Laser Guide Star Facility) and expanded through an ESO Large Program in collaboration with the "zCOSMOS" team. Over 100 nights were devoted for observations of 110 $z \sim 1 - 3$ MS galaxies, focusing on H α and [NII] emission, mostly in seeing-limited mode (4 - 5 kpc resolution) and with adaptive optics (AO) for a sharper view of 35 of the targets (1 - 2 kpc resolution). SINS/zC-SINF probes the bulk of the $z \sim 2$ star-forming galaxy (SFG) population over two orders of magnitude in stellar mass and SFR (Förster Schreiber et al. 200, 2009, 2013; Mancini et al. 2011). The deep SINFONI+AO data were complemented with sensitive ~ 1.5 kpc resolution mapping of the stellar component using HST NICMOS and WFC3 near-IR imaging. In parallel, our detailed studies of galaxy morphologies from HST ACS optical and WFC3 near-IR imaging in the "CANDELS" survey fields and our emission line survey of another 100 $z \sim 2$ MS galaxies with the multi-object spectroscopic mode of LUCI (built in part by MPE) at the Large Binocular Telescope (LBT) have provided concurring evidence strengthening several of our main SINFONI results.

Galaxy kinematics and structure at $z \sim 2$. SINS/zC-SINF shows that more than half of the galaxies are rotationally supported disks. The rest consists of interacting/merging systems and more compact, velocity dispersion-dominated objects but even in the latter a significant rotation component is detected at AO resolution (Fig. IR.9, Shapiro et al. 2008; Förster Schreiber et al.

2009; Mancini et al. 2011; Newman et al. 2013). The rotation velocity v_{rot} scales roughly linearly with galaxy size, consistent with centrifugally-supported baryonic disks of constant angular momentum parameter within virialized dark matter halos. The rest-optical light and stellar mass maps of the SINS/zC-SINF AO galaxies also shows a majority of disk-like profiles and reveals the presence of a bulge-like component in the most massive galaxies (Förster Schreiber et al. 2011a; Lang et al., in prep.). The prevalence of disks among distant SFGs is further strengthened by our study of rest-UV/optical morphologies of large mass-selected samples out to $z \sim 2.5$: the tight locus defined by the vast majority of SFGs in the M-SFR plane is dominated by disk-like systems while rarer "outliers" above and below this "main sequence" show more compact, cuspier morphologies (Fig. IR.9, Wuyts et al. 2011). This result makes a compelling case that a correlation between galaxy structure and stellar populations, i.e. a Hubble sequence, was already in place just about 3 Gyr after the Big Bang. Our resolved measurements of the kinematics and structure of high- z galaxies suggest that smoother accretion and internal dynamical processes play a dominant role in growing galaxies. Theoretical support for these findings also comes from our analysis of halo merger fractions and mass accretion rates based on the Millenium Simulation (Springel et al. 2005, Genel et al. 2008).

Properties and evolution of $z \sim 2$ disks. High- z disks exhibit high intrinsic velocity dispersions of $\sigma_0 \sim 30 - 80$ km/s, 5-10 times great than in $z \sim 0$ "thin" disks (Genzel et al. 2006, 2008; Förster Schreiber et al. 2006, 2009; Cresci et al. 2009; Newman et al. 2013). Velocity dispersions show little if any dependence on galaxy size or star formation surface density, explaining the larger fraction of dispersion-dominated objects among smaller galaxies. The $z \sim 2$ disks often exhibit luminous kpc-sized clumps in H α and rest-UV/optical light, each clump contributing up to $\sim 20\%$ of the galaxies' SFRs (Genzel et al. 2008, 2011; Förster Schreiber et al. 2011b; Wuyts et al. 2012). In pilot studies of a subset of galaxies, we found trends of increasing central dynamical mass fraction with galaxy evolutionary stage, and of older clump ages at smaller galactocentric radii. These trends are consistent with theoretical arguments and numerical simulations of turbulent gas-rich disks in which giant star-forming clumps result from violent gravitational instabilities and bulges form via efficient secular processes on timescales < 1 Gyr (e.g. Genel et al. 2012). Inward clump migration could be an important path for bulge formation if clumps survive to strong stellar feedback and tidal torques.

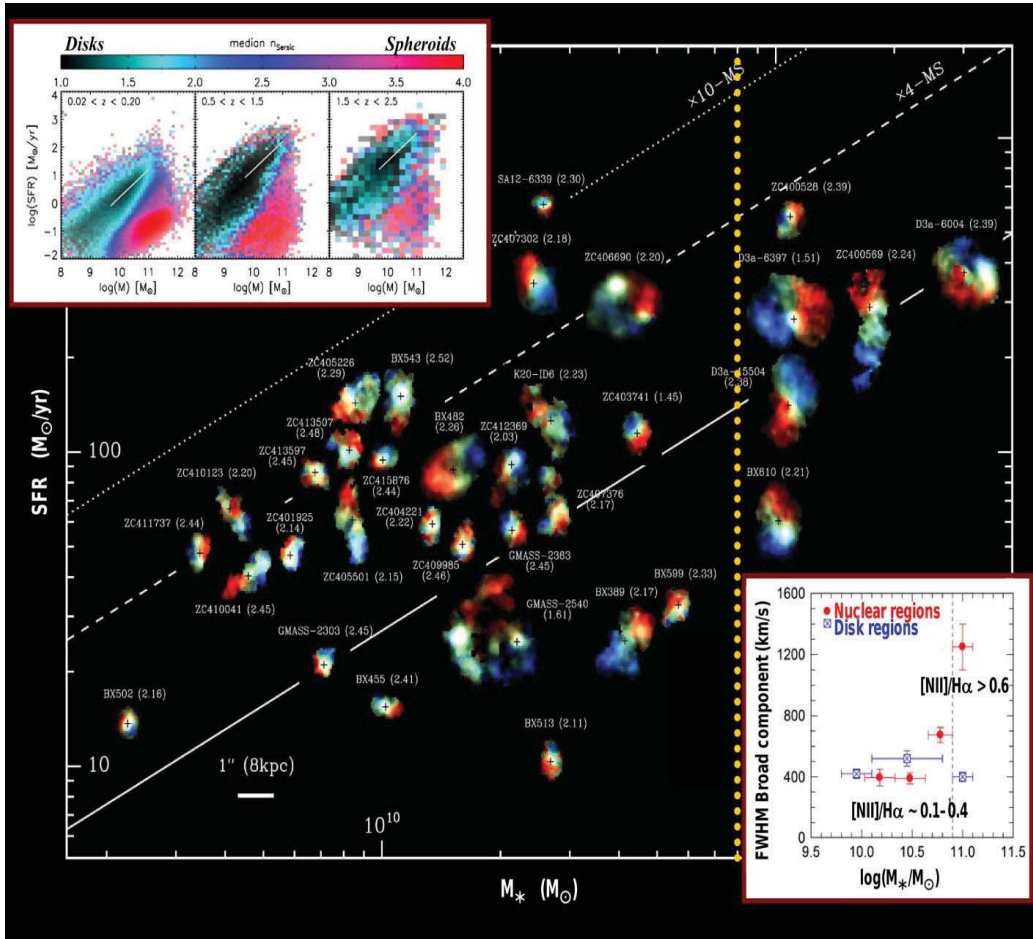


Fig. IR.9: Velocity fields at ~ 1.5 kpc resolution from our SINFONI+AO H α observations of $z \sim 2$ SFGs, sorted according to the stellar mass and SFR of the galaxies. All sources are shown on the same angular scale, with color-coding ranging from blue to red for blueshifted to redshifted emission relative to the systemic velocity, and with intensity scaled by the H α surface brightness. The galaxies probe the star-forming population within a factor of a few around the $z \sim 2$ “main sequence” (MS, solid white line). A majority exhibits disk-like kinematics, in line with the dominance of disk-like morphologies among SFGs that is observed out to $z \sim 2.5$ (top inset). Smaller, lower-mass objects tend to have higher ratios of random-to-rotational/orbital motions, lower metallicities, and younger stellar ages and could represent earlier evolutionary stages. A broad H α + [NII] emission component signals the pervasive presence of strong star formation-driven outflows at $z \sim 2$ (bottom inset, see also Fig. 2). Galaxies with $\log(M_*/M_{\odot}) > 10.9$ show evidence for a bulge component and an AGN driving a powerful nuclear outflow, which could contribute to the shutdown of star formation at the high-mass end.

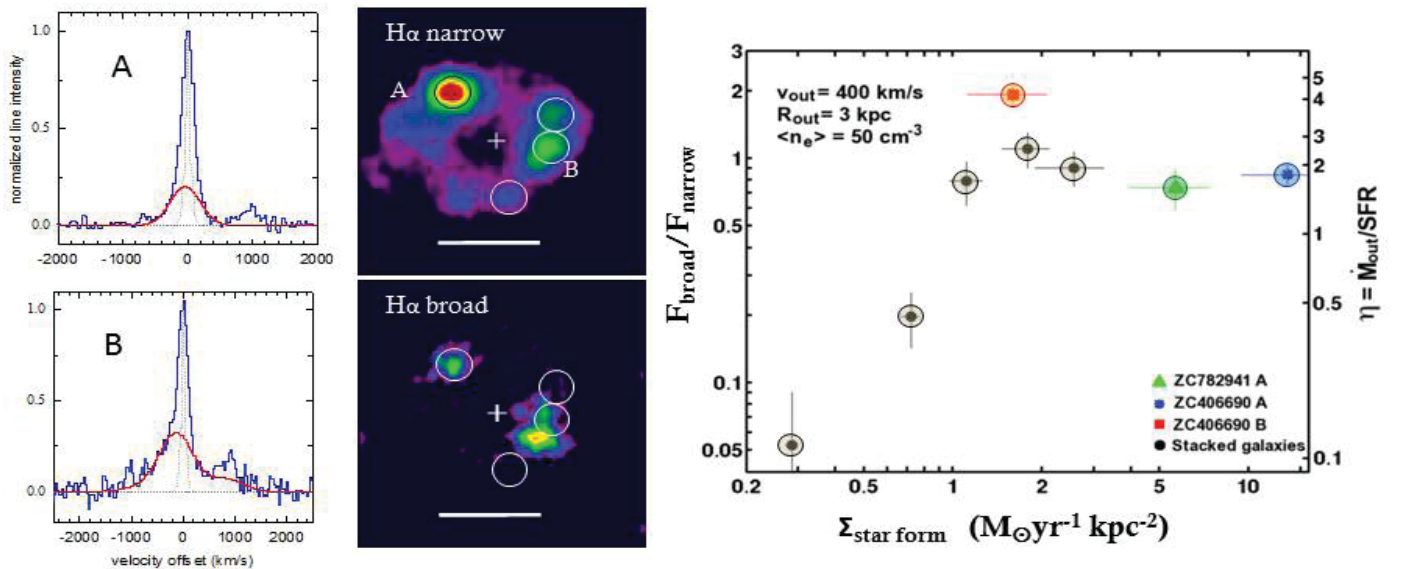


Fig. IR.10: Stellar ‘feedback’ in high- z main sequence star forming galaxies. Left: Maps of the narrow and broad H α emission in zC406690 ($z=2.19$), with the profiles of H α /[NII] toward the prominent star forming clumps A and B. The broad emission ($\Delta v_{\text{FWHM}} \sim 500$ -700 km/s) is spatially resolved and is clearly associated with the prominent clumps, which are obviously driving powerful ionized gas outflows into the circum-galactic environment of the galaxy (Genzel et al. 2011, Newman et al. 2012a). Right: The ratio of broad to narrow line flux (left) and inferred wind mass loading factor (right) of the ionized outflows, as a function of star formation surface density, in individual clumps, as well as stacked galaxy spectrum. There appears to be a sharp onset of galactic winds above $\sim 1 M_{\odot}\text{yr}^{-1}\text{kpc}^{-2}$ (Newman et al. 2012b).

Vigorous feedback from star formation and AGN. The SINS/zC-SINF survey uncovered strong, spatially-extended ionized gas outflows revealed by a broad FWHM ~ 450 km/s $\text{H}\alpha$ + $[\text{NII}]$ component underneath the narrower emission tracing star formation, and which, in some of the disks, originates from individual bright clumps (Fig. IR.10, Genzel et al. 2011; Newman et al. 2012a,b). This discovery pinned down the roots of the ubiquitous galactic-scale winds at high- z so far only observed on > 10 kpc scales (e.g., Steidel et al. 2010, Shapiro et al. 2009). The winds appear to set in at a SFR surface density $\sim 1 \text{ M}_{\odot}/\text{yr}/\text{kpc}^2$, 10 times higher than the break-out threshold in nearby starbursts and attributed to enhanced gas pressure in $z \sim 2$ disks. Outflow rates from clumps and from the galaxies reach up to several times their SFRs -- the first empirical constraint at $z > 1$ on mass loading, a key parameter in theoretical models of star formation-driven feedback (Fig. IR.10). Gas-rich clumps may be self-destroyed by the vigorous feedback before they migrate to the galaxy center, as seen the simulations of Genel et al. (2012). Our HST studies demonstrate that massive $z \sim 0.5 - 2.5$ SFGs appear smoother in stellar mass than in rest-UV/optical light; clumps thus trace local peaks in star formation rather than in mass, and their typical stellar properties are consistent with rapid in-situ disruption unless they are able to migrate inward within ~ 1 orbital timescale (Wuyts et al. 2012). Our SINFONI data further uncover strong nuclear outflows in all of the most massive galaxies ($\log M_{\ast} > 10.9 \sim \log M_{\ast}^{\text{Schechter}}$), all of which are large disks with evidence for a significant bulge. The broad nuclear component has enhanced $[\text{NII}]/\text{H}\alpha > 0.5$ and FWHM $\sim 1000-1500$ km/s, highly suggestive of outflows driven by an AGN (Fig. IR.9 bottom right). The average wind densities and mass loading factors are comparable to those of the star formation-driven outflows. The frequency of these AGN-driven outflows at the high-mass end suggests they have a large duty cycle and may thus contribute significantly to the shutdown of star formation activity observed at galaxy masses above $\sim 10^{11} \text{ M}_{\odot}$.

Nebular gas excitation and metallicity. Analysis of $\text{H}\alpha$, $[\text{NII}]$, $[\text{OIII}]$, and $\text{H}\beta$ line emission among our SINFONI+LUCI samples confirms enhanced global nebular excitation at $z \sim 2$ compared to typical $z \sim 0$ SFGs, implying higher ionization parameters and electron densities in the non-AGN galaxies (Newman et al. 2013b). Shock excitation attributed to star formation-driven outflows is detected around bright clumps (Newman et al. 2012a). At fixed stellar mass, galaxies with higher SFRs do not tend to be more metal-poor, challenging a recently proposed fundamental $M_{\ast}-Z$ -SFR relation, at least in the mass range probed by our measurements. Metallicities inferred from $[\text{NII}]/\text{H}\alpha$ ratios appear to drop radially but are shallower than those of present-day spiral galaxies. This finding may be consistent with beam-smearing effects at $z \sim 2$ and the fact that our SINS/zC-SINF galaxies likely evolve into more massive, earlier-type galaxies by $z \sim 0$ (Förster Schreiber et al. 2013).

Taking the next step with KMOS^{3D}. The obvious next step is to expand our studies to larger, homogeneous, and more complete samples. We are undertaking KMOS^{3D}, a comprehensive multi-year survey of $\text{H}\alpha$ + $[\text{NII}]$ + $[\text{SII}]$ emission leveraging the $24\times$ multiplexing capabilities of the new KMOS multi-object near-IR integral field spectrograph at the VLT to study spatially-resolved kinematics, star formation, outflows, nebular excitation, and metallicities of ~ 600 $z = 0.7 - 2.6$ mass-selected galaxies. This survey is a joint venture of the MPE IR/Submm and OPINAS groups, dedicating ~ 70 nights of GTO for building KMOS (see below 2.3.4). KMOS^{3D} capitalizes on the 3D-HST and CANDELS HST Treasury Surveys, providing unique multi-wavelength data and large mass-limited samples with accurate redshifts. The survey will enable us for the first time to establish firmly the connection between galaxy kinematics and stellar structure, to determine the role of star formation and AGN in governing stellar mass growth, to test systematically the imprint of feedback on galaxy formation efficiency, and to explore the influence of environment. KMOS^{3D} will offer an unbiased view in unprecedented detail of galaxy evolution across the peak of cosmic SFR, tracing key transformations at the origin of today's Hubble sequence. A preview of things to come is given in Fig. IR.16 (below) that shows the extracted position wavelength diagrams for two $z\sim 2$ galaxies observed during the commissioning.



Natascha Förster Schreiber is a W2 Senior Scientist at MPE and was a MPG Minerva Fellow at MPE between 2007 and 2012. She led the highly successful SINS and zC-SINF integral field spectroscopy surveys of $z\sim 1.5-3$ star forming galaxies with SINFONI @ VLT. She currently is the Principal Investigator of the KMOS^{3D} GTO survey of the MPE-IR+OPINAS groups that aim at IFU data for $600+ z\sim 0.8-3$ star forming galaxies.



Stijn Wuyts

(Other MPE team members include Kaushala Bandara, Nicolas Bouché, Andreas Burkert, Peter Buschkamp, Ric Davies, Shy Genel, Reinhard Genzel, Erin Hicks, Jaron Kurk, Philipp Lang, Dieter Lutz, Sarah Newman, Kristen Shapiro Griffin, Linda Tacconi, Emily Wisnioski, Eva Wuyts)

Selected References:

- Cresci, G.; Hicks, E. K. S.; Genzel, R.; Schreiber, N. M. Förster; Davies, R.; et al. 2009, *ApJ*, 697, 115
 Förster Schreiber, N. M.; Genzel, R.; Lehnert, M. D.; Bouché, N.; Verma, A.; et al. 2006, *ApJ*, 645, 1062
 Förster Schreiber, N. M.; Genzel, R.; Bouché, N.; Cresci, G.; Davies, R.; et al. 2009, *ApJ*, 706, 1364
 Genel, S.; Genzel, R.; Bouché, N.; Sternberg, A.; Naab, Th.; et al. 2008, *ApJ* 688, 789
 Genel, S.; Naab, Th.; Genzel, R.; Förster Schreiber, N.M.; Sternberg, A.; et al. 2012 *ApJ* 745, 11
 Genzel, R.; Tacconi, L. J.; Eisenhauer, F.; Förster Schreiber, N. M.; Cimatti, A.; et al. 2006, *Nature* 442, 786
 Genzel, R.; Burkert, A.; Bouché, N.; Cresci, G.; Förster Schreiber, N. M.; et al. 2008 *ApJ* 687, 59
 Genzel, R.; Newman, S.; Jones, T.; Förster Schreiber, N. M.; Shapiro, K.; et al. 2011 *ApJ* 733, 101
 Mancini, C.; Förster Schreiber, N. M.; Renzini, A.; Cresci, G.; Hicks, E. K. S.; et al. 2011, *ApJ*, 743, 86
 Newman, S.F.; Shapiro Griffin, K.; Genzel, R.; Davies, R.; Förster-Schreiber, N.M.; et al. 2012a, *ApJ*, 752, 111
 Newman, S.F.; Genzel, R.; Förster-Schreiber, N.M.; Shapiro Griffin, K.; Mancini, C.; et al. 2012b, *ApJ*, 761, 43
 Newman, S.F.; Genzel, R.; Förster Schreiber, N.M.; Shapiro Griffin, K.; Mancini, C.; et al. 2013, *ApJ*, 767, 104
 Shapiro, K.L.; Genzel, R.; Förster Schreiber, N.M.; Tacconi, L.J.; Bouché, N.; et al. 2008, *ApJ*, 682, 231
 Shapiro, K.L.; Genzel, R.; Quataert, E.; Förster Schreiber, N.M.; Davies, R.; et al. 2009, *ApJ*, 701, 955
 Steidel, C.C.; Erb, D.K.; Shapley, A.E.; Pettini, M.; Reddy, N.; et al. 2010 *ApJ* 717, 289
 Springel, V.; White, S.D.M.; Jenkins, A.; Frenk, C.S.; Yoshida, N.; et al. 2005 *Nature* 435, 629
 Wuyts, Stijn; Förster Schreiber, Natascha M.; Genzel, Reinhard; Guo, Yicheng; et al. 2012, *ApJ*, 753, 114

2.3.2 IRAM: Tracing the Molecular Gas Contents of Main Sequence SFGs

Stars form from cold, dense molecular interstellar gas clouds. Measurements of mass fractions, spatial distributions and kinematics of the cold molecular gas component across cosmic time, and the evolution of the relation between gas content and star formation activity, together provide critical observational tests of the ‘equilibrium growth’ framework described at the beginning of this chapter. The last six years have witnessed studies of molecular gas taking center stage in the research on galaxy evolution in the IR/submm group. Taking full advantage of new generation, sensitive broad-band receivers at IRAM’s PdBI Interferometer and 30-meter telescope we have successfully carried out three Large Programs that take a census of the molecular gas contents in MS star forming galaxies both in the local Universe (the COLD-GASS program) and at the peak epoch of cosmic

star formation from $z \sim 1-2$ (PHIBSS). We describe the main results from both of these important studies here.

PHIBSS. In late 2008, we began the IRAM Plateau de Bure high- z blue sequence CO 3-2 survey (PHIBSS), the first systematic and highly successful effort to assess the molecular gas properties in massive MS SFGs near the cosmic star formation peak, pushing to 3-10 times fainter sources than in our previous CO studies of SMGs (e.g. Tacconi et al. 2008, Engel et al. 2010, Bothwell et al. 2013). PHIBSS provides for the first time sizeable samples of CO 3-2 line detections in two redshift slices selected by stellar mass ($>2.5 \times 10^{10} M_{\odot}$) and star formation rate ($>30 M_{\odot} \text{yr}^{-1}$). The lower redshift slice at $z \sim 1.2$ contains 50 CO detections, including 12 SFGs from the literature. The higher redshift slice at $z \sim 2.2$ consists of

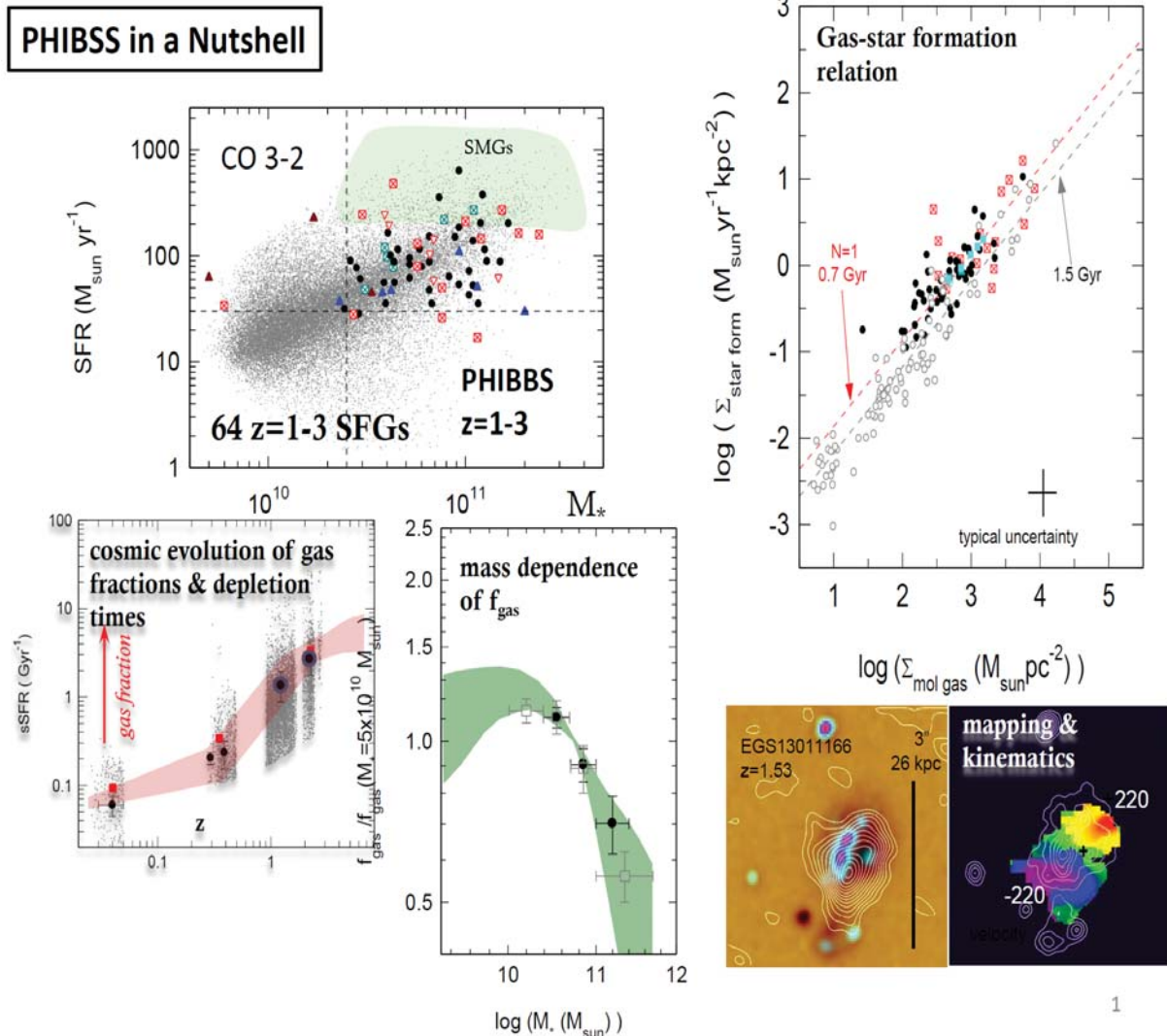


Fig. IR.11: PHIBSS in a Nutshell. Upper left: The location of the PHIBSS survey SFGs in the stellar mass – star formation planes, with PHIBSS sources indicated by the black circles, red squares and red triangles. Upper right: Molecular gas – star formation surface density relationship (‘Kennicutt-Schmidt’ relation), for $z \sim 0$ “near main-sequence” SFGs (open grey circles), $z \sim 1-1.5$ SFGs (black filled circles: PHIBSS), $z \sim 1.53$ EGS13011166 (filled cyan squares), $z \sim 2-2.5$ detected SFGs (red squares). Lower left: cosmic evolution of sSFR (SFR/ M^*) from multiband imaging surveys (red shaded area, red squares and grey dots) and inferred from CO data and a linear KS relation with PHIBSS data in large black circles; Bottom right: A PHIBSS $z \sim 1.5$ SFG, where we have been able to map the CO distribution (in white contours) and kinematic at $0.7''$ resolution. Bottom center: The dependence of normalized gas fractions (relative to value at $\log M^* = 10.7$) on stellar mass (filled black circles from PHIBSS, open circles from $z=0$ COLDGASS, and green shaded area from imaging surveys with an inverse KS-estimate of gas).

23 SFGs, 17 with detected CO emission, including three lensed galaxies from the literature. PHIBSS has tripled the number of normal high- z SFGs with directly measured cold gas properties. We sketch the key results from PHIBSS in Fig. IR.11 and summarize them here.

Through PHIBSS we have uncovered large molecular gas reservoirs in these main-sequence SFGs, with average gas fractions of 30–50%, i.e. 4–10 times higher than main-sequence SFGs in the local Universe (Tacconi et al. 2010, 2013, Genzel et al. 2010, 2013). These molecular gas fractions are stellar mass dependent. They drop by 60% between $\log M^* = 10.5$ and 11.3, at both high and low redshift, consistent with the expectations from cosmological simulations with strong star formation feedback (Fig IR.11, bottom right). Most importantly, we find that gas fractions correlate strongly with the specific star formation rate, $sSFR = SFR/M^*$, both at a given redshift as a function of star formation rate near the main sequence, and also as a function of redshift (Fig IR.11, top right). The important implication from this work is that at constant stellar mass, both the vertical location of a galaxy in the M^* -SFR plane, and the variation of $sSFR$ over cosmic time, are mainly driven by the available molecular gas reservoir. On both galactic and sub-galactic scales, $z \sim 1$ main-sequence SFGs obey a near-linear relation between molecular gas mass and SFR (Fig. IR.11, top left; Genzel et al. 2010, 2013), with a gas depletion time scale ($t_{\text{depl}} = M_{\text{mol}}/SFR$) of about 0.7 Gyr, similar to what is found at $z=0$ (Saintonge et al. 2011b).

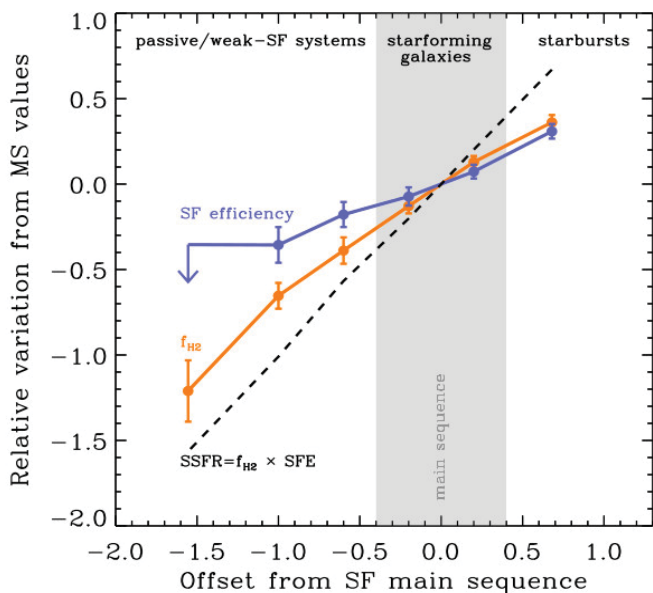


Fig. IR.12: Because COLD GASS fully samples the SFR- M^* plane, we can study the molecular gas properties of galaxies not only on and above the main sequence, but also far below. Using spectral stacking we find that the molecular gas mass fraction varies strongly as a function of main sequence offset (orange line), but that this variation is not enough to explain the full range of specific star formation rates (black dashed line).

A slow variation in star formation efficiency (SFR/ M_{H2}) with main sequence offset (blue line) is also observed and required to explain the very high SSFRs of starbursts, and the very low values measured in early-type galaxies.

In a second stage of the survey we have been able to map the CO emission in ~ 12 galaxies at sub-arcsecond resolution (Fig. IR.11, bottom left). These sensitive observations reveal gas distributions extended over regions comparable to the rest-frame optical/UV emission. Most of these targets have regular velocity fields, indicative of ordered rotational motion, and reminiscent of the findings from our SINS near-IR $H\alpha$ survey at $z \sim 2$ (e.g. Förster Schreiber et al. 2009). From modeling the intrinsic gas kinematics we find that the ratio of rotational velocity to local velocity dispersion is ~ 7 , consistent with, but a bit larger than dispersions in similar SFGs from $H\alpha$ imaging spectroscopy (Förster Schreiber et al. 2009), indicating that large velocity dispersions are characteristic of the entire gas layer of high- z SFGs.

With new capabilities coming online with IRAM's NOEMA program, a major upgrade for the interferometer, we are in a perfect position to take a next major step in surveying the gas contents of high- z SFGs. We have just started PHIBSS2, a 4-year Legacy class survey at IRAM (>1000 hours of integrated on PdBI/NOEMA), which will more than triple the number of MS SFGs with CO observations, sample a wider redshift range from $z=0.5-3$, and more systematically sample the mass-SFR plane of the underlying parent population. The combination of PHIBSS and PHIBSS2 will enable us to comprehensively study the molecular content of galaxies during the epochs that are associated with the rapid build-up ($z > 2$), peak, and subsequent winding down ($z < 1$) of star formation in the Universe.

COLD GASS. Closer to home and together with Guinevere Kauffmann and colleagues at MPA, over the last three years we have been assembling a legacy database of molecular gas in nearby galaxies with the IRAM 30-meter telescope. We have measured the CO (1-0) line in 350 galaxies selected purely on stellar mass ($\log M^* > 10.0$), without any additional selection criteria on quantities such as star formation rate, infrared luminosity, morphology, environment. Our COLD GASS survey is the first completely unbiased and representative study of molecular gas across the low redshift galaxy population. In combination with a large observing campaign at the Arecibo observatory and at several optical facilities, COLD GASS has established some of the first unbiased scaling relations between the cold gas contents of galaxies (both atomic and molecular), their star formation rates, and their physical, structural and chemical properties (Saintonge et al. 2011a,b, 2012).

Among the results to come out of COLD GASS is the observation that molecular gas mass fractions depend most strongly on morphological parameters such as concentration index or stellar mass surface density (Saintonge et al. 2011a). This observation is not reproduced by semi-analytic galaxy formation models, suggesting that the implementation AGN feedback needs to be revised. We have also used the COLD GASS sample to study the Kennicutt-Schmidt (KS) star formation relation over a representative sample. We reproduce the slope and scatter typically found in recent studies of the KS

relation, but discover some structure within the scatter around the relation. For example, bulge-dominated galaxies fall systematically below the mean relation, suggesting that gas surface density is not the only parameter driving star formation efficiency (Saintonge et al. 2012). Finally, using stacking we have probed the molecular gas contents both along and across the star formation main sequence. We find that the low specific star formation rates (SSFRs) of early-type galaxies are caused not only by low molecular gas contents, but also by lower star formation efficiency than in main sequence galaxies. Conversely, the high sSFRs of starbursts are caused in similar proportions by higher H₂ masses and an increased efficiency at converting this gas into stars (Fig. IR.12).

Because the COLD GASS sample is large and covers the full SFR-M* plane at z=0, the survey is becoming the reference against which the predictions of galaxy formation models are tested. The COLD GASS sample also serves as the ideal reference for high redshift studies, as it can be pruned to match the selection criteria of different surveys (see Fig. IR.11). We have recently begun observations on an extension of the COLD GASS survey, to push our systematic study down to lower stellar masses. The combined sample of 500 galaxies, fully sampling the SFR-M* plane over the full mass interval $9.0 < \log M^* < 11.5$, will be an invaluable tool both to put into context low- and high-z studies of specific galaxy populations with NOEMA and ALMA, but also to constrain models of galaxy evolution.



Linda Tacconi



Amelie Saintonge

(Other MPE team members include Nicolas Bouché, Andreas Burkert, Hauke Engel, Natascha Förster Schreiber, Reinhard Genzel, Javier Gracia-Carpio, Dieter Lutz, Sarah Newman, Kristen Shapiro Griffin, Stijn Wuyts)

Selected References:

- Bothwell, M. S.; Smail, I.; Chapman, S. C.; Genzel, R.; Ivison, R. J.; et al. 2013 *MNRAS* 429, 3047
 Engel, H.; Tacconi, L. J.; Davies, R. I.; Neri, R.; Smail, I.; et al. 2010 *ApJ* 724, 233
 Förster Schreiber, N. M.; Genzel, R.; Bouché, N.; Cresci, G.; Davies, R.; et al. 2009, *ApJ*, 706, 1364
 Genzel, R.; Tacconi, L. J.; Gracia-Carpio, J.; Sternberg, A.; Cooper, M. C.; et al. 2010, *MNRAS*, 407, 2091
 Genzel, R.; Tacconi, L. J.; Combes, F.; Bolatto, A.; Neri, R.; et al. 2012 *ApJ* 746, 69
 Genzel, R.; Tacconi, L. J.; Kurk, J.; Wuyts, S.; Combes, F.; et al. 2013 *arXiv* 1304.0668
 Saintonge, A.; Kauffmann, G.; Kramer, C.; Tacconi, L.J.; Buchbender, C.; et al. 2011, *MNRAS* 415, 32
 Saintonge, A.; Kauffmann, G.; Wang, J.; Kramer, C.; Tacconi, L.J.; et al. 2011, *MNRAS* 415, 61
 Saintonge, A.; Tacconi, L.J.; Fabello, S.; Wang, J.; Catinella, B.; et al. 2012 *ApJ* 758, 73
 Tacconi, L. J.; Neri, R.; Chapman, S. C.; Genzel, R.; Smail, I.; et al. 2006, *ApJ*, 640, 228
 Tacconi, L. J.; Genzel, R.; Smail, I.; Neri, R.; Chapman, S. C.; et al. 2008 *ApJ* 680, 246
 Tacconi, L. J.; Genzel, R.; Neri, R.; Cox, P.; Cooper, M. C.; et al. 2010 *Nature* 463, 781
 Tacconi, L. J.; Neri, R.; Genzel, R.; Combes, F.; Bolatto, A.; et al. 2013 *ApJ* 768, 74

2.3.3 PACS-PEP: Herschel Infrared Galaxies

Star formation rates and infrared SEDs from Herschel provide us with a comprehensive view of the galaxy population evolving from $z \sim 2$ to $z \sim 0$, and challenge the applicability of the traditional locally calibrated picture of the merger-nature of (ultra)luminous infrared galaxies. Infrared SEDs and other properties of galaxies are naturally explained in relation to the evolving 'main sequence' of star forming galaxies, and are consistent with the equilibrium, gas-regulated growth model discussed above.

Much of the interpretation of ISO and Spitzer extragalactic surveys has been made in the context of luminosity-dependent SED families that encode locally well calibrated trends from normal disk galaxies to merger-dominated ULIRGs, and implicitly a wealth of connotations concerning other properties. These trends and properties are poorly tested at high redshift, and may not apply. Using our PEP guaranteed time Herschel extragalactic survey of key multi-wavelength deep fields (Lutz et al. 2011), we are now directly measuring the calorimetric rest frame far-infrared emission of massive high redshift galaxies. This allows us to re-calibrate other star formation indicators such as the mid-infrared, UV- and radio emission. We confirm the 'mid-infrared excess', which was previously hinted at in Spitzer data, and which leads to an over prediction of $z \sim 2$ star formation rates based on mid-infrared fluxes and local luminosity dependent SED families. We find that this excess is not related to AGN-emission, but is due to the systematic increase with redshift (at given infrared luminosity) of the ratio of star formation related mid-infrared PAH features to total infrared emission (Fig. IR.13 right, Nordon et al. 2010, 2012).

The Herschel data indicate that the mid- to far-IR SEDs of near MS SFGs are luminosity and redshift independent (Fig. IR.13 left). MS galaxies have large PAH/IR ratios similar to local disk galaxies, while galaxies above the main sequence show the suppressed PAH/IR typical of the intense radiation fields in strong local starbursts/mergers (Fig IR.13 right).

We have combined Herschel, mid-infrared, and optical/near-infrared based star formation rates into a consistently calibrated 'ladder' of star formation indicators. It is then possible to place consistently galaxies throughout the star formation rate / stellar mass plane at different redshifts, characterize the importance of different regions, and define typical properties. Among star forming galaxies, MS galaxies dominate starburst-merger outliers greatly by number ($\sim 98\%$) and in the contribution to the total star formation rate ($\sim 90\%$) (Wuyts et al. 2011a, Rodighiero et al. 2011).

A PACS/SPIRE study of a large sample of submillimeter galaxies (SMGs) has confirmed the very large luminosities (and star formation rates) of the brightest cases (Fig. IR.14). This study shows, however, that at lower submillimeter flux levels the SMG population is a mixture of these starbursts far above the main sequence, and of colder, very massive objects near the main-sequence (Magnelli et al. 2010, 2012a). In addition recent ALMA studies indicate that a fraction of the brightest SMGs are multiple sources in the large beams of the discovery surveys. The combination of these effects significantly decreases the tension between the observed SMG number counts and recent simulations.

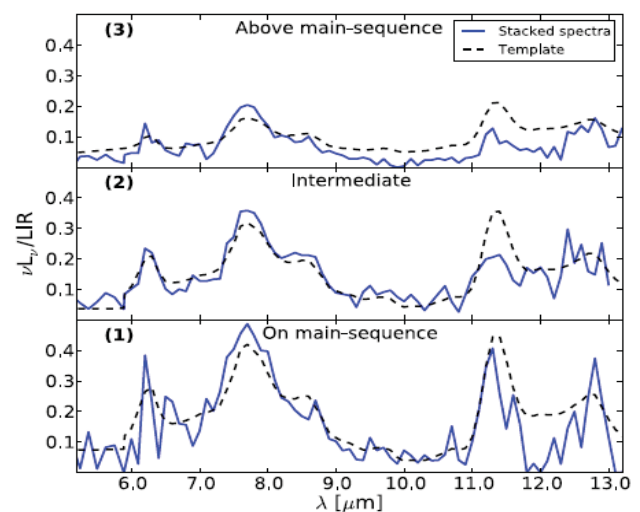
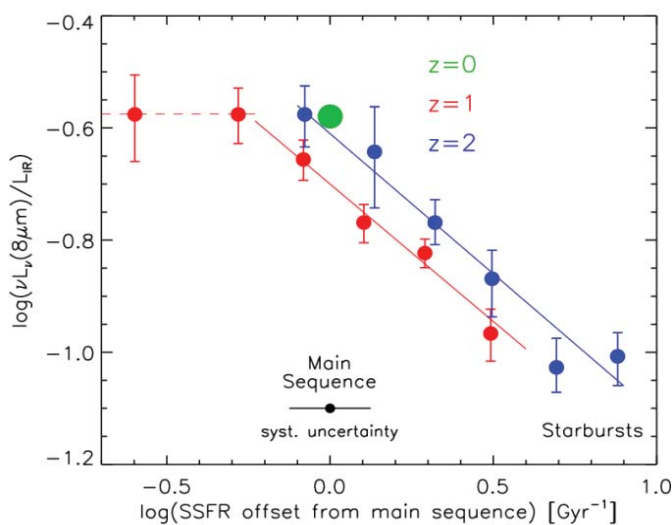


Fig. IR.13: Left: The Herschel/Spitzer infrared SED shape (coded by the ratio of rest $8\mu\text{m}$ and total infrared emission) follows a relation with offset from the star forming main sequence, consistently between $z \sim 0$ and $z \sim 2$. Right: Ultra-deep Spitzer spectra, grouped by offset from the main sequence, show that the $8\mu\text{m}$ emission is always dominated by PAH features (star formation), and that the SED trends are caused by the smaller PAH/IR ratio in the intense radiation fields of starbursts above the main sequence (Nordon et al. 2010, 2012).

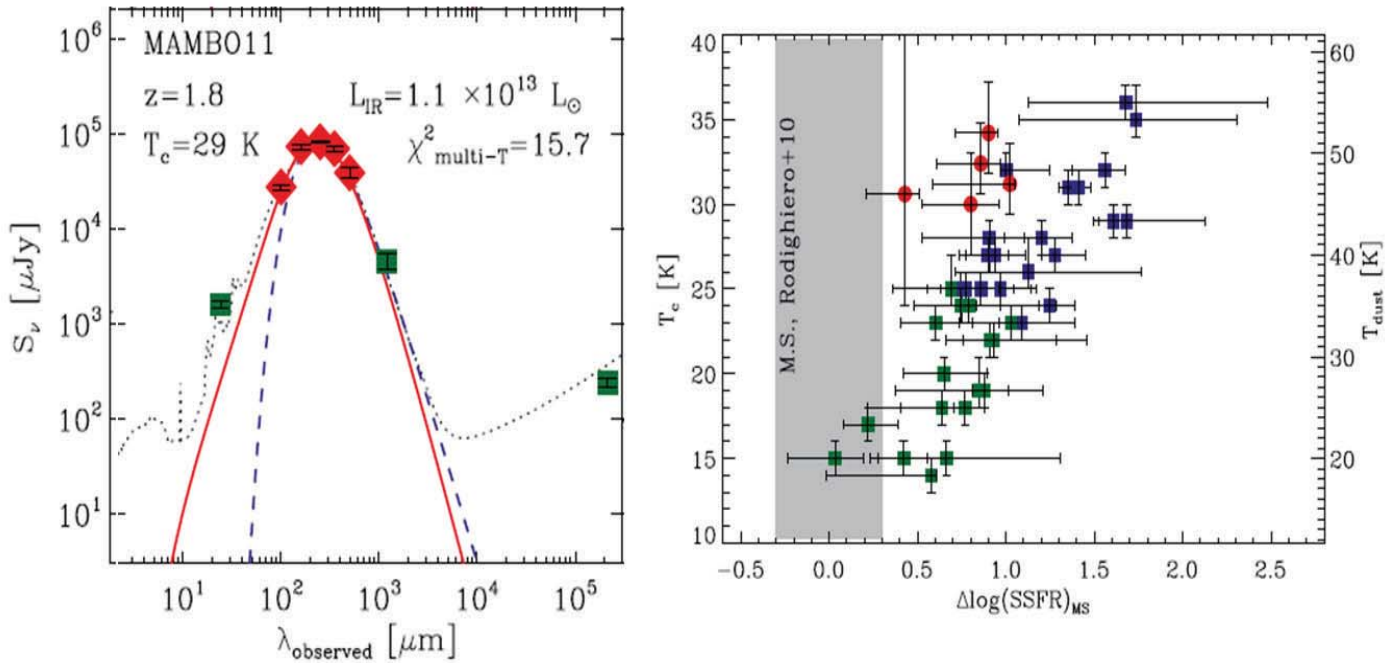


Fig. IR.14. Herschel PACS/SPIRE observations of SMGs. Top: IR to radio SED of one of 61 SMGs of our sample, where PACS/SPIRE data (red) have unambiguously confirmed the remarkably large luminosities and star formation rates of the most extreme SMGs ($\sim 10^3 M_{\odot} \text{yr}^{-1}$ in MAMBO11). However, for the sample as a whole it is becoming clear that the SMG population is a ‘mixed bag’, with the majority of the most luminous sources being extreme starbursts way above the main sequence, but with an increasing admixture of colder, very massive near main-sequence galaxies at the fainter levels (Magnelli et al. 2010, 2012a)

With full PACS/SPIRE Herschel SEDs we can also derive dust masses and (via a metallicity dependent gas-to-dust ratio) gas masses for high- z galaxies on and above the main sequence (Santini et al. 2010, Magnelli et al. 2012b, Saintonge et al. 2013). Our results confirm the notion from CO studies that there is a systematic change in the CO emission to molecular gas mass ‘conversion factor’, when going from the main sequence galaxies to starbursts above.



Dieter Lutz

(Other MPE team members include Stefano Berta, Natascha Förster Schreiber, Reinhard Genzel, Benjamin Magnelli, Raanan Nordon, Albrecht Poglitsch, Paola Popesso, David Rosario, Amelie Saintonge, Li Shao, Linda Tacconi, Stijn Wuyts)

Selected References:

- Lutz, D.; Poglitsch, A.; Altieri, B.; Andreani, P.; Aussel, H.; et al. 2011, A&A 532, A90
 Magnelli, B.; Lutz, D.; Berta, S.; Altieri, B.; Andreani, P.; et al. 2010, A&A 518, L28
 Magnelli, B.; Lutz, D.; Santini, P.; Saintonge, A.; Berta, S.; et al. 2012a, A&A 539, A155
 Magnelli, B.; Saintonge, A.; Lutz, D.; Tacconi, L. J.; Berta, S.; et al. 2012b, A&A 548, A22
 Nordon, R.; Lutz, D.; Shao, L.; Magnelli, B.; Berta, S.; et al. 2010, A&A 518, L24
 Nordon, R.; Lutz, D.; Genzel, R.; Berta, S.; Wuyts, S.; et al. 2012, ApJ 745, 182
 Popesso, P.; Rodighiero, G.; Saintonge, A.; Santini, P.; Grazian, A.; et al. 2011 A&A 532, A145
 Popesso, P.; Biviano, A.; Rodighiero, G.; Baronchelli, I.; Salvato, M.; et al. 2012 A&A 537, A58
 Rodighiero, G.; Daddi, E.; Baronchelli, I.; Cimatti, A.; Renzini, A.; et al. 2011, ApJ 739, L40
 Santini, P.; Maiolino, R.; Magnelli, B.; Silva, L.; Grazian, A.; et al. 2010, A&A 518, L154
 Saintonge, A.; Lutz, D.; Genzel, R.; Magnelli, B.; Nordon, R.; et al. 2013, ApJ, submitted
 Wuyts, S.; Förster Schreiber, N.M.; Lutz, D.; Nordon, R.; Berta, S.; et al. 2011, ApJ, 738, 106
 Wuyts, S.; Förster Schreiber, N.M.; van der Wel, A.; Magnelli, B.; Guo, Y.; et al. 2011, ApJ 742, 96

2.3.4 MOS & Laser Guide Star Adaptive Optics Instrumentation for Galaxy Evolution

As in the past, our ground-based instrumentation for high-*z* galaxy evolution program is driven by our science goals. The multi-object spectroscopic instruments LUCI at the LBT and KMOS at the VLT, as well as ERIS at the VLT aim at measuring the properties of distant galaxies more efficiently and with greater sensitivity than ever before. With the high multiplexing capabilities of the near-IR MOS instruments, the spectroscopic survey speeds are 10-20 times greater than in the past, making the ambitious systematic surveys (such as KMOS^{3D}) discussed above possible. The combination of the MOS capabilities of LUCI with ARGOS – the ground layer laser guide star adaptive optics system for the LBT - will for the first time open spatially multiplexed, AND spatially resolved spectroscopic observations across a wide field of view. Sharpening the LBT's view with laser guide star adaptive optics will not only give access to a more detailed view, but as well increases the sensitivity and thus shortens the required observation time. As soon as the E-ELT receives the green light, we will add the development of the first light instrument MICADO to this suite of instrumentation developments.

LUCI & KMOS. Spectroscopic observations of distant galaxies are a time consuming and telescope demanding process: even at the world's largest telescopes a few to a few tens of hours of integration time are required to achieve the required signal to noise ratio. In order to achieve robust statistics a high multiplexing capability is desired. Two projects of the MPE-IR group strive at pushing the frontier of multiplexed infrared spectroscopy for large spectroscopic look-back surveys: LUCI at the LBT in the northern hemisphere and KMOS at the VLT in the south. LUCI I/ -II is the LBT's near infrared imager and multi object spectroscopic instrument. LUCI I is in full operation at the LBT and routinely used for observations. Its twin instrument LUCI II will be shipped soon to Mt Graham, such that both eyes of LBT can be used simultaneously for MOS observations (Fig. IR.15).

The LUCI-MOS units developed by our group allow spectroscopic observations in the near infrared bands Z,I,J,H and K. The object selection within the 4x2 arcmin field of view is done with laser cut masks that allow observations of up to 40 objects simultaneously. Since a new mask is required for each observation, LUCI contains a magazine of pre-prepared cold masks and a cryogenic robot mechanism to position them in the

focal plane. An exchange of the whole mask cabinet can be carried out without breaking the cryogenic conditions.

The second generation VLT instrument KMOS for the first time provides spatially multiplexed IFU spectroscopy. With this unique instrument 24 cryogenic arms can position pick-off mirrors in the VLT UT1 focal plane, each relaying a 2.8 arcsecond field onto integral field units. With a sampling of 0.2 arcseconds spatially resolved spectroscopic information can be obtained. The arms can be freely positioned within the whole 7.2 arcminute field of the telescope, giving access to simultaneous observations of many objects in a single pointing. The wavelength coverage between 0.8 to 2.45 microns is obtained with five gratings, with a resolving power of 3000 to 4000. Wavelength bands spanning IZ, YJ, H or K can be measured in a single setting. KMOS is a collaboration between Durham University, MPE, the LMU Munich Observatory, Oxford University and the UK Astronomy Technology Centre. On the MPE/LMU side the project is led by Ralf Bender and his OPINAS/LMU teams (for details see the OPINAS report). The MPE-IR group has provided the data analysis software for KMOS. KMOS (Fig. IR.16) passed commissioning in March 2013 and is since in the scientific operation phase.

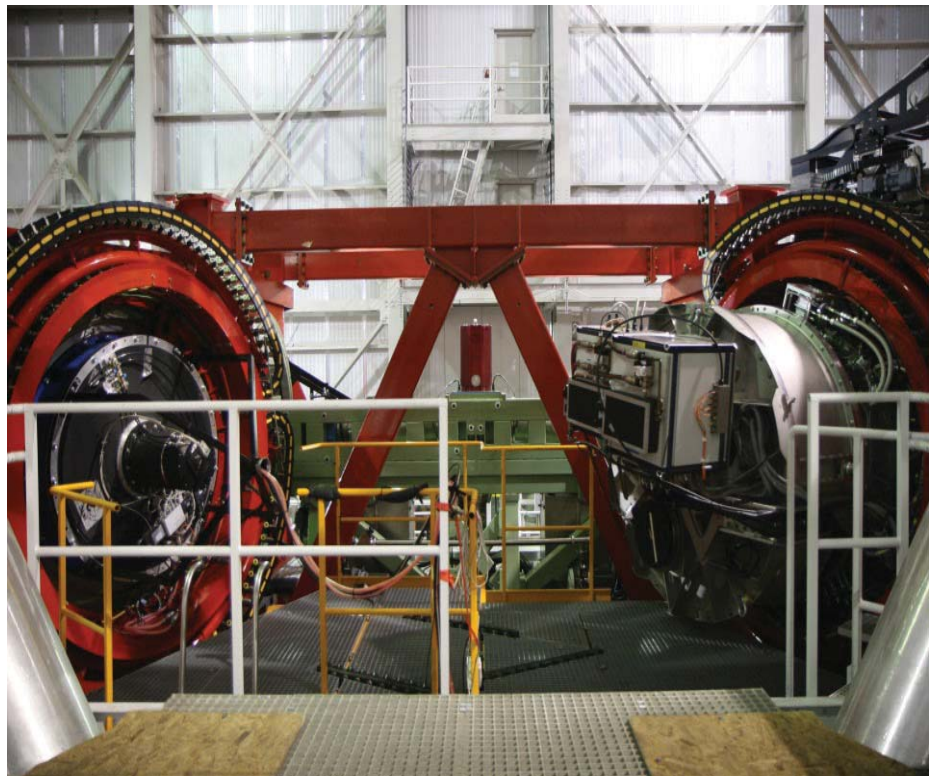


Fig. IR.15: The LUCI platform at LBT. To the right LUCI I can be seen mounted and in operation, while to the left the telescope focus is prepared to take the twin instrument LUCI II. With both sides of LBT highly multiplexed observations can be performed with the collecting power of two 8.4m apertures.

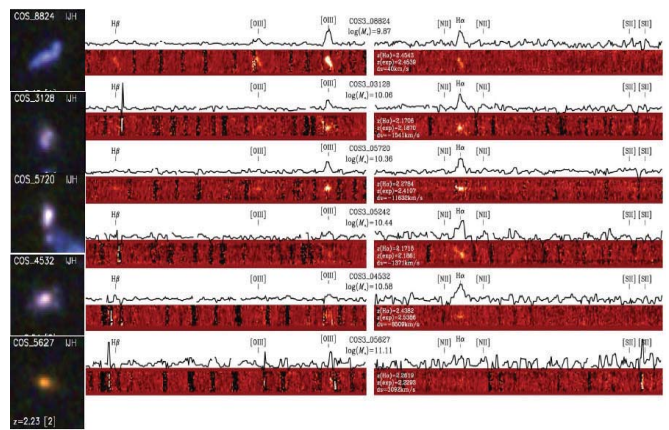


Fig. IR.16: Left: KMOS installed at the VLT. The huge vacuum vessel with the cryogenic pick off arms, integral field units and spectrometer is attached to the VLT UT1 Nasmyth rotator. Right: Images and extracted position-wavelength (velocity) diagrams for 6 $z \sim 2$ star forming galaxies observed for 2 hours during the commissioning of KMOS, showing the H- and K-band spectra of H α , [NII], [OIII] and H β .

ARGOS. ARGOS is the Laser Guide Star adaptive optics system for the Large Binocular Telescope. Aiming for a wide field adaptive optics correction, ARGOS will equip both sides of LBT with a multi laser beacon system and corresponding wavefront sensors, driving LBT's adaptive secondary mirrors.

The basic motivation for the development of ARGOS @ LBT (Fig. IR.17) is spatially resolved spectroscopy, simultaneously of up to 40 objects across the 2'x4' FOV of LUCI. The ground layer adaptive optics (GLAO) correction of ARGOS will improve the 50% encircled energy diameter to $\leq 0.2''$ in good seeing, and $\leq 0.4''$ in relatively poor seeing. This is well matched to the typical sizes of high- z galaxies ($0.3''$ - $1''$), and will in addition increase the efficiency of the telescope even in poorer conditions.

ARGOS employs high power pulsed green lasers for generating the artificial beacons via Rayleigh scattering in the lower Earth atmosphere ($h \sim 12$ km). ARGOS will create a set of three guide stars above each of LBT's mirrors in a wide constellation. The returning scattered light is sensitive to the ground layer turbulence, and is detected in a gated wavefront sensor system. Measuring and correcting the ground layer of the optical distortions enables ARGOS to achieve a stable field correction across several arcminutes that is well matched to the LUCI MOS field of view. Taking advantage of this wide field correction, the science that can be done with the multi object spectrographs LUCI will be boosted by higher spatial resolution and strongly enhanced flux for spectroscopy. Apart from the wide field correction ARGOS delivers in its ground layer mode, we foresee a future upgrade of the system for diffraction limited operation, with a hybrid Sodium laser Rayleigh beacon combination. The first parts of the instrument are currently on their way to Mt. Graham with installation and initial commissioning planned for summer and fall 2013.

ERIS. ERIS is the ESO Enhanced Resolution Imager and Spectrograph for the Very Large Telescope (Fig. IR.18). Following the success of NACO and SINFONI

over the last decade, ERIS will take the next steps in high angular resolution imaging and spectroscopy of high redshift galaxies and the Galactic Center. It will be installed behind ESO's Adaptive Optics Facility, combining an 1170 element adaptive secondary mirror and multiple 20 W lasers with a new wave-front sensor, a state-of-the-art near-infrared imaging camera, and an enhanced SPIFFI spectrometer. After leading the development of the SPIFFI spectrometer for SINFONI and co-leading the development of the CONICA camera for NACO, MPE has recently been selected in a competitive call-for-proposals to build the ERIS infrared camera and to upgrade SPIFFI for ERIS. Like CONICA, the ERIS camera will be a general purpose adaptive optics camera



Fig. IR.17. Left: Artist concept of the ARGOS ground layer AO system for each eye of the LBT.

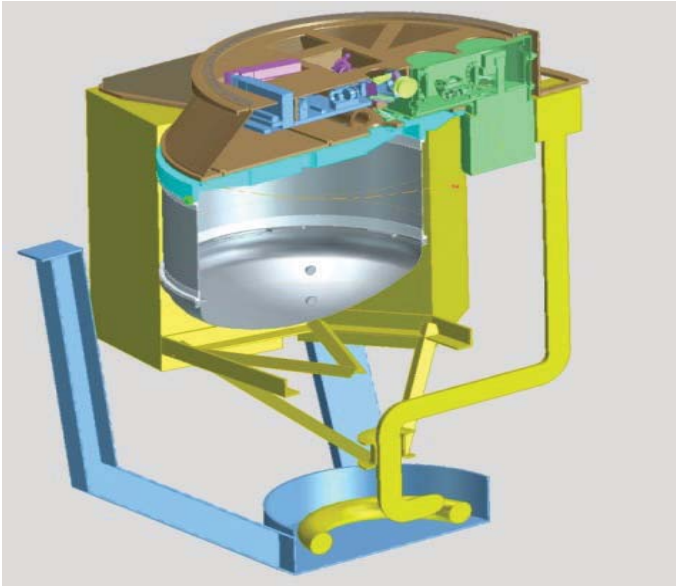


Fig. IR.18: ERIS – the Enhanced Resolution Imager and Spectrograph for the ESO Very Large Telescope (image courtesy ESO). ERIS will be installed behind ESO's new adaptive optics facility and will push the VLT's diffraction-limited imaging and spectroscopy to the next level of resolution and sensitivity. MPE will develop and build its infrared camera (green) and upgrade the SPIFFI integral field spectrograph (grey).

for the 1-5 μm wavelength range, now taking advantage of the latest generation of four megapixel infrared detectors and optimized for very high resolution observations with a Strehl-ratio $>75\%$ in K-band. It is specifically tuned for high precision astrometry and ultra-deep imaging to serve our core science programs on the Galactic Center and high redshift galaxies. In addition it will also include sparse aperture masks and a pupil plane coronagraph to open up new science frontiers at the ultimate VLT diffraction limit.

Other than CONICA, the SPIFFI/SINFONI integral field spectrometer will have a second life in ERIS. SPIFFI/SINFONI has been outperforming its contenders at other 10m class telescopes, but the ERIS adaptive optics will bring its performance to yet another level of angular resolution and sensitivity. We will use the ERIS opportunity to upgrade SPIFFI with an even better optics and to implement a new grating for a very high spectral resolution $R \sim 10.000$, a new step in diffraction limited integral field spectroscopy. First light of ERIS is foreseen in 2017. The following picture shows the ERIS instrument concept with its infrared camera (green) and the upgraded SPIFFI integral field spectrometer (grey).



Sebastian Rabien



Frank Eisenhauer

(Other MPE team members include Nancy Ageorges, Lothar Barl, Alex Agudo Berbel, Peter Buschkamp, Ric Davies, Helmut Feuchtgruber, Natascha Förster Schreiber, Hans Gemperlein, Michael Hartl, Reiner Hofmann, Srikrishna Kanniganti, Jaron Kurk, Christina Loose, Gilles Orban de Xivry, Erich Wiezorrek)

2.4 The Harvest of PACS @ Herschel

After a decade of development and testing, the Photo-detector Array Camera and Spectrometer (PACS) was integrated into the Herschel satellite in 2007/2008 and launched into orbit in May 2009. During the following six months, our PACS team accomplished the commissioning and calibration of the instrument and demonstrated that the advertised performance was fully reached (Poglitsch et al. 2010 [521cites to date]). Over the entire routine phase of the mission – more than three years – our Instrument Control Center was responsible for all PACS-specific aspects of operation (PACS was active during 65% of the Herschel observing time), characterization, and data processing of Herschel. This substantial effort was rewarded by a rich harvest – particularly through the large amount of guaranteed time, which MPE earned in return for the provision of PACS – of absolutely unique data. Some of the highlights are: the conclusion, based on our deep-field photometric surveys, that merger/“ULIRG” phenomena have played a lesser role in the history of star formation over cosmic times than previously assumed; the discovery of extreme, AGN-driven molecular outflows, capable of terminating star formation in the host galaxy, providing the first, direct evidence of such a mechanism; and the ubiquitous presence and role of water in the process of star formation.

PACS operation. With the successful 2009 launch of Herschel and Planck, the PACS project made its transition into the operational phase. As the PI institute, MPE was not only responsible for the design, construction and qualification of the PACS instrument, but also for the coordination of the PACS Instrument Control Center (ICC), with a total staff of over 30 scientists and engineers, distributed over 9 partner institutes. The ICC had to deal with all aspects of the operation, calibration, and software development related to PACS. After commissioning, PACS operated almost flawlessly, with just a handful of hick-ups in the electronics and on-board software, but – notably – no failures in the cold focal plane unit. Mostly during the Science Demonstration Phase, but partly also later into the Routine Phase, we kept optimizing the observing modes and even introduced a new mode for more efficient spectroscopic mapping. In order to verify these modifications we kept our complete flight spare instrument setup in the lab running in stand-by condition, such that checks could be performed without any delay.

The PACS instrument was actually observing for more than 50% of the total Herschel science time (~22,000 hours) in its prime instrument modes, about equally distributed between photometry and spectroscopy, plus about 15% of the total science time in the SPIRE/PACS parallel photometry mode (Fig. IR.20). In line with this high share of observing time, out of the 50 most-cited Herschel publications to date, 32 are based on PACS data, of which 15 are resulting from MPE-led observing programs. At the time of writing, our Herschel-PACS science has resulted in 60 refereed papers with about 2600 citations to date. Although this may be hard to quantify, we feel that, having developed the instrument and most of its data analysis tools ourselves, gave us an advantage for timely publication of our results, particularly during the early phases of the mission, where Herschel and its community compare favorably to other missions (Fig. IR.20 right). One of the core tasks of our ICC was the detailed characterization and calibration of the instrument and also of the satellite attitude control system. Here we address only a few key points out of the many aspects one has to consider for a complete characterization of a complex instrument like PACS.

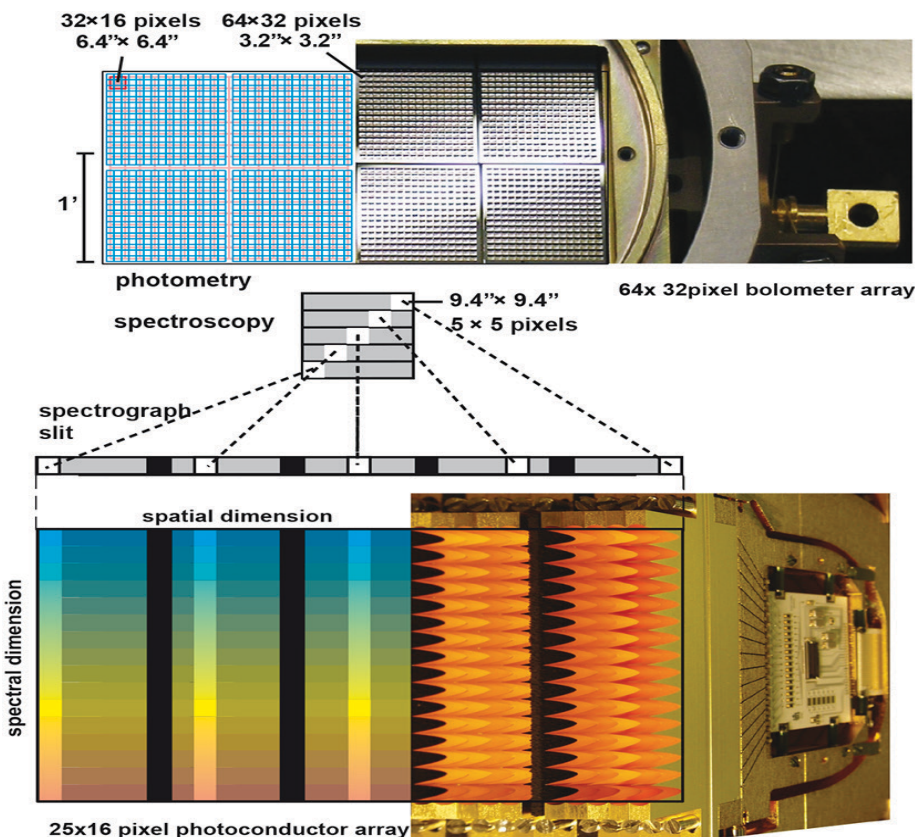


Fig. IR.19: PACS in a nutshell. A fixed mirror splits the focal plane into the photometry (top) and spectroscopy (bottom) channels of the instrument. For integral-field spectroscopy, an optical image slicer re-arranges the 2-dimensional field along the entrance slit of the grating spectrograph such that for each spatial element in the field of view, a spectrum can be simultaneously observed with a 2D detector array. Right: The close-up photos show, at the appropriate scale, half of the short wavelength bolometer array with its tiled monolithic sub-arrays and part of the long wavelength photoconductor array with its area-filling light-cones.

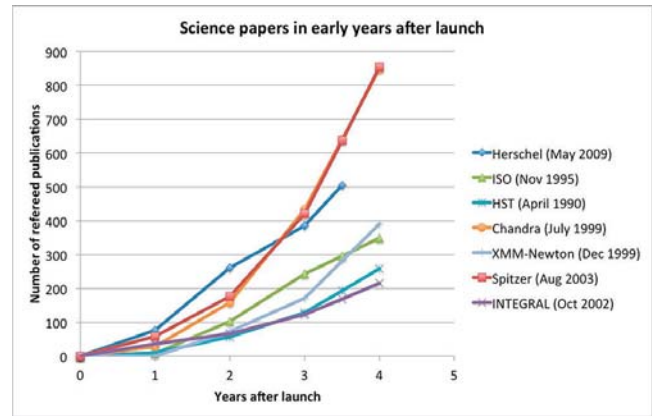
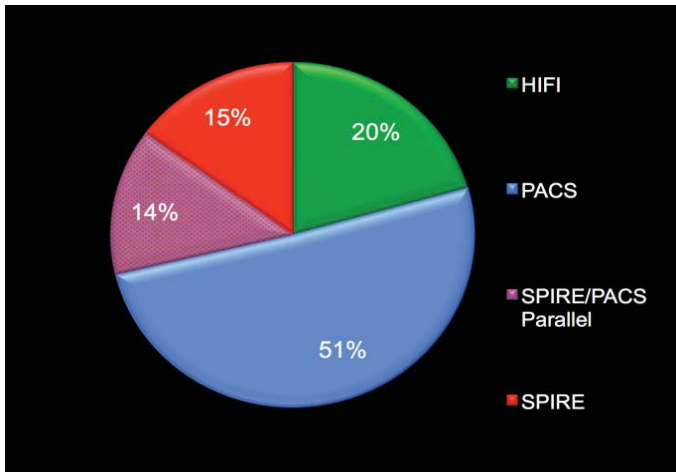


Fig. IR.20: Left: Distribution of the total Herschel scientific observing time between the three instruments. Right: Cumulative number of refereed publications during the first years of Herschel compared to other, relevant astronomy space missions.

Spatial calibration. This task encompassed focal plane geometry as well as the establishment of “beams” (the coupling factor of each pixel to a point source as a function of point source position) and point spread functions (PSF, i.e., the resulting image of a point source as the output from a mapping algorithm). For the photometer with its highly redundant observing scheme, only the PSF is relevant, and a great effort was made to accurately measure it down to very faint levels at large radii, in order to allow source extraction in fields with a high dynamic range (Fig. IR.21 left).

For the spectrometer, which normally cannot observe with much spatial redundancy, the effort was mainly on the characterization of the individual beams of each spaxel, to provide consistent flux calibration between point-like and extended sources (Fig. IR.21 right). In both cases we compared the measured beams/PSFs

with the predictions from an end-to-end physical optics analysis of the telescope/instrument optical train and found very good agreement, indicating no optical degradation in orbit. However, even the subtle differences in the measured PSFs compared to the model predictions turned out relevant for accurate source extraction / aperture photometry techniques. The focal plane geometry (line of sight, scale and distortion) was measured to better than 1/10 of a pixel precision in all bands.

Flux calibration. For absolute flux calibration we used a set of “fiducial” stars, for which accurate photospheric models exist (5% absolute error), as well as Neptune, for which detailed spectral modeling has been done, with a less than 5% error in flux density within the PACS wavelength range (Fig. IR.22 right). Due to the totally different detector technology in photometry vs. spectroscopy, the emphasis had to be quite different in the two parts of PACS.

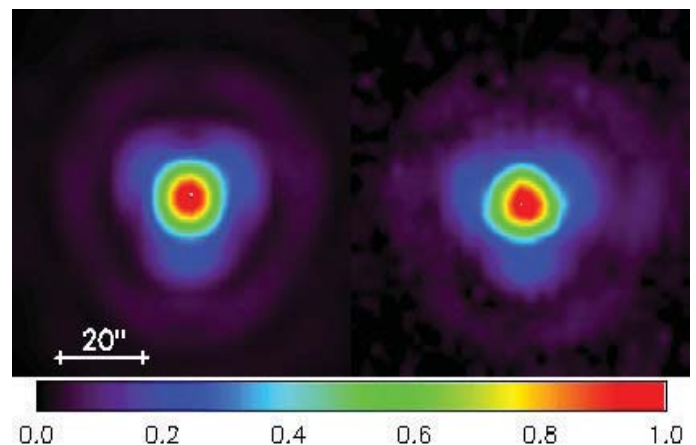
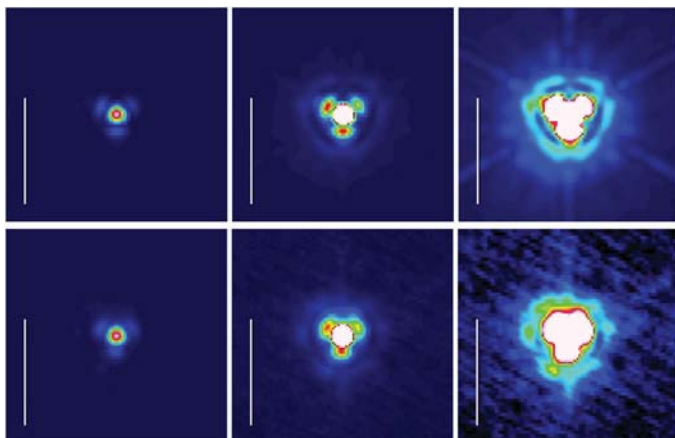


Fig. IR.21: left: photometer point spread function (PSF) in the “green” (100 μ m) band, clipped at – from left to right – 100%, 10%, and 1% of the peak value. Top row: polychromatic physical optics calculation; bottom row: measurement on Vesta. Right: Calculated spectrometer PSF at 124 μ m (left) and measured on Neptune (right) at the same wavelength. Both are normalized to the peak and scaled by square root, to enhance the faint wing pattern. The calculation includes the predicted telescope wave-front error, which dominates the overall aberrations. PACS is the first realization of a diffraction-limited, integral-field spectrometer in the far infrared.

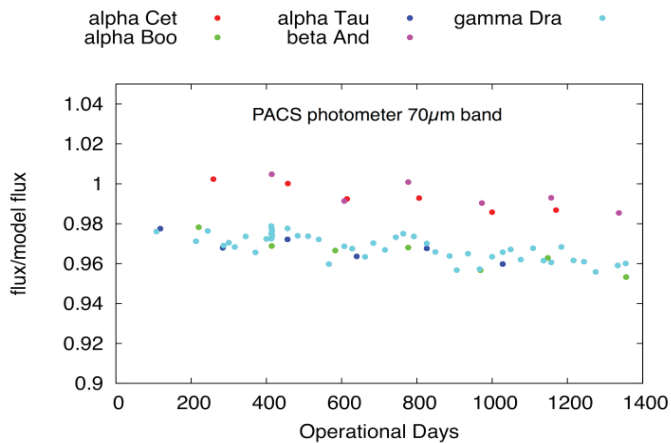


Fig. IR.22: Comparison of measured vs. model fluxes for our 5 “fiducial” calibration stars over time. The seasonal change and overall increase of the telescope emission with time is clearly seen as a yet unaccounted for load, which we still plan to address in the final calibration for the Herschel archive, but we also see systematic differences ($\sim 2\%$) between stars, which may be indicative of the actual accuracy of the stellar models.

For the photometer with its bolometric detectors, it was important to quantify the influence of various external parameters on the absolute response, in particular, of the bath temperature, but also that of the total flux on the detector (non-linearity). Over the course of the mission we were able to establish a flux calibration at the 1-2% precision level over a wide range in flux – unprecedented in this wavelength range, and finally limited by the accuracy of the models for the celestial calibration standards. For the photoconductors in the spectrometer branch, there was some concern about their calibration stability in orbit, due to cosmic ray effects on the detector response and the curing of such effects. As indicated by our ground tests with a light ion synchrotron, these effects were expected to be manageable, though. However, it turned out that not all observations could be reduced with the same calibration scheme; for those observations (mostly, faint sources), where precise “nulling” of longer chop/nod sequences was essential, we devised a scheme to use the self-emission of the telescope as a calibration source, which is observed simultaneously with the celestial object, to achieve the required precision. For absolute flux calibration we used Neptune, and with the telescope normalization method were able to achieve a precision, as derived from many, repeated observations of our calibration stars, of 5% (1σ), which is comparable to the absolute accuracy as defined by our primary standard, Neptune.

In-flight sensitivity. When we started the operation of PACS in orbit, one of the most urgent questions was what effects cosmic rays would have on the detector performance. The actually observed hit rates (photoconductors: 0.08...0.2/s/pixel; bolometers: ~ 1 /min/pixel) were very close to expectation, and there were no effects other than what we had seen on ground during the radiation tests. For the spectrometer, we had been concerned about excess noise from cosmic ray glitches and their “tails” in the detector response, but found no unex-

pected degradation. Actually, the in-flight sensitivity was slightly better than (conservatively) predicted, based on the ground tests. Also, deep observations reached their nominal sensitivity; our record is a 3σ detection of a line flux of 9×10^{-19} W/m² after 6.5 hours of integration. For the photometer, we found that in the 70 μ m and 100 μ m bands the sensitivity was, indeed, as predicted, but that in the 160 μ m band there was some extra background, probably stray light from an intermediate-temperature component of the cryostat/baffle system, which caused some degradation in sensitivity, but without any serious consequences for the execution of our observing programs. In fact, our deepest maps reach a 3σ detection limit of 0.9, 0.6, and 1.3 mJy at 70, 100, and 160 μ m, respectively, which drives the 1000 and 160 μ m maps into the confusion limit.

Data pipeline development. This effort had been started long before launch, and when the PACS photometer was used for Herschel’s very first glimpse of the sky the pipeline was able to produce images straight away. With growing knowledge about the instrument/satellite system and ongoing calibration efforts, substantial improvements and extensions to the pipeline and also many specialized scripts have been implemented in the course of ten major releases of the Herschel Common Science System (Fig. IR.23).

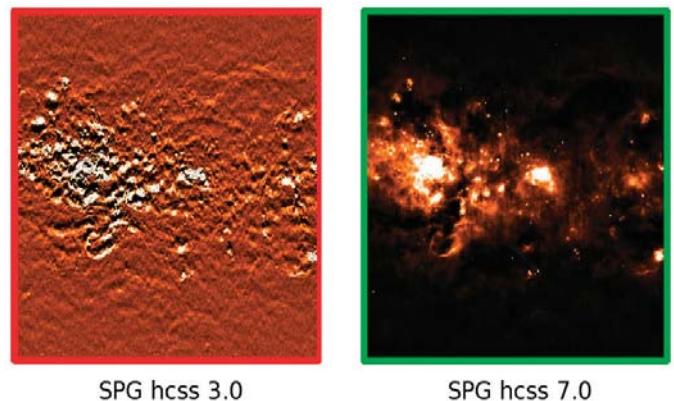


Fig. IR.23: Continued development and improvement of the PACS automatic data pipeline. Shown is the same photometric map (Level2 data product), generated by versions HCSS3.0 (April 2010 and HCSS 7.0 (May 2011).

On the photometer side, two main branches were pursued: one for the mapping of deep fields, optimized for point source sensitivity at the expense of larger-scale structures, and one for general mapping, where low spatial frequencies must be recovered. Different algorithms were investigated; the most suitable ones (MADmap, Scanamorphos) have been or will be implemented within the HCSS framework. The spectrometer pipeline has a number of modules to deal with the different observing modes, from which it will always derive homogeneous, individual data cubes. Special scripts are optimized for line observations or continuum/SED observations and for bright or faint sources. Recently, we were also able to provide a 3D drizzle method, which combines multiple, spatially redundant observations, set up for fully sam-

pled spectral mapping, into one, large data cube, from which maps of line flux, radial velocity, or velocity dispersion can be extracted. Tools for analyzing extended/multiple sources from single pointed observations are under development.

Science results: Resolving the cosmic infrared background (CIB). One of the original science drivers of the Herschel mission was the question of the nature of the sources which constitute the CIB, and what we can learn from them about the history of star formation and galaxy evolution over cosmic times.

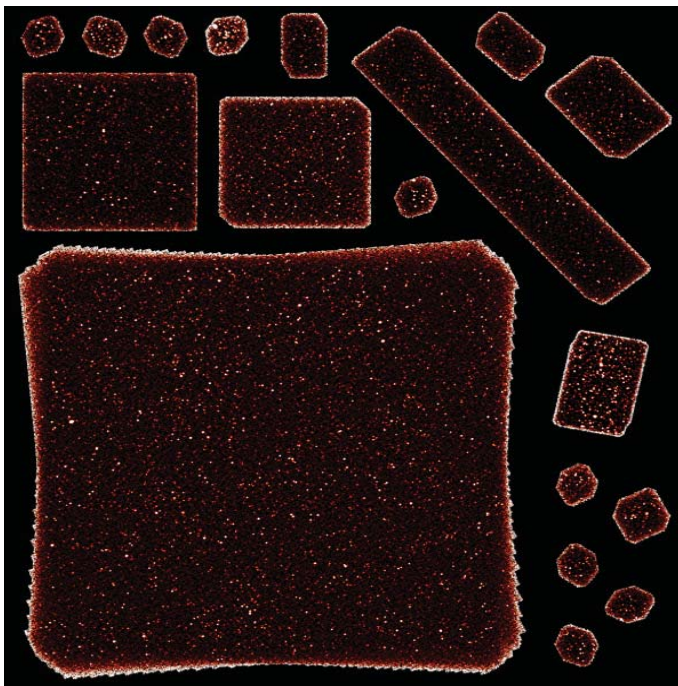
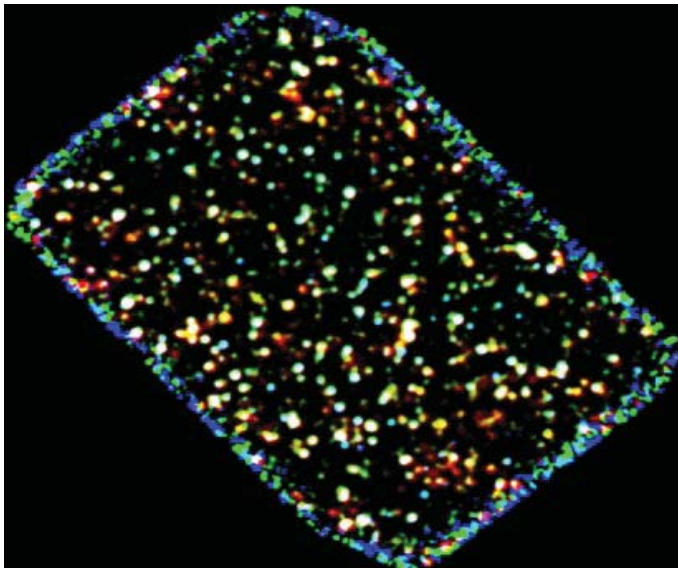


Fig. IR.24: Top: three-color image of the GOODS-North cosmological deep field ($17' \times 11'$), observed with Herschel/PACS at 100 micron (blue) and 160 micron (green) and with Herschel/SPIRE at 250 micron (red), and based on 124 hours of integration (Elbaz et al. 2011). Bottom: Summary of the overall PEP program with all the deep fields. The largest is the COSMOS field ($85' \times 85'$) (Lutz et al. 2011).

We therefore spent the bigger part of our guaranteed time on deep photometric look-back surveys (PACS Evolutionary Probe (PEP): Lutz et al. 2011) of the most widely studied extragalactic blank fields, following a “wedding cake” strategy (Fig. IR.24). Its tiers include the wide (2 deg^2) and shallow COSMOS field, medium depth areas like the ECDFS, EGS, and Lockman Hole, and pencil-beam, very deep observations of GOODS-N/S (reaching $\leq 1 \text{ mJy}$ at 3σ , at $100\mu\text{m}$, Fig. IR.24 left). These are complemented by ten nearby lensing clusters and two $z \sim 1$ clusters. By integrating the number counts we derive the cumulative CIB as a function of flux (Fig. IR.25, red dots) and compare it to the direct measurement by COBE. Roughly 75% of the COBE CIB is resolved in individual sources at $100\mu\text{m}$ and $160\mu\text{m}$. PEP observations of lensing clusters (e.g. Abell 2218) extend this estimate to even fainter fluxes. Finally, employing the “probability of deflection” statistical analysis, $P(D)$, we break the confusion limit and reach 89% of the total CIB at $160\mu\text{m}$. We have now reached the point where the CIB lower limits from the source counts are more constraining than direct, integral measurements (Berta et al. 2010, 2011).

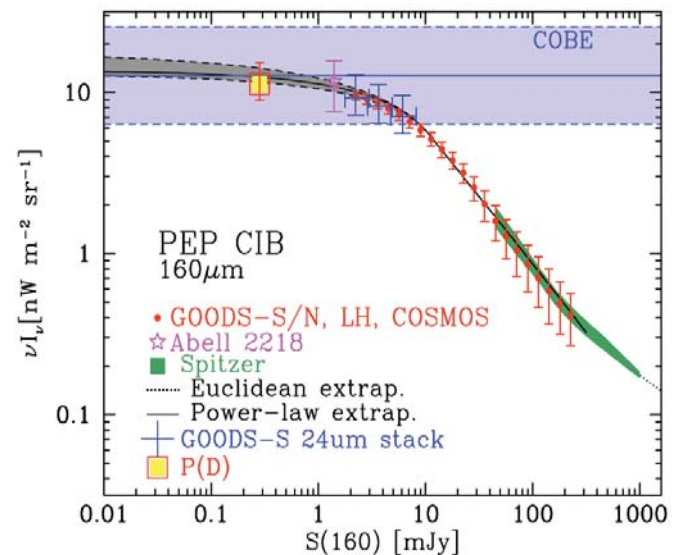


Fig. IR.25: Cumulative Cosmic Infrared Background as a function of flux. Red circles, blue crosses and the yellow square represent completeness-corrected counts, stacking, and $P(D)$ analysis, respectively. The grey shaded area is an extrapolation based on a power-law fit to the resolved number counts. The blue shaded area indicates the $\pm 1\sigma$ range of the direct, integrated measurement of the CIB with COBE. The green shaded represents previous surveys carried out with IRAS, ISO and Spitzer (Berta et al. 2010, 2011).

With PACS-PEP we now have available rest-frame FIR luminosities, IR SEDs and star formation rates unaffected by extinction, not only the most luminous objects, but also many of the “main sequence” galaxies out to redshifts of $z \sim 2$. One basic finding is that the bulk of the star formation at the peak of the cosmic star formation activity has occurred in a more continuous mode, albeit at higher rates in earlier epochs, related to also an increase in the reservoir of available molecular gas, rather than in starbursts and mergers (2.3).

A fraction of the population of star forming galaxies in the survey also hosts active galactic nuclei (AGN), which allowed us to study signatures of co-evolution, focusing on the two aspects of black hole feeding and AGN feedback on star formation (2.5.2). The key papers are Elbaz et al. 2010, Nordon et al. 2010, 2012, Rodighiero et al. 2010, 2011, Magnelli et al. 2010, 2012, Shao et al. 2010, Santini et al. 2012, Rosario et al. 2012.

Science results: The [C II] line deficit revisited. One of the somewhat puzzling results from the ISO LWS spectroscopy program on ultra-luminous infrared galaxies (ULIRG) had been an apparent “deficit” in the relative brightness of the 158 μm [C II] line, which was assumed to be one of the best tracers of star formation activity and, thus, was expected to be bright in these objects. We have now studied many atomic and ionic FIR fine structure lines in a large sample of galaxies in the local and high- z Universe, leading to a much clearer picture (Fig. IR.26). We find that the relative brightness of the fine structure lines shows a much stronger correlation with the ratio $L_{\text{FIR}}/M_{\text{mol}}$ between the FIR luminosity and the molecular gas mass – the material, from which stars are formed – than with the absolute luminosity, L_{FIR} , itself. Systems with intense star formation tend to have weaker lines relative to their FIR continuum than less actively star-forming galaxies. These line deficits are found, both, in local galaxies and in the high- z Universe, and are probably a consequence of their more intense interstellar radiation fields (Gracia Carpio et al. 2011, 2013).

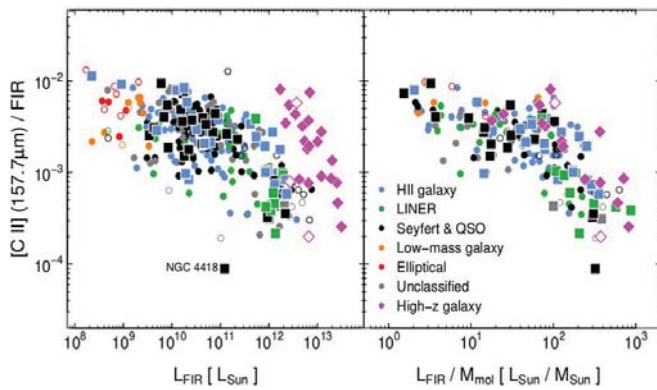


Fig. IR.26: The global [C II] line to FIR continuum ratio in different types of galaxies. While there is some trend with the total luminosity L_{FIR} (left panel), there is a significantly tighter correlation with the ratio $L_{\text{FIR}}/M_{\text{mol}}$ (right panel), indicating that the local physical conditions in the ISM determine the relative line brightness, rather than absolute luminosity (Gracia Carpio et al. 2011, 2013)

The $L_{\text{FIR}}/M_{\text{mol}}$ value, where the line deficit sets in, is similar to the limit that sets apart the two modes of star formation recently found in galaxies on the basis of studies of their gas-to-star formation relation (“main sequence”). By resolving the spatial emission in local galaxies, we have been able to extend our analysis to kiloparsec and sub-kiloparsec scales. We find low line to continuum ratios in regions with high FIR surface brightness and warm dust temperatures. However, only the most compact and obscured regions in some local HII galaxies

present line deficits as strong as those found globally in ULIRGs, which highlights the extreme and episodic nature of these systems.

Science results: Galactic outflows. Winds, driven, e.g., by stars and supernovae, or by AGN, may play an important role in the overall balance of the reservoir of gas available for star formation in galaxies. With PACS spectroscopy we have access to virtually extinction-free tracers of all components of the interstellar medium – molecular, neutral atomic, and ionized – and can thus contribute to a more complete picture of these phenomena. One of the key results of our guaranteed time program “SHINING” is the direct evidence for AGN-driven, molecular outflows in a sample of local ULIRGs, observed in several FIR lines of the hydroxyl molecule, OH, which is a good tracer of the warm and dense gas predominantly abundant in the nuclear regions. The amount of molecular gas in the outflow and its velocity imply that this outflow – if sustained – would void the central part of the galaxy of its gas reservoir much faster than the gas can be converted into stars, given the present, observed star formation rate. In other words, it provides a mechanism for the long sought-after, strong, QSO-mode feedback onto the host galaxy required by galaxy evolution models (2.5.1, Fischer et al. 2010, Sturm et al. 2011).

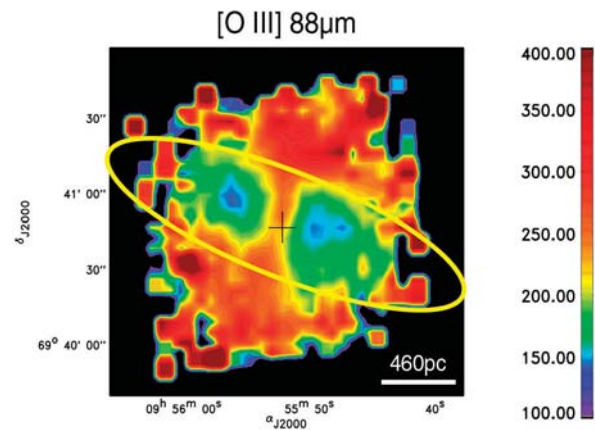


Fig. IR.27: Velocity dispersion map of the [O III] 88 μm line in the starburst galaxy M82, where we have studied the starburst-driven winds in the ionized as well as in the neutral atomic medium (Contursi et al. 2013).

Our maps of the starburst galaxy M82 in the strongest fine structure lines within the PACS wavelength range ([O I] at 63 μm and 145 μm , [C II] at 158 μm , and [O III] at 88 μm) provide – for the first time – the spatial and spectral resolution to separate disk and outflow components (Fig. IR.27). We find that the FIR lines are spatially and kinematically linked to the molecular outflow, rather than the ionized component traced by H α , and suggest that the bulk of the material in the outflow must be in the form of clumps or cloudlets, where the [O III] line traces gas surrounding the PDR layer, observed in the [C II] and [O I] lines, on the surface of the molecular clump. The derived mass loading factor, $\dot{M}_{\text{outflow}}/\text{SFR}$, of the combined molecular and neutral atomic gas in the outflow is ~ 2 , much less than what we find for the AGNs.



Fig. IR.28: This three-color image of the W3 giant molecular cloud combines PACS bands at $70\mu\text{m}$ (blue) and $160\mu\text{m}$ (green) with the $250\mu\text{m}$ SPIRE band (red). The image spans about 2×2 degrees. W3 hosts low- and high-mass star formation. In this image, the low-mass protostars are seen as tiny yellow dots embedded in cool red filaments, like pearls on a string, while the highest-mass stars ($M > 8M_{\odot}$) emit intense radiation, heating up the gas and dust around them and showing up in blue (taken from Rivera-Ingraham et al. 2013, http://www.nasa.gov/mission_pages/herschel/news/herschel20130328.html).

Science results: Filamentary cloud structure and star formation. The spatial resolution of Herschel allowed for the first time, to map in great detail and with high angular resolution, clumps and filamentary dust structures in star forming molecular clouds. The broad spectral coverage of PACS in addition allows disentangling dust temperature and column density (Fig. IR.28). The clump mass function (CMF) strongly resembles the Initial Mass Function (IMF) of stars forming from them. The overall star formation efficiency is 20-25%, suggesting that the IMF is already preset during the cloud fragmentation phase. The clumps or cores form within tubular structures or filaments, which seem to be characterized by a narrow distribution of widths with a median value of 0.10pc . This characteristic scale is similar in gravitationally bound and unbound structures, and corresponds to within a

factor of ~ 2 to the sonic scale below which interstellar turbulence becomes subsonic in diffuse gas. This finding supports the argument that the filaments form primarily as a result of the dissipation of large-scale turbulence, rather than by gravity or magnetic fields (André et al. 2010, Molinari et al. 2010, Men'shchikov et al. 2010, Miville-Deschenes et al. 2010, Könyves et al. 2010, Arzoumanian et al. 2011, Hill et al. 2011).

Science results: The role of water in star formation. Water is one of the most important molecules in interstellar space. It is a unique diagnostic of warm gas and energetic processes taking place during star formation, and plays an active role in the gas cooling. In cold regions, water ice may help the coagulation process that ultimately produces planets. As part of the "Water in

Star-forming regions with Herschel (WISH) key program (PI: E. van Dishoeck), water and related molecules have been observed in about 80 sources covering a wide range of masses and luminosities – from the lowest to the highest mass protostars – and a large range of evolutionary stages – from the first stages represented by the pre-stellar cores to the last stages represented by the by the pre-main sequence stars surrounded only by their protostellar disks (Fig. IR.29). The full story is given in van Dishoeck et al. 2011, Kristensen et al. 2010, Nisini et al. 2010, Hogherheijde et al. 2011, Bruderer et al. 2010, Chavarria et al. 2010)

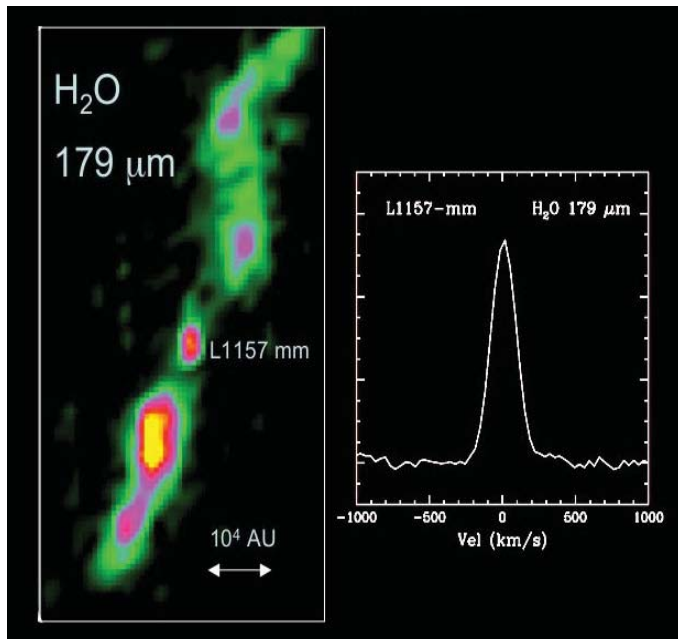


Fig. IR.29: PACS image of water toward the young solar analog L 1157, lighting up the outflow of gas (Nisini et al. 2010).



Albrecht Poglitsch is a W2 Senior Scientist at MPE. Since 1997 he has been the Principal Investigator for the PACS instrument onboard of ESA's Herschel mission. He has a longstanding track record in developing state of the art cryogenic spectrometers for the far-infrared wavelength region. PACS combines broadband photometric imaging with bolometers, with the world's first far-infrared integral field spectrometers with Ge:Ga photoconductors, together based on 4 large, very sensitive array detectors.

(Other MPE PACS team members include: Lothar Barl, Stefano Berta, Alessandra Contursi, Jeroen DeJong, Vanessa Doublier Pritchard, Helmut Feuchtgruber, Reinhard Genzel, Dieter Lutz, Thomas Müller, Paola Popesso, Eckhard Sturm, Ekkehard Wieprecht, Erich Wiezorrek)

Selected References:

- André, Ph.; Men'shchikov, A.; Bontemps, S.; Könyves, V.; Motte, F.; et al. 2010, *A&A*, 518, L102
 Arzoumanian, D.; André, Ph.; Didelon, P.; Könyves, V.; Schneider, N.; et al 2011, *A&A* 529, L6
 Berta, S.; Magnelli, B.; Lutz, D.; Altieri, B.; Aussel, H.; 2010 *A&A* 518, L30
 Berta, S.; Magnelli, B.; Nordon, R.; Lutz, D.; Wuyts, S.; et al. 2011 *A&A* 532, A49
 Bruderer, S.; Benz, A. O.; van Dishoeck, E. F.; Melchior, M.; Doty, S. D.; et al. 2010 *A&A* 521, L44
 Chavarria, L.; Herpin, F.; Jacq, T.; Braine, J.; Bontemps, S.; et al. 2010 *A&A* 521, L37
 Contursi, A.; Poglitsch, A.; Gracia Carpio, J.; Veilleux, S.; Sturm, E.; et al. 2013, *A&A*, 549, A118
 Elbaz, D.; Hwang, H. S.; Magnelli, B.; Daddi, E.; Aussel, H.; et al. 2010 *A&A* 518, L29
 Elbaz, D.; Dickinson, M.; Hwang, H. S.; Díaz-Santos, T.; Magdis, G.; et al. 2011, *A&A*, 533, A119
 Fischer, J.; Sturm, E.; González-Alfonso, E.; Graciá-Carpio, J.; Hailey-Dunsheath, S.; et al. 2010, *A&A* 518, L41
 Graciá-Carpio, J.; Sturm, E.; Hailey-Dunsheath, S.; Fischer, J.; Contursi, A.; et al. 2011, *ApJ* 728, L7
 Hill, T.; Motte, F.; Didelon, P.; Bontemps, S.; Minier, V.; et al. 2011 *A&A* 533, A94
 Hogerheijde, M.R.; Bergin, E.A.; Brinch, C.; Cleeves, L.I.; Fogel, J.K.J.; et al. 2011 *Science* 334, 338
 Könyves, V.; André, Ph.; Men'shchikov, A.; Schneider, N.; Arzoumanian, D.; et al. 2010 *A&A*, 518, L106
 Kristensen, L. E.; Visser, R.; van Dishoeck, E. F.; Yildiz, U. A.; Doty, S. D.; et al. 2010 *A&A* 521, L30
 Lutz, D.; Poglitsch, A.; Altieri, B.; Andreani, P.; Aussel, H.; et al. 2011 *A&A* 532, A90
 Magnelli, B.; Lutz, D.; Berta, S.; Altieri, B.; Andreani, P.; et al. 2010 *A&A* 518, L28
 Magnelli, B.; Lutz, D.; Santini, P.; Saintonge, A.; Berta, S.; et al. 2012 *A&A* 539, A155
 Men'shchikov, A.; André, Ph.; Didelon, P.; Könyves, V.; Schneider, N.; et al. 2010 *A&A* 518, L103

2.5. Massive Black Holes and Black Hole–Galaxy Co-Evolution

2.5.1. Feeding and Feedback in Nearby Active Galactic Nuclei

During the last decade evidence has accumulated that accreting MBHs (=Active Galactic Nuclei (AGN)) play an important role in the evolution of galaxies. Throughout cosmic history, AGN and their host galaxies have grown together and probably influenced each other, via common gas accretion and feedback mechanisms. In order to understand the key physical processes that couple the growth of MBHs to their host galaxies we are pursuing an extensive program to observe local template galaxies from the near-IR to the mm range. A recent breakthrough came from PACS @ Herschel. We find unambiguous evidence for massive molecular outflows in OH molecular transitions, in the PACS spectra of 30 AGN dominated, ultra-luminous infrared galaxies (ULIRGs). These outflows may represent evidence for strong ‘QSO mode’ feedback onto the host galaxy, as predicted by galaxy evolution models.

As discussed in section 2.3, galaxy evolution models predict, and observations find, that the co-evolution of galaxies and AGN must depend on feedback processes linking accretion and ejection. In these models, galaxies and their black holes grew rapidly at early times because of the large gas accretion rates from the cosmic web. As the SMBH grows the AGN luminosity sometimes reaches the Eddington limit (QSO phase) and may drive winds that potentially could expel much of the gas in the host galaxy. This “QSO mode” feedback is thought to self-regulate both star formation in the host galaxy and black hole fuelling, in the process setting up the black hole-galaxy mass relation observed in local galaxies. While there is much evidence for a jet-driven ‘radio feedback’ from MBHs in the most massive cluster ellipticals, direct observational evidence for the ‘QSO mode’ has been more anecdotal. Outflows have been observed in starbursts and QSOs, but mostly in the ionized and neutral atomic gas components, and with poorly known rates. To inhibit star formation in the host galaxy, outflows have to affect the molecular gas out of which stars form.

Powerful molecular outflows in AGN-dominated ULIRGs. As part of our Herschel Guaranteed Time Key Project SHINING we have detected P-Cygni profiles in the OH spectra of ~ 30 ULIRGs, with blue shifted absorption and red shifted emission, unambiguous evidence for molecular outflows. In some of these objects the (terminal) outflow velocities exceed 1000 km/s, and their outflow rates (up to $\sim 1200 M_{\odot}/\text{yr}$) are several times larger than their star formation rates (Fig. IR.30). We compare the outflow signatures in different types of ULIRGs and in starburst galaxies to address the issue of the energy source (AGN or starburst) of these outflows. ULIRGs with a higher AGN luminosity (and higher AGN contribution to L_{IR}) have higher terminal velocities and shorter gas depletion timescales, i.e. these outflows may be AGN-driven. The outflows in the observed ULIRGs are able to expel the cold

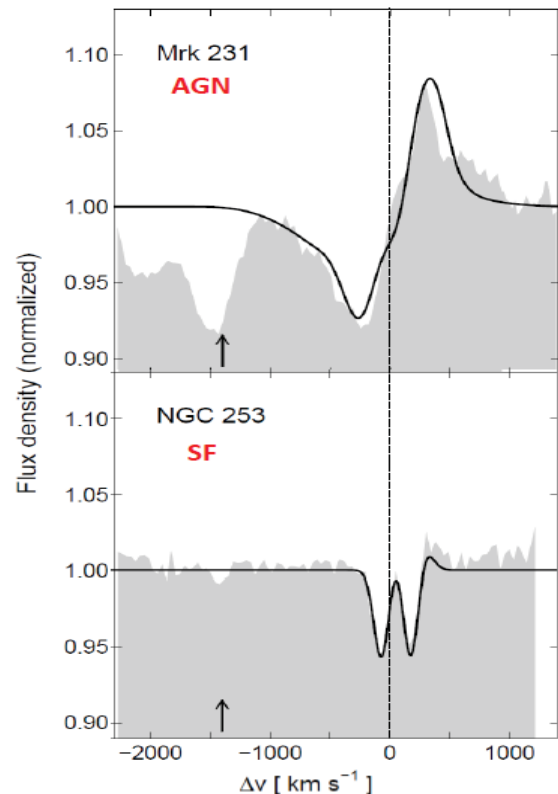


Fig. IR.30: Profiles of the $79\mu\text{m } 2\pi_{1,2} J=1/2 - 2\pi_{3,2} J=3/2$ transition of OH toward the ultraluminous infrared galaxy/QSO Mrk231 (top, Fischer et al. 2010), and the starburst galaxy NGC253 (bottom), along with best fit outflows model (black line). The arrows denote the position of an H_2O line that also shows a P-Cygni profile with blue wings to $\sim 1000 \text{ km/s}$, as in the case of OH.

gas reservoirs from the centers of these objects within $\sim 10^6$ – 10^8 years (Fischer et al. 2010, Sturm et al. 2011). Our modeling of the OH spectra using radiative transfer models and an outflowing shell-like geometry yields a mass outflow rates ranging between 10^2 to $10^3 M_{\odot}/\text{yr}$, up to 10 times the star formation rate. We have detected the same molecular outflow in CO(1-0) with the PdBI@IRAM interferometer, independently supporting our OH outflow modeling. We are now pursuing an extensive follow-up program with Herschel, PdBI and ALMA, expanding the sample to PG QSOs and lower luminosity AGN at various evolutionary stages, confirming the correlation of outflow strength with AGN luminosity, and spatially resolving the outflow geometries

Highly excited molecular line emission from the nucleus of NGC1068. Another aspect of AGN – the direct detection of the torus emission in NGC1068 via high excitation CO lines – was an obvious, and highly anticipated, goal of PACS. This was achieved (Fig. IR.31), although not in the way foreseen.

The detection of 11 CO lines from upper levels as high as $J=30$ enabled us to show that there were 3 distinct contributions to the CO spectral line energy distribution. The coolest component is known to be dominated by the circum-nuclear ring which has a 1kpc radius. In contrast, the medium and high excitation components, at 170K and 570K respectively, arise from the central few hundred parsecs of NGC1068. The excited CO emission may come from dense photo-dissociation regions, X-ray dominated regions, or shocks, or a combination thereof. The energetics suggests that the highest excitation component is most likely heated by X-rays from the AGN. Taking this further, we combined the spectral diagnostic power of PACS with spatially resolved kinematics of SINFONI. Matching the spectrally distinct CO components to the near infrared H_2 line emission from spatially distinct locations, we showed that the medium excitation emission arises primarily from the bright massive molecular region about 70pc east of the AGN, while the highest excitation component only matches the tongue of H_2 that lies just 20pc north of the AGN – and, based on a detailed analysis of the SINFONI kinematics, is believed to be falling almost directly towards it (Müller Sanchez et al. 2009, Hailey-Dunsheath et al. 2012). There is no direct evidence, however, for a separate component associated with a few parsec dense molecular torus.

What triggers AGN activity? Modeling the gas inflow mechanisms towards AGN, including the impact of star formation, and also the spatially resolved AGN-driven outflows, has been a focus of our SINFONI observations.

Our AO data-sets reach spatial resolutions as small as a few parsecs. One of the highlights of this work has been to show that nuclear starbursts on scales of tens of parsecs may play a decisive role in initially moderating, and then assisting, gas inflow. There appears to be a delay of order 100 Myr between the onset of star formation on these scales and the more active phase of accretion onto the central black hole (Davies et al. 2007). This conclusion has been further corroborated by other observations, as well as 3D hydrodynamical simulations. In essence, the turbulent early phases of a short starburst (OB winds and type II supernovae) tend to drive gas outward, while in the later more quiescent phases, outflows from AGB stars are able to accrete to smaller scales – at least to the limit allowed by their residual angular momentum (Schartmann et al. 2008, 2009). In planned future work, we want to place this ‘limit-cycle’ concept on a more robust statistical footing by targeting a complete sample of nearby AGN selected from the Swift-BAT 14-195 keV catalogue (which is widely thought to be the least biased with respect to host galaxy properties), complemented by a matched sample of inactive galaxies. Because the luminosity range in our nearby template samples overlaps that of AGN at higher redshift, and because there is increasing observational and theoretical evidence that disk processes remain important in driving gas inwards at higher redshift, what we learn from our sample of local AGN can be applied directly to AGN at $z > 1$ where co-evolution largely occurs but where small scales cannot be spatially resolved.

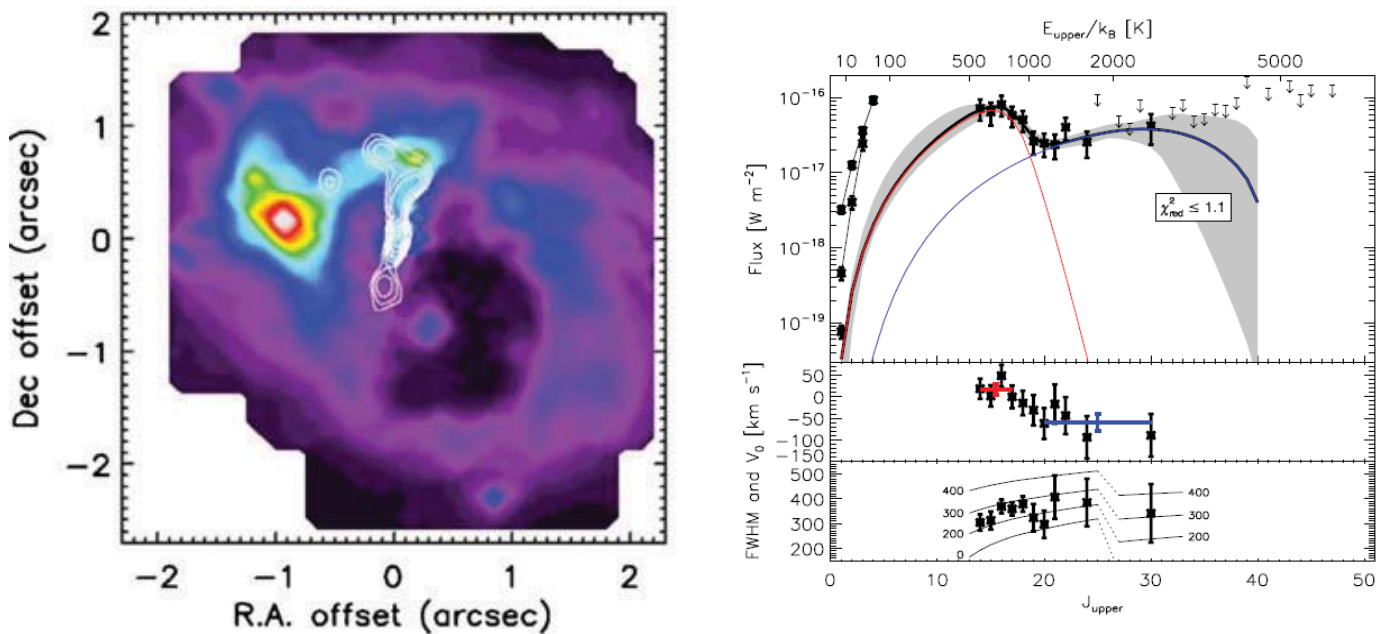


Fig. IR.31: High excitation molecular gas in the nucleus of the Seyfert 2 galaxy NGC 1068. Left: H_2 1-0 S(1) (color) SINFONI image of the central $4'' \times 6''$, showing the circum-nuclear disk/ring in NGC1068 (Müller Sánchez et al. 2009), as well as in white contours the $12\mu m$ hot dust emission from the narrow-line region/jet region. H_2 emission associated with the latter structure delineates two streamers of molecular gas falling from the ring inwards toward the nucleus (red cross) from the north and south. Right: The CO line spectral energy distribution (SED) as measured with PACS, identifying two separate emission components, a medium and a high excitation component (ME (red) and HE (light blue)). Comparison of the velocity and line width of the high excitation CO emission suggests that the ME emission originates in the ring east of the nucleus, while the HE emission comes from the northern narrow-line region/ infalling H_2 streamer (adapted from Müller Sanchez et al. 2009, Hailey-Dunsheath et al. 2012).

Dense molecular gas in AGN. An immediate question that arises is, given the abundance of molecular gas, why these nuclear post-starbursts are not now forming stars. This is best addressed using the millimeter emission of molecular lines such as HCN. The spatial resolution of the IRAM PdBI is just sufficient to spatially resolve the central region of interest, providing crucial dynamical information (Sani et al. 2012). Our initial exploration of the molecular properties suggests that the dense gas lies in disks that are intrinsically turbulent and so have a significant scale height; and that filaments of hot molecular gas (traced by the near infrared 1-0S(1) line) are blown or scattered to even greater distances above the galaxy plane (Hicks et al. 2009). There is tantalizing evidence that the molecular clouds in these disks may not be self-gravitating but are instead pressure confined. Probing the physical properties of the innermost regions of galaxies in this way is fundamental to our understanding of the processes that lead to gas inflow and ultimately accretion onto AGN, and this area is ripe for studies in the near future with both the NOEMA upgrade to PdBI as well as ALMA.

Selected References:

- Davies, R.; Müller Sánchez, F.; Genzel, R.; Tacconi, L. J.; Hicks, E. K. S.; et al. 2007, *ApJ*, 671, 1388
 Feruglio, C.; Fiore, F.; Maiolino, R.; Piconcelli, E.; Ausser, H.; Elbaz, D.; et al. 2013, *A&A*, 549, A51
 Fischer, J.; Sturm, E.; González-Alfonso, E.; Graciá-Carpio, J.; Hailey-Dunsheath, S.; et al. 2010, *A&A*, 518, L41
 González-Alfonso, E.; Fischer, J.; Graciá-Carpio, J.; Sturm, E.; Hailey-Dunsheath, S.; et al. 2012, *A&A*, 541, A4
 Gracia-Carpio, J.; Sturm, E.; Hailey-Dunsheath, S.; Fischer, J.; Contursi, A.; Poglitsch, A.; et al. 2011, *ApJ*, 728, L7
 Hailey-Dunsheath, S.; Sturm, E.; Fischer, J.; Sternberg, A.; Graciá-Carpio, J.; et al. 2012, *ApJ*, 755, 57
 Hicks, E.; Davies, R. I.; Malkan, M. A.; Genzel, R.; Tacconi, L.J.; et al. 2009, *ApJ*, 696, 448
 Müller Sanchez, F.; Davies, R. I.; Genzel, R.; Tacconi, L.J.; Eisenhauer, F.; et al. 2009, *ApJ*, 691, 749
 Sani, E.; Davies, R. I.; Sternberg, A.; Graciá-Carpio, J.; Hicks, E. K. S.; et al. 2012, *MNRAS*, 424, 1963
 Sturm, E.; González-Alfonso, E.; Veilleux, S.; Fischer, J.; Graciá-Carpio, J.; et al. 2011, *ApJ*, 733, L16



Ric Davies



Eckhard Sturm

(Other MPE team members include Leonard Burtscher, Alessandra Contursi, Reinhard Genzel, Javier Gracia-Carpio, Steve Hailey-Dunsheath, Erin Hicks, Annemieke Janssen, Dieter Lutz, Francisco Müller Sanchez, Gilles Orban de Xivry, Albrecht Poglitsch, Linda Tacconi)

2.5.2 Herschel Studies of the Co-Evolution of Galaxies and Black Holes: Secular Processes Dominate over Merging

In our PACS Evolutionary Probe (PEP) guaranteed time key program we have studied the relationship between star formation and AGN activity in galaxies across cosmic time. Exploiting the fact that far-infrared continuum emission traces star formation, and is little affected by AGN activity, we have traced star formation in the hosts of AGN over a wide range of luminosities and accretion regimes. We find a strong correlation between concurrent host star formation and AGN activity limited to the most luminous AGN at $z < 1$. Most high- z AGN are instead located in steadily evolving hosts with star formation similar to ‘main sequence’ star forming galaxies.

AGN are fuelled by the accretion of gas from their environs onto MBHs in the nuclei of their host galaxies. They can be powerful sources of radiative, mechanical and thermal energy, and are capable of returning a substantial fraction of this energy to galaxy scales, which may regulate the formation of stars in their hosts. Indeed, AGN “feedback” is now an essential element of most successful simulations of galaxy evolution. In addition, mechanisms that regulate the supply of gas on large spatial scales could be indirectly linked to the feeding of the AGN that occurs on very small scales. Current AGN co-evolutionary models include elements of black hole feeding and feedback when describing the star formation rates and transformations of galaxies over time. These come in various flavors, but may be categorized as those that link AGN activity to short perturbations of the host galaxy, for example through galaxy mergers, or those which employ more continuous or “secular” processes to bring gas from large radii to the nucleus.

At redshifts $z > 1$ and among massive galaxies, in situ star formation (SF) accounts for most of the stellar growth. In addition to the well-defined scaling relations between MBH masses and the masses of spheroids in local galaxies, the correspondence between the cosmic star formation rate (SFR) density and the accretion density to these redshifts, suggests a close connection between SF and MBH growth operating over much of cosmic history. The connection may be “direct” or “synchronized”, in which case AGN episodes maintain a fairly close temporal relationship with respect to SF, such that luminous AGN activity is always associated with strong SF, modulo a lead or lag time (Fig. IR.32 right). Another relationship, somewhat less appreciated, exists even without a direct link between AGN and SF. Even if SF and AGN activity proceed stochastically in a galaxy, they still both depend on the same supply of gas. Integrated over time, MBHs grow faster in galaxies with higher levels of SF because they also have more cold gas that can fuel more AGN phases.

Since the launch of the Herschel Space Observatory in May 2009, our PEP survey has collected deep far-infrared (FIR) maps in several key extragalactic fields, with deep and well-characterized multi-wavelength data obtained by collaborating teams. Compared to other star formation tracers in the UV to mid-IR, which are easily contaminated by the AGN, the FIR has the best host to AGN contrast, and is best suited to study the star formation of AGN hosts. Having established and tested the performance of the FIR as a star-formation tracer in

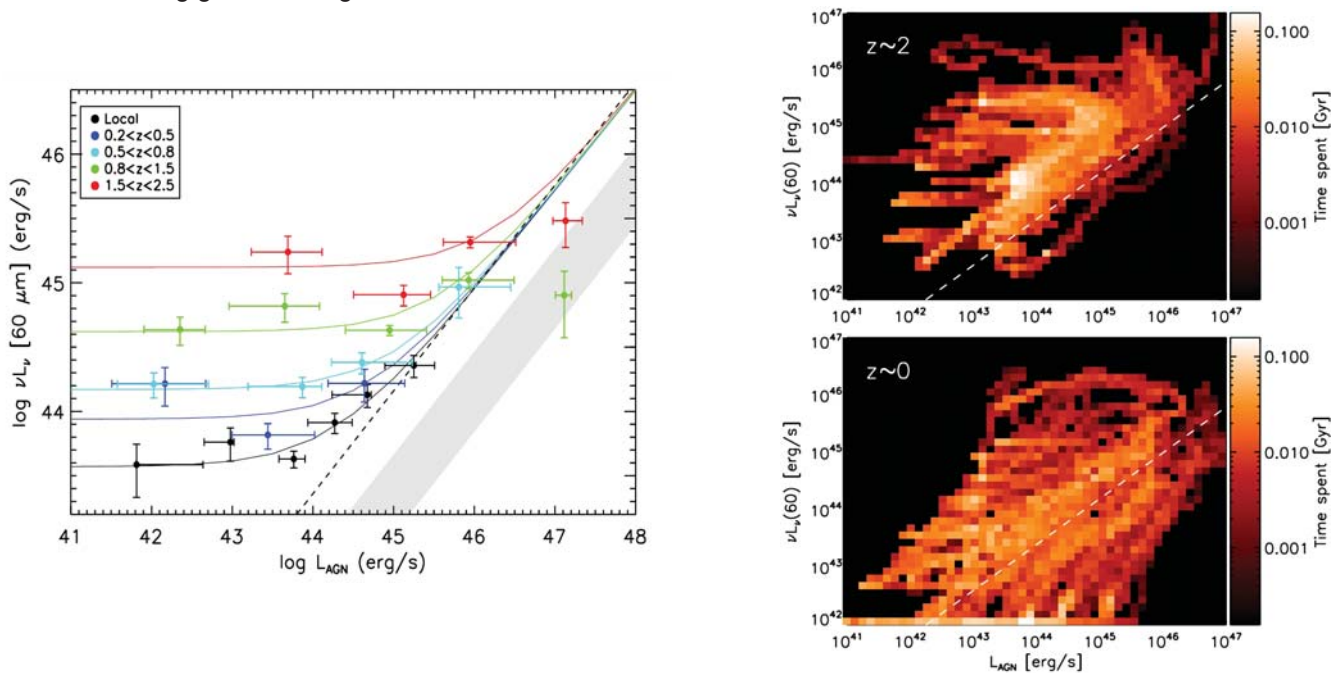


Fig. IR.32: (Left) Mean rest-frame $60 \mu\text{m}$ luminosity (L_{60}) of X-ray selected AGN as a function of AGN bolometric luminosity and redshift. The local points come from IRAS measurements of Swift/BAT AGN, while all other points are derived from stacking Herschel/PACS maps. At $z < 1$, luminous AGN show a consistent correlation between L_{60} and L_{AGN} . This correlation appears to weaken or disappear at $z > 1$. (Right): Predictions of the correlation from a suite of hydrodynamic major merger simulations. The dashed lines are the same as that plotted in the left panel (Rosario et al. 2012).

AGN, we have undertaken a series of studies exploring the relationship between SF and AGN luminosity, AGN obscuration and MBH properties, as well as placing the SF properties of AGN host galaxies in the context of the overall field galaxy population. These studies rely on some of the most developed AGN samples in the PEP fields, based on X-ray, IR and optical selections.

Starting with the very first Herschel Science Demonstration Phase data and later expanding both sample size and depth by including both GOODS fields and the COSMOS field, we put forward a heuristic framework to explain measurements of the mean SFR (traced by the rest-frame $60\mu\text{m}$ luminosity L_{60}) as a function of redshift and AGN luminosity L_{AGN} . In this picture (Fig. IR.32 left), two regimes were identified where different L_{60} - L_{AGN} relationships appear to hold. For $z < 1$ and low L_{AGN} , SFR is uncorrelated with AGN luminosity,

but at high L_{AGN} , a positive correlation is seen, with a slope consistent with that demonstrated by major merger models. At high redshifts ($z > 1$), the correlation with SFR seen among luminous AGN seems to weaken or disappear, and essentially all X-ray AGN, across five orders of magnitude in nuclear luminosity, exhibit comparable mean SFRs. In parallel with inactive galaxies, the mean SFRs of AGN hosts are much higher at $z \sim 2$ than locally. This behavior may be plausibly interpreted through the following scenario. At all redshifts, secular fuelling of the SMBH dominates among low luminosity AGN and erases any direct link between the nuclear accretion event and global SF. At $z < 1$, the most luminous phases of nuclear activity can only be sustained in disruptive events such as major mergers, which simultaneously inspire strong starbursts and drive the correlation we observe. However, at $z > 1$, the highly turbulent nature of SF gas disks can also sustain luminous AGN by secular fuelling without much impact on global star formation, since gas inflow rates to the nucleus are expected to be much higher, through various possible mechanisms such as inward migration of gas clumps but possibly also including minor mergers. These findings agree with current morphological studies, which do not find a significant excess of mergers among high- z AGN hosts, compared to matched non-AGN samples.

Another handle on the SF properties of AGN hosts is through a comparison to the Main Sequence of star forming galaxies. Starburst galaxies are defined to be the few objects that lie well above this relation. After estimating the stellar masses of AGN hosts while accounting for optical and near-IR light from the nucleus, we have compared the average star formation of AGN hosts and stellar mass-matched inactive galaxies to $z = 2.5$. We find a clear star formation enhancement for the most luminous AGNs, in line with the results described above. In addition, we also find a small but consistent enhancement in the mean SFRs of the hosts of lower luminosity AGN. This enhancement could be either due to a larger proportion of intense starbursts, or due to a larger fraction of normal star forming galaxies compared to quiescent galaxies, among AGN hosts. Our preference for the latter interpretation is strongly confirmed by analysis of the deepest PACS survey which combines all data for the GOODS fields, resolving a major fraction of the AGN population into individually detected FIR sources. We find that, while star-forming AGN hosts are drawn at random from the massive end of the Main Sequence, they are also, at all redshifts and consistently in both GOODS fields, much more likely to be in a SF galaxy than similarly massive inactive galaxies (Fig. IR.33). Our statistics are compatible with the notion that all low and mod-

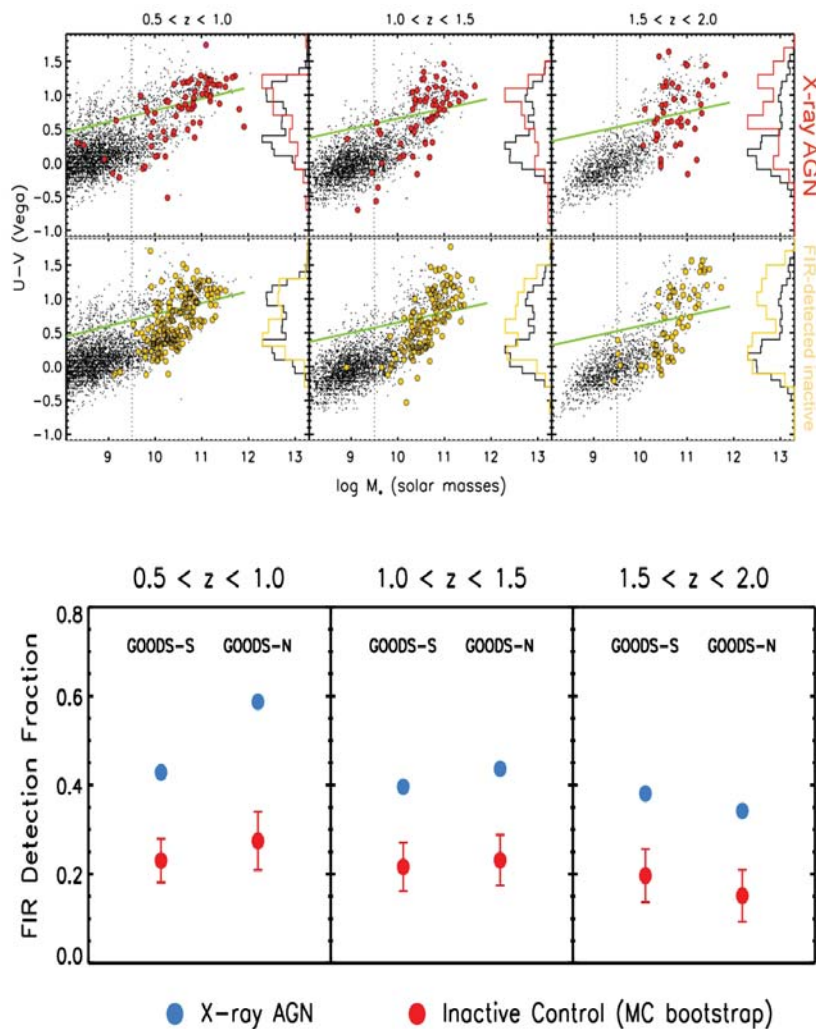


Fig. IR.33: Top: Color magnitude diagrams of X-ray AGN (top) and PACS detected (i.e., dusty star-forming) inactive galaxies (bottom) compared to that of the field galaxy population (small black points) in the GOODS-S field. Both sets of objects occupy similar parts of the diagram and there is no preference for AGN hosts to lie in the “Green Valley” (marked by the green line in all panels, Rosario et al. 2013). Bottom: FIR detection rates for X-ray selected AGN (blue points) in the two GOODS fields, compared to a stellar mass-matched control sample of inactive galaxies (red points). The errors on the latter are derived from a Monte-Carlo bootstrap resampling into the complete inactive galaxy population. AGN are about twice more likely to be FIR detected than similarly massive non-AGN (Rosario et al. 2013).

erate luminosity X-ray selected AGN are in star forming galaxies, if one corrects for the incompleteness of the FIR survey. These observations give credence to a scenario where the common supply of cold gas is what ultimately mediates a connection between nuclear activity and SF in galaxies. It also weakens a long-standing claim that AGN are typically associated with galaxies in which star formation has already been largely quenched (Fig. IR.33).

Since the majority of the growth in the black hole mass density comes from AGN around the knee of the bolometric luminosity function, the host properties of low and moderate luminosity AGN may not be particularly important for setting MBH scaling laws. A detailed exploration of the SF properties of more luminous AGN can reveal the critical processes at play in these systems. The best understood population of luminous AGN are QSOs, in which the central nuclear source is unobscured along the line of sight, yielding information on the accretion rate and mass of the black hole. We have compiled a complete sample of spectroscopic QSOs in the COSMOS field with uniformly estimated properties.

Studying their mean SF properties in detail, we do not find evidence that the fastest growing SMBHs are associated with massive starbursts, despite predictions from merger models. Direct co-evolution may only occur in heavily obscured systems which are not accessible through traditional X-ray or optical selection methods. We have probed some of this parameter space in X-ray AGN: we find no systematic variation in SFR over 4 orders of magnitude in X-ray obscuration. We are currently expanding into studies of luminous obscured AGN, selected through mid-IR or emission-line based methods. The link between star-formation and AGN activity is a test of the relevant physics that governs the co-evolution of black holes and galaxies. Through an extensive study of the SF properties of AGN across a wide range of host and accretion properties, we have revealed the importance and defined the scope of secular and stochastic processes in black hole growth across most of cosmic time (Shao et al. 2010, Santini et al. 2012, Rosario et al. 2012, 2013)



David Rosario



Dieter Lutz

(Other MPE team members include Stefano Berta, Marcella Brusa, Natascha Förster Schreiber, Reinhard Genzel, Benjamin Magnelli, Raanan Nordon, Albrecht Poglitsch, Paola Popesso, Amelie Saintonge, Mara Salvato, Li Shao, Eckhard Sturm, Linda Tacconi, Stijn Wuyts)

Selected References:

- Lutz, D.; Sturm, E.; Tacconi, L. J.; Valiante, E.; Schweitzer, M., et al. 2008 *ApJ* 684, 853
 Lutz, D.; Mainieri, V.; Rafferty, D.; Shao, L.; Hasinger, G., et al. 2010 *ApJ* 712, 1287
 Shao, L.; Lutz, D.; Nordon, R.; Maiolino, R.; Alexander, D. M., et al. 2010 *A&A* 518, L26
 Santini, P.; Rosario, D. J.; Shao, L.; Lutz, D.; Maiolino, R., et al. 2012 *A&A* 540, A109
 Rosario, D. J.; Santini, P.; Lutz, D.; Shao, L.; Maiolino, R., et al. 2012 *A&A* 545, A45
 Rosario, D. J.; Santini, P.; Lutz, D.; Netzer, H.; Bauer, F. E., et al. 2013 *ApJ in press* (arXiv 1302.1202)

2.6 Star and Planet Formation

Within our own Galaxy, many of the same IR/submm instruments (Herschel, Spitzer, VLT, PdBI, ALMA) have opened up new avenues in the study of the dense interstellar medium in star- and planet-forming regions (133 refereed papers with MPE involvement). Highlights include quantifying star formation rates and efficiencies in nearby clouds as function of gas density, elucidating the physical processes by which young stars impact their surroundings ('feedback'), following the trail of water and complex organic molecules from collapsing cores to protoplanetary disks, and characterizing a new class of transitional disks that are likely actively forming planets.

Feedback from protostars: Water and the CO ladder. Young protostars interact violently with their parent clouds. As the protostar grows in mass, it heats the collapsing envelope and simultaneously spews out jets of gas which plow into the surrounding dark cloud. At the same time, UV radiation can escape through the outflow cavities and dissociate and heat the gas. PACS provides unique diagnostic tools to probe and image these

highly energetic processes in regions close to the protostar that cannot be seen at visible wavelengths. The water molecule is a particularly sensitive probe of where a young star dumps energy into its surroundings. Its signatures are strongly detected and imaged by PACS along the two-sided outflow lobes. An illustrative example is provided in Fig. IR.29 (section 2.4), the low-mass protostar L1157, an analog of the young Sun. The water emission shows up most strongly in "hot spots" due to strong shocks symmetrically displaced from the young star.

A survey of ~ 20 low mass protostars with PACS has revealed very rich far-infrared spectra, which provide a direct measurement of the gas cooling budget. A spectacular example is provided by the low-mass protostar NGC 1333 IRAS4B (Fig. IR.34). The total far-infrared cooling is dominated by H_2O and CO, with the [O I] contribution increasing with protostellar evolution. Many lines of CO are detected in all sources, up to very high levels ($J=49-48$, $E_{\text{up}}=6724$ K). Interestingly, two distinct compo-

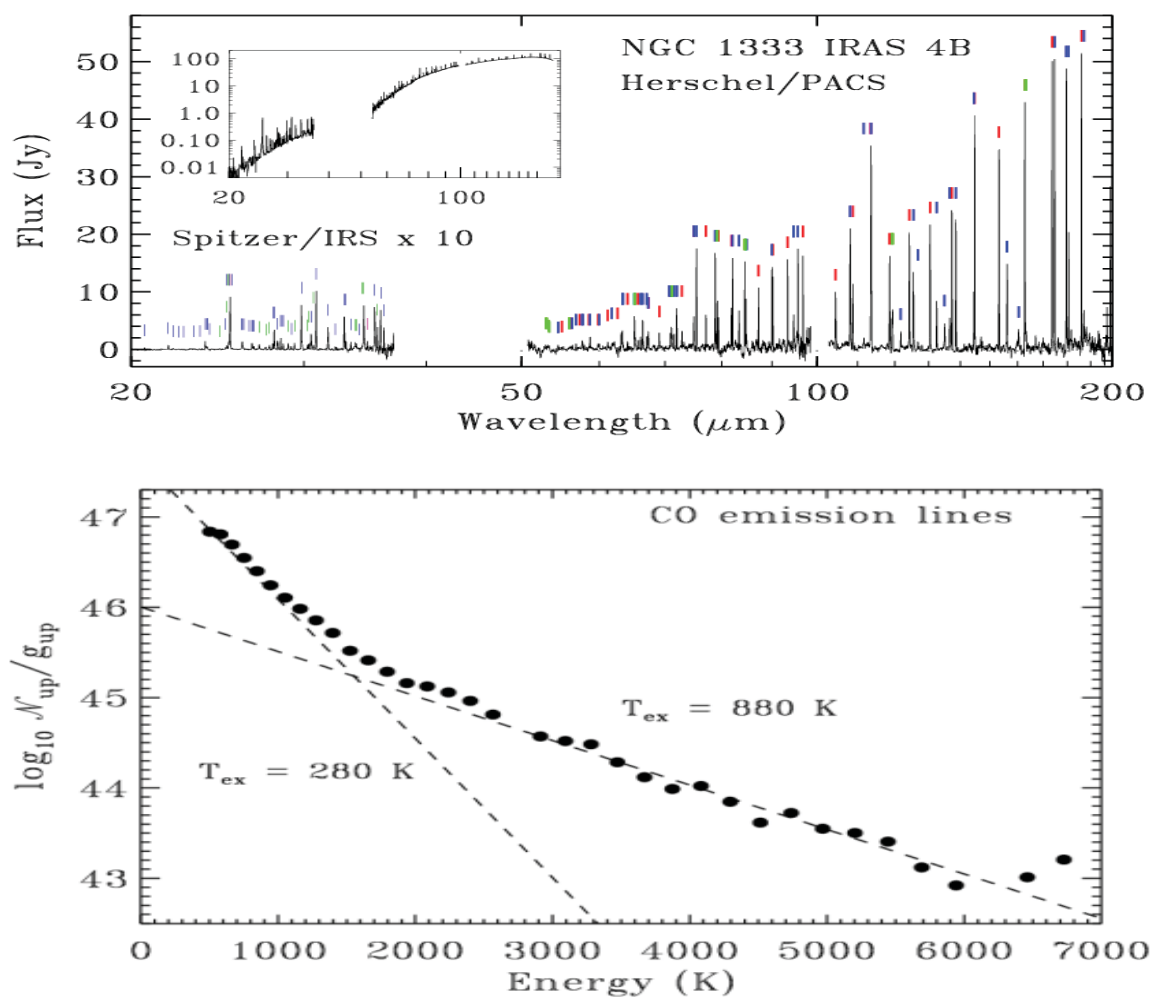


Fig. IR.34: Top: The Herschel/PACS and Spitzer-IRS continuum-subtracted spectra of the low-mass protostar NGC 1333 IRAS 4B ($d=235$ pc, $L=4.4 L_{\text{sun}}$), with bright emission in many H_2O , CO, OH and atomic or ionized lines indicated. The inset shows the combined spectrum including the continuum. Bottom: CO rotational ladder showing the warm and hot CO components (Herczeg et al. 2012).

nents are seen on Boltzmann diagrams with rotational temperatures of ~ 350 K and ~ 700 K, indicating different physical processes involved (dissociative vs. irradiated non-dissociative shocks). CO isotopologs measured by HIFI trace the effect of UV heating. These temperature components seen in the CO ladder turn out to be universal, seen in many galactic and extragalactic sources. Sophisticated 1D and 2D models have been developed.

The water trail from cores to disks. Water is one of the most important molecules in interstellar space. As a dominant form of oxygen, the third most abundant element in the universe, it controls the chemistry of many other species. It is a unique diagnostic of warm gas and energetic processes taking place during star formation, and plays an active role in the gas cooling. In cold regions, water ice may help the coagulation process that ultimately produces planets. Asteroids and comets containing ice have likely delivered water to our oceans on Earth, where water is directly associated with the emergence of life. Tracing the distribution of water vapor and ice during the entire star and planet formation process is therefore a fundamental question relevant to our own origins.

As part of the 'Water in Star-forming regions with Herschel' (WISH) key program (PI: van Dishoeck), water and related molecules have been observed in about 80 sources covering a wide range of masses and luminosities -from the lowest to the highest mass protostars-, and a large range of evolutionary stages -from the first stages represented by the pre-stellar cores to the last stages represented by the pre-main sequence stars surrounded only by their protostellar disks. Both the HIFI and PACS instruments are used to put together the trail of water during star formation. Gaseous water abundances are very low in cold cores and disks, but reach high values in the shocks associated with outflows. A highlight is the

first measurement of the cold water reservoir in a protoplanetary disk, pointing to the presence of about 6000 oceans of water ice (Fig. IR.35).

As a complement to WISH, the IRAM PdB interferometer has been used in a collaboration with the university of Copenhagen to image the warm gas-phase water abundance in the inner hundred AU of three deeply embedded low-mass protostars, revealing for the first time the distribution of water in forming disks.

The warm gas atmosphere of disks revealed by Herschel-PACS. The surface layers of protoplanetary disks are heated by the UV radiation from the young star resulting in high gas temperatures >1000 K. However, this prediction has never been tested. Herschel-PACS has detected the high-J CO lines in the atmospheres of protoplanetary disks for the first time. Comparison with a new generation of thermo-chemical disk models shows that the observed CO ladder can be reproduced, but indeed only for a warm atmosphere with $T_{\text{gas}} \gg T$. When combined with ground-based APEX-CHAMP+ data, all principle forms of carbon can be studied. The data indicate a low abundance of volatile carbon in the disk, perhaps due to transformation of solid CO to more complex species in the cold phase. Disks around intermediate mass stars have high OH/H₂O abundance ratios and show little warm water compared with disks around low mass stars. These findings have consequences for the composition of the atmospheres of any planets that may form in this gas.

Determining disk masses with PACS. The gas mass of a protoplanetary disk is key in determining the disk's ability to form a planetary system but is notoriously difficult to determine. CO is not a good tracer due to freeze-out and photodissociation. Even for the best studied systems, estimated gas masses vary by up to two orders

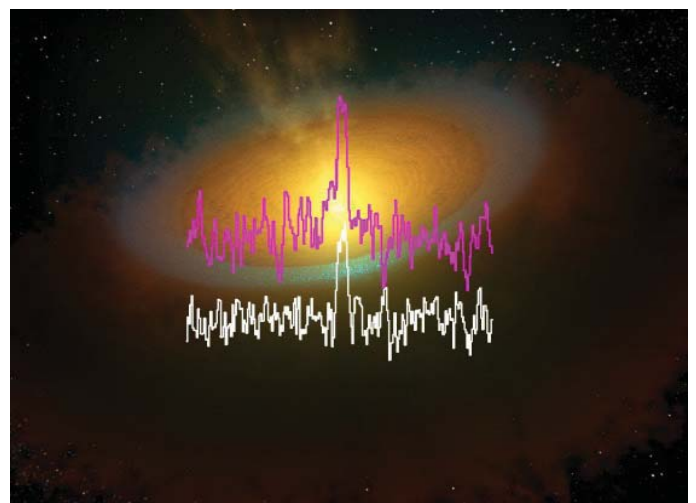
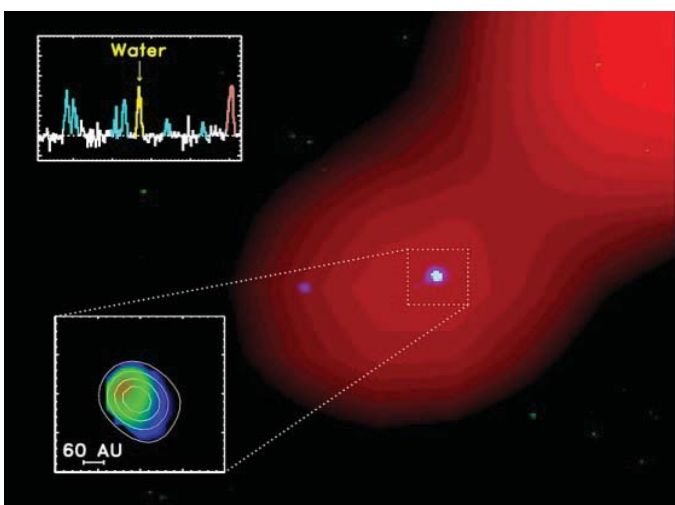


Fig. IR.35: Left. Detection of cold water vapor in the disk around the young star TW Hya with Herschel-HIFI, obtained as part of the WISH program (van Dishoeck et al. 2011). Both the ground-state $o\text{-H}_2\text{O}$ (557 GHz) and $p\text{-H}_2\text{O}$ (1113 GHz) lines are shown (Hogerheijde et al. 2011). Right: Warm water emission toward a low-mass protostar imaged with the IRAM Plateau de Bure Interferometer. The background image shows the distribution of cold dust and gas (red colors) distributed over scales a few thousand times larger than our solar system. The blue color indicates the location of the water vapor detected with IRAM in a rotating disk. The lower inserted Fig. shows the water image with the colors corresponding to the velocities of the gas.

of magnitude. The HD molecule provides a new tool to tackle this issue, since its abundance is directly related to that of H_2 . Using PACS, the $J=1-0$ line at 112 micron has been detected in one disk (only the second time this line has been seen in the ISM). The inferred mass indicates that this disk still has enough gas to form giant planets.

Detection of the simplest sugar in a solar-type protostar with ALMA. Glycolaldehyde ($HCOCH_2OH$) is the simplest sugar and an important intermediate in the path toward forming more complex biologically relevant molecules. Using ALMA science verification data in a collaboration with the University of Copenhagen, the first detection of this molecule around a solar-type young star was obtained, the protostellar binary IRAS 16293-2422. The glycolaldehyde lines have their origin in warm (200-300 K) gas within 25 AU radius (orbit of Uranus) of the individual components of the binary. All transitions show redshifted absorption profiles toward one component in the binary indicative of infall. Thus, the sugar molecules are at the right place and moving in the right direction to be incorporated into future solar systems. The order of magnitude increase in line density even in these early ALMA data illustrates its huge potential to reveal the full chemical complexity associated with the formation of solar system analogs.



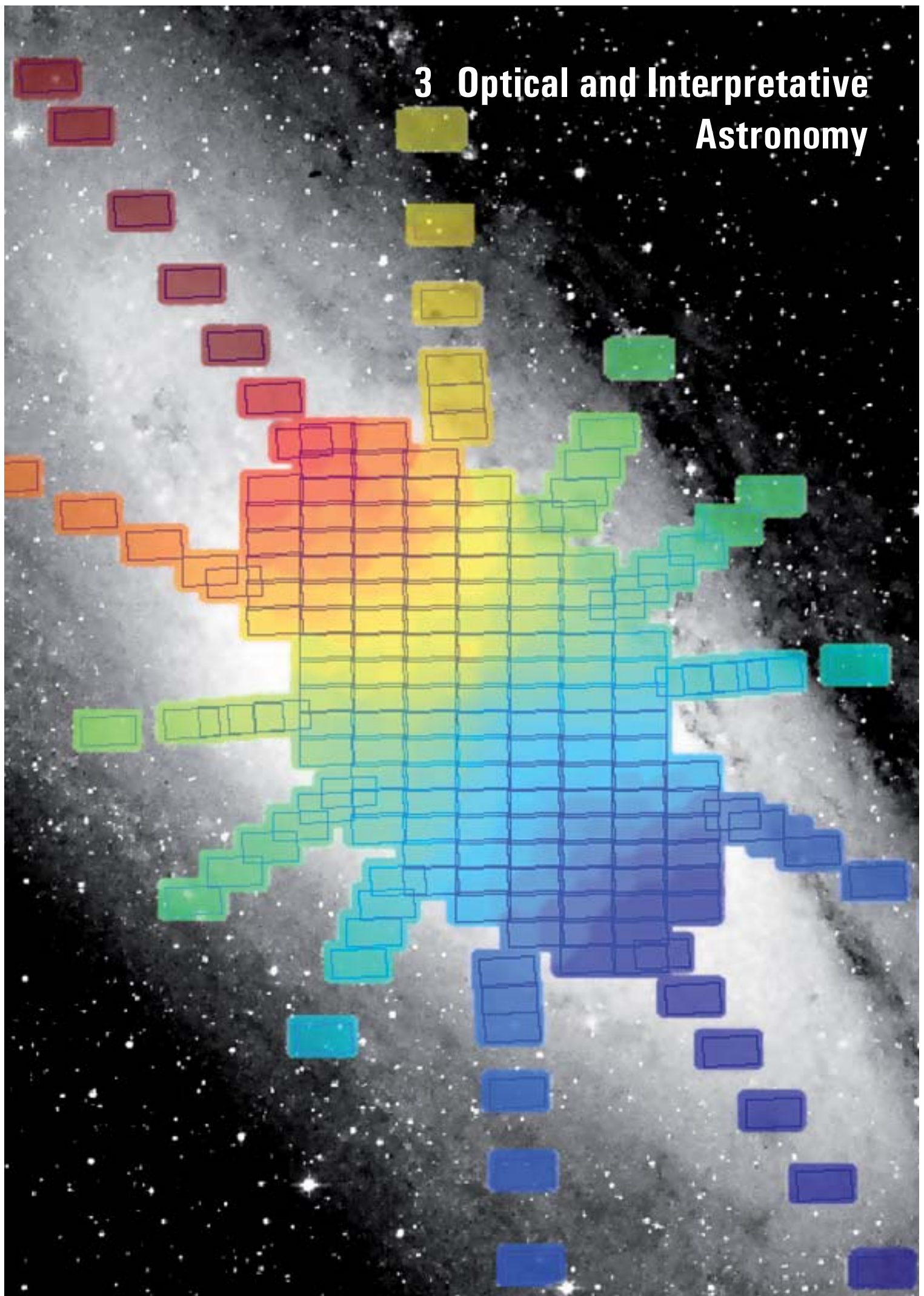
Ewine van Dishoeck is Professor of astrophysics and astrochemistry at Leiden University, The Netherlands. She is also an External Scientific Member of MPE and has an active research group on star and planet formation at MPE and hosted by the IR-group. Ewine is the PI of the 'WISH' program on Herschel, where she uses PACS and HIFI for a detailed study of the role of water vapor in star forming regions and protostellar disks. She is also one of the scientific drivers of the ALMA project, which she is beginning to exploit for spatially resolved studies of protostellar disks.

(Other MPE team members include Joanna Brown, Simon Bruderer, Davide Fedele, Gregory Herzceg, Agatha Karska, Nadia Murillo)

Selected References:

Herczeg, G. J.; Karska, A.; Bruderer, S.; Kristensen, L. E.; van Dishoeck, E. F.; et al. 2012 A&A 540, A84
Hogerheijde, M. R.; Bergin, E. A.; Brinch, C.; Cleeves, L. I.; Fogel, J. K. J.; et al. 2011 Science 334, 338
van Dishoeck, E. F.; Kristensen, L. E.; Benz, A. O.; Bergin, E. A.; Caselli, P.; et al. 2011 PASP 123, 138

3 Optical and Interpretative Astronomy



3. Optical and Interpretative Astronomy (OplnAs)

3.1 Overview

Our central research topic is galaxies. We strive to understand their internal structure, their origin and evolution and how these are related to the properties of their dark halos and central supermassive black holes. Branching off from this core theme, we also have developed interests in the large scale distribution of galaxies and its relation to cosmological parameters, and on smaller scales in, e.g., machos and variable stars in M31.

The OPINAS group is a joint group of the MPE and the University Observatory Munich (Ralf Bender is full professor at the University of Munich and Director at MPE). About half of the group is located at the Observatory, the other half at MPE. Instrument development for ground-based observatories takes place in the observatory (we had PI or leading roles in the VLT-instruments FORS, OmegaCAM, and KMOS, and we are building the complete instrumentation for the Wendelstein 2m telescope). Our contribution to the ESA space mission EUCLID is instead hosted at MPE, as is the development of data analysis software (we are in charge of the Cure-WISE package for HETDEX and of the Photometric Classification Server for Pan-STARRS). Science projects are carried out at both places, as is the education of graduate students. The group members at the observatory are also heavily involved in undergraduate teaching. The requirement to provide bachelor and master thesis topics for a wide variety of students inevitably also leads to a somewhat broader research portfolio than in other MPE groups.

One of our most ambitious science projects in recent years was the search for supermassive black holes with SINFONI and Adaptive Optics at the ESO VLT. In 22 VLT nights, the project has produced in total 31 new black hole detections, more than any other project so far, with the exception of the Nuker HST project, of which we are part as well. Several new results on mergers, extremely compact bulges and pseudo-bulges, the consequences of core-scouring by binary black holes and the influence of dark halos on black hole mass determinations (to name just a few) have been published already. We are currently working on two summary papers that will be submitted in the course of 2013 (plus a few more papers on interesting individual galaxies). In addition, we have published a number of black hole papers with various external colleagues (notably John Kormendy, University of Texas, an external MPE member). On the time scale of a decade, major break-throughs in black hole research can be expected from the advent of Extremely Large Telescopes. We are optimistic that we can continue to play a leading role then, too, as we are a member of the MICADO consortium, which will build the first-light camera/spectrograph for the ESO-ELT. More details on our black hole projects can be found in Section 3.2 below.

In the field of galaxy structure and evolution, we have mostly concentrated on galaxies in the local universe and up to $z \sim 1$ and pursued a broad variety of projects, including studies of the different types of bulges (classical and pseudo), the origin of S0's and spheroidal galaxies, general scaling properties of galaxies, the analysis of environmental effects and stellar populations. The analysis of the dark halo properties of galaxies has received particular attention, both via dynamical analysis and gravitational lensing. Both approaches now deliver very consistent results showing an impressive homogeneity in halo properties for the different types of galaxies. This research has also led to new constraints on the stellar IMF of elliptical galaxies. With the recent completion of KMOS, a 2nd generation NIR multi-integral-field-spectrograph for the VLT, the focus of our galaxy research will now shift to higher redshift. In collaboration with the MPE Infrared Group, we are carrying out a 75 night survey of field galaxies from $z \sim 1$ to $z \sim 4$ with the aim to build up a representative sample of objects covering the full range of star formation activity at all redshifts. We will investigate the relations between the key properties of galaxies, like star formation, rotational properties, mass, metallicity and environment. In addition, we will study the evolution of passive galaxies in clusters with KMOS absorption line spectroscopy in the J-band. Our galaxy research is described in Sections 3.3, 3.4 and 3.5 below.

Driven by the ambition to better understand the relation between galaxies and large scale structure, we have in more recent years also engaged in large surveys like Pan-STARRS and SDSS-III BOSS. Of course, these surveys also allow to address fundamental questions of cosmology. In particular the BOSS survey has recently enabled us to obtain valuable new insights into Dark Energy using the power spectrum/correlation function of the large scale distribution of galaxies. This line of research will gain increasing importance in the future, as we are participating in a series of projects which aim for tighter constraints on the nature of Dark Energy: starting in 2014, the Hobby-Eberly Dark Energy Experiment will investigate the large-scale distribution of Ly α emitters at $1.8 < z < 3.5$ (we are a founding member of HETDEX); in the same year, the SDSS-IV project eBOSS will commence to extend the redshift space coverage of BOSS; and in the more distant future, the ESA mission EUCLID (launch: 2020) will analyse the gravitational shear signal of 109 galaxies and the spatial distribution of ~ 50 million star-forming objects over 15000 square degrees. Needless to say that all these experiments will also produce data sets of tremendous value for the understanding of galaxy formation and galactic structure, too. For more information on large scale structure analyses and the EUCLID mission, see Sections 3.6 and 3.8 of this report, respectively.

Finally, motivated by our long-term search for MACHOs in M31 at the Wendelstein Observatory (WeCAPP project) and our participation in Pan-STARRS, but also because of the broad range of interests of our bachelor and master students at the university, we have also carried out a number of smaller to medium-size research projects on MACHOS, variable stars and planets during the last 6 years. The Pan-STARRS sub-project PAndromeda has been particularly efficient in detecting MACHO events in M31, as well as variable stars that are relevant in a broader astrophysical or cosmological context (e.g. cepheids and eclipsing binaries). With the Pan-STARRS sub-project Pan-Planets we are searching for planet transits, as we have done with the WTS-RoPACS survey. Radial velocity follow-up of transit candidates is currently performed with the HRS at the Hobby-Eberly-Telescope. In the nearby future, we will also be able to use the high-resolution spectrograph FOCES-Comb at the 2m telescope of the Wendelstein Observatory in the Bavarian Alps (which is operated by the OPINAS branch of the University Observatory). Further information on these research topics can be found in Section 3.7.

As in the past, the longer term strategy of the OpInAs group will focus on a few key themes (those described above) but will also allow smaller projects to try out new directions. We will continue to develop dedicated instrumentation and data analysis software to pursue our research more efficiently. And, of course, the steady improvement of our interpretational and modeling tools will remain central for our research.



Ralf Bender

3.2 Supermassive Black Holes

The last two decades made clear that supermassive black holes are ubiquitous at the centres of galaxies with bulges. The galaxy velocity dispersion, bulge mass and the mass of the black hole scale within a factor of 2, which implies that galaxy bulges and black holes were grown in lock step, at least to some degree. Important clues about this interrelation are encoded in the steepness and physical scatter of scaling laws like the $M_{\text{BH}}-\sigma$ and the $M_{\text{BH}}-M_{\text{Bu}}$ relations. Different regimes of these scaling relations isolate different stages and modes of BH and/or bulge growth. At the low-mass end galaxies are disk dominated, mergers are unimportant and scaling relations mostly probe secular evolution processes in disks. At the high-mass end gas poor mergers dominate and leave their imprint in the scaling laws. Studying the link between global galaxy properties and central supermassive black holes was one of the major science activities of the OPINAS group in the last 6 years. In particular our SINFONI survey, the largest ground-based campaign to measure masses of supermassive BHs with the help of adaptive optics, is currently achieving important new insights into BH growth and bulge formation.

When black holes accrete mass, they shine as quasars or AGN, and this activity interferes with the star formation which contributes to bulge growth. Gas can make it to the central BH of a galaxy when distortions in the gravitational potential are strong enough. This can happen through secular evolution of a disk which also leads to the build-up of a bulge. These ‘pseudo-bulges’ structurally resemble disks, e.g. in their flattening and rotational support. Mergers are another channel to feed a central BH. Mergers produce classical bulges and elliptical galaxies. Ultimately these processes govern galaxy evolution with time (see our parallel contribution on ‘Galaxy evolution’). Whether or not and how bulge growth is related to the build-up of a central supermassive BH

can best be studied in galaxies where specific growth modes dominate, like galaxies with pseudo-bulges, bulgeless disk galaxies, the most massive ellipticals or merger remnants. Before we started our campaign, the available databases suffered from the paucity of dynamical BH measurements for these classes. For example, measurements of the BH masses for the merger remnants CenA and NGC 4382 (for the latter see Gültekin et al. 2011), became available only recently. Our Sinfoni BH survey aimed at filling these gaps, after the parameter space accessible using HST was exhausted (a last effort produced 5 new measurements by Gültekin et al. (2009a) and the important stellar dynamical confirmation of the black hole mass in the maser galaxy NGC 4258 by Siopis et al. 2009). Low- σ galaxies are mainly disks with dusty, small (pseudo-) bulges. High- σ galaxies are often large early-type galaxies with relatively low surface brightness. The large collecting power of the VLT, combined with the excellent spatial resolution achieved in the NIR with adaptive optics, offered the right solution to the problems (dust absorption, lack of photons and the need to resolve the small angular size of the BH sphere of influence) that hampered HST to study this type of objects.

The Sinfoni Black Hole Survey: During the last 6 years we invested 22 nights of VLT observations with the Sinfoni integral field spectrograph and adaptive optics to study the centers of 33 local galaxies, (16 Es and S0s, 3 mergers, 11 pseudo-bulges, and 3 classical bulges), resulting in the determination of the BH masses in 31 objects. This is the largest sample of local galaxies observed in the NIR with adaptive optics-based resolution ever put together from the ground and enlarges by 30% the available database of dynamically determined black hole mass measurements. We measured BH masses by modelling the stellar line-of-sight velocity distributions derived by fitting the first and second CO band heads. We complemented these high-resolution (FWHM~0.1

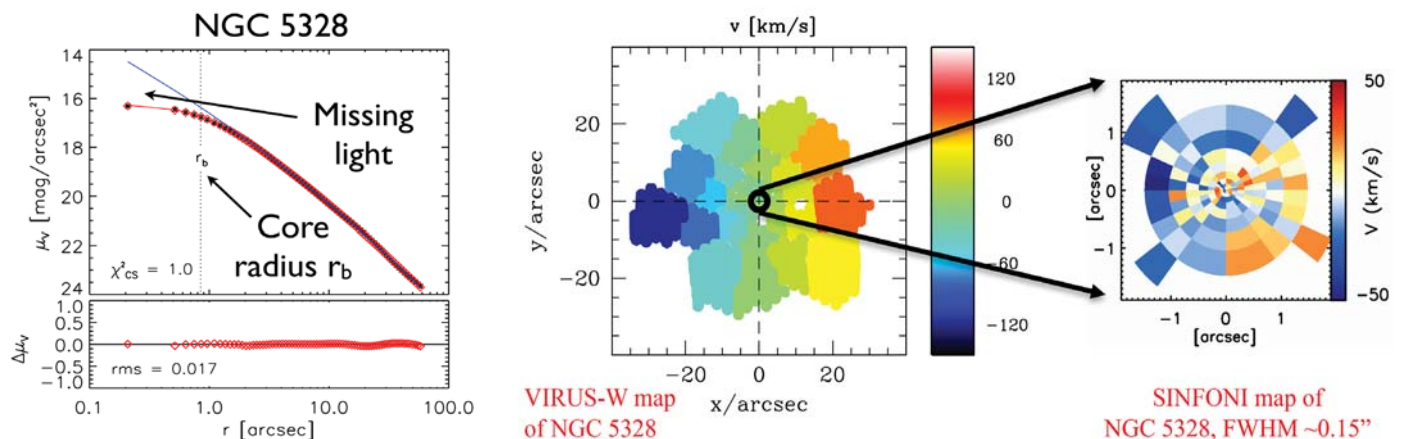


Fig. OP.1: The surface brightness profile (left), the extended 2D kinematics (middle) and high resolution SINFONI data (right) used to derive the black hole mass in the massive elliptical NGC 5328.

arcsec) stellar kinematic maps with deep wide-field 2D or long-slit data covering the outer regions of the galaxies. For each galaxy we also measured high-resolution, extended surface photometry. Fig. OP.1 shows an example of such a combination. We modelled these data using our Schwarzschild axisymmetric orbit superposition code (see also our ‘Galaxy structure’ report), fitting the BH mass, the mass-to-light ratio of the stars and, when needed, the parameters of the dark matter halo. We published first ‘prototype’ results in a series of papers (Nowak et al 2007, 2008, 2010, Rusli et al. 2011) discussing the galaxies NGC 4486a (an elliptical galaxy companion of M87), NGC 1316 (Fornax A, a merger remnant with a dusty central region), NGC 3368 and NGC 3489 (two disk galaxies harbouring both a pseudo- and a classical bulge), NGC 1332 (a lenticular galaxy with high velocity dispersion). In Mazzalay et al. (2013) we study the distribution of the warm molecular and ionized gas we detect at the centers of 6 spiral galaxies of our sample.

Massive galaxies: Our sample of high- σ galaxies is presented in Rusli et al. (2013a and b). In Rusli et al. (2013a) we measure accurate BH masses for 10 early-types, 9 of which have $\sigma > 270$ km/s, enlarging the available sample in this regime by 50%. As discussed for the first time for the case of the black hole in M87 by Gebhardt and Thomas (2009), we find that it is essential to take into account the gravitational contribution of the dark matter halos when modelling these massive ellipticals. Otherwise, the mass-to-light ratio of the stellar component is too high (to compensate for the missing halo) and the BH masses can be underestimated by factors 2 to 6, depending on the spatial resolution of available kinematics. Our BH masses are systematically higher than predicted by the $M_{\text{BH}}-\sigma$ relation determined by Gültekin

et al (2009b). This solves the first problem pointed out by this reference paper, which summarized the results obtained in a decade of HST observations. Since there are no local galaxies with velocity dispersions larger than ~ 440 km/s, it was impossible find the dead counterparts of $10^{10} M_{\text{sol}}$ black holes powering high redshift luminous quasars: the implied dispersion would be $\sigma \sim 560$ km/s. Our measurements confirm the steepening of the $M_{\text{BH}}-\sigma$ relation at large σ (already suggested based on two high mass BH measurements by McConnell et al. 2011, Nature, 480, 215): our best-fit correlations now allow for $10^{10} M_{\text{sol}}$ BHs in local galaxies with $\sigma \sim 440$ km/s can host (see Fig. OP.2).

The second problem discussed in Gültekin et al (2009b) remains somewhat mysterious. The local density of massive BHs predicted by the $M_{\text{BH}}-\sigma$ relation using the SDSS σ -function, is still lower than the density derived using the $M_{\text{BH}}-\text{Bulge Luminosity}$ relation using the SDSS bulge luminosity function (see Fig. OP.3). Our BH measurements imply larger black hole masses for a given bulge luminosity than Gültekin et al. (2009b) predicted and this compensates to some extent the steepening of the $M_{\text{BH}}-\sigma$ relation. Still, the predicted density of local black holes is an order of magnitude larger than derived from models of quasar counts (which, objectively, are also affected by considerable uncertainties).

Depleted cores & BH binaries: Nine of the high- σ galaxies discussed above are so-called core ellipticals (see Fig. OP.1, left, for an example). Compared to power-law ellipticals, shallow cores have been interpreted as signs of ‘missing light’ in the centre Lauer et al. (2007). During the dry mergers that are believed to form core ellipticals the hardening of the binary black hole expels stars

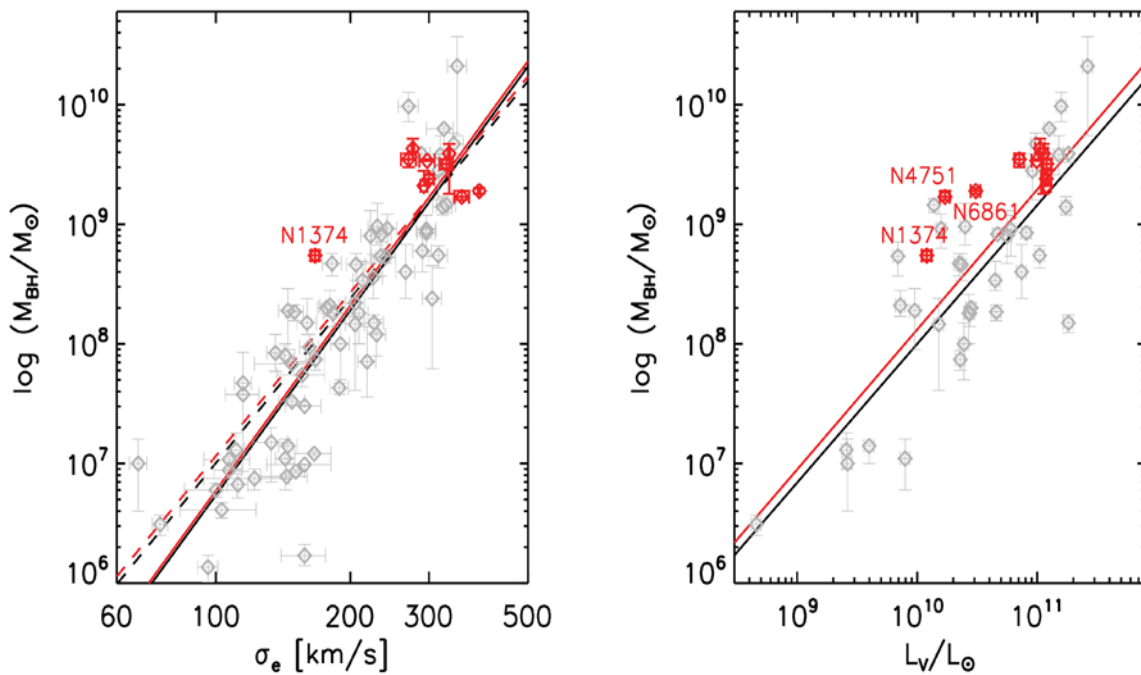


Fig. OP. 2: the $M_{\text{BH}}-\sigma$ (left) and the $M_{\text{BH}}-L_V$ (right) diagrams with our updated relations (red full lines). Gray diamonds are the galaxies from the literature, red ones our 10 high- σ objects. The black lines show the results from the literature. Dashed lines refer to fits restricted to early-type galaxies.

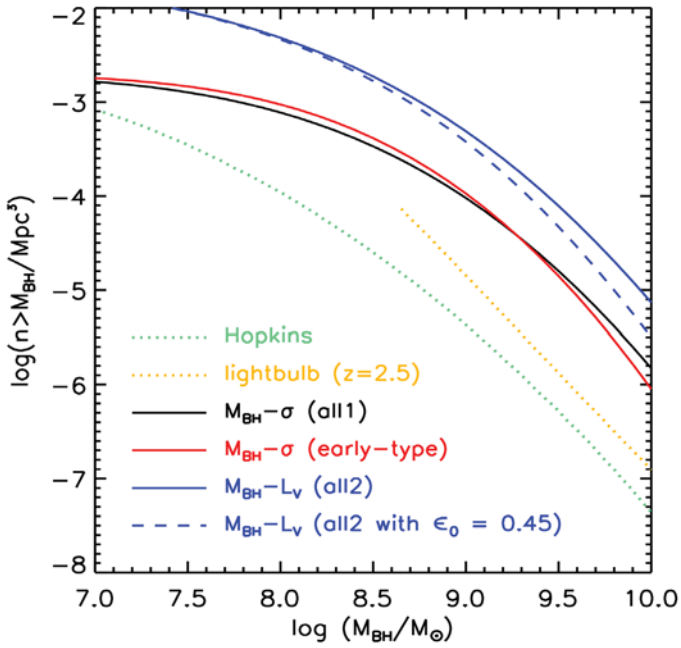


Fig. OP. 3: Black hole cumulative space density derived from the $M_{\text{BH}}-\sigma$ (black and red lines) and the $M_{\text{BH}}-L_v$ (blue lines, the dashed one is computed for a small intrinsic scatter, see Rusli et al. 2013a) relations. Green and yellow dotted lines show models of quasar counts as in Lauer et al. (2007, ApJ, 662, 808).

from the centre. We investigated the interconnection between missing light and BH mass in two papers (Rusli et al. 2013b, Kormendy and Bender 2009). Having now doubled the number of core galaxies with accurate BH masses, including the effects of dark matter for the first time, we find that the core radius r_b , that measures the size of the ‘missing light’ region, correlates very well with the BH mass, as good as the correlation with σ (i.e. within a factor 2). This underlines the physical link between black hole and core size and opens the possibility to estimate BH masses without spectroscopy, at least for core galaxies. Numerical N-body simulations predict that the amount of stars ejected from the centre in each merger equals 1-5 times the mass of the binary BH in the centre.

Our measurements are consistent with these predictions as 75% of the core galaxies in our sample have deficit masses between 1 and 5 times the BH mass. Our detailed orbit models allowed us to go a step further and search for more direct evidence for the core scouring picture. Stars can only be ejected by a binary BH when they reach its sphere of influence. It is therefore the stars on radial orbits which are most affected. After the core-scouring, radial orbits remain depopulated for long times. Therefore the imprint of a BH merger is a lack of radial orbits in the very centre. Our SINFONI galaxies show exactly this characteristic depletion of radial orbits inside the core radius (see Fig. OP.4). This matches the predictions of core formation models based on binary black hole scouring and rules out models where the cores are formed through expansion when an active black hole ejects gas from the center. Power-law galaxies have a different central orbital structure. Our SINFONI survey is a major step forward in understanding the black-holes of the most massive galaxies. The different pieces of evidence from the steepening of the scaling relations, the mass deficits and the orbital structure in core galaxies are the consistent fingerprints of dry merging being the most important evolutionary channel for the most massive elliptical galaxies.

BHs in pseudo-bulges and bulgeless galaxies: We discuss in our parallel contribution on ‘Galaxy evolution’ how late-type galaxies have central structures different from ‘classical bulges’. These so-called ‘pseudo-bulges’ are made of young stars, flattened and rotationally supported, built up by secular evolution possibly driven by the formation of a bar in contrast to merger-driven classical bulge formation. In the last years we showed that BH masses do not correlate with disk or pseudo-bulge K-band luminosity Kormendy and Bender (2011a) and neither with the mass of the surrounding dark-matter halo: there are many bulge-free disks with dark matter halos as massive as the ones of galaxies with big bulges. However, bulge-less disks have BHs much smaller in

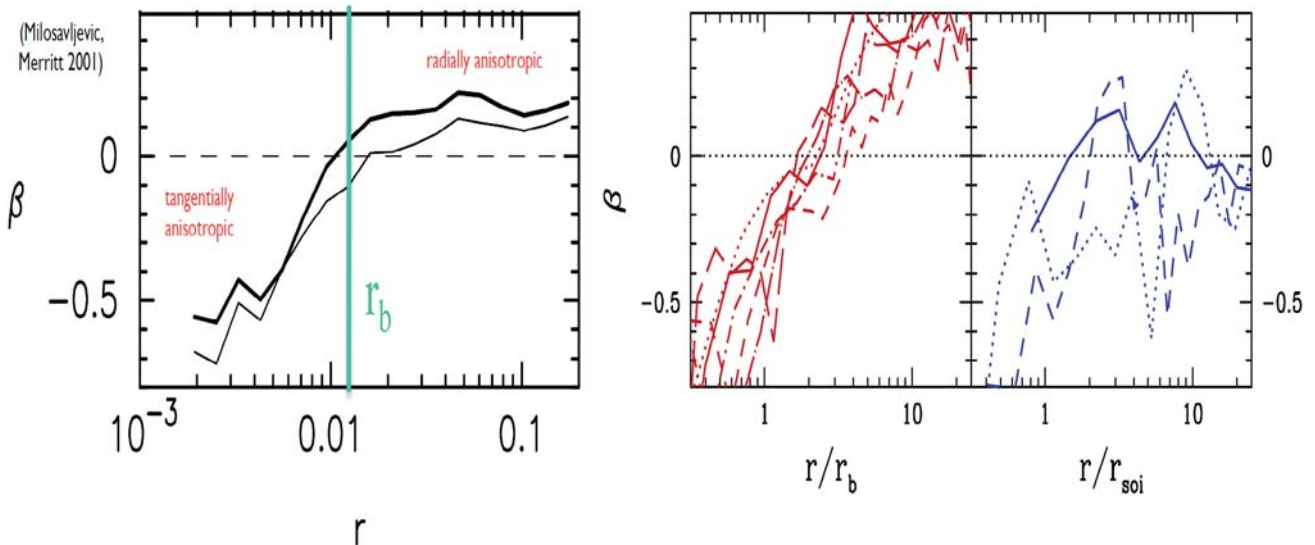


Fig. OP. 4: Left: the anisotropy profiles β ($=1-\sigma_t^2/\sigma_r^2$, where σ_t and σ_r are the tangential and radial velocity dispersions) predicted by the core formation models of Milosavljevic & Merritt (2001, ApJ 563, 34). Right: The anisotropy profiles of core (red) and cuspy power-law (blue) Sinfoni galaxies.

mass Kormendy and Bender (2011b). The physical conditions leading to the growth of classical bulges therefore drive the black-hole bulge coevolution. This makes ‘composite systems’, where both a (small) classical and a (large) pseudo-bulge co-exist particularly important. We presented the first two of them (NGC 3368 and NGC 3489) in a pilot study and find that their BH masses are in reasonable agreement with the $M_{\text{BH}}-\sigma$ relation, but are much smaller than the pseudo-bulge K luminosities predict (Nowak et al. 2010).

Bulge densities and formation scenarios: Incorporating the results of our spiral sample of galaxies, we have produced a merged SINFONI-literature database, that now lists BH masses for more than 80 galaxies. Two important results are emerging from the analysis of this sample, for which we compute dynamical bulge mass estimates M_{Bu} , determine the bulge spherical half-luminosity radius r_h and averaged spherical density ρ_h within r_h . Bulge densities turn out to be important. High densities imply a large baryonic concentration near the centre and make a very efficient mass accretion onto the black hole likely. Bulge densities, in turn, are set mainly by two factors: (1) the formation redshift – earlier formation implies higher halo and gas densities – and (2) the merging history – gas poor mergers reduce the density in each merger generation.

We find that early-type galaxies and classical bulges follow a similar trend in the $M_{\text{BH}}/M_{\text{Bu}}$ ratio, while pseudo-bulges are different (see Fig. OP.5, left). Two-parameter correlations best predict the BH mass for early-types and classical bulges (see Fig. OP.5, right). At the lowest densities we find core galaxies. In these objects, at a given σ or M_{Bu} , the most massive BHs are found at the largest sizes or lowest ρ_h . Further developing earlier suggestions and discussions, we speculate that large, ‘slow

rotator’ galaxies (that often have a core) are the result of dry mergers of ‘fast rotator’, ‘cuspy’ power-law early-type galaxies. While keeping σ constant, the mergers reduce the average density (by $1/4$ for equal mass mergers) of the resulting galaxies, increase the central black hole masses through black hole merging (by a factor 2 for equal mass mergers), a process that is also responsible for the creation of the cores. In a ‘dry’ (i.e. without gas and therefore dissipationless) merger these cannot be ‘refilled’ to reform central cusps. Several minor dry mergers can also enlarge sizes and lower average densities, while keeping the $M_{\text{BH}}/M_{\text{Bu}}$ ratio almost constant. Measuring M_{BH} in galaxies known to be recent mergers of disk galaxies (with gas and therefore ‘wet’) allows one to sketch what could be the evolution with time in the more common gaseous rich mergers supposed to generate the majority of ‘fast-rotating’ early-type galaxies. If these progenitors follow the $M_{\text{BH}}-M_{\text{Bu}}$ relation and the black hole(s) do not accrete substantial amounts of gas during the merging process, the merger remnant would now fall below the relation by a factor corresponding to the mean bulge-to-total ratio of the progenitors. This is indeed what we see for NGC 1316, NGC 2960, NGC 5018, and NGC 5128, all rather young, gas-rich, merger remnants. NGC 3923 is likely to be (the late phase of) a merger between an existing elliptical with low velocity dispersion dwarf galaxy. As the gas fraction decreases with cosmic time, it is plausible that galaxies that merged earlier had a better chance to grow their black holes in lock-step with the spheroid than present-day mergers. Thus, we would expect the $M_{\text{BH}}/M_{\text{Bu}}$ ratio to increase with increasing redshift. This is indeed observed in various samples of quasars at $z > 2$. Extrapolated even further, we would expect those objects that were assembled early and did not undergo later major mergers to harbour the relatively most massive black holes at a given bulge mass. These objects should have formed from

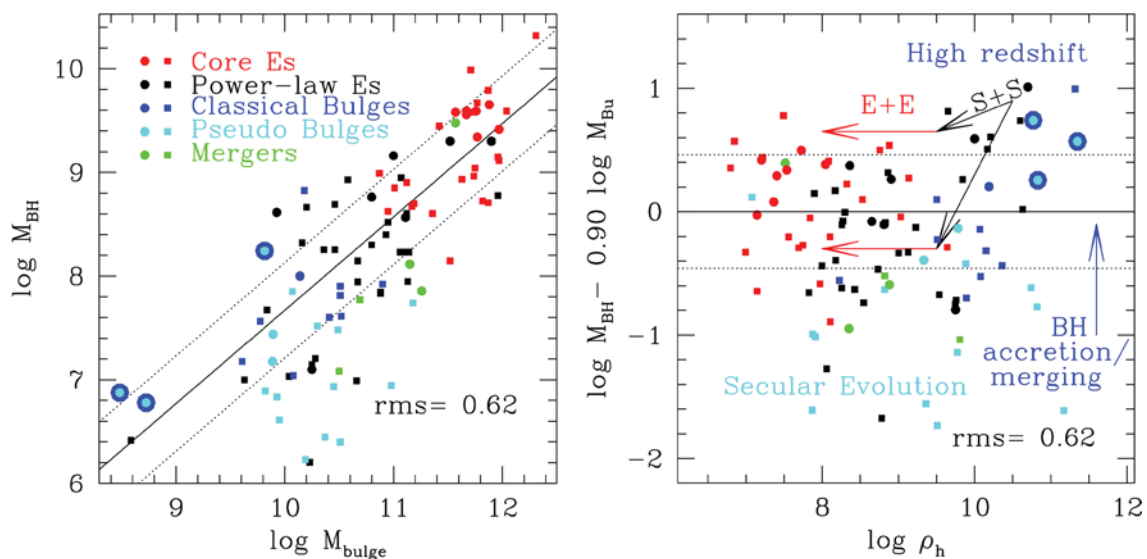


Fig. OP.5: the $M_{\text{BH}}-M_{\text{Bu}}$ relation (left) and the residuals as a function of bulge density ρ_h . Squares are data from the literature, circles are galaxies from our Sinfoni survey. We plot core galaxies in red, power-law early-types in black, classical bulges in blue, pseudo-bulges in cyan and merger remnants in green. Cyan dots with a blue annulus are the classical bulge components of pseudo-bulges. The dotted lines indicate the estimated intrinsic scatter for the early-type plus classical bulge sample, the rms is measured on the whole sample (i.e. including pseudo-bulge). Arrows describe qualitatively the effects of the different channels of BH and bulge growth.

very gas-rich material that allowed their black holes to grow efficiently. They also should have high stellar densities because earlier formation implies higher dark matter and gas densities. As dry mergers decrease the mean stellar density, a high density today also implies that the objects did not undergo such events more recently. Examples for such objects could be very compact bulges in old S0's or early-type spirals, where the existence of a substantial disk indicates the lack of late major mergers.

In fact, some of the most compact bulges known, like NGC 4486b, NGC 4342, NGC 3998, NGC 4594, NGC 5845, NGC 3245, NGC 1332 do harbour unusually large black holes. M32 (NGC 221) is also extremely dense, but with a black hole only slightly more massive than average for its bulge mass. Except for NGC 4486b, these galaxies are not particularly deviant when the $M_{\text{BH}}-\sigma$ relation is considered, an indication that the velocity dispersion (through the $M_{\text{BH}}-\sigma$ relation) is a more robust black hole mass predictor than the bulge mass (through the MBH-MBu relation).

In contrast, the mass of BHs in pseudo-bulges (cyan points in Fig. OP.5, typically they have lower ρ_h than classical bulges) correlates weakly with σ , with a shallower slope and a lower zero point than found for early-types and classical bulges, without further dependencies on other parameters. In particular, it does not correlate with the pseudo-bulge mass. This is in agreement with the results of Kormendy and Bender (2011a). To conclude, the growth of black holes in galaxies that did not undergo mergers and therefore do not have a 'classical bulge', follows a path decoupled from the rest of the galaxy and set by the amount of gas that secular processes (such as bars) manage to funnel towards the galaxy centers. The resulting black hole masses are much smaller than the ones measured in early-type or classical bulges of the same bulge density. However, we also found 'composite systems' where both a 'classical' and a 'pseudo'-bulge co-exist. In Fig. OP.5 we plot the position of NGC 3368, NGC 3489 and NGC 4699, all galaxies with 'pseudo'-bulges, using the mass of their small 'classical' bulges. Possibly these high-density components were formed together with their BH at high redshifts.

Instrument developments: MICADO. Together with the NIR group we participate in the definition and design of MICADO, the high-resolution near-infrared imager (likely with a long-slit grism spectroscopy capability) for the ELT. Thanks to the multi-conjugate adaptive optics, MICADO will deliver a 1×1 arcmin² diffraction limited field (10 mas in the K band) with unprecedented sensitivity. With this instrument we expect to measure stellar kinematics and black hole masses in distant (massive) bulges and possibly follow the motions of resolved stars in the cores of the nearest galaxies.



Roberto Saglia



Jens Thomas

(Other OPINAS team members include R. Bender, P. Erwin, M. Fabricius, J. Kormendy, X. Mazzalay, N. Nowak, M. Opitsch, S. Rusli)

Selected References:

- Gebhard and Thomas, 2009, *ApJ*, 700, 1690
 Gültekin et al. 2009a, *ApJ*, 695, 1577
 Gültekin et al. 2009b, *ApJ*, 698, 198
 Gültekin et al. 2011, *ApJ*, 741, 38
 Kormendy and Bender 2009, *ApJ*, 691, L142
 Kormendy and Bender 2011a: *Nature*, 469, 374
 Kormendy and Bender 2011b: *Nature*, 469, 377
 Lauer et al. 2007, *ApJ*, 664, 226
 Lauer, Bender et al. 2012, *ApJ* 745, 121
 Mazzalay et al. 2013, *MNRAS*, 428, 2389
 Nowak et al. 2007, *MNRAS*, 379, 909
 Nowak et al. 2008, *MNRAS*, 391, 1629
 Nowak et al. 2010, *MNRAS*, 403, 646
 Rusli et al. 2011, *MNRAS*, 410, 1223
 Rusli et al. 2013a, *AJ*, in press
 Rusli et al. 2013b, *AJ*, in press
 Siopis et al. 2009: NGC 4258, *ApJ* 693, 946

3.3 Galaxy Structure

Dark matter is the key ingredient of our current picture for the formation and evolution of galaxies. It provides the seed gravitational concentrations into which baryons dissipate to form stars and build up galaxies. One of the strongest predictions of the Λ -CDM paradigm is a cuspy density distribution in the centres of dark-matter halos. The distribution of dark matter is altered during the infall of the baryons and many of the related processes are not understood in detail: How strong is the gravitational contraction of dark matter halos exerted by the baryons when they assemble in the central parts of the halos? Do dark matter halos expand as a result of feedback from stars (in low-mass galaxies) or central supermassive black holes (in massive galaxies)? To answer these questions we study the fossil records of the formation processes in the structure of local galaxies. We are using state-of-the-art dynamical modelling techniques that provide precision mass profiles of unprecedented detail.

Precision mass measurements for early-type galaxies: Unlike the rotation curves for spiral galaxies there is no direct tracer for the mass distribution in early-type galaxies. Masses have to be obtained through dynamical modelling of the kinematics of the stars. Stellar orbits, in turn, reflect the merging and formation history of a galaxy and are not known in advance. In the last years we advanced the so-called extended Schwarzschild orbit-

superposition method. It allows us to recover not only the mass profiles of galaxies, but also the distribution of stellar orbits. We tested the method extensively on analytic models and N-body merger remnants and applied it to 24 cluster early-type galaxies: 16 in Coma and 8 in the cluster Abell 262. Advances in strong gravitational lensing methods enabled us – for the first time – to directly compare our masses of real galaxies to independent measurements (Thomas et al. 2011; Wegner et al. 2012). The orbit superposition models we developed achieve a level of accuracy in mass similar to strong gravitational lensing (see Fig. OP.6). Systematic uncertainties in both methods are on the same low level ($\sim 10\%$), as the small scatter shows. Opposed to lensing, dynamical models provide precision masses spatially resolved over the whole region covered by the stellar kinematic data and are applicable to all galaxies and not only to the rare galaxies in lensing configurations.

Maximum or submaximum bulges? Stars respond to the overall gravitational field and there is no direct way to distinguish whether the gravitational pull that shapes a star's orbit originates from dark matter or from other stars. Dynamical models offer spatially resolved mass profiles of elliptical galaxies and give us the information how much of this mass is traced by the light and how much is not. If all the mass that follows the light is in stars

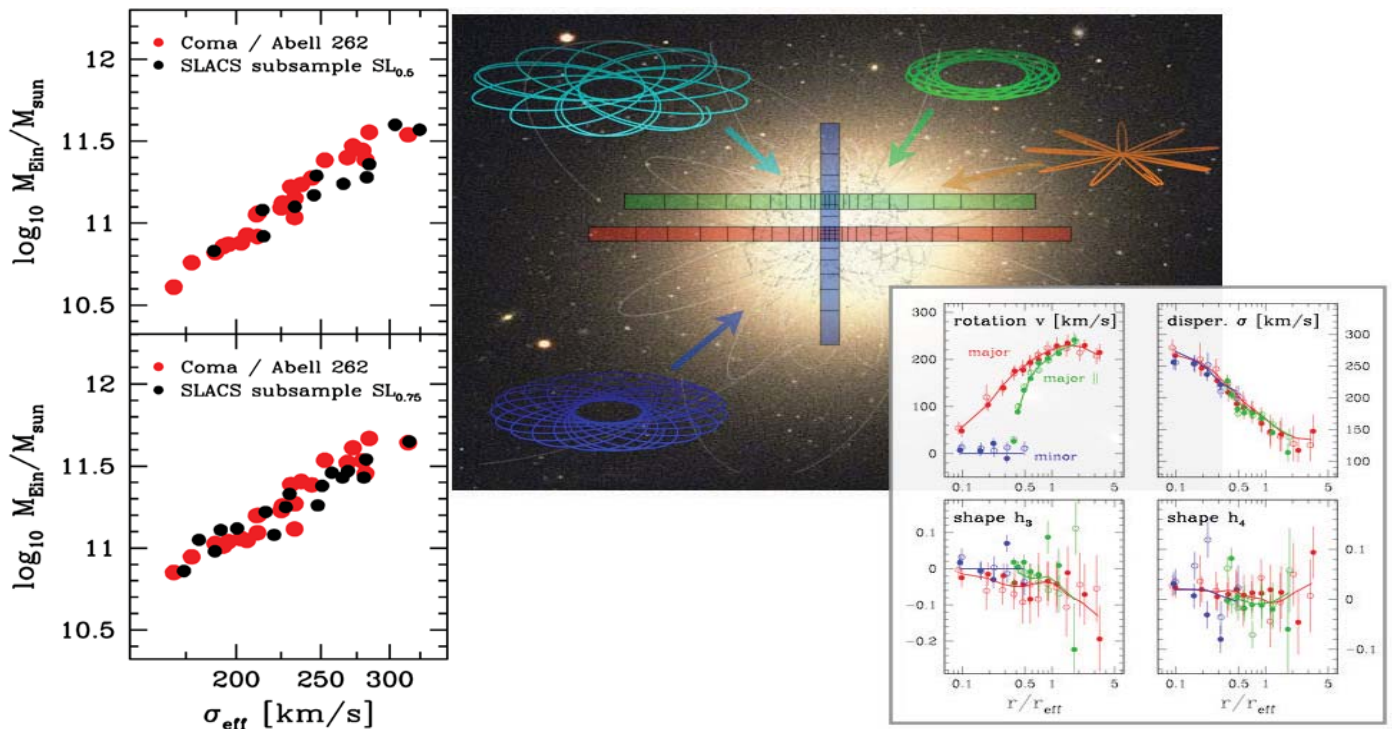


Fig. OP.6: Predicted Einstein masses of our dynamical orbit-superposition models (red, left panels) versus a test sample of SLACS strong gravitational lenses (black; the observed lenses in the top panel have Einstein radii = $\frac{1}{2}$ of their half-light radii, lenses in the bottom panel = $\frac{3}{4}$ of the half-light radius). Our dynamical models achieve the same precision as strong gravitational lensing masses. Systematic uncertainties are lower than $\sim 10\%$, as judged from the scatter in both methods. The right panels show how well the orbit model reproduces the stellar kinematics (the rotation, dispersion and Gauss-Hermite parameters of the line-of-sight velocity distribution) along three different slits (separated by color and illustrated on the image).

then we can easily separate stellar from dark matter. In spiral galaxies this assumption is well known as the maximum disk hypothesis, and in analogy to the case of spirals, we can call it the maximum-bulge hypothesis (counting elliptical galaxies as bulges). We were the first to relax this assumption and also investigate the consequences of submaximum bulges, i.e. that some of the mass that is traced by the light might not be baryonic (Thomas et al. 2011; Wegner et al. 2012).

The stellar initial-mass-function (IMF): In the Milky Way and its direct neighbourhood the stellar IMF, i.e. the distribution of the masses of stars at their birth, can be measured through star counts and is known to flatten below one solar mass (Kroupa IMF). In more distant galaxies star counts are not feasible and the IMF is not known. While stellar-population ages and metallicities can be determined from spectral line indices through stellar-population synthesis models, the corresponding stellar masses are uncertain to a factor of ~ 2 as long as the IMF is not known. To constrain the IMF, we compared our dynamical stellar mass estimates with stellar-population synthesis predictions based on a Milky Way IMF. Maximum bulges require the stellar IMF in early-type galaxies to vary, because dynamical stellar masses turn out to be higher than predicted by a Milky Way IMF in many galaxies, as recently also found in the ATLAS3d survey (Cappellari et al. 2012, Nature 484, 485): at galaxy velocity dispersions of $\sigma=200$ km/s the IMF is similar to our own Galaxy, but more massive galaxies ($\sigma=300$ km/s) reveal an excess of mass that is traced by the light. This extra mass could be the footprint of a population of low-mass stars and thus indicating an IMF that is steeper at the low-mass end than in our Galaxy (e.g. Salpeter IMF; see Fig. OP.7). Independent, direct measurements of the stellar IMF beyond the neighbourhood of our Galaxy are still uncertain. A universal IMF cannot be ruled out by stellar kinematic data, but would imply that the most massive bulges are submaximal and that some dark matter follows the light in the most massive galaxies. Our cluster galaxy study clearly shows that bulges are either maximal or that the IMF is universal, but not both (Thomas et al. 2011; Wegner et al. 2012).

Halo profiles: isothermal, Λ -CDM or cored? Maximum bulges are consistent with both Λ -CDM halos and halos that have a flat central core. The evidence against either of the two profiles turns out to be weak in the cluster early-types we studied. In the majority of our galaxies cored halos even fit slightly better such that the direct evidence for Λ -CDM halos is weak (Thomas et al. 2011; Wegner et al. 2012). Independently of which halo profile we assume, the fraction of dark matter inside the half-light radius is $\sim 25\%$ of the total mass. In the Draco dwarf spheroidal galaxy we recently applied a new, non-parametric mass reconstruction method that suggests a dark halo profile similar to Λ -CDM predictions (Jardel et al. 2013). We showed that a universal IMF (i.e. submaximum bulges) requires almost isothermal dark halos, steeper than implied by Λ -CDM and dark matter fractions twice as large as in maximum bulges (over 50%). The bulge-halo degeneracy cannot be broken by any method tracing just

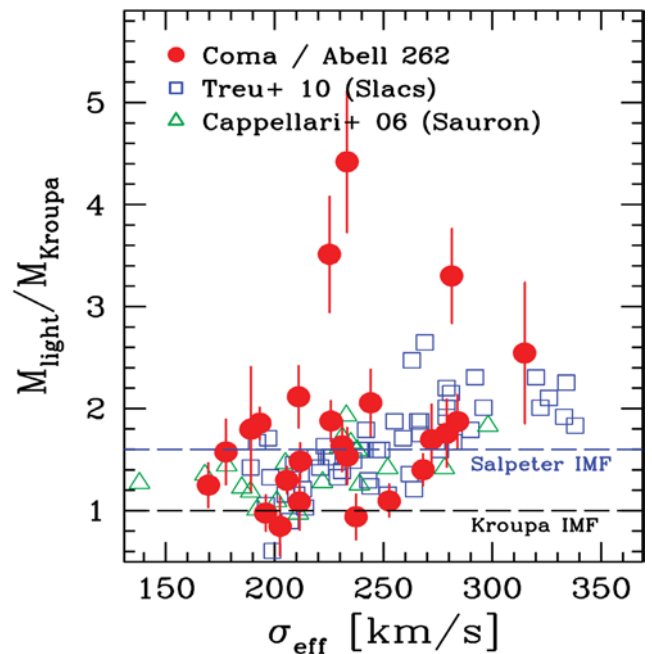


Fig. OP.7: Variation of the stellar IMF implied by maximum-bulge models, i.e. assuming that all the mass M_{light} that follows the light is in stars. At galaxy velocity dispersions of $\sigma=200$ km/s the IMF in early-type galaxies appears as in our Galaxy (Kroupa IMF; $M_{\text{light}} \sim M_{\text{Kroupa}}$). At higher dispersions ($\sigma=300$ km/s) we observe an excess of mass that follows the light. It could be tracing a population of low-mass stars (as e.g. implied by a Salpeter IMF, for which $M_{\text{light}} \sim 1.6 M_{\text{Kroupa}}$). Alternatively, high- σ galaxies must have submaximum stellar masses (i.e. some of the mass that is traced by the light is not baryonic).

the gravitational field, but the requirement that one of these interpretations is correct puts strong constraints on galaxy formation models.

Dark-matter densities & halo-assembly epoch: Our elliptical galaxies have 10 times higher dark matter densities than spiral galaxies of the same stellar mass (see Fig. OP.8). This rules out that ellipticals as a class have formed through binary mergers of present-day spirals. Instead, it puts strong constraints on galaxy formation simulations. Higher dark matter densities imply an earlier formation epoch. We derived for the first time formation redshift estimates for local cluster ellipticals (between $z=1$ and $z=3$, or roughly 8-10 Gyrs ago). Half of the galaxies assembled their halos at the same time as their stars were born. These galaxies must have formed in a dynamically violent, collapse-like process (Thomas et al. 2009).

Search for MACHOS in M31: We are monitoring Andromeda (M31) to search for microlensing events and variable stars (see description of the Pandromeda project in Planets & Stars). In order to disentangle events due to the MACHOS of the dark halos from self-lensing, it is important to construct the tri-dimensional mass distribution of the galaxy, and in particular its bulge. This can be done best by complementing imaging with a kinematic survey. In a first step we measured the stellar and gas kinematics along 4 directions of the central bulge and disk regions of M31 using the HET low-resolution spectrograph (Saglia et al. 2010). We confirmed the presence

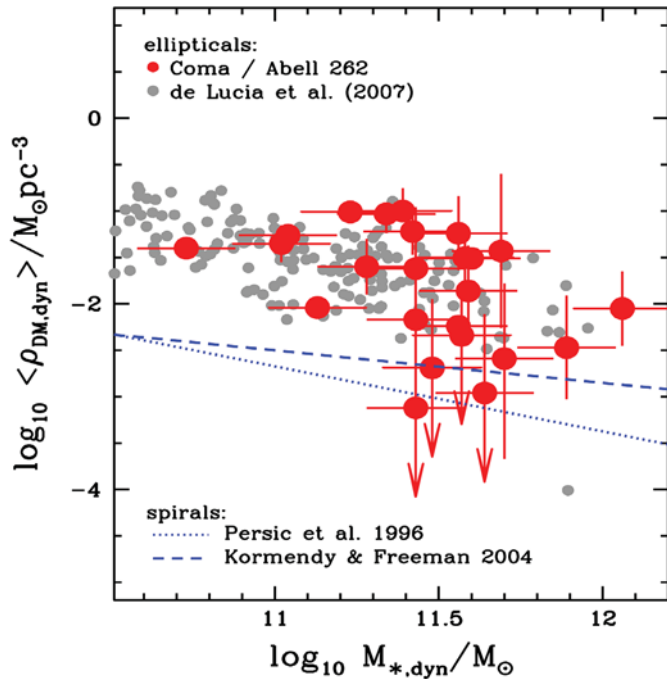


Fig. OP.8: Dark-matter densities of early-type galaxies in the Coma and Abell 262 clusters (in red) are higher than in spiral galaxies of the same stellar mass (blue lines). Denser halos imply an earlier formation redshift and rule out that ellipticals as a class have formed through binary mergers of present-day spirals.

of bulge triaxiality and estimated its age (>12 Gyr), metallicity (solar) and its being slightly α -overabundant (0.2 dex). As a further step, we mapped the kinematics of the whole bulge using the VIRUS-W spectrograph at the 2.7m McDonald telescope (Fig. OP.9). The data analysis is in progress. We also continued the study of the clus-

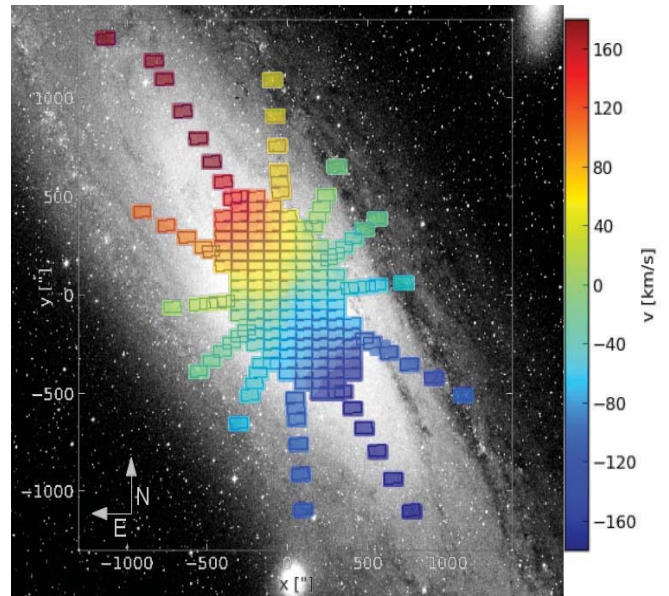


Fig. OP.9: The rotation field of the M31 bulge as a mosaic of 190 pointings observed with VIRUS-W.

ter of blue stars surrounding the M31 nuclear black hole (Lauer et al. 2012).

Dynamical structure of bulges: We are currently conducting a study of the dynamical structure of bulges in nearby disks. With its large field of view and high spectral resolution VIRUS-W (see below) is ideally suited to study the stellar and gaseous kinematics of local disk galaxies and specifically to study the kinematic signature of different structural components (bulges/disk/bars)

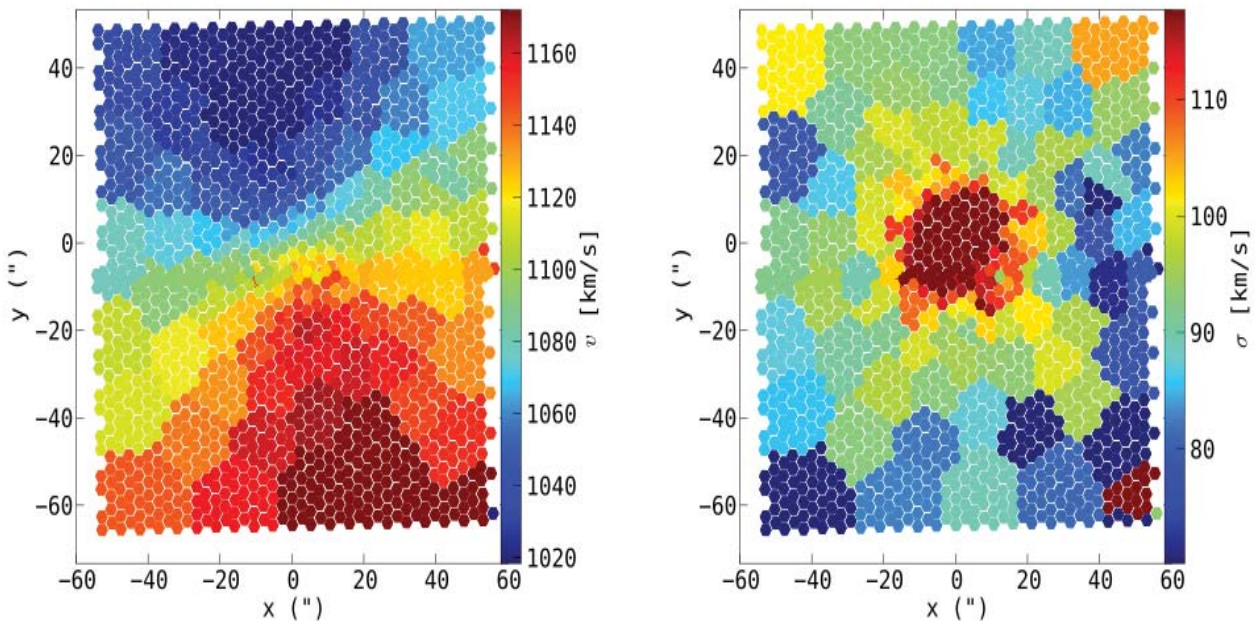


Fig. OP.10: A map of the stellar line-of-sight velocities (left) and velocity dispersions (right) of NGC4203.

giving a unique insight into their formation history. For this work, we are targeting a sample of local ($D < 20$ Mpc) bulges in S0 to Sc type galaxies. As example, Fig. OP.10 shows kinematic maps for the lenticular galaxy NGC4203 that we obtain from the VIRUS-W data. A clear increase of stellar velocity dispersion is seen towards the centre of this galaxy. The central region in this galaxy is clearly dominated by dispersion, as expected for classical bulges.

Instrument developments: VIRUS-W. In order to study the orbital structure of galaxies, we need to spectroscopically measure the line of sight velocity distributions of the stars. This is only feasible if the intrinsic dispersion of the targeted objects is larger than the instrumental dispersion of the instrument that is used to obtain these

In November and December 2010 we successfully commissioned a new optical fibre-based Integral Field Unit (IFU) spectrograph (see Fig. OP.11) at the 2.7 m Harlan J. Smith Telescope of the McDonald Observatory in Texas (Fabricius et al. 2012). Regular science observations commenced in spring 2011. The instrument achieves a spectral resolution of $\lambda/\Delta\lambda = 8700$ with a spectral coverage of $4850 \text{ \AA} - 5480 \text{ \AA}$ and a spectacular throughput of 35% including the telescope optics. The design is related to the VIRUS-P instrument that was developed for the HETDEX experiment, but was modified significantly in order to achieve the large spectral resolution that is needed to recover the dynamical properties of disk galaxies. In addition to the high resolution mode, VIRUS-W offers a stellar population mode with a resolution of $\lambda/\Delta\lambda = 3300$ and a spectral coverage of $4340 \text{ \AA} - 6040 \text{ \AA}$. The

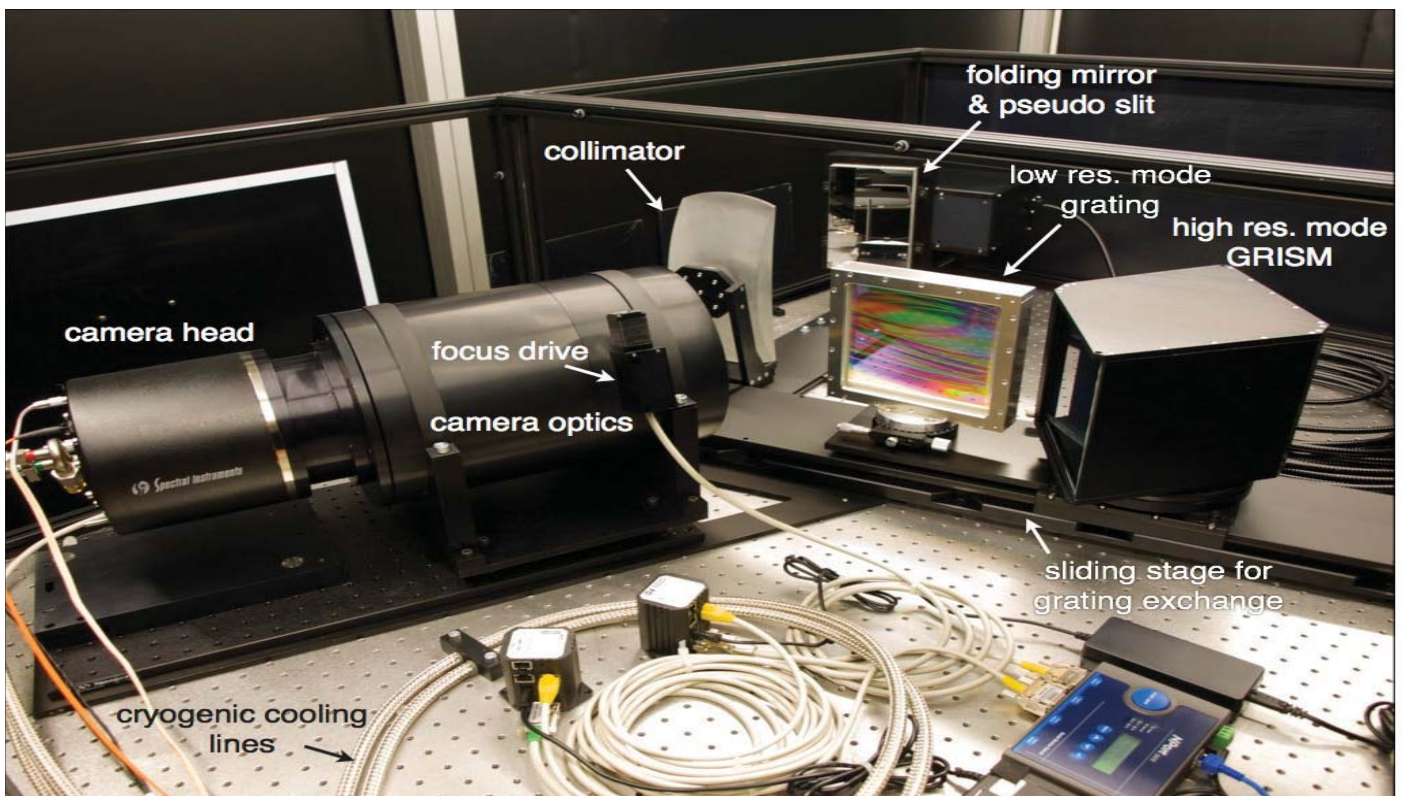


Fig. OP.11: VIRUS-W. The image was taken in the optical laboratory in Munich shortly before the instrument was packed and shipped to the McDonald Observatory. The spectrograph is benchmounted. The devices seen in the bottom half are the motor controllers for the grating exchange and the camera focus drive, the ethernet to RS232 converter, and power supplies.

spectra. For early type galaxies with dispersions well in excess of 100 km/s, spectral resolutions of a few thousands are sufficient and a number of instruments exists that have been used to study the properties of these objects in great detail. Spiral galaxies on the other hand exhibit dispersions often well below 100 km/s and dwarf galaxies typically show a few tens of km/s. Few instruments exist which have sufficient resolution to derive dispersions - let alone higher moments - in these galaxies and typically the offered field of view is too small to capture their global dynamical properties.

IFU (see Fig. OP.12) is composed out of 267 $150 \mu\text{m}$ -core optical fibers with a fill factor of 1/3. With a beam of $f/3.65$, the core diameter translates to $3.2''$ on sky and a large field of view of $105'' \times 55''$ that is ideally suited to study the bulge regions of local spiral galaxies. Light loss due to focal ratio degradation in the fibers is minimized by a design that operates close to their numerical aperture. Further, a large 200 mm aperture refractive camera with no central obscuration, highly efficient volume phase holographic gratings, and a high-QE CCD are responsible for the overall large throughput of this instrument.

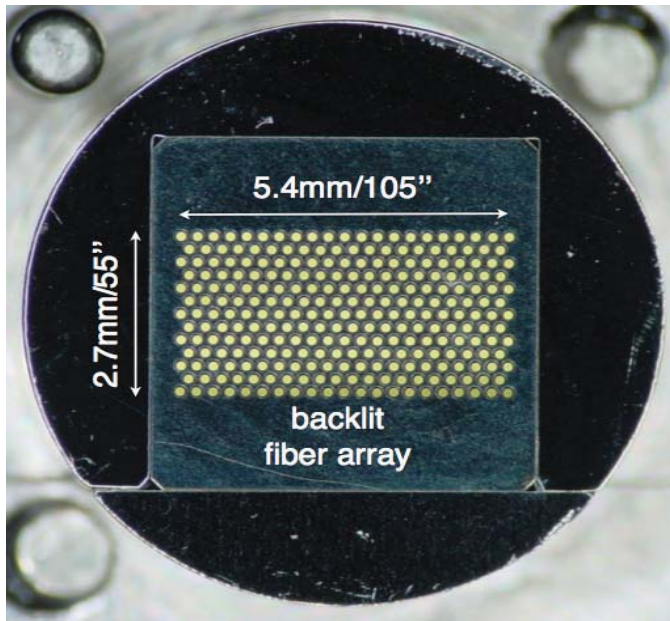


Fig. OP.12: VIRUS-W. Micrograph of the IFU. The 267 fibers are arranged in a hexagonal densepack scheme. The total fill factor is 1/3. The fiber slit was illuminated while this image was taken. A 25 m long fiber bundle connects the IFU to the spectrograph that is located in the control room.

Selected References:

- Corsini et al. 2008, *ApJS* 175, 462
 Fabricius et al. 2012, *SPIE* 8446, 5
 Hilz et al. 2012, *MNRAS* 425, 3119
 Jardel et al. 2013, *ApJ* 763, 91
 Lauer et al. 2012, *ApJ* 2012, 745, 121
 Pu et al. 2010, *A&A* 516, 4
 Remus et al. 2013, *ApJ* 766, 71
 Saglia et al. 2010, *A&A* 509, 61
 Teodorescu et al. 2011, *ApJ* 736, 65
 Thomas et al. 2007, *MNRAS* 381, 1672
 Thomas et al. 2007, *MNRAS* 382, 657
 Thomas et al. 2009, *MNRAS* 393, 641
 Thomas et al. 2009, *ApJ* 691, 770
 Thomas et al. 2011, *MNRAS* 418, 2815
 Wegner et al. 2012, *AJ* 144, 78
 Williams et al. 2012, *MNRAS* 427, 99



Jens Thomas, Roberto Saglia, Max Fabricius

(Other OPINAS team members include Ralf Bender, Michael Opitsch, Shibi Pu, Michael Williams)

3.4 Dark Matter in Galaxies and Clusters of Galaxies from Weak and Strong Lensing

One major emphasis of our work in the last 4 years was to understand the mass distribution of galaxies from small scales, where they turn from baryon dominated to dark matter dominated, out to scales where their halo ends. To achieve this goal, we studied individual galaxies acting as strong lenses, the lensing effect of galaxies embedded in a high-density cluster environment, and the weak galaxy-galaxy lensing signal of field galaxies. We also mapped the dark matter distribution of clusters of galaxies with strong and weak lensing. Recently we concentrated our effort on the determination of the mass distribution of the CLASH-cluster RXJ2248, which will be one of the 6 HST Frontier Fields to be mapped with 140 orbits of HST-time each.

The mass density profile and stellar mass to light ratio in elliptical galaxies:

Elliptical galaxies obey the Faber-Jackson and Fundamental Plane scaling relations linking the luminosity, effective radius and surface brightness to the central velocity dispersion of their stars. According to strong lensing results (Bolton et al. 2008, ApJ, 682, 964) the mass distribution of massive elliptical galaxies at around half the effective radius is correctly described by a nearly isothermal total (dark plus luminous) profile with velocity dispersion equal to the central stellar velocity dispersion. This conclusion has been obtained by assuming that galaxies

have either nearly isotropic stellar orbits or that galaxies with different luminosities have self-similar profiles. Our goal was to measure the mass profile of massive ellipticals without such assumptions from lensing alone. This can be achieved if particular (“golden”) lens systems are investigated which map extended sources with surface brightness substructure or with several subcomponents into extended images or rings. We published the analysis of two such (SLACS) systems: SDSSJ1538+5817, (Grillo et al. 2010) and SDSSJ1430+4105 (Eichner et al. 2012). In the second case we split the mass distribution into one following the galaxy’s de Vaucouleurs light profile and a NFW component. Thanks to the large radial range over which multiple image constraints are available we could measure the mass of the de Vaucouleurs component and the additional component separately. The mass to light ratio of the luminous component is higher than for a Chabrier IMF and requires a Salpeter IMF (if all matter of the de Vaucouleurs component is baryonic). The dark matter is fairly flat within the effective radius. Results for further 3 lensing systems (in prep.) are similar. Our findings for $z=0.1-0.3$ massive galaxies concerning Salpeter-like mass to light ratios for the de Vaucouleurs components and the total mass density profile agree with results for local, massive Coma elliptical galaxies derived by our group (Thomas, J. et al. 2011) with dynamical modelling.

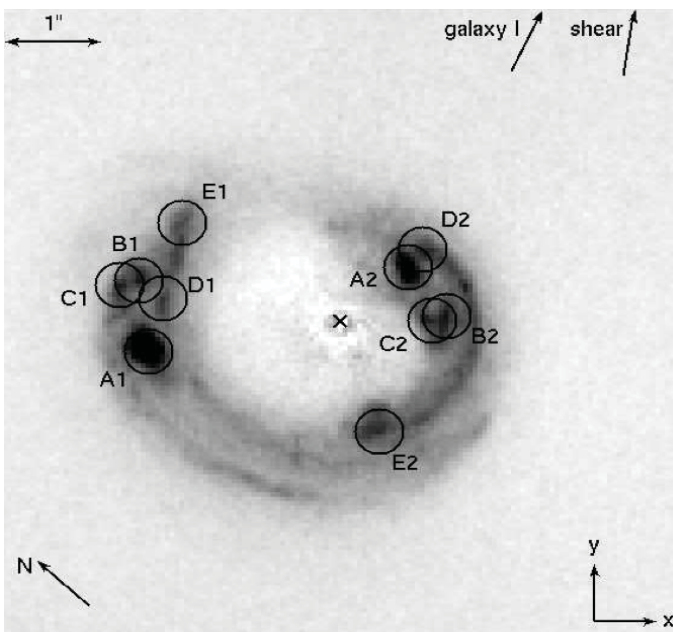


Fig. OP.13: This image shows the lensed galaxy (with source redshift of $z_s = 0.575$) for the system SDSSJ1430+4105, the lensing galaxy (at a redshift of $z_l = 0.285$) is already subtracted. The extended source is imaged twice to form an almost complete Einstein ring. The labels A to E mark corresponding sub-components.

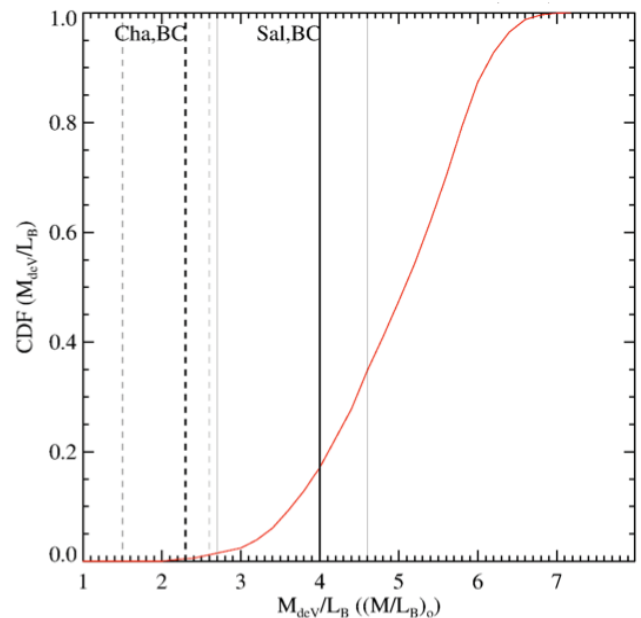


Fig. OP.14: The red curve shows the cumulative distribution function for the mass to light ratio of SDSSJ1430+4105-de Vaucouleurs component, as derived from our lensing analysis. The vertical lines illustrate estimates obtained from the SDSS photometry and modelling the star formation history of the lensing galaxy for Chabrier- and Salpeter IFMs by Grillo et al. (2009, A&A, 501, 461).

The tidal radius of galaxy dark matter halos in cluster cores:

Galaxy halos in dense environments are expected to be smaller than in the field due to tidal stripping. Halo sizes in clusters can be measured by weak galaxy-galaxy lensing for regions outside the highest projected densities where strong lensing takes place. In the strong lensing regions galaxy halos (mass profile and total masses) are measurable because they influence the positions of multiple image systems and because they change the surface brightness distributions of giant arcs and other extended images. The CLASH-cluster MACS1206 provides a spectacular example where the light bending due to cluster galaxies can be seen easily by eye (we are a core team member of the CLASH Multi-Cycle Treasury HST project). We measured the halo sizes by studying both the multiple image positions and the surface brightness (SFB) distribution of the giant arc and

its counter-image. Results of both methods agree, with the arc providing the stronger constraints. According to this the size (half mass radius) of a halo with central velocity dispersion of $\sim 190\text{km/s}$ is only $35\pm 8\text{kpc}$ at 95 per cent confidence (Eichner et al. 2013). Our analysis did not make use of the Faber Jackson relation or Fundamental Plane relation in order to obtain the estimate of the velocity dispersion of cluster galaxy halos. It however predicts these relations correctly, which confirms that the degeneracy between halo size and halo potential depth is correctly broken. Comparing cluster halo masses with halo masses measured by us for elliptical field galaxies (Brimioulle et al. 2013) yields that the central cluster galaxies in MACS1206 have lost about 90 per cent of their mass by tidal stripping. This result is in agreement with hydro-dynamical simulations of clusters by Limousin et al. (2009, ApJ, 696, 1771).

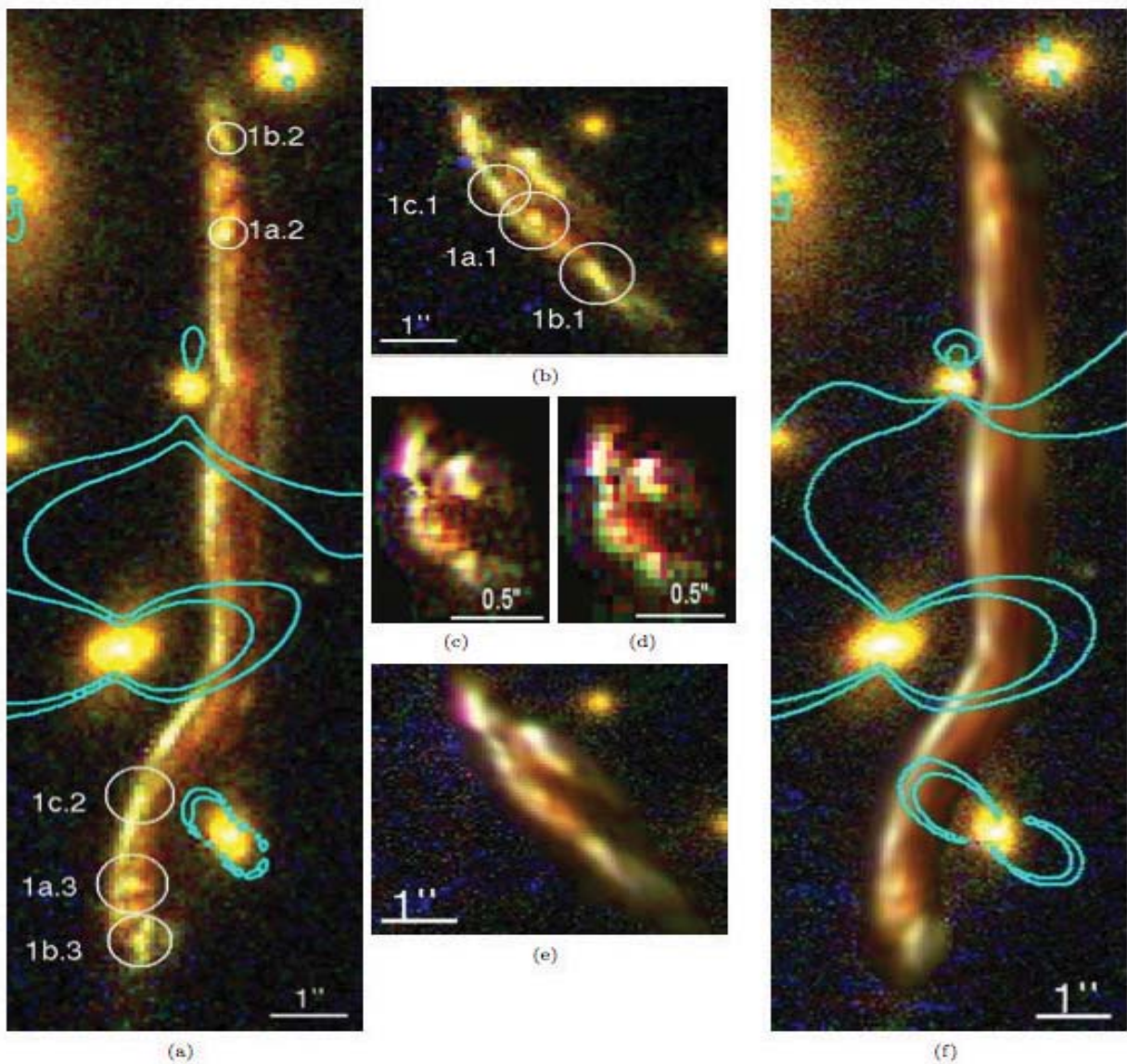


Fig. OP.15: The giant arc (at a source redshift of $z_s = 1.033$) and its counter-image observed in MACSJ1206.2-0847 are shown in the left row and the middle, top panel. The reconstruction of the arc by our strong lensing model is shown in the right and middle, bottom panel. The colors of the observations and reproductions are composed of the HST/ACS F435W-F606W-F814W filters. Cyan lines mark regions of very high magnification.

Scaling relations for field galaxy dark matter halo parameters:

Another focus of our work was to measure how galaxy light and dark matter halo properties are related for field galaxies. In Briouille et al. 2013 we studied this by analysing the galaxy-galaxy lensing effect in about 100 square degrees of the public CFHTLS-Wide data set taken in the $u^*g'r'l'z'$ filter system. We used the photometric data to estimate the SED-type and photometric redshifts and then analysed the shape distortion that foreground galaxies impose on galaxies in their background. If we describe the mass profiles out to 100 h^{-1} kpc as isothermal spheres then the scaling relations for the velocity dispersion σ for the red and blue galaxies are $\sigma_{\text{red}} = 162 \pm 2 \text{ km/s} \times (L/L^*)^{0.24 \pm 0.03}$ and $\sigma_{\text{blue}} = 115 \pm 3 \text{ km/s} \times (L/L^*)^{0.23 \pm 0.03}$, with an r' -band reference luminosity of $L^* = 1.6 \times 10^{10} h^{-2} L_{\odot}$. We alternatively describe the mass distribution with NFW profiles and a Duffy et al. (2008, MNRAS, 390, 64) concentration-mass relation. In this case we obtain a broken power law relation for the scaling of the virial masses M_{200} with luminosity. For the red galaxies we can turn the luminosities into stellar masses and obtain a minimum of the M_{200}/M_{star} – ratio for a stellar mass of $M_{\text{star}} \sim 3-4 \times 10^{10} h^{-2} M_{\text{star}}$. Our halo mass to light ratio values and the location of the minimum agrees with results from satellite kinematics from More et al. (2011, MNRAS, 410, 210), see Dutton et al. (2010, MNRAS, 407, 2) for a compilation of further results.

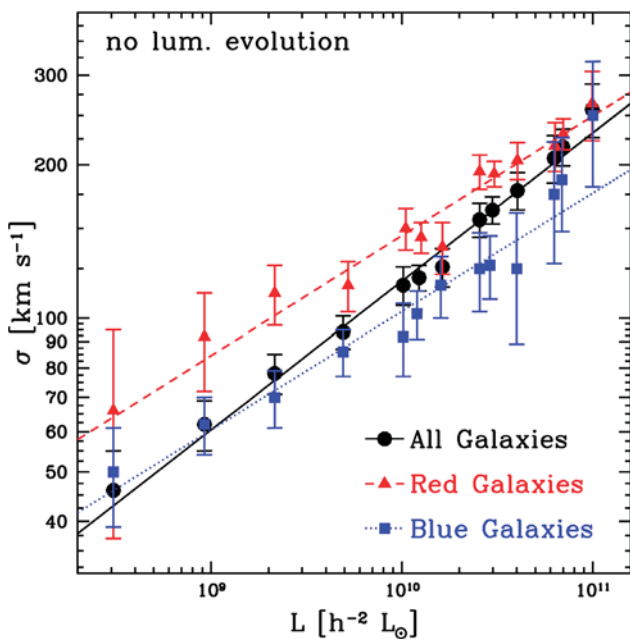


Fig. OP.16: Velocity dispersions of isothermal sphere halos from fitting the weak lensing signal to scales $< 100 h^{-1}$ kpc. We show the scaling with r' -band luminosity for galaxies with red and blue spectral energy distributions and for the combined galaxy sample.

Matter profiles of galaxies and gravitational telescopes:

The Cluster Lensing And Supernovae with Hubble (CLASH) program lead by M. Postman (Postman et al., 2012, ApJS, 199, 25) aims to precisely map the (dark and luminous) matter distribution in 24 clusters, to iden-

tify gravitationally magnified high redshift galaxies and Supernovae along their line of sights.

Within the CLASH team we lead the analysis of the RXJ2248 cluster. We measured the large-scale mass distribution of this cluster with weak lensing (Gruen et al. 2013a) using ground based data and constrained the central mass distribution by analysing the strong lensing systems identified by us in the HST data (Monna et al. 2013). We also carried out a systematic search for $z > 5$ galaxies in this field. We found a candidate for a $z \sim 6$ galaxy lensed into 5 images (Monna et al. 2013). A spectroscopic confirmation will be attempted within the next run of the CLASH-VLT spectroscopic programme. The cluster RXJ2248 recently became one of the HST-Frontier Fields and thus will be mapped much deeper by HST within the next 2.5 years. In our future work on CLASH and Frontier-Field data we will continue to measure the substructure traced by galaxies and obtain limits on “dark” halos (masses and abundances) not hosting galaxies to obtain a halo-mass function in cluster core. We will also continue to participate in the search for the highest redshift galaxies.

Regarding cluster weak lensing analyses have shown that the Large Binocular Telescope is suitable to measure weak lensing masses for $z \sim 1$ clusters (Fassbender et al. 2011 and Lerchster et al. 2011) and we have also obtained weak lensing masses for 8 massive SZ clusters (Gruen et al. 2013b). We also carried out a theoretical study to find out how weak lensing data are optimally weighted as function of cluster centric distance to obtain minimum-variance cluster masses (Gruen et al. 2011). With this effort we contribute to the understanding of how precisely one can measure cluster masses with weak lensing, and whether clusters of galaxies can finally serve for a method to measure not only the matter density of the universe but also the dark energy equation of state.

Developments of Algorithms for data reduction, photometric redshift and shear measurements:

Weak lensing analyses require special attention for data reduction regarding astrometric accuracy and the identification and elimination of image artefacts, like cosmics, satellites and ghost images of bright stars. We developed an algorithm which is particular suited to identify extended, low-surface brightness artefacts like faint ghost images and faint satellite trails. The code will be provided to the public (Gruen et al. 2013c).

We work on bias free gravitational shear estimates with neural networks (Gruen et al. 2010) and on improving the measurement of the PSF in wide field data as far as related to weak lensing analyses (Kitchings et al. 2013).

Accurate photometric redshift measurements and shape measurements of galaxies are an essential ingredient to measure mass distributions with the weak lensing effect. Consequently we improved the accuracy of our photometric redshift method (Bender et al. 2001) by improving the SED-templates for red galaxies (Greisel et al. 2013).

Instrument developments:

Wendelstein Wide Field Imager (WWFI)

Our group has built the 27'x27' Wide Field Imager for the Wendelstein 2m Fraunhofer telescope (Gössl et al. 2010a&b) This instrument is tailored to carry out science projects requiring the good PSF-conditions of our sight, like weak lensing analyses: combined with the telescope optics the CCD pixel size translates to 0.2", the optics itself is designed to minimize ghost images, and the charge transfer inefficiency and charge persistence of the WWFI detectors were shown to be at a level low enough to be irrelevant for gravitational shear measurements we aim for. The instrument will also be used to continue our effort to find and characterize variables and transient source and microlensing events towards nearby galaxies like M31 (see section 3.7).

Wendelstein 3KK

The Wendelstein 3KK (Lang-Bardl et al. 2010) is a 3 channel imager providing 2 optical channels for imaging with the u', g', r'-filters (blue channel) and with the l' and z'-filters (red channel) and one near infrared channel for imaging with the Y, J, H, Ks, H2, Bry -filters. The pixel size and FOV of images will be 0.2" and 6.8'x6.8' in the optical and 0.24" and 8.2'x8.2' in the NIR. W3KK will allow us to efficiently obtain photometric redshifts for clusters identified in Xray surveys (like eRosita) and shallow optical surveys (like PanSTARRS-1) and to analyse the weak lensing signal in the central regions of these clusters. In addition we will use this instrument to follow up, e.g. transients sources, for which the simultaneous observations of fluxes at different wavelengths is particularly beneficial.



Stella Seitz

(Other OPINAS team members include R. Bender, F. Brimiouille, T. Eichner, N. Greisel, D. Gruen, M. Kodric, J. Koppenhoefer, R. Kosyra, A. Monna, A. Riffeser, R.P. Saglia, C. Goessl, U. Hopp, F. Lang-Bardl)

Selected References:

- Bauer A. H., Seitz S., Jerke J., et al., 2011, *ApJ*, 732, 64
 Bender R. et al., 2001, *Deep Fields: ESO Astrophysics Symposia*, ISBN 3-540-42799-6.
 Brownstein J. R., Bolton A. S., Schlegel D. J., et al., 2012, *ApJ*, 744, 41
 Coe D., Umetsu K., Zitrin A., et al., 2012, *ApJ*, 757, 22
 Coe D., Zitrin A., Carrasco M., et al., 2013, *ApJ*, 762, 32
 Eichner T., Seitz S., Bauer A., 2012, *MNRAS*, 427, 1918
 Fassbender R., Boehringer H., Santos J. S., et al., 2011, *A&A*, 527, A78
 Gössl, C. et al., *Society of Photo-Optical Instrumentation Engineers (SPIE) Conference Series*, 2010, 7735
 Gössl, C. et al., *Society of Photo-Optical Instrumentation Engineers (SPIE) Conference Series*, 2010, 8446
 Greisel N., Seitz S., Drory N., et al., 2013, *ApJ*, 768, 117
 Grillo C., Eichner T., Seitz S., et al., 2010, *ApJ*, 710, 372
 Gruen D., Bernstein G. M., Lam T. Y., et al., 2011, *MNRAS*, 416, 1392
 Gruen D., Brimiouille F., Seitz S., et al., 2013, *MNRAS*, 1221
 Gruen D., Seitz S., Koppenhoefer J., et al., 2010, *ApJ*, 720, 639
 Halkola A., Seitz S., Pannella M., 2007, *ApJ*, 656, 739
 Lang-Bardl, F. et al., *Society of Photo-Optical Instrumentation Engineers (SPIE) Conference Series*, 2010, 7735-133
 Lerchster M., Seitz S., Brimiouille F., et al., 2011, *MNRAS*, 411, 2667
 Nesvadba N. P. H., Lehnert M. D., Genzel R., et al., 2007, *ApJ*, 657, 725
 Ofek E. O., Seitz S., Klein F., 2008, *MNRAS*, 389, 311
 Postman M., Coe D., Benitez N., et al., 2012, *ApJS*, 199, 25
 Saglia R. P., Tonry J. L., Bender R., et al., 2012, *ApJ*, 746, 128
 Spinelli P. F., Seitz S., Lerchster M., et al., 2012, *MNRAS*, 420, 1384
 Thomas J., Saglia R. P., Bender R., et al., 2011, *MNRAS*, 415, 545
 Umetsu K., Medezinski E., Nonino M., et al., 2012, *ApJ*, 755, 56
 Zheng W., Postman M., Zitrin A., et al., 2012, *Natur*, 489, 406
 Zitrin A., Broadhurst T., Coe D., et al., 2011, *ApJ*, 742, 117
 Zitrin A., Meneghetti M., Umetsu K., et al., 2013, *ApJ*, 762, L30
 Zitrin A., Rosati P., Nonino M., et al., 2012, *ApJ*, 749, 97

3.5 Galaxy Evolution

To develop a picture of how galaxies evolve in a Universe where assembly proceeds hierarchically, a few key ingredients are required: an understanding of the galaxy properties themselves; the star formation history; scaling relations between photometric properties tracing the stars and dynamical properties tracing total mass; a statistical description of the full galaxy population, most importantly the mass function of galaxies; and a description of an evolving galaxy population in the context of an evolving (hierarchical) environment. Our research pushes for a clearer understanding of these topics by taking a leading role in the development of ground-breaking instrumentation and utilizing the highest quality data in collaborations with the best people. Over the last 6 years much of our research focused on understanding bulge growth, which holds the key to much of galaxy evolution. There are two types of bulge, and two types of elliptical galaxy (pure bulges) described by different formation paths. The merger-induced growth predicted by hierarchical models would form more ellipticals than we observe. Instead, the high frequency of S0s leads us to intriguing conclusions relating bulge growth to the quenching of star formation. We also find a separate formation path for S0s as satellites in massive halos. We extend the sequence of S0 galaxies to low mass, bulgeless spheroidals which appear to partially drive a steep slope at low masses in the mass function of galaxies. The next step is to move to high redshift, tracking the peak epoch of star formation with our GTO access to KMOS on the VLT.

There follows a brief description of some of our research highlights.

Two types of bulge: Classically Dead or Pseudo Active?

Using high resolution imaging and kinematics of nearby galaxies (Kormendy et al. 2009; Kormendy et al. 2010; Kormendy & Bender 2012; Drory & Fisher 2007; Fisher, Drory & Fabricius 2009; Fisher & Drory 2008, 2010, 2011; Fabricius et al. 2012), we identify bulges as either classical-bulges (passively evolving, pressure-supported “mini-ellipticals” at the centre of disc galaxies, Fig. OP.17, top panel), or pseudo-bulges (flattened, rotationally supported, star forming disc-like enhancements at the centre of the main disc of a galaxy, Fig. OP.17, bottom panel). Classical bulges probably form via violent relaxation when two galaxies merge and their hosts are almost all on the red sequence with quenched star formation (Drory & Fisher 2007). The hosts of pseudo-bulges are almost all actively star forming: gas seems to be required for the development, probably via secular instabilities in the galaxy's disk.

Puffing-up Ellipticals: When, How and Where?

We measured stellar velocity dispersions and sizes for the ESo Distant Cluster Survey (EDisCS) cluster and field early-type galaxies to measure dynamical masses, densities and stellar mass fractions at redshifts $z \sim 0.4$ - 0.9 (Saglia et al. 2010). Consistently with our previous

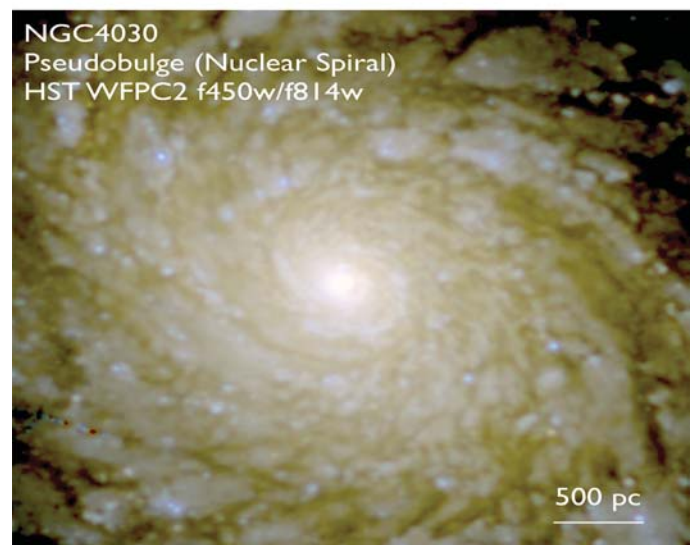


Fig. OP.17: HST two colour images of a typical classical bulge (top panel) and pseudobulge (bottom panel).

work (Longhetti et al. 2007), galaxy sizes increase while dispersions decrease as the Universe ages. Removing younger galaxies from the sample to account for progenitor-bias (Valentinuzzi et al. 2010), a milder evolution still exists. The data suggests that dynamical mass to stellar mass ratios in early-type galaxies increase with time, which implies an increasing contribution of dark matter as a result of size growth. This growth seems to be accelerated in cluster galaxies, with stellar populations ~ 1 Gyr older than the field galaxies (as we also find in Sánchez-Blázquez et al. 2009) suggesting an earlier formation time.

Dwarfs do it their own way: A second Schechter function for low mass galaxies

Our deep, relatively wide area measurement of the stellar mass function of galaxies in the COSMOS field led to the discovery that a double Schechter function is needed to describe the mass function with a second, lower mass component required to describe the number of low mass galaxies (Drory et al. 2009). This imposes a dip at $\sim 10^{10} M_{\odot}$ and steeper slope at lower masses, and is also necessary to describe the individual mass functions of both passive and star forming populations. The challenge is to describe the efficiency of formation and assembly of stars in halos and how this varies with halo mass. We also derive important constraints on galaxy evolution by comparing the expected mass-dependent growth of galaxies from measured star formation with the observed evolution of the mass function (Drory & Alvarez 2008).

Bulgeless and Spherical?

Kormendy & Bender (2012) have produced a revised version of the Hubble sequence, noting that the photometric properties of “spheroidal” galaxies scale in the same way as passive, S0 galaxies. They form a natural extension to low mass of pure-disc galaxies (see Fig. OP.18). This population has been identified with the second Schechter component for passive, low mass galaxies (Drory et al. 2009). We have also quantified the relatively high frequency of pure disc (bulgeless) galaxies in the local Universe (Kormendy, Drory, Bender & Cornell 2010; Fisher & Drory 2011) and compared this with expectations from hierarchical models in Fontanot et al. (2011). The observed high frequency is consistent with the predictions: merger induced bulges are not expected to be ubiquitous, but bulgeless galaxies are predicted to be more common among satellites.

A Dichotomy of enhanced centres and scoured cores in Ellipticals

By compiling a large set of elliptical galaxies in the Virgo cluster with accurate, high-resolution photometric pro-

files from the centre to the outskirts, we confirmed the clear dichotomy in the central properties of elliptical galaxies (Kormendy et al. 2009). Light profiles depart from the inward extrapolation at the centre with some missing light (cores) and some showing excess-light. The former are slow rotating, have anisotropic velocity distributions, boxy isophotes (see Fig. OP.18), their stellar population is old and they appear to be formed in a short time scale, while the latter are rapidly rotating, more isotropic, have disky isophotes, are younger and formed on longer time-scales. Cores can be generated when supermassive black holes scour the centre while orbiting one another during a gas-poor merger of galaxies and excess light can be generated in a gas-rich merger via a central starburst (see section on Supermassive Black Holes).

Stars at the edge: Truncated and anti-truncated outer galactic disks

By fitting accurate photometric profiles, Erwin et al. (2008) recognized that outer galaxy stellar discs fall into three broad categories: single-exponential, truncated, and “anti-truncated” (upward-turning). Surprisingly, in the Virgo cluster there are no S0 discs with truncated profiles, but more single-exponential profiles. This suggests that the mechanism of formation for truncated stellar disc profiles in S0 galaxies does not occur in the Virgo environment (Gutiérrez et al. 2011; Erwin et al. 2012).

Spirals die in groups: The realm of S0s

We discovered that at $z \sim 0.4$ S0s are just as common in groups as in clusters, while they are significantly less common in the lower density field (Wilman et al. 2009). This suggested that the group environment significantly enhances – but is not absolutely required for – the production of passive galaxies with significant discs (Wilman et al. 2008; Poggianti et al. 2008; McGee et al. 2008, 2011; Balogh et al. 2009, 2011; Tyler et al. 2011; Mok et al. 2013). Moving to the local Universe for a more detailed picture, we confirmed that S0s exist either as central galaxies of halos of any mass, or as the satellites of group-mass halos ($M_{\text{halo}} \geq 10^{13} M_{\odot}$) with stellar

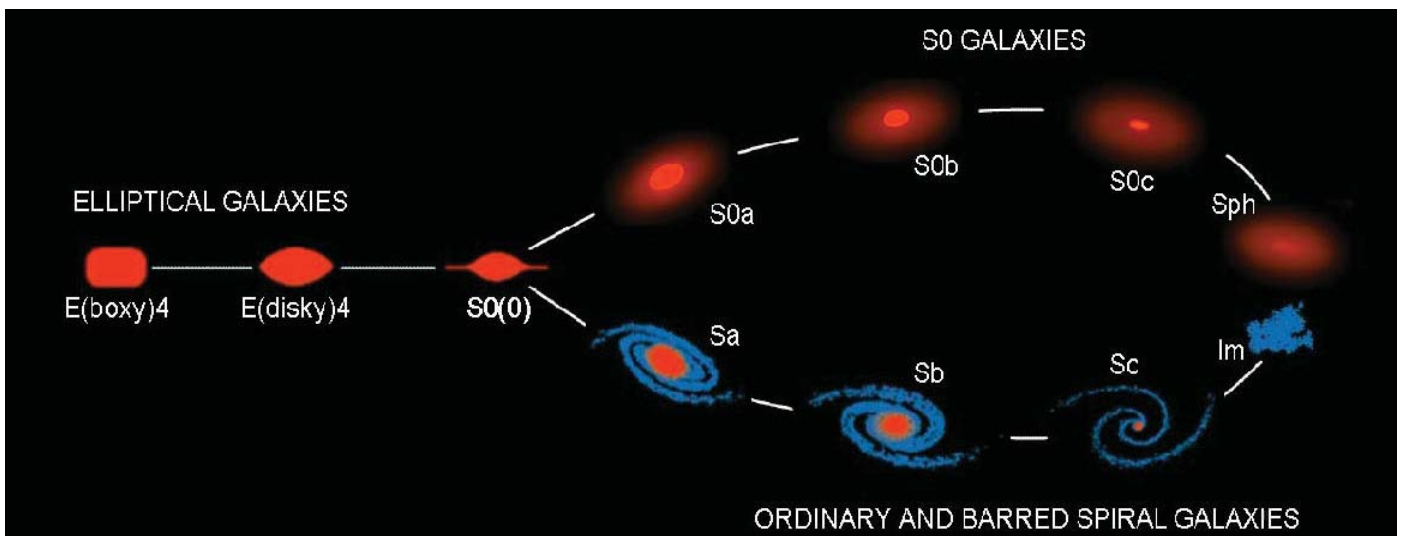


Fig. OP.18: Revised parallel-sequence morphological classification of galaxies. Bulge-to-total ratios decrease toward the right; Sc and S0c galaxies have tiny or no pseudobulges. Sph and Im galaxies are bulgeless (from Kormendy & Bender 2012).

masses $< 10^{11} M_{\odot}$. Their discs are likely quenched by different processes in the two cases (Wilman & Erwin 2012). “Environmental quenching” of low mass galaxies drives the enhanced fraction of quenched, low mass galaxies in groups and clusters with respect to lower density environments at fixed mass.

How big is your Neighbourhood? Quenching and the Multiscale Environment

We have developed the multiscale framework to trace the density field of galaxies as a function of scale. This takes empirical definitions of environment beyond typical single-value measurements and allows us to trace the physical importance of scale. The quenched fraction of galaxies increases with local density, but only on $< 1\text{Mpc}$ scales (Wilman, Zibetti & Budavari 2010). The data can be accurately modelled using a Halo Occupation Distribution (HOD) in which the number of galaxies which are assigned to halos and subhalos is a function of the halo mass M_{halo} , and where the quenched fraction depends only on M_{halo} . This only fits the data if there is a shallow dependence of quenched satellite galaxy fraction on halo mass, illustrating the hierarchical nature of galaxy environment and the quenching of star formation (Phleps et al., submitted).

It's all Hierarchical – Growth of Bulges and Quenching of Massive Galaxies

Evidence is growing that quenching of massive galaxies correlates strongly with the growth of classical bulges. We see that galaxies containing a classical bulge are mostly quenched (Drory & Fisher 2007), and find that sig-

nificant stellar bulge components are common among a large sample of recently quenched galaxies (identified to have little ongoing star formation but a large component of young, A stars, Mendel et al. 2013), consistent with the co-evolution of star formation and structure. Ellipticals form hierarchically via major mergers, producing an increasing fraction with halo mass (for central galaxies, Wilman et al., submitted). But elliptical ($B/T > 0.7$) fractions are overpredicted by two independent hierarchical models, even assuming ellipticals and bulges form only in mergers (from De Lucia et al, 2011) when compared to the fraction of observed, visually classified ellipticals (from Wilman & Erwin 2012) as seen in the left panel of Fig. OP.19. The impact of major mergers may be reduced if tidal stripping of satellite galaxies reduces the mass ratio of mergers and thus the frequency of major mergers. Meanwhile, the observed passive, population of massive central galaxies (star formation rate $\times 100 \text{ Gyr} < \text{stellar mass}$, Fig. OP.19, right panel) is re- (or over-) produced by the models. To successfully reproduce both elliptical and passive fractions, galaxies with $B/T \geq 0.2$ must have their star formation effectively quenched. In models this occurs because energy from the AGN suppresses the cooling flows which otherwise supply the star-forming gas. This only happens in central galaxies with a significant bulge and super-massive black hole, and living in massive halos.

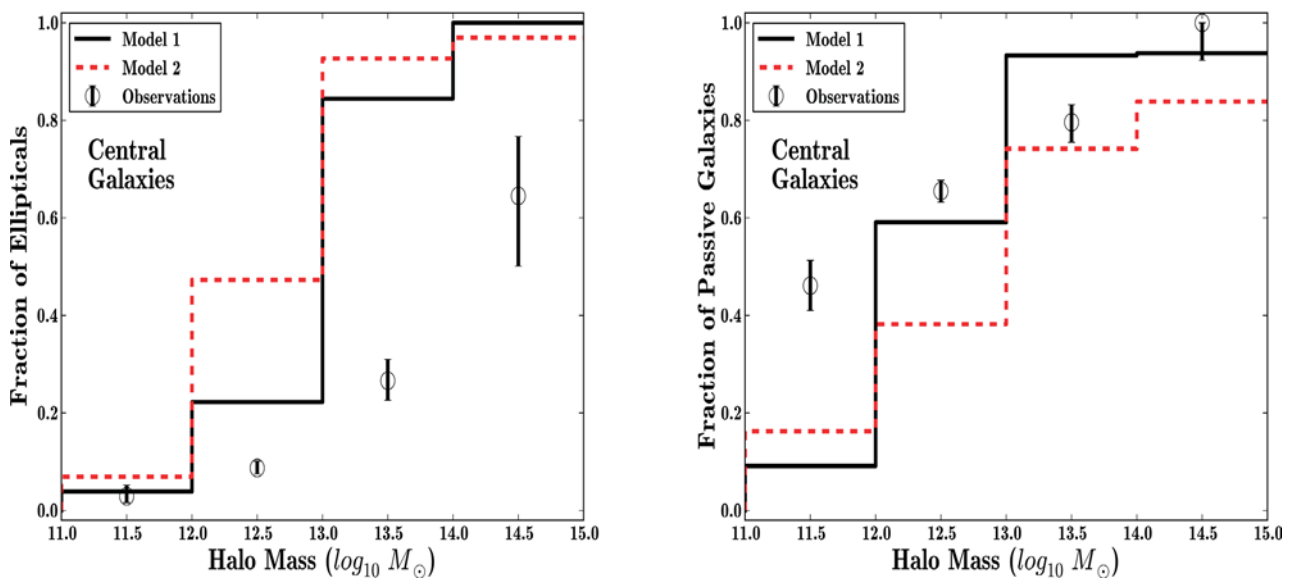


Fig. OP.19: Elliptical (left) and passive ($SSFR \leq 10^{-11} \text{ yr}^{-1}$, right) fraction of $M_{\ast} \geq 10^{10.5} M_{\odot}$ central galaxies, as a function of halo mass. Observed SDSS RC3 fractions are open black points. Data are compared with the fraction of model elliptical ($B/T > 0.7$) and passive central galaxies in two hierarchical formation models in which bulges only form in galaxy mergers (see De Lucia et al. 2011 for a description of the models). From Wilman et al. (submitted).

3.5.1 Understanding Galaxy Growth: the KMOS View

KMOS (K-band Multi Object Spectrograph) is a NIR Multi-Object IFU Spectrograph for the ESO VLT. MPE-OPINAS/USM is a key partner in the consortium along with MPE-IR and the UK (R. Bender was first PI, then co-PI of KMOS). Our group is co-leading large surveys with KMOS focused on the understanding of the processes regulating galaxy growth. Our combination of detailed and statistical studies puts us in an ideal position to take advantage of these surveys.

The unique design of KMOS allows us to obtain two-dimensional spatially-resolved spectra for large samples of galaxies at high redshift by delivering integral field unit (IFU) spectroscopy in *iz*, YJ, H, HK or K-bands (for example, sampling the H α emission line up to $z\sim 2.6$) and ~ 15 km/s spectral resolution with seeing-resolved spatial resolution and 0.2" spaxel size. KMOS samples up to 24 targets simultaneously within a 7.2' diameter field of view. Each robotic arm, with an IFU at the tip, selects a sub-field on the sky of 2.8" x 2.8" and can be positioned anywhere in the field of the VLT focus. The IFU size is well suited to the extent of galaxies at high- z . KMOS is designed with 3 identical spectrographs with a resolving power of ~ 3500 , each with a single 2kx2k Hawaii-2RG HgCdTe detector. Its unique method of target selection using 24 robotic pick-off arms, located in two layers, required we overcome significant technological challenges. OPINAS/USM provided the electronics, instrument control software and observing preparation software. KARMA (KMOS ARM Allocation) is an interactive tool designed to maximise the efficiency of target allocation using the 24 arms, accounting for targets priorities and restricting arms motions to prevent arm collisions and shadowing effects. The full instrument and software was tested here in Munich before delivery to Chile. KMOS

has now been successfully commissioned on the VLT in Paranal (November 2012 – March 2013).

As part of the instrument team, we have 87.5 guaranteed nights which, combined with the 37.5 guaranteed nights from the IR group at MPE, totals 125 nights over 5 years. A large fraction of this time will be used for the KMOS3D survey in collaboration with the IR group, capitalising on the unique multiplexing capability provided by the instrument, to trace star-forming gas using H α emission, and study spatially resolved star formation, nebular excitation, metallicities, and outflow properties for a representative sample of ~ 600 galaxies in deep fields at $z\sim 0.7-2.5$ (see also IR-group report). By studying galaxies at high redshift, we can move to the epoch of galaxy formation characterized by high star formation rates, strongly evolving galaxy sizes and the quenching of massive galaxies.

We are also targeting passive galaxies in both deep fields and high redshift clusters, using absorption features to trace stellar populations and kinematics. KMOS' multiplexing combined with the VLT collecting power will provide stellar velocity dispersions and line strengths for an unprecedented number of galaxies at $z\sim 1.5$. This will allow us to derive dynamical masses and examine the fundamental plane when the Universe was only ~ 4 Gyr old. The near infrared spectra trace rest-frame optical wavelengths, which contains the strongest and best studied absorption features. This yields tracers of stellar content and kinematics which can be compared directly with local galaxies.

Our ultimate goal with KMOS is to combine information on the evolution of mass density within galaxies with our understanding of quenching mechanisms and feedback



Fig. OP.20: KMOS at the VLT Nasmyth B ANTU focus (UT1)

within star forming galaxies. This has to fit into our picture – enhanced through comparisons with models – of how galaxies grow and are quenched in a hierarchical Universe.



Dave Wilman



Alessandra Beifiori

(Other OPINAS team members include Ralf Bender, Jennifer Connelly, Niv Drory, Peter Erwin, Maximilian Fabricius, Natascha Greisel, Ulrich Hopp, John Kormendy, Trevor Mendel, Stefanie Phleps, Roberto Saglia, Stella Seitz and Bernard Muschielok, Reinhold Haefner, Achim Hess, Ivica Ilievski, Helmut Kravcar, Josef Richter, Joerg Schlichter, Christoph Schwab, Michael Wegner)

Selected References:

- Balogh M. L., Wilman D. J., et al. 2007, *MNRAS*, 374, 1169
 Balogh M. L., McGee S. L., Wilman D., et al. 2009, *MNRAS*, 398, 754
 Balogh M. L., McGee S. L., Wilman D. J., et al. 2011, *MNRAS*, 412, 2303
 Barazza F. D., et al. 2009, *A&A*, 497,713
 Bundy K., Scarlata C., Carollo C. M., Ellis R. S., Drory N., et al., 2010, *ApJ*, 719, 1969
 Connelly J. L., Wilman D. J., Finoguenov A., et al. 2012, *ApJ*, 756, 139
 De Lucia, et al. 2007, *MNRAS*, 374, 809
 De Lucia G., Fontanot F., Wilman D., Monaco P. 2011, *MNRAS*, 414, 1439
 De Lucia G., Fontanot F., Wilman D. 2012, *MNRAS*, 419, 1324
 Desai V., et al. 2007, *ApJ*, 660, 1151
 Domínguez-Palmero L., Balcells M., Erwin P., et al. 2008, *A&A* 488, 1167
 Drory N. & Fisher D. B. 2007, *ApJ*, 664, 640
 Drory N. & M. Alvarez 2008, *ApJ*, 680,41
 Drory N., et al. 2009, *ApJ*, 707, 1595
 Elsner F., Feulner G., Hopp U., 2008, *A&A*, 477, 503
 Erwin P., Pohlen M., Beckman J. E., 2008, *AJ*, 135, 20
 Erwin P., Gutiérrez L., & Beckman J. E., 2012, *ApJ*, 744, L11
 Fabricius M. H., Saglia R. P., Fisher D. B., Drory N., Bender R., & Hopp U., 2012, *ApJ*, 754, 67
 Faltenbacher A., Finoguenov A., & Drory N., 2010, *ApJ*, 712, 484
 Feulner G., Goranova Y., Hopp U., Gabasch A., Bender R., Botzler C. S., Drory N., 2007, *MNRAS*, 378, 429
 Finoguenov A., Connelly J. L., Parker L. C., Wilman D. J., Mulchaey J. S., Saglia R. P., et al. 2009, *ApJ*, 704, 564
 Fisher D. B., Drory N., 2008, *AJ*, 136, 773
 Fisher D. B., Drory N., Fabricius M. H., 2009, *ApJ*, 697, 630
 Fisher D. B., Drory N., 2010, *ApJ*, 716, 942
 Fisher D. B., Drory N., 2011, *ApJ*, 733, 47
 Fontanot F., De Lucia G., Wilman D., Monaco P., 2011, *MNRAS*, 416, 409
 Gabasch A., Goranova, Y., Hopp, U., Noll, S., Panella, M. 2008, *MNRAS*, 383, 1319
 Gerssen J., Wilman D. J., et al., 2009, *MNRAS*, 393, L45
 Gerssen J., Wilman D. J., Christensen L. 2012, *MNRAS*, 420, 197
 Greisel N., Seitz S., Drory N., Bender R., Saglia R., Snigula J., 2013, *ApJ*, in press, arXiv:1303.3005
 Gutiérrez L., Erwin P., Aladro R., Beckman J. E., 2011, *AJ*, 142, 145
 Hou A., Parker L. C., Harris W. E., Wilman D. J. 2009, *ApJ*, 702, 1199
 Hou A., Parker L. C., Wilman D. J., et al. 2012, *MNRAS*, 421, 3594
 Jaffé Y. L., Aragón-Salamanca A., De Lucia G., Jablonka P., Rudnick G., Saglia R., & Zaritsky D. 2011, *MNRAS*, 410, 280
 Jaffé Y. L., et al. 2011, *MNRAS*, 417, 1996
 Johansson J., et al. 2013, *MNRAS*, submitted, arXiv: 1211.1386
 Kormendy J., Fisher D. B., Cornell M. E., Bender R. 2009, *ApJS*, 182, 216
 Kormendy J., Drory, N., Bender R., Cornell M. E. 2010, *ApJ*, 723, 54
 Kormendy J. & Bender R. 2012, *ApJS*, 198, 2
 Leaman R. et al., 2013, 767, 131
 Lerchster M., Seitz S., et al. 2011, *MNRAS*, 411, 2667
 Longhetti M., Saracco P., Severgnini O., Della Ceca R., Mannucci F., Bender R., Drory N., et al. 2007, *MNRAS*, 374, 614
 López-Sanjuan C., et al. 2009, *ApJ*, 694, 643
 Marinova I., Jogee S., Weinzirl T., Erwin P., et al. 2012, *ApJ*, 746, 136
 Maraston C., Nieves Colmenárez L., Bender R. & Thomas, D. 2009, *A&A*, 493, 425
 Maraston C., et al. 2013, *MNRAS*, submitted, arXiv: 1207.6114
 Masters K. L., Maraston C., Nichol R. C., Thomas D., Beifiori A., et al. 2011, *MNRAS*, 418, 1055
 McGee S. L., Balogh, M. L., Henderson R. D. E., Wilman D. J., et al. 2008, *MNRAS*, 387, 1605
 McGee S. L., Balogh, Mi. L., Wilman D. J., et al. 2011, *MNRAS*, 413, 996
 Mendel J. T., Simard L., Ellison S. L., Patton D. R. 2013, *MNRAS*, 429, 2212
 Mendel J. T., et al. 2013b, *MNRAS*, submitted
 Milvang-Jensen B., Noll S., Halliday C., Poggianti B. M., Jablonka P., Aragon-Salamanca A., Saglia R. P., Nowak N., et al. 2008, *A&A*, 482, 419
 Mok A., Balogh M. L., McGee S. L., Wilman D. J. et al. 2013, *MNRAS*, 431, 1090
 Muldrew S. I., et al. 2012, *MNRAS*, 419, 2670
 Pannella M., Gabasch A., Goranova Y., Drory N., Hopp U., Noll S., Saglia R. P., Strazzullo V., & Bender R., 2009, *ApJ*, 701, 787
 Pelló, R., et al. 2009, *A&A* 508, 1173
 Phleps S., et al., 2007, *A&A*, 468, 113
 Phleps S., Wilman D. J., et al. 2013, *MNRAS*, submitted
 Poggianti B. M., et al. 2008, *ApJ*, 684, 888
 Poggianti B. M., et al. 2009, *ApJ*, 693, 112
 Prieto M., Eliche-Moral M. C., Balcells M., Cristóbal-Hornillos D., Erwin P., et al. 2013, *MNRAS*, 428, 999
 Rudnick G., et al. 2009, *ApJ*, 700, 1559
 Saglia R. P., Tonry J. L., Bender R., Greisel N., Seitz S., Senger R., Snigula J., Phleps S., Wilman D., et al. 2012, *ApJ*, 746, 128
 Saglia R. P., Sánchez-Blázquez P., Bender R., et al. 2010, *A&A*, 524, A6
 Sánchez-Blázquez P., et al. 2009, *A&A*, 499, 47
 Simard L., et al. 2009, *A&A*, 508, 1141
 Strazzullo V., Pannella M, Owen F.N, Bender R., et al. 2010, *ApJ*, 714,1305
 Strazzullo V., et al. 2010, *A&A*, 524, 17
 Tanaka M., Finoguenov A., Mirkazemi M., Wilman D. J., et al. 2013, *PASJ*, 65, 17
 Thomas D., Steele O., Maraston C., Johansson J., Beifiori A., et al., 2013, *MNRAS*, 431, 1383
 Tyler K. D., Rieke G. H., Wilman D. J., et al. 2011, *ApJ*, 738, 56
 Valentiniuzzi, T., Poggianti, B. M., Saglia, R. P., et al. 2010, *ApJ*, 721, L19
 Vennik J., Hopp U. 2008, *A&A*, 481, 79
 Whiley I. M. et al. 2008, 2008, *MNRAS*, 387, 1253
 Wilman D. J., et al. 2008, *ApJ*, 680, 1009
 Wilman D. J., et al. 2009, *ApJ*, 692, 298
 Wilman D. J., Zibetti S. & Budavári T. 2010, *MNRAS*, 406, 1701
 Wilman D. J. & Erwin P. 2012, *ApJ*, 746, 160
 Wilman D. J., et al. 2013, *MNRAS*, submitted
 Zibetti S., et al. 2007, *ApJ* 659, 161

3.6 Precision Cosmology from Large-Scale Structure Observations

The discovery of the accelerated expansion of the Universe has revolutionized the field of physical cosmology. Understanding the origin of this phenomenon is one of the most challenging problems in physics today. Observations of the large-scale structure (LSS) of the Universe are expected to play a major role in shedding light on this puzzle. For this reason, several new ground-breaking galaxy surveys, such as Pan-STARRS1, BOSS, HETDEX and Euclid, are currently under way. These surveys, in which the MPE OPINAS group has a major involvement, will measure the LSS of the Universe with unprecedented precision, providing new insights not only on the origin of cosmic acceleration, but also on many other important physical parameters. However, the quality of these observations demands the use of accurate models to avoid introducing systematic errors or biases into the obtained constraints. We develop and apply novel models and techniques to extract cosmological information from these new LSS datasets, helping to ensure that their full scientific potential is realised.

Dark energy and the large-scale structure of the Universe

One of the most significant scientific discoveries of recent years is that our Universe is not only expanding, but that it is doing so at an increasing rate. In the context of general relativity, this phenomenon implies that the total energy-density of the Universe is dominated by an exotic component, dubbed dark energy, whose repulsive effect drives the acceleration of cosmic expansion. A key property that can be used to characterize this component is the dark energy equation of state, $w_{\text{DE}} = p_{\text{DE}}/\rho_{\text{DE}}$, where p_{DE} and ρ_{DE} correspond to the pressure and density of dark energy, respectively. Current observations are consistent with the so-called Λ CDM cosmological model, in which dark energy can be characterized by a constant equation of state $w_{\text{DE}} = -1$, equivalent to Einstein's cosmological constant. A detection of a deviation from this value, at any time in cosmic history, would have strong implications for our understanding of cosmic acceleration.

The first step into solving the mystery of cosmic acceleration is to obtain accurate measurements of the expansion history of the Universe. Observations of the large-scale clustering of galaxies can provide us with such measurements. Galaxies form a variety of structures that encode valuable cosmological information. This clustering pattern is usually characterized in terms of two-point statistics such as the correlation function, $\xi(s)$, or its Fourier transform, the power spectrum, $P(k)$. These measurements have played a central role in establishing the current standard cosmological model, and it is expected that they will continue to do so in the coming years.

A special feature of large-scale galaxy clustering provides a powerful method to probe the expansion history

of the Universe: the signal of the baryon acoustic oscillations (BAO). These are fluctuations in the density field caused by acoustic waves that propagated through the photon-baryon fluid prior to recombination. The signature from these waves is imprinted in the galaxy distribution, where it appears as a broad peak in the two-point correlation function. In the power spectrum, the BAO signal can be seen as a small oscillatory amplitude modulation. The position of the peak in $\xi(s)$ and the wavelength of the oscillations in $P(k)$ are closely related to a particular scale, called sound horizon, of about 150 comoving Mpc. As the same physical scale can be measured to high accuracy from observations of the cosmic microwave background (CMB), the BAO signal inferred from galaxy clustering measurements can be used as a standard ruler. The apparent size of the BAO ruler in the directions parallel and perpendicular to the line-of-sight can be used to measure the redshift evolution of the Hubble parameter, $H(z)$, and the angular diameter distance, $D_A(z)$, which depend on the equation of state of dark energy. However, when dealing with angle-averaged measurements such as $\xi(s)$ or $P(k)$, the BAO signal is only sensitive to an average distance, $D_V(z) \propto (D_A(z)^2/H(z))^{1/3}$. Thanks to the BAO, galaxy clustering measurements offer one of the most promising routes to obtain accurate constraints on w_{DE} and its possible evolution with time.

Driven by the potential of LSS observations for shedding light on the nature of dark energy, the size and quality of galaxy redshift surveys has increased dramatically. A new generation of galaxy surveys is currently being constructed or designed. Our group has a major involvement in some of the most exciting examples of these new surveys, including the on-going Baryon Oscillation Spectroscopic Survey (BOSS), which is a part of SDSS-III, and future surveys such as SDSS-IV, the Hobby-Eberly Telescope Dark Energy Experiment (HETDEX) or the ESA space mission Euclid. By probing larger volumes, these surveys will deliver views of the large-scale galaxy clustering pattern with greater accuracy than ever before.

The data corresponding to the first two years of observations of BOSS have been released to the community as part of the SDSS Data Release 9 (DR9). Even though this sample corresponds to about one third of the final survey, it is already the largest galaxy catalogue available, making it ideally suited for large-scale structure analyses. Our group has been heavily involved in the analysis of galaxy clustering measurements based on this dataset, which have shown clear detections of the BAO feature. The red circles in the left-hand panel of Fig. OP.21 correspond to the measurement of the correlation function of the CMASS galaxy sample of BOSS-DR9 (Sánchez et al. 2012). The BAO signal can be clearly seen as a broad bump on large scales.

Galaxy surveys contain more information than what can be extracted from angle-averaged measurements. With

this in mind, we proposed a new statistical tool, called clustering wedges, $\xi_{\parallel}(s)$ and $\xi_{\perp}(s)$ (Kazin, Sánchez & Blanton 2012). These functions contain the same information as the correlation function, but for structures primarily aligned in the directions parallel and perpendicular to the line-of-sight, respectively. In this way, they provide separate constraints on $H(z)$ and $D_A(z)$, increasing the constraining power of the BAO test. The right-hand panel of Fig. OP.21 shows the measurements of the clustering wedges of the BOSS-DR9 sample (Sánchez et al. 2013, Kazin et al. 2013). The BAO peak appears in both clustering wedges. The information from the full shape of these measurements can be used to obtain tight constraints on cosmological parameters.

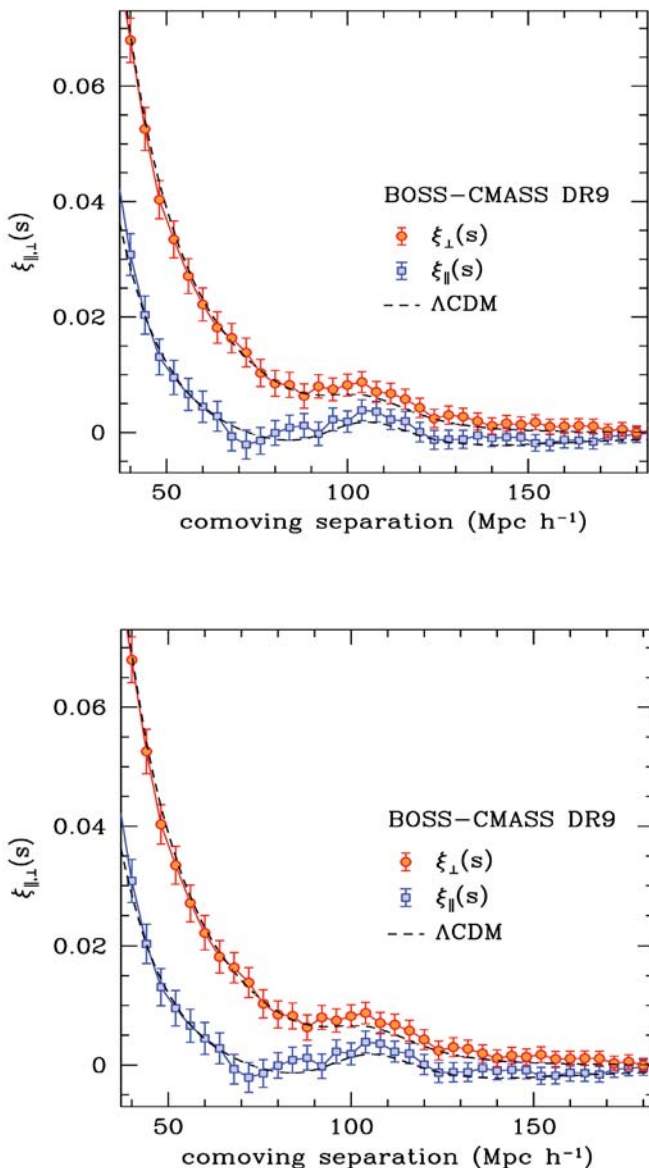


Fig. OP.21: Two-point correlation function (left panel) and clustering wedges (right panel) of the CMASS sample of BOSS DR9 (Sánchez et al. 2012, 2013). These functions characterize the large-scale clustering properties of this galaxy sample. The signature of the BAO can be seen as broad peaks on all these measurements. The dashed lines correspond to the predictions of the Λ CDM model, which gives an excellent description of these results.

Modelling large-scale structure observations

The increase in the amount and quality of the observational data in recent years led to a drastic reduction in the statistical errors of LSS measurements. This data revolution poses a challenge for our theoretical understanding and modelling of these observations. As the statistical errors decrease, the control of the systematic errors introduced by our analysis techniques becomes crucial as these can dominate the final error budget. Thanks to the analysis of large-volume N-body simulations, we have helped to show that, even on large scales, LSS observations are distorted by a number of scale-dependent effects, such as the non-linear evolution of density fluctuations, redshift-space distortions and galaxy bias (Sánchez et al. 2008). If not taken into accurately accounted for, these distortions might jeopardise the use of LSS measurements as precision cosmological probes.

Much theoretical work has been devoted to improving the modelling of the clustering signal measured in galaxy surveys. Based on new developments in perturbation theory, we have developed and tested new models and parameterizations of LSS statistics (Sánchez et al. 2008; Montesano et al. 2010). These models give an accurate description of the results from N-body simulations and mock catalogues at various redshifts and provide us with robust methods to extract unbiased cosmological constraints from large-scale clustering measurements. By adopting a perturbation-theory based model in the mildly non-linear regime, we are able to exploit the information in the full shape of two-point clustering measurements, beyond that in the scale of the BAO peak alone.

We used these new methods to explore the cosmological implications of galaxy clustering measurements from SDSS-II and BOSS, combining this information with recent CMB, Type Ia supernova (SN), and additional BAO measurements from other surveys (Sánchez et al. 2009, 2012, 2013; Montesano et al. 2012; Anderson et al. 2012, 2013; Kazin et al. 2013). An example of the obtained results can be seen in Fig. OP.22, which shows the joint constraints on the matter density parameter, Ω_m , and the dark energy equation of state, w_{DE} , obtained from different dataset combinations. The CMB-only results (blue contours) exhibit a strong degeneracy that extends beyond the boundaries of the plot, covering a wide range of values of w_{DE} . The grey contours show the effect of including the information of the BOSS-CMASS $\xi(s)$ in the analysis. The constraints on $D_V(z)$ provided by this measurement partially break the degeneracy obtained from the CMB observations, tightening the constraints on the dark energy equation of state. The red contours correspond to the results obtained when the information from $\xi(s)$ is replaced by that of the clustering wedges of the same sample, which provide separate constraints on $H(z)$ and $D_A(z)$. This information is much more efficient at breaking the CMB degeneracy than the average distance obtained from $\xi(s)$, leading to a significant improvement of the obtained constraints. The green contours show the effect of also including additional BAO and SN data

in the analysis, which leads to a final constraint of $w_{DE} = -1.02 \pm 0.06$, in excellent agreement with a cosmological constant (Sánchez et al. 2012, 2013).

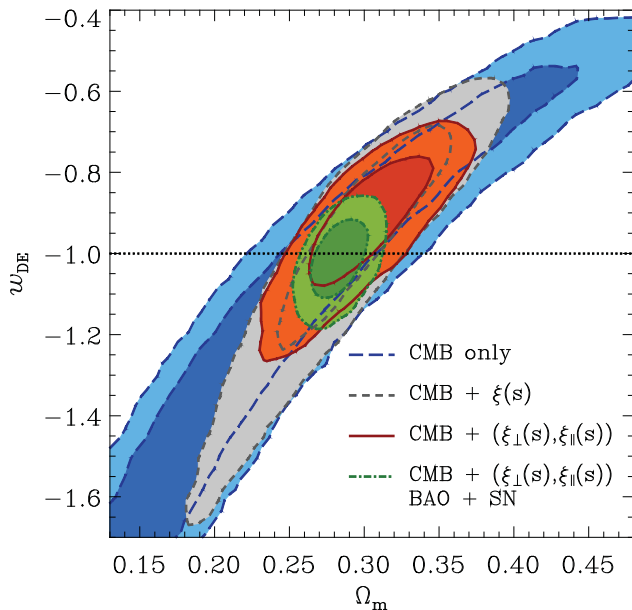


Fig. OP.22: Joint 1σ and 2σ constraints on the matter density parameter, Ω_m , and the dark energy equation of state parameter, w_{DE} . The different sets of contours correspond to the results obtained using different combinations of datasets: CMB information alone (blue lines), CMB combined with the BOSS two-point correlation function (grey lines), CMB combined with the BOSS clustering wedges (red lines), and when this last combination is extended by including additional BAO and SN datasets (green lines). The final constraints are in good agreement with the Λ CDM model value of $w_{DE} = -1$, shown by the dotted line (Sánchez et al. 2013).

Although effects such as non-linear evolution and redshift-space distortions can be modelled and included in the theoretical description of a given measurement, the degradation of the BAO signal they produce decreases the achievable accuracy. A complementary approach is to apply corrections to the galaxy positions prior to the estimation of any clustering statistic to reduce the impact of these systematic effects. This is the general idea behind the so-called “reconstruction” techniques.

The dominant sources of the degradation of the BAO feature are the coherent flows that arise from the clustering pattern itself. This means that the same galaxy sample used to detect the BAO feature can also map the cosmic structure responsible for its degradation. One can therefore use these data to infer the large-scale flow field and partially undo the distortion of the BAO feature, restoring the information lost by these processes. In general however, this reconstruction will not be perfect and residual non-linearities must be taken into account by means of accurate models. We are currently working on the combination of these two approaches, reconstruction techniques and accurate modelling of non-linearities, which hold the key to maximizing the constraining power of LSS observations.

Linking light and matter

As galaxies are biased tracers of the underlying dark matter density field, the observed clustering of galaxies can be quite different from the theoretically predicted clustering of dark matter or dark matter haloes. A precise characterization of the relation between the distribution of galaxies and dark matter is crucial when galaxy clustering measurements are used to constrain cosmological parameters.

The size of present-day galaxy surveys allows for studies of sub-samples defined as a function of properties such as colour, luminosity, star formation rate, etc. with a high signal-to-noise ratio. We have carried out several investigations of the clustering properties of sub-samples defined in this way in order to measure their relative bias based on spectroscopic data from the VVDS and zCosmos surveys (Meneux et al. 2008, 2009). Besides characterizing the relation between the galaxy and matter distributions, these results also offer important clues on the physical processes that govern the formation and evolution of galaxies.

The bias of a given galaxy population depends on the way in which they populate dark matter halos of different masses. This can be characterized by means of halo occupation distribution (HOD) models. For a given cosmology, the HOD can be inferred by comparing the observed galaxy clustering with that of dark matter haloes in N-body simulations (Nuza et al. 2012). Alternatively, the parameters characterizing the HOD can be fitted for directly from galaxy clustering measurements. We are currently using correlation functions of different galaxy types in independent redshift bins up to $z = 1$ derived from Pan-STARRS1 data to determine the typical dark matter halo masses in which these galaxies live (Phleps et al. in prep).

Future galaxy surveys: SDSS-IV, HETDEX and Euclid

The tendency to build increasingly large galaxy surveys will continue into the future, with MPE playing a leading role in some of the most promising galaxy surveys of the coming years, such as SDSS-IV, HETDEX and Euclid.

The legacy of BOSS will be continued by eBOSS, a part of SDSS-IV that will target emission line galaxies (ELG) to fill in the redshift gap between the galaxy and quasar samples of BOSS. This new sample will then allow us to obtain BAO distance measurements in the full redshift range $0.1 < z < 3$.

HETDEX (Hill et al. 2004, AIPC, 743, 224) will map the three-dimensional positions for 0.8 million Lyman- α emitting (LAE) galaxies at $1.9 < z < 3.6$ over an area of 420 deg^2 , covering a volume of 9 Gpc^3 . This sample will provide us with a powerful window into the growth of structure and expansion history of the universe at high redshift, reaching sufficient precision in $H(z)$ and $D_A(z)$ to directly detect the presence of dark energy at $z \sim 3$ at 3σ . HETDEX will also provide competitive constraints on

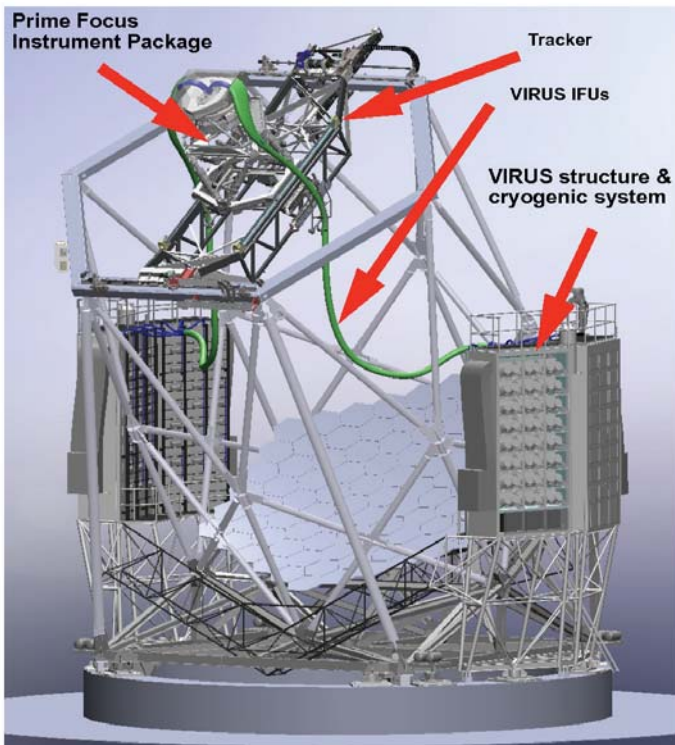


Fig. OP.23: The upgraded 10m Hobby-Eberly Telescope with the new prime focus assembly. The tracker allows the instruments to follow the objects across the sky during the exposure. 20 m long fiber bundles (green) transport the light from the prime focus to the 150 VIRUS spectrographs which are mounted on a co-rotating frame on the side of the telescope.

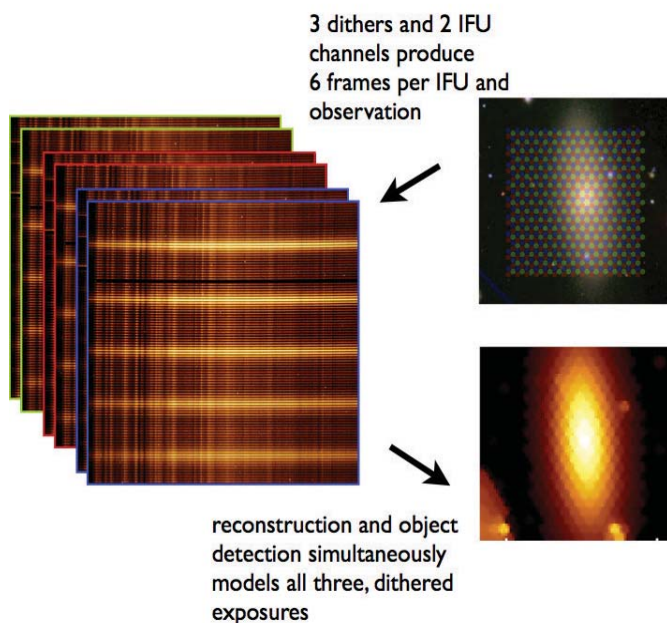


Fig. OP.24: Raw HETDEX-like data from our simulation pipeline and reconstructed image of a galaxy. The fiber-based IFUs of VIRUS have a 1/3 fill factor. Three dithers are needed to cover the sky completely. Each observation therefore produces a number of frames which need to be combined using a Bayesian approach for faint object detection. Cure-WISE will automatically run the reduction and object detection for the 75 IFUs and ~4000 individual HETDEX observations.

the total neutrino mass (from small scale clustering) and on inflationary models (from the clustering on the largest scales). Our group leads the data analysis software development and survey scheduling (Gössl et al. 2007; Snigula et al. 2012) and is contributing to the hardware of VIRUS.

The primary survey instrument of HETDEX is the VIRUS spectrograph (Hill et al. 2010, 2012), an array of 75 integral-field spectrographs on the 10m Hobby-Eberly Telescope (see Fig. OP.23). Each IFU spectrograph will cover 3500-5500Å at ~5Å resolution, sampling 50" × 50" using 448 fibres on the sky. The 75 IFUs are distributed within a 22' field. The footprint of HETDEX will be surveyed blindly by this instrument during 3 years starting in early 2014, with a likely 2 year extension. Our group has participated in the construction of a prototype of the VIRUS unit spectrograph (VIRUS-P; Hill et al. 2008), which is operating on the McDonald 2.7 m since 2007. VIRUS-P has been used for a pilot survey to better characterize the properties of LAEs in support of HETDEX and to develop and test data reduction procedures (Adams et al. 2011; Blanc et al. 2011; Finkelstein et al. 2011). Furthermore, we made contributions to the VIRUS calibration unit and the purchasing of fibers.

Our largest contribution to HETDEX however lies in the development of the data analysis system. HETDEX will deliver a massive amount of information during its operation: it is expected that more than 35000 individual FITS images will be produced on a typical night of observations. To accomplish the challenging task of analysing this volume of data, we developed the CURE pipeline within the Astro-WISE system (Astronomical Wide-field Imaging System for Europe). The Cure-WISE pipeline will provide automated object detection, flux and redshift measurements for HETDEX (see Fig. OP.24). First tests with mock HETDEX data show that CURE will be able to reduce the observations in real time (Snigula et al. 2012).

The ability to calibrate the instrument swiftly at multiple times during a night is critical to our ability to detect faint emission line sources. This requires frequent calibrations of the spectrograph. To minimize the impact of repeated calibrations on the survey efficiency we developed a dedicated Facility Calibration Unit (FCU) (Lee et al. 2012; Hill et al. 2012). This device provides ten different spectral-calibration lamps and a tuneable flat field unit: an array of 16 different LEDs that can be adjusted in power output to provide almost constant signal over the whole spectral range from 3500-5500Å, eliminating the problem of strongly varying flux levels as function of wavelength of traditional light sources.

On a longer time scale, the ESA Euclid satellite will combine imaging and spectroscopic information optimized for two complementary cosmological probes, weak lensing and BAO measurements, in the most ambitious attempt so far at explaining the origin of cosmic acceleration. Euclid will be described in some detail in Section 3.8 below.

Outlook

Current galaxy clustering measurements can place strong cosmological constraints. So far, all results are completely consistent with the standard Λ CDM model. This is illustrated in Fig. OP.21 where the dashed lines correspond to the predictions of this model, which give an excellent description of the clustering measurements in BOSS DR9. Subsequent data releases from BOSS and future galaxy surveys such as SDSS-IV, HETDEX and Euclid will deliver even more accurate views of the large-scale clustering pattern in the Universe. With MPE's involvement in these new surveys, we are in an ideal position to fully participate in the science exploitation of these datasets. By means of precise theoretical models and techniques, we will use these data to derive new, more stringent constraints on cosmological parameters, putting the Λ CDM model to a much more rigorous test.



Ariel Sanchez, Stefanie Phleps, Max Fabricius

(Other OPINAS team members include Andres Balaguera-Antolinez, Ralf Bender, Yi-Hao Chen, Niv Drory, Claus Gössl, Jan Grieb, Marco Haeuser, Ulrich Hopp, Martin Landriau, Baptiste Meneux, Francesco Montesano, Roberto Saglia, Salvador Salazar, Holger Schlagenhauer, Jan Snigula, Jochen Weller and Philipp Wullstein)

Selected References:

- Adams J. J., Blanc G. A., Hill G. J., et al., 2011, *ApJS*, 192, 5
 Anderson L., Aubourg E., Bailey S., et al., 2012, *MNRAS*, 427, 3435.
 Anderson, L.; Aubourg, E.; Bailey, S., et al., 2013, submitted to *MNRAS* (arXiv1303.4666).
 Balaguera-Antolínez A., Sánchez A.G., Böhringer H., Collins C., Guzzo L., Phleps S., 2011, *MNRAS*, 413, 386.
 Balaguera-Antolínez A., Sánchez A.G., Böhringer H., Collins C., 2012, *MNRAS*, 425, 2244.
 Barreira, A., Baojiu L., Sánchez A.G., Baugh C.M., Pascoli S., 2013, submitted to *MNRAS* (arXiv1302.6241).
 Blanc G. A., Adams J. J., Gebhardt K., et al., 2011, *ApJ*, 736, 31
 Chuang C., Prada F., Cuesta A., et al., 2013, submitted to *MNRAS* (arXiv1303.4396).
 Finkelstein S. L., Hill G. J., Gebhardt K., et al., 2011, *ApJ*, 729, 140
 Gössl C. A., Hopp U., Köhler R., et al., 2007, *ASPC*, 376, 281
 Hill G.J., MacQueen P. J., Smith M. P., et al., 2008, *SPIE*, 7014
 Hill G.J., Lee H., Vattiat B. L., et al., 2010, *SPIE*, 7735
 Hill G.J., Tuttle S. E., Lee H., et al., 2012, *SPIE*, 8446
 Hill G. J., Booth J. A., Cornell M. E., et al., 2012, *SPIE*, 8444
 Kazin E., Sánchez A.G., Blanton A., 2012, *MNRAS*, 419, 3223.
 Kazin, E., Sánchez, A.G., Cuesta A., et al., 2013, submitted to *MNRAS* (arXiv1303.4391).
 Lee H., Hill G. J., Vattiat B. L., Smith M. P., Haeuser M., 2012, *SPIE*, 8444
 Manera M., Scoccimarro R., Percival W., et al., 2012, *MNRAS*, 428, 1036
 Meneux B., Guzzo L., Garilli B., et al. 2008, *A&A*, 478, 299.
 Meneux B., Guzzo L., de la Torre S., et al. 2009, *A&A*, 505, 463.
 Montesano F., Sánchez A.G., Phleps S., 2010, *MNRAS*, 408, 2397.
 Montesano F., Sánchez A.G., Phleps S., 2012, *MNRAS*, 421, 2656.
 Nuza S., Sánchez A.G., Prada F., et al. 2013, *MNRAS in press* (arXiv1202.6057).
 Ross A., Percival W., Sánchez A.G., et al., 2012, *MNRAS*, 424, 564.
 Saglia R.P., Tonry J.L., Bender R., et al., 2012, *ApJ*, 746, 128.
 Sánchez A.G., Cole S., 2008, *MNRAS*, 385, 830.
 Sánchez A.G., Baugh C.M., Angulo R., 2008, *MNRAS*, 390, 1470.
 Sánchez A.G., Crocce M., Cabré A., Baugh C.M., Gaztañaga E., 2009, *MNRAS*, 400, 1643.
 Sánchez A.G. Scóccola C., Ross A.J., et al., 2012, *MNRAS*, 425, 415.
 Sánchez A.G., Kazin E., Beutler F., et al., 2013, submitted to *MNRAS* (arXiv1303.4486).
 Schlagenhauer H., Phleps S., Sánchez A.G., 2012, *MNRAS*, 425, 2099
 Scóccola C., Sánchez A.G., Rubiño-Martin, J. A., et al., 2012, submitted to *MNRAS* (arXiv1209.1394)
 Snigula J. M., Cornell M. E., Drory N., Fabricius M., Landriau M., Hill G. J., Gebhardt K., 2012, *SPIE*, 8451

3.7 Machos, Stars and Planets

The search for a possible baryonic constituent of dark matter halos around galaxies, the so-called ‘Machos’ (massive compact halo objects), motivated our efforts in time-domain studies. The microlensing effect provides the only possibility to find such invisible MACHOs by monitoring the light curves of distant stars which brighten in a characteristic way when lensed. Since a decade, we are one of the leading groups in monitoring the disk and bulge regions of the Andromeda Galaxy. We developed techniques for very precise measurements of faint light variations close to the noise level. The same techniques are used to study variable stars (like Cepheids) or eclipsing binaries, and to search for planets. During the last 6 years we expanded our activities in time domain astrophysics by participating in several large projects which investigated stellar objects in the Milky Way and the Andromeda Galaxy (M31). Our involvement in the Pan-STARRS Survey (Pan-Planets and PAndromeda) and the ‘Rocky Planets Around Cool Stars’ project (RoPACS), as well as the guaranteed access to high resolution spectrographs on the northern and southern hemisphere, enabled us to detect several micro-lensing events M31, study variable stars and eclipsing binaries in the Milky Way and our neighboring galaxies M31 and M32, and search for extra-solar planets in different environments (the Galactic Disk, the open cluster M67 and the globular cluster M71).

Microlensing in M31: Microlensing surveys toward Local Group galaxies have the prospect to measure the amount of act dark matter (Machos) in these halos independent of the baryonic or non-baryonic nature of Machos. So far observations on the LMC and SMC by the EROS, MACHO and OGLE collaborations yielded around 20 candidates compatible with gravitational lensing by Machos or with self lensing (lensing of stars by stars). These numbers are yet too small to allow to derive precise halo fractions beyond just yielding upper limits, e.g. of order 20% for the M31 galaxy (see overview by Calchi Novati, 2012, JPhCS, 354a, 2001).

Our PAndromeda survey was designed to identify microlensing events toward M31 with high-cadence observations (20 min per night) using the 1.8m Pan-STARRS 1 telescope on Haleakala (Maui, Hawaii) with its large 7 deg² field-of-view. From July 2009 till October 2012 we monitored the entire disk of M31 with close to daily sampling (just limited by weather) for up to 5 months per year. In a first analysis of 91 nights from the 2010 season (Lee et al. 2012a) we studied six 20' x 20' sub-fields including the central region of M31 and detected six candidate microlensing events in the central 40' x 40' region of M31 (see Fig. OP.25 and Fig. OP.26). This is a very promising rate compared to previous M31 microlensing surveys.

The identification of four short-duration microlensing events with $t_{\text{FWHM}} \sim 1\text{--}3$ days shows that the time resolution of the PAndromeda project is comparable with the best two seasons of the WeCAPP project (where two tel-

escopes were coordinated to monitor M31, see Riffeser et al. 2001, 2003). We are currently analyzing the full data set (4453 frames of in total 22.4 TeraBytes) of all three PAndromeda seasons. An excess in the measured lensing rate or an incompatible spatial distribution rela-

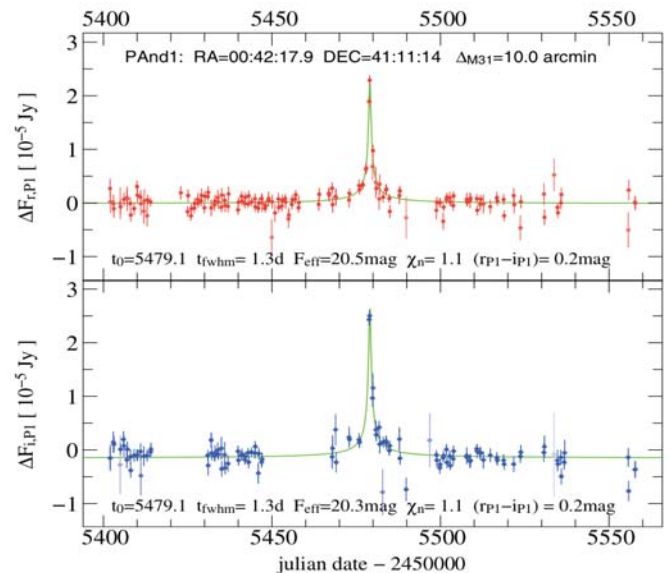


Fig. OP.25 - Light curves of the PAnd-1 microlensing event. red dots: r_{PS1} -band, blue dots: i_{PS2} -band, grey: difference image postage stamps.

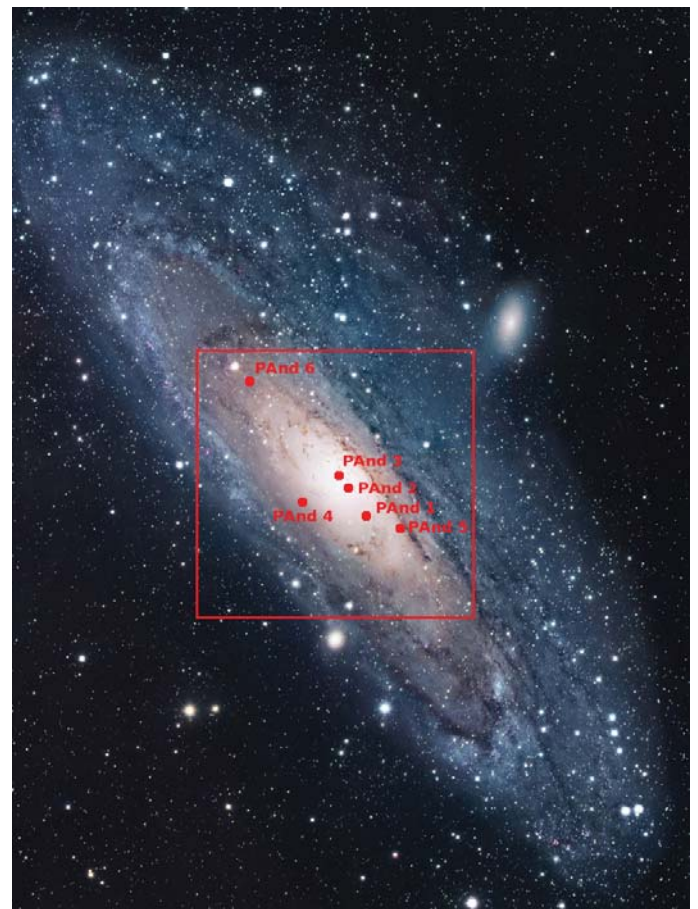


Fig. OP.26 - Position of the six microlensing event candidates detected in the central 40' x 40' region of M31 from PAndromeda.

tive to the pure self-lensing rate will point to Macho lensing in the halo of M31 (see our theoretical work in Riffeser et al. 2006). Observational studies of the dynamics of the M31 bulge (see Saglia et al. 2010 and Opitsch et al., 2013) help to quantify the bulge–bulge self-lensing contribution at a better level (see also the “Galaxy Structure” contribution in section 3.3).

Variable stars in M31: In the context of the PAndromeda project we also study the stellar population properties of M31. We have carried out similar analyses before in the WeCAPP project (see Fliri et al. 2006 and Lee et al. 2012b). In a recent publication, we presented 2009 Cepheids, the largest sample in M31 published so far (Kodric et al. 2013). As can be seen in Fig. OP.27, the Population I Cepheids nicely trace the dust pattern of the M31 disk, whereas the Type II Cepheids are distributed throughout the halo of M31. Fig. OP.28 shows the Period-Luminosity-Relation (PLR) for the three Cepheid populations. A comparison to previously published PLRs indicates a curvature term in the wavelength dependency of the PLR. By transforming the period measurements into stellar ages we find a radial age gradient within the previously detected ring of star formation at 10kpc. We identify and study eclipsing binaries in order to measure the physical properties of the involved stars and to obtain a sample that can be used for M31 distance measurements. Using a modified box-fitting algorithm we detected more than 300 detached and semi-detached eclipsing binary systems of which 36 are brighter than $V=20$ mag and thus suitable for spectroscopic follow-up and determination of the distance to M31 (Lee et al. 2013). We also work on other types of variable stars, e.g. LBVs, LPVs and novae.

Planets in the Galactic Disk: Pan-Planets. Within the Pan-STARRS 1 survey, we are also co-leading the Pan-Planets project which is a search for transiting extra-solar

planets in the Galactic Disk. The survey is a collaboration between the Max Planck Institute for extraterrestrial Physics (MPE), the Max Planck Institute for Astronomy (MPIA) and the Pan-STARRS Science Consortium. With Pan-Planets we study the frequency of Jupiter-sized planets around M-dwarfs increasing the number of target stars by an order of magnitude compared to the WTS survey at ULIRT (see below). In addition, Pan-Planets opens up a new research field, the detection of planets

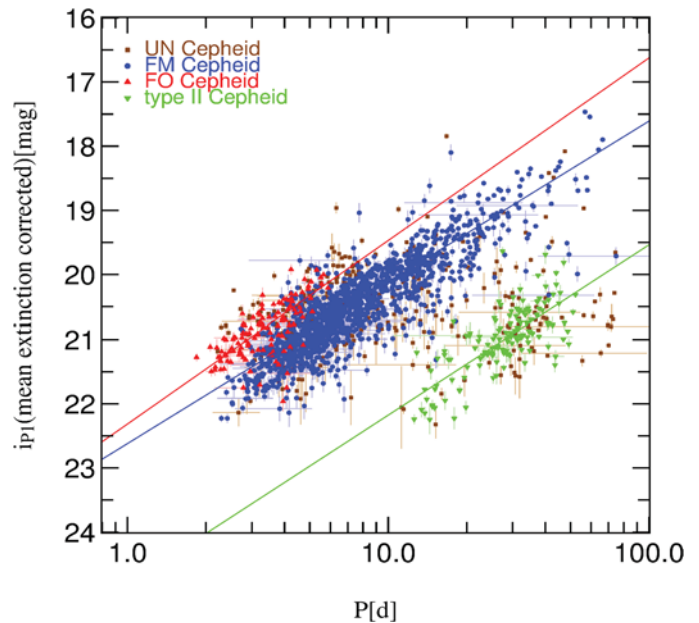


Fig. OP.28: Period–apparent-magnitude relation in the i_{p_1} -band

around white dwarfs in short orbits. Such systems would show very deep but extremely short eclipses (\sim few minutes only). With a high number of white dwarfs in the Pan-Planets target sample (\sim 5.000) the survey has the potential to detect such systems if they exist. During the period 2009–2012 we observed \sim 50.000 M-dwarfs down to 18th I-band magnitude in seven slightly overlapping fields (\sim 40 sq.deg.). The survey strategy has been optimized using Monte-Carlo simulations (Koppenhoefer et al. 2009). We developed the Munich Difference Imaging Analysis tool (Koppenhoefer et al. 2013) which we use to create high precision light curves for 4 million sources in the Pan-Planets fields. So far, we have analyzed \sim 25% of the whole Pan-Planets data set. We detected a few planet candidates around M-dwarfs. In addition, we found a good candidate around a 15th magnitude late-F type star which is currently being followed-up with high resolution spectroscopy at the Hobby-Eberly-Telescope. Fig. OP.29 shows the phase-folded light curve together with the best fitting transit model.

Planets in the Galactic Disk: The RoPACS project. The Rocky Planets Around Cool Stars project is an Initial Training Network of the FP7 Marie-Curie Program of the European Community. Based on the J-band light curves collected during the Widefield Transit Survey (WTS) at UKIRT, we searched for planets using the transit method, aiming to maximize the chances to find candidate plan-

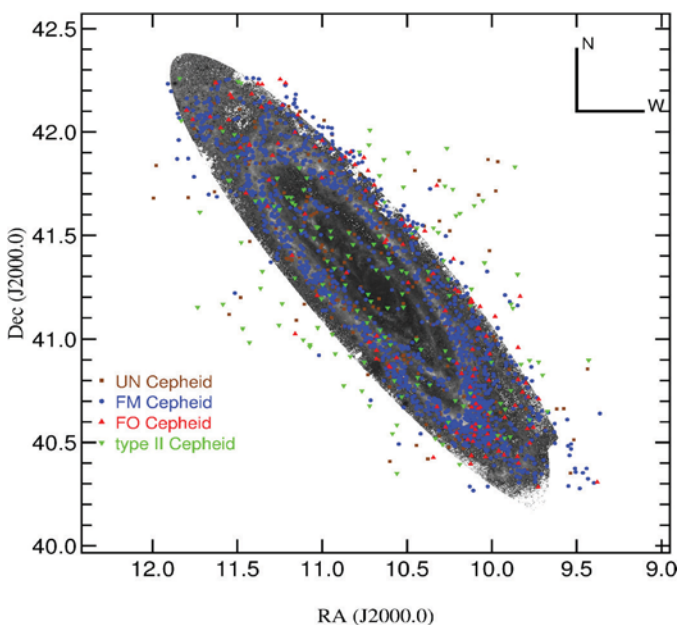


Fig. OP.27: Positions of the PAndromeda fundamental mode (blue), first overtone (red) and Type II Cepheids (green), plotted over the $E(B-V)$ map of Montalto et al. (2010).

ets around cool (M-dwarf) stars. We followed up our best candidates spectroscopically with the Hobby-Eberly Telescope, confirming two planets, both of them (very) hot Jupiters orbiting an F7V and an K2V star respectively (see Cappetta et al. 2012 and Birkby et al. 2013). WTS-1b has one of the largest radius anomalies among the known hot Jupiters in the mass range 3-5 MJ. We show its phased light and radial velocity curves in Fig. OP.30.

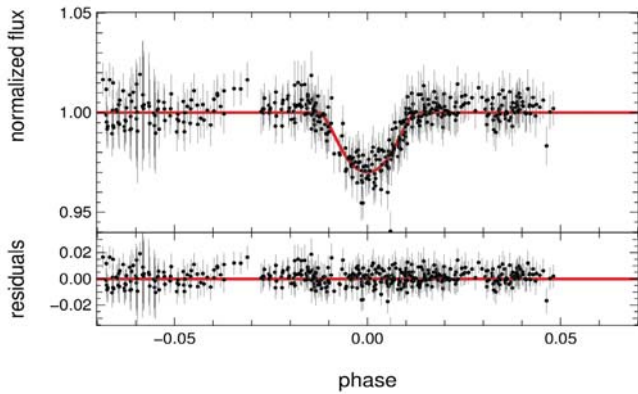


Fig. OP.29: Phase-folded light curve of a $1.7 R_{Jup}$ candidate orbiting a late-F star in the PanPlanets field.

WTS-2b is unusually close to its star, at just 1.5 times the distance at which it would be destroyed by Roche lobe overflow, with a predicted lifetime of just ~ 38 Myr. In contrast, we did not find any hot Jupiter around M-dwarfs, our prime target population. This allowed us to set up an upper limit (1.7-2% at 95% confidence) to the fraction of M-dwarfs brighter than 17 J mag hosting Jupiter-like planets on orbits with periods shorter than 10 days (Kovacs et al. 2013). This is twice as tight as the Kepler constraint and goes towards discriminating between the two available competing formation theories. While the core accretion scenario is not able to form Ju-

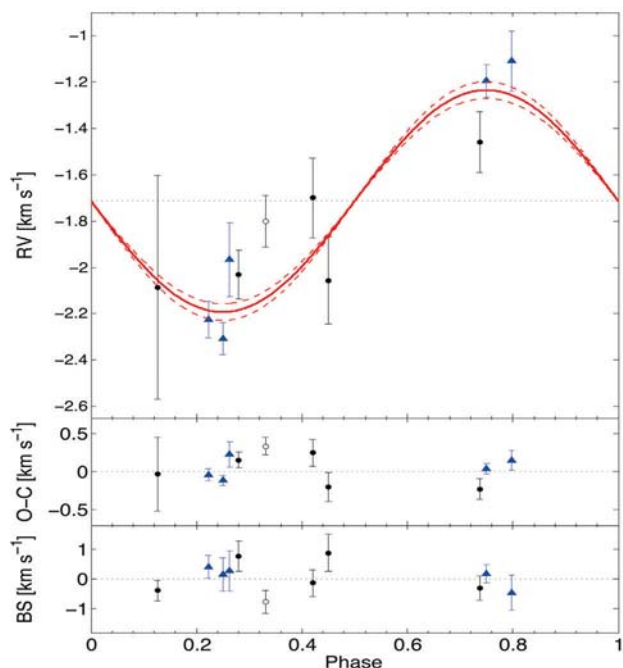
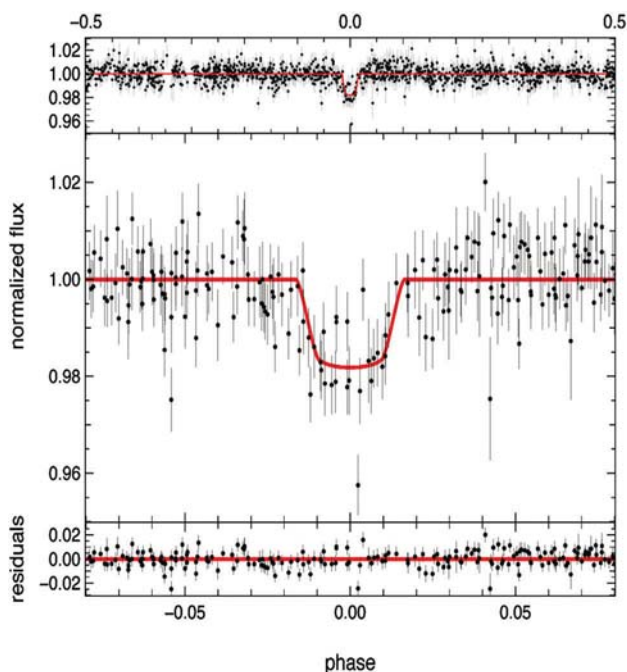


Fig. OP.30: The light (left) and radial velocity (right) curves of WTS1-b.

piters around M-dwarfs, the gravitational instability is a possible formation channel. Furthermore, we pushed the analysis of the light curves to J=18 mag using difference imaging, again without finding any candidate planet around M-dwarfs (Zendejas et al. 2013). The RoPACS project also organized an interational conference on planets at MPE in 2012 (Saglia 2013).

Planets in star clusters: We used the high-resolution spectrograph at the Hobby-Eberly Telescope (HET) to search for planets in a systematic way around stars in the open cluster M67 with the radial velocity method (Pasquini et al. 2012). Up to now only two planets around a star in an open cluster (the Pleiades) have been detected. Our search, that combines spectroscopic data from the Hobby-Eberly-Telescope with observations of HARPS at ESO, SOPHIE at the OHP and CORALIE at the 1m Euler Swiss telescope in La Silla, finds several very promising candidates around giants and main sequence stars of different masses. Two of the most interesting phased radial velocity curves are shown in Fig. OP.31. One of the Pan-Planets fields includes the globular cluster M71, which has been targeted for extra-solar planets by other groups before. The cluster has a high metallicity ($[Fe/H]=0.4$) which increases the chance for a detection. So far, no transiting planet has been reported in the literature. A detection in M71 would have a large impact on the understanding of planet formation and evolution in the very interesting environment of a dense star cluster.

Variable stars in the Milky Way: A by-product of the RoPACS survey is the discovery of several detached M dwarf eclipsing binaries, in particular four with ultra-short periods $\leq 0.18d$ (Nefs et al. 2012). Such systems are interesting for both measuring in a model independent way the fundamental parameters of these poorly understood yet numerous stars, and for probing the models

of formation of low-mass binaries (Birkby et al. 2012). In our Hobby-Eberly-Telescope search for binaries we also found a white dwarf – brown dwarf (of 56 Jupiter masses) system rotating with an amazingly short period of 102 minutes, the shortest ever detected (Steele et al. 2013). The Pan-Planets data base of light curves will enable us to extend our studies of variable stars to a large number of targets in the coming years.

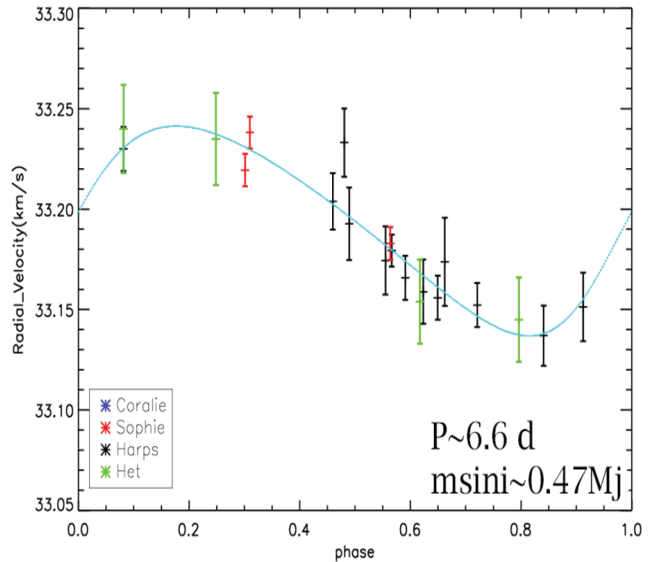
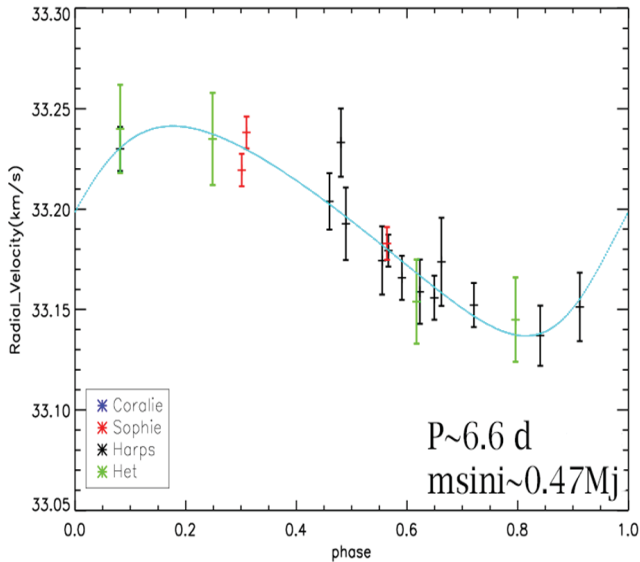


Fig. OP.31: The phased radial velocity curves of two stars in M67 with candidate Jupiter-like exoplanets.

Software development: The Photometric Classification Server (PCS) for PanSTARRS-1

Our contribution to the analysis pipeline for the PanSTARRS-1 data is PCS. The software allows the automatic classification of objects into star/galaxy/quasar classes based on colors (PanDiSC) and the measurement of photometric redshifts for extragalactic objects (PanZ). The object classification PanDiSC is based on a support vector machine, a statistical learning algorithm. The photometric redshifts produced by PanZ are derived performing Bayesian spectral energy distribution fitting. The codes are interfaced to the PS database, run unsupervised on our multi-node cluster when new data become available, and push the results back to the database in Hawaii. We used the photometry derived from the Medium-Deep Fields of Pan-STARRS1 to test the system in combination with available spectroscopic surveys as training and or verification sets (Saglia et al. 2012). PanDiSC classifications are accurate (85% for stars, 97% for galaxies, 83% for QSOs). The purity of the corresponding samples is highest for galaxies (99%); for stars and QSOs we reach 81% and 72%, respectively. These numbers can be improved by taking morphologies into account. Photometric redshifts are of excellent qualities for red luminous galaxies (2.4% in $\Delta z/(1+z)$) thanks to a newly developed set of spectroscopic templates (Greisel et al. 2013).

Instrument development: FOCES-Comb

We are currently upgrading the echelle-spectrograph FOCES, which was built by the University Observatory Munich 15 years ago for the Calar Alto 2.2m telescope, with a frequency comb and a temperature- and pressure-stabilization system. The upgraded instrument (called FOCES-Comb) will provide a spectral resolution of $\lambda/\Delta\lambda \sim 70000$ and very high stability which will enable us to search and characterize exo-planetary systems with our

new 2m Fraunhofer telescope on Mt. Wendelstein. This program will not only allow efficient follow-up of planet candidates from an increasing number of transit surveys but we will also enable us to carry out stand-alone radial velocity searches for planets. With FOCES-Comb we will be able to execute a >5-year spectroscopic monitoring of approximately one hundred bright stars observable from Mt. Wendelstein.

FOCES is currently set-up in a pressure- and temperature stabilized box at the University Observatory Munich (Fig. OP.32). Temperatures are stable to better than 0.01 K, pressures to better than 0.1 hPa, which translates into a spectrograph stability of better than 0.001 pixels. Therefore, already now FOCES is able to reach the required stability for highly precise radial velocity (\sim m/s) work over shorter periods of time (days). To achieve high precision long-term stability, we are installing a frequency comb (see Fig. OP.32, right) referenced to its zero-frequency (thus wavelength) to a rubidium atomic clock. With a drift of less than 10^{-13} , this clock can nominally achieve the required stability over timescales of decades. In order to test fiber modal effects as well as spectrograph stability independent from each other, we will build a fiber link consisting of four fibers, two multi-mode fibers and two single mode fibers.

It will then be possible to test all combinations of single-vs-single, single-vs-multi and multi-vs-multi without having to mechanically change the spectrograph setup. In addition, another mode, allowing to mix comb and starlight at the entrance of a single multi mode fiber is under investigation. First simulations show that an accuracy of $<1\text{m/s}$ can be achieved with this mode. Software to analyze classical (2 fiber) simultaneous calibration data is also in the state of testing. FOCES is expected to reach a limiting magnitude of $V\sim 8.5$ with the 2m Fraunhofer telescope on Mt. Wendelstein.



Arno Riffeser, Johannes Koppenhoefer, Roberto Saglia

(Other OPINAS team members include R. Bender, A. Brucalassi, M. Cappetta, C. Goessl, N. Greisel, F. Grupp, M. Kodric, C. H. Lee, S. Seitz, R. Senger, J. Snigula, P. Steele, J. Zendejas)

Selected References:

- Birkby et al. 2012, MNRAS 426, 1507*
Birkby et al. 2013, submitted to MNRAS
Cappetta et al. 2012, MNRAS 427, 1877
De Mooij et al. 2012, A&A 538, 46
Fliri et al. 2006, A&A, 445, 423
Fouque et al. 2010, A&A, 518, A51
Greisel et al. 2013, ApJ, astro-ph/1303.3005
Henze et al. 2013, A&A, 549, A120
Kodric et al. 2013, AJ, 145, 106
Koppenhoefer et al. 2009, A&A, 494, 707
Koppenhoefer et al. 2013, ExA, 35, 329
Kovacs et al. 2013, MNRAS, in press, astro-ph/1304.1399
Lee et al. 2009, ApJ, 695, 200
Lee et al. 2010, MNRAS, 407, 1597
Lee et al. 2012a, AJ, 143, 89
Lee et al. 2012b, A&A, 537, A43
Lee et al. 2013, in prep.
Lendl et al 2010, A&A 522, 29
Middleton et al., 2013, Nature, 493, 187
Montalto et al. 2009, A&A, 507, 283
Montalto, M. 2010, A&A, 521, 60
Montalto et al 2011, A&A, 535, 39
Nefs et al., 2012, MNRAS, 425, 950
Nikolov et al. 2012, A&A 539, 159
Opitsch et al. 2013, in preparation
Pasquini et al. 2012, A&A, 545, A139
Pietsch et al. 2007, A&A, 465, 375
Riffeser et al. 2001, A&A, 379, 362
Riffeser et al. 2003, ApJL, 599, L17
Riffeser et al. 2006, ApJS, 163, 225
Riffeser A., Seitz S., Bender R., 2008, ApJ, 684, 1093
Saglia et al. 2010, A&A, 509, A61
Saglia et al. 2012, ApJ, 746, 128
Saglia (Editor): EPJ Web of Conference, 2013, Vol. 47
Snellen et al. 2009, A&A 497, 545
Steele et al. 2013, MNRAS 429, 3492
Zendejas et al. 2013, submitted to A&A

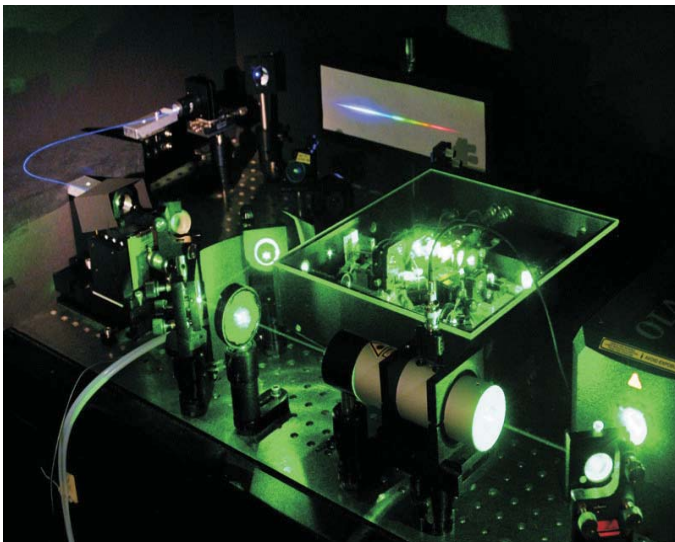


Fig. OP.32: Top: FOCES in its pressure box, note the outer layer heating elements on the walls. Bottom: Frequency comb system developed at the Max-Planck-Institute for Quantum Optics in collaboration with Menlo Systems, a more integrated system will be used to calibrate FOCES.

3.8 Euclid

Understanding the acceleration of the expansion of the Universe is one of the most compelling challenges of cosmology and fundamental physics. The ESA mission Euclid will determine how cosmic acceleration modifies the expansion history and the 3-dimensional distribution of matter in the Universe. To achieve this, Euclid will measure the shapes of over a billion galaxies and accurate redshifts of tens of millions of galaxies for weak gravitational lensing and galaxy clustering studies. Euclid was adopted by ESA for implementation in summer 2012, launch is foreseen for 2020. The MPE OpInAs group is a founding member of the Euclid mission. We are responsible for the optical design of the NIR Spectro-Photometer, for which we also provide the key optical components. In addition, MPE will host the German Euclid Science Data Center and is involved in developing data analysis components. Ralf Bender is a member of the Euclid Board, Frank Grupp is the Lead Optical Architect of the Euclid Consortium, and several further OpInAs scientists (Koppenhöfer, Saglia, Sanchez, Seitz, Weller) are participating in Science Working Groups and other activities.

Euclid is designed to understand the origin of the Universe's accelerating expansion. It will use several cosmological probes to investigate the nature of dark energy, dark matter and gravity by tracking their observational signatures on the geometry of the universe and on the cosmic history of structure formation. Euclid will map large-scale structure over a cosmic time covering the last 10 billion years, more than 75% the age of the Universe. The mission is optimised for two independent **primary cosmological probes**: Weak gravitational Lensing (WL) and Baryonic Acoustic Oscillations (BAO). Surveyed in the same cosmic volume, these two probes provide necessary cross-checks on systematic errors. They also provide a measurement of large scale structure via different physical fields (potential, density and velocity), which are required for testing dark energy and gravity at all scales. Beyond the two primary probes, the Euclid surveys yield data of several important complementary cosmological probes such as galaxy clusters, redshift space distortions and the integrated Sachs Wolfe effect. WL requires a high image quality on sub-arcsec scales for the galaxy shape measurements, and photometry at visible and infrared wavelengths to measure the photometric distances of each lensed galaxy out to $z \geq 2$. BAO requires near-infrared spectroscopic capabilities to measure accurate redshifts of galaxies out to $0.7 < z < 2.1$. Both probes require a very high degree of system stability to minimise systematic effects, and the ability to survey a major fraction of the extra-galactic sky. Such a combination of requirements cannot be met from the ground, and demands a wide-field-of-view space mission like Euclid.

To understand the nature of dark energy, its equation of state needs to be determined. Euclid uses WL and BAO

to measure the constant and time varying terms of the dark energy equation of state to a unprecedented precision (see Fig.32), sufficient to make a hopefully decisive statement on the nature of dark energy. Euclid will also test the validity of General Relativity by measuring the rate of cosmic structure growth to a 1-sigma precision of < 0.02 , sufficient to distinguish General Relativity from a wide range of modified-gravity theories. As Euclid maps the dark matter distribution with unprecedented accuracy, subtle features produced by neutrinos are measured, providing constraints on the sum of the neutrino masses with a 1-sigma precision better than 0.03 eV. Likewise, the initial conditions of the seeds of cosmic structure growth are unveiled by determining the power spectrum of density perturbations to one percent accuracy. Euclid and Planck together measure deviations to a Gaussian distribution of initial perturbations with a precision one order of magnitude better than current constraints, allowing Euclid to test a broad range of inflation models. Euclid is therefore poised to uncover new physics by challenging all sectors of the cosmological model.

Beyond unprecedented constraints on cosmology and dark energy, the Euclid wide and deep surveys will produce data with **unique legacy science** value in various fields of astrophysics and a primary data base for next generation multi-wavelength surveys (see Fig. OP.33). Euclid will obtain images and photometry of more than a billion galaxies and several million spectra of emission line objects, out to redshifts $z > 2$. At low redshift, Euclid resolves the stellar population of all galaxies within ~ 5 Mpc, providing a complete census of all morphological and spectral types of galaxies in our neighborhood. It also delivers morphologies, masses, and star-formation rates out to $z \sim 2$ with a 4 times better resolution, and 3 NIR magnitudes deeper, than possible from ground. Euclid derives the mass function of galaxy clusters (in combination with eROSITA, Planck and SZ telescopes), and finds over 105 strong lensing systems. Gravitational lensing together with near infrared photometry of lensing sources explores the relationship between light, baryons and dark matter between galaxy and super cluster scales as a function of look-back time and environment.

The Euclid deep survey area will be the primary target for follow-up observations. Deep data contain thousands of objects at $z > 6$ and several tens of $z > 8$ galaxy or quasar candidates that will be critical targets for JWST and E-ELT. As the deep survey fields are visited repeatedly over a time span of several years they are also a unique baseline for the discovery of variable sources.

Our hardware contribution to Euclid consists primarily in the optical design of the NIR Imaging Spectrometer (NISIP) and the provision of the corresponding optical elements. In addition, we contribute to the development and implementation of data analysis components and we will host the German Euclid Science Data Center.

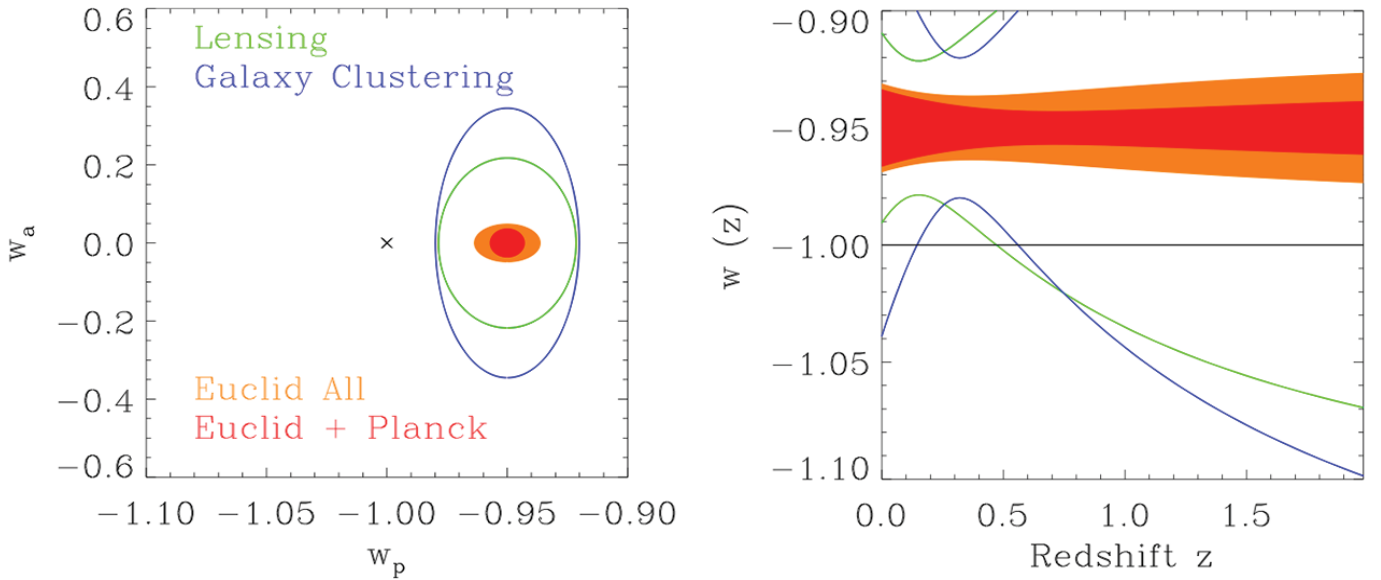


Fig. OP.32: The expected constraints from Euclid in the dynamical dark energy parameter space. The Fig. shows lensing only (green), galaxy clustering only (blue), all the Euclid probes (lensing+galaxy clustering+clusters+ISW; orange) and all Euclid with Planck CMB constraints (red). The cross shows a cosmological constant model. Left panel: the expected 68% confidence contours in the (w_p, w_a) . Right panel: the 1 constraints on the function $w(z)$ parameterised by (w_p, w_a) as a function of redshift (green-lensing alone, blue-galaxy clustering alone, orange-all of the Euclid probes, red-Euclid combined with Planck).

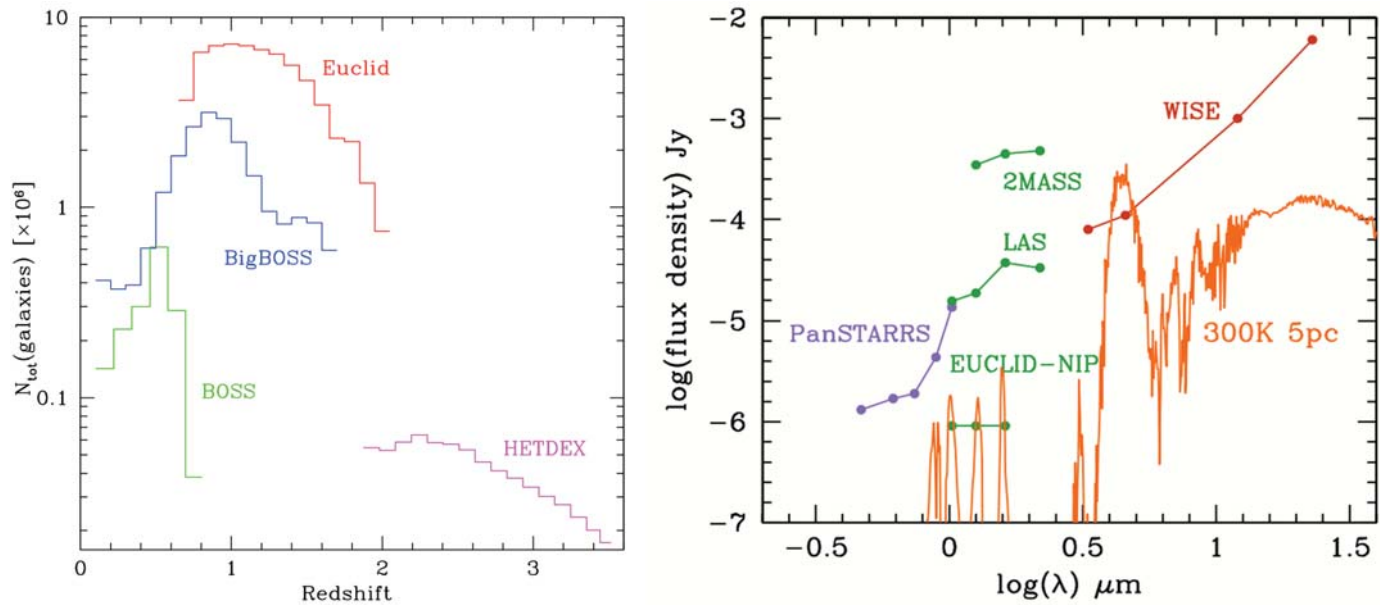


Fig. OP.33: Left: comparison of number of galaxies in redshift bins of width $z=0.1$, for the Euclid spectroscopic survey compared with various ongoing and proposed ground-based surveys. Right: 5σ point-source depths in imaging for a selection of surveys as a function of wavelength: PanSTARRS, 2MASS, UKIDSS- LAS, Euclid-NIR, and WISE. Overplotted is a Y-dwarf at 5pc distance.

To achieve the science goals of the Euclid mission, a 168mm diameter NIR optical system with close to diffraction limited performance is needed. This is the largest ever flown lens optics in combination with the most stringent tolerances on lens shapes and positions (see Fig. OP.34). In the photometer mode, the NISP instrument images the telescope light in the wavelength range from 920 nm to 2000 nm (Y, J, H, K bands) on an array of 16 detectors. The resolution is required to be approximately 0.33 arcsec per pixel in J-band at 1259nm wavelength. The field-of-view of the instrument is 0.763 deg \times 0.722 deg. In the spectrometer mode the light of the observed target is dispersed by means of gratings in the wavelength

range of 0.92 μm to 2 μm . In order to provide a constant resolution over the specified wavelength range, two sets of two gratings each are applied in a filter wheel. The two sets of gratings provide two dispersion directions tilted against each other by 90 deg to allow better disentangling of the taken spectra. The field and waveband definition used in the individual configurations for spectroscopy and photometry are shown in Table 2.

The overall parameters of the Euclid mission are given in Table 1.

Main Scientific Objectives					
Understand the nature of Dark Energy and Dark Matter by:					
<ul style="list-style-type: none"> Reach a dark energy $FoM > 400$ using only weak lensing and galaxy clustering; this roughly corresponds to 1 sigma errors on w_p and w_a of 0.02 and 0.1, respectively. Measure γ, the exponent of the growth factor, with a 1 sigma precision of < 0.02, sufficient to distinguish General Relativity and a wide range of modified-gravity theories Test the Cold Dark Matter paradigm for hierarchical structure formation, and measure the sum of the neutrino masses with a 1 sigma precision better than 0.03eV. Constrain n_s, the spectral index of primordial power spectrum, to percent accuracy when combined with Planck, and to probe inflation models by measuring the non-Gaussianity of initial conditions parameterised by f_{NL} to a 1 sigma precision of ~ 2. 					
SURVEYS					
	Area (deg ²)	Description			
Wide Survey	15,000 (required) 20,000 (goal)	Step and stare with 4 dither pointings per step.			
Deep Survey	40	In at least 2 patches of $> 10 \text{ deg}^2$ 2 magnitudes deeper than wide survey			
PAYLOAD					
Telescope	1.2 m Korsch, 3 mirror anastigmat, $f=24.5 \text{ m}$				
Instrument	VIS	NISP			
Field-of-View	$0.787 \times 0.709 \text{ deg}^2$	$0.763 \times 0.722 \text{ deg}^2$			
Capability	Visual Imaging	NIR Imaging Photometry			NIR Spectroscopy
Wavelength range	550– 900 nm	Y (920-1146nm),	J (1146-1372 nm)	H (1372-2000nm)	1100-2000 nm
Sensitivity	24.5 mag 10 σ extended source	24 mag 5 σ point source	24 mag 5 σ point source	24 mag 5 σ point source	$3 \cdot 10^{-16} \text{ erg cm}^{-2} \text{ s}^{-1}$ 3.5 σ unresolved line flux
Detector Technology	36 arrays 4k \times 4k CCD	16 arrays 2k \times 2k NIR sensitive HgCdTe detectors			
Pixel Size	0.1 arcsec	0.3 arcsec			0.3 arcsec
Spectral resolution					R=250
SPACECRAFT					
Launcher	Soyuz ST-2.1 B from Kourou				
Orbit	Large Sun-Earth Lagrange point 2 (SEL2), free insertion orbit				
Pointing	25 mas relative pointing error over one dither duration 30 arcsec absolute pointing error				
Observation mode	Step and stare, 4 dither frames per field, VIS and NISP common FoV = 0.54 deg^2				
Lifetime	7 years				
Operations	4 hours per day contact, more than one ground station to cope with seasonal visibility variations;				
Communications	maximum science data rate of 850 Gbit/day downlink in K band (26GHz), steerable HGA				
Budgets and Performance					
	Mass (kg)		Nominal Power (W)		
industry	TAS	Astrium	TAS	Astrium	
Payload Module	897	696	410	496	
Service Module	786	835	647	692	
Propellant	148	232			
Adapter mass/ Harness and PDCU losses power	70	90	65	108	
Total (including margin)	2160		1368	1690	

Table OP.1: Overall mission parameters of Euclid.

Configuration	λ_{start} [nm]	λ_{end} [nm]	Orientation [°]	Dispersion [nm/pix]
Y	920	1146	–	–
J	1146	1372	–	–
H	1372	2000	–	–
Spec Blue 0	1100	1457	0	0.98
Spec Red 0	1445	2000	0	0.98
Spec Blue 90	1100	1457	90	0.98
Spec Red 90	1445	2000	90	0.98

Table OP.2: The imaging and spectroscopic modes of the Euclid NIR Imaging Spectrometer.

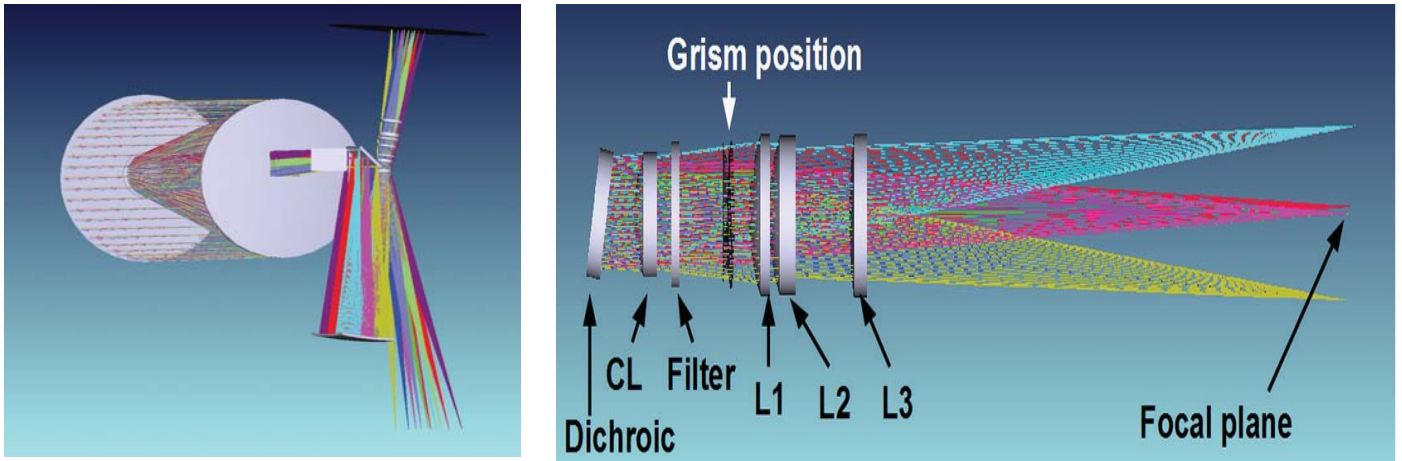


Fig. OP. 33: Left: the optical design of the complete Euclid telescope and instrument system. The NIR focal plane is at the top right, the optical focal plane at the bottom left. Right: The optical design of the NIR Imaging Spectrometer including the dichroic at the left that reflects the optical part. The system reduces the f -ratio from 20 to 10 to achieve an apparent pixel size of 0.33 arcsec.



Ralf Bender



Frank Grupp

Selected References:

- Fuchs U., Grupp F., Kiontke S., Bender R. 2011, SPIE, 8146
 Grupp F., Prieto E., Geis N. et al. 2012, SPIE, 8442
 Grupp F., Prieto E., Spano P. et al. 2011, SPIE, 8146
 Laureijs R., Amiaux J., Arduini S., et al. 2011, arXiv, arXiv:1110.3193
 Morgante G., Maciaszek T., Martin L., et al. 2012, SPIE, 8442
 Prieto E., Amiaux J., Augueres J.-L., et al. 2012, SPIE, 8442

(Other OPINAS team members include A. Bode, C. Bodendorf, N. Geis, R. Katterloher, J. Koppenhöfer, M. Neumann, F. Raison, R. Saglia, A. Sanchez, S. Seitz, J. Snigula, C. Vogel, I. Weiss, J. Weller)

3.9 Research Group "Dynamics" Ortwin Gerhard

3.9.1 Summary/Overview

Our research is broadly directed towards understanding the dynamical structure and evolution of nearby galaxies, including our Milky Way. We are also interested in dark matter, galactic nuclei and intracluster light, a product of galaxy evolution in clusters. Observations of nearby galaxies tell us about the current dynamical configuration of stars and dark matter, and at the same time provide a record of their formation and evolution from high redshift until now. Similarly, the spatial distribution and kinematics of stellar generations in the Milky Way are the focus of extensive observational programs in order to clarify the history of our Galaxy. We develop dynamical models and tools to understand the implications of these new data for galaxy dynamics and evolution.

The following briefly describes past and on-going research projects in the Dynamics Group. Results from three of these projects are described in some more detail at the end.

Structure and origin of the Milky Way bulge and bar (MW): Recent spectroscopic surveys have measured the velocities and abundances of several 10'000 stars in the inner MW, giving a unique view on the composition and formation history of the Galactic bulge. Other ground-based surveys are returning unprecedented data for the Galactic disk and halo. Our strong interest is in the dynamical structure and origin of the MW bulge and bar. We are interested in how the bulge assembled, how its dynamical structure varies with abundance, and whether signatures of several bulge formation episodes can be found, as might be expected from galaxy evolution studies at high redshift. We are using N-body models and the powerful NMAGIC particle technique to help answer these questions. Results from this project are described in section 3.9.2 [I. Martinez-Valpuesta, C. Wegg, M. Portail].

Dynamics of barred bulges: Our N-body simulation studies have shown that pre-existing classical bulges in now barred galaxies can be spun-up by angular momentum transfer from the bar and may reach cylindrical rotation [1,2]. The implications of this finding for the distinction between classical and boxy bulges remain to be fully understood. We have started to construct dynamical models for barred galaxy bulges, such as M31 [3], using the NMAGIC particle technique, in order to obtain a better understanding of their internal dynamics. In future, we intend to include their central black holes, in collaboration with the OpInAs group at MPE [I. Martinez-Valpuesta, M. Portail, (p: K. Saha)].

Nuclear star cluster in the MW: The cluster of old stars around the black hole in the Galactic centre is unique in that many 1000's of proper motions and radial velocities are available to constrain its dynamics [4]. In collaboration with the IR/Submm Astronomy group at MPE, we are constructing dynamical models in order to determine the mass, angular momentum, orbit structure and distance of the Galactic nuclear star cluster (see poster by Chatzopoulos et al.) [S. Chatzopoulos].

Stellar and dark matter halos of early-type galaxies (ETGs): Massive ETGs are believed to grow continuously from after their formation at redshift $\sim 2-3$ up until the present time. While integral field spectroscopy has allowed a detailed characterisation of the stellar motions and orbits in the inner parts of nearby ETGs, much of the "late galaxy formation" happens in their outer halos, where volumes are large and surface brightnesses faint. The outer halos of ETGs has been one of our main research topics in the last years, including their angular momentum, dark matter halo mass, and orbit distribution, as summarized in section 3.9.3 below [I. Martinez-Valpuesta, (p [past group members]: L. Coccato, P. Das, F. de Lorenzi, L. Morganti, X. Wu)].

NMAGIC made-to-measure modelling of equilibrium stellar systems: This is a very promising method to determine particle models for given target galaxy data, to infer the unobservable internal dynamical structure of these systems. By varying the gravitational potential, the dark matter halo and black hole mass parameters can also be determined [5-10]. NMAGIC is particularly useful for making dynamical models of barred galaxies such as the MW, but we also used it to model composite data sets for elliptical galaxies, and to predict pseudo-data. We are also working on increasing the models' generality, versatility, and speed [I. Martinez-Valpuesta, M. Portail, C. Wegg, (p: P. Das, F. de Lorenzi, L. Morganti)].

Origin of intracluster light (ICL): Galaxy clusters generally contain an unbound, ICL component, consisting of stars torn off galaxies by dynamical processes. Observing and interpreting the kinematics of the faint ICL is a new way to understand the evolution of galaxy clusters. Cluster centres are found invariably dynamically evolving, through accretion of cluster galaxies and mergers with the cluster-central massive galaxy; see section 3.9.4 below. In future, we intend to refocus this project on the transition regions between ETGs and the surrounding unbound stars [A. Longobardi, (p: L. Coccato, G. Ventimiglia)].

Members of the Dynamics Group: Besides the author of this summary, the group consists of typically 2-3 PhD students and a post-doctoral fellow from MPE funds; however, in the last few years, we were able to attract a Humboldt fellow (K. Saha) and an additional post-doc through a DFG Schwerpunktprogramm. Depending on the project, we collaborated with scientists at MPE, MPA, and ESO, the international PN.S team, and other international collaborators as can be seen from the references.



Ortwin Gerhard is a senior scientist at MPE (W2) who came to the institute in 2005 from the University of Basel. He leads the Dynamics Group and also has been coordinating the annual recruitment of new PhD students at MPE since 2006. During 2006-2009, he was president of Div. VII (The Galactic System) of the International Astronomical Union.

(Other team members include I. Martinez-Valpuesta, S. Chatzopoulos, A. Longobardi, M. Portail, C. Wegg

Former team members include L. Coccato, P. Das, F. de Lorenzi, L. Morganti, K. Saha, G. Ventimiglia, X. Wu)

Selected References:

- [1] Saha et al. 2012, *MNRAS*, 421, 333
- [2] Saha & Gerhard 2013, *MNRAS*, 430, 2039
- [3] Saglia et al. 2010, *AA*, 509, 61
- [4] Trippe et al. 2008, *AA*, 492, 419
- [5] de Lorenzi et al. 2007, *MNRAS*, 376, 71
- [6] —, 2008, *MNRAS*, 385, 1729
- [7] —, 2009, *MNRAS*, 395, 76
- [8] Das et al., 2011, *MNRAS*, 415, 1244
- [9] Morganti & Gerhard 2012, *MNRAS*, 422, 1571
- [10] Morganti et al. 2013, *MNRAS*, in press
- [11] Martinez-Valpuesta & Gerhard, 2011, *ApJL*, 734, L20
- [12] Gerhard & Martinez-Valpuesta 2012, *ApJL*, 744, L8
- [13] Martinez-Valpuesta & Gerhard, 2013, *ApJL*, 766, L3
- [14] Coccato et al. 2009, *MNRAS*, 394, 1249
- [15] McNeill et al. 2010, *AA*, 518, 44
- [16] — 2012, *AA* 539, 11
- [17] Napolitano et al. 2012, *MNRAS*, 411, 2035
- [18] Cortesi et al., 2013, *MNRAS* in press
- [19] Churazov et al. 2008, *MNRAS*, 388, 1062
- [20] —, 2010, *MNRAS*, 404, 1165
- [21] Das et al. 2010, *MNRAS*, 409, 1362
- [22] Longobardi et al., 2013, *AA*, submitted
- [23] Gerhard et al. 2007, *AA*, 468, 815
- [24] Coccato et al. 2010, *MNRAS*, 407, L26
- [25] Ventimiglia et al. 2011, *AA*, 528, A24
- [26] Arnaboldi et al. 2012, *AA*, 545, A37
- [27] Castro-Rodriguez et al. 2009, *AA*, 507, 621
- [28] Doherty et al. 2009, *AA*, 502, 771

3.9.2 Structure and Origin of the Galactic Bulge

The Galactic bulge is unique in that the kinematics and element abundances of a large number of its stars can be measured individually, allowing us to study the fossil record of its formation history in much greater depth than for any other galaxy. On-going large surveys have confirmed the barred nature of the Milky Way's boxy bulge and, aided by dynamical models, are beginning to reveal its detailed morphological, dynamical, and stellar population properties. Our results suggest that the so-called long bar is the planar continuation of the boxy bulge, and that the density structure, kinematics, and metallicity gradients of the bulge are essentially consistent with a disk instability origin.

From studies of the gas flow in the inner galaxy, from COBE NIR photometry, and star counts, we have long known that the Galactic bulge is barred and boxy. More recently, NIR star counts near the Galactic plane have shown apparent evidence for a planar long bar tilted with respect to the bulge. The vertical gradient seen in the measured metallicity distribution, on the other hand, has been interpreted as a signature of a classical, merger-collapse built bulge, and most studies agree that the bulge stars are uniformly old, >10 Gyr, at least in fields several degrees above the Galactic plane like Baade's window. So how does all this fit together, and what is the origin of the Milky Way (MW) bulge?

Recent and on-going photometric and spectroscopic surveys are greatly enhancing our knowledge about bulge stars and are leading to a consistent picture. The

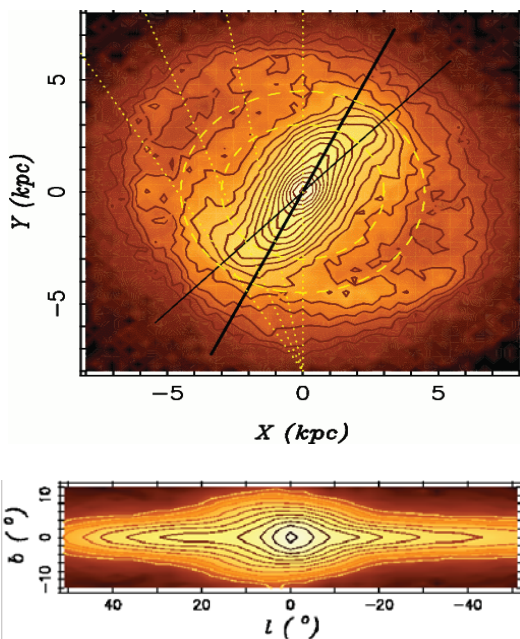


Fig. OP.34, left: Face-on and edge-on projections of the model [11] for the Milky Way boxy bulge and long bar. The Sun is at $X=0$ ($l=0$) and $Y=-8$ kpc.

'split red clump' found in star counts is a characteristic signature of a rotating barred potential, as is the near-cylindrical rotation found in the BRAVA and ARGOS surveys. The latter survey shows that the vertical metallicity gradients may plausibly be explained as a superposition of different Galactic components with different scale-heights.

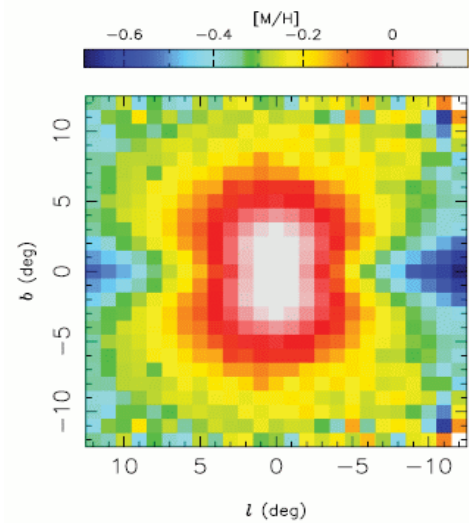


Fig. OP.35, right: Metallicity map of the boxy bulge of the model after bar and buckling instabilities, for assumed radial gradient in the initial disk [13].

In our work, we use various models to understand the bulge data. The N-body model in Fig. OP.34 shows a bulge that grew from the disk through bar and buckling instabilities. We used it to show how the star count data can be interpreted in terms of a unified bar whose inner 3D-part is the boxy bulge and whose outer parts form the long bar [11]. The model also explains a structural change in the red clump magnitude distributions for $|b| < 4^\circ$ as due to the inner, rounder parts of the bulge [12]. Recently, we used it to show that a bar formed in rapid evolution does not destroy radial metallicity gradients in the initial disk. The metallicity map shown in Fig. OP.34 was obtained with parameters adjusted such as to fully match the observed vertical gradients in the MW bulge [13]. Thus vertical gradients in the bulge are consistent with a disk instability origin; they are not convincing evidence for a classical bulge. Yet, a classical bulge of the size compatible for the MW would show cylindrical rotation, after being spun up by the gravitational field of the bar [1,2]; see also poster by Saha et al. Thus a more detailed chemo-dynamical analysis is needed to settle the question whether the MW contains a small classical bulge. So far, the data are consistent with a disk instability origin for the Galactic bulge.

To look forward, we are currently constructing a detailed density model for the MW bulge from VVV star counts, and have started to make NMAGIC dynamical models for the BRAVA and ARGOS kinematic data (posters by Wegg & Gerhard and Martinez-Valpuesta et al.). The goal is to understand better the interrelation between chemistry and dynamics and their implications for the origin of the Galactic bulge.

3.9.3 Faint Outer Regions and Dark Matter Halos of Early-Type Galaxies

The outer regions of galaxies is where dark matter dominates, and where the signatures of merger and accretion events are preserved longest. We have used planetary nebulae (PNe) as tracers to measure the kinematic structure, angular momentum, and mass in the outer halos. Dynamical masses were determined using sophisticated particle-dynamical models, and show that also quasi-Keplerian ETGs have dark matter (DM) halos, some with strong central concentration of the baryonic components. In bright elliptical galaxies, the comparison of masses determined from optical data with X-ray measurements was used to estimate the non-thermal pressure fraction in their hot gas halos.

In current hierarchical models, early-type galaxies (ETGs) are believed to form in a two-stage process. An early, dissipative merger-collapse forming a dense centre of in situ stars is followed by a prolonged phase of growth through minor mergers and accretion. This scenario, supported by hydrodynamic cosmological simulations, provides an explanation for the observed size evolution of old ETGs. It also predicts that much of the late evolution of these systems should occur in the diffuse outer halos of ETGs where dynamical time-scales are long. In these outer regions, traditional spectroscopy is very difficult because of the rapidly falling surface brightness.

To overcome this problem we use PNe as kinematic tracers. Their radial velocities can be measured from bright [OIII] emission lines. Our group is part of the PN spectro-

graph (PN.S) team operating a special-purpose instrument for this purpose, but also VLT slitless spectroscopy has been employed (e.g. [14-18]). Based on PNe velocity fields, we showed that the fast/slow rotator dichotomy is largely preserved in the halos ([see [14,18] and poster by Longobardi et al.]), and found an apparent second dichotomy between ETGs with nearly constant velocity dispersion and a class of intermediate luminosity ETGs with rapidly falling, quasi-Keplerian dispersion profiles.

These latter systems were once argued to contain only very diffuse if any DM halos; however, our dynamical modelling with the flexible NMAGIC particle method has shown that the combined slit and PN kinematic data require DM halos, quite massive in one case, and with considerable mass-anisotropy degeneracy in others (see Fig. OP.36, [6,7,10], and poster by Morganti et al.). In bright ETGs the diffuse X-ray emission and hydrostatic equilibrium provide for independent mass measurements. Comparing X-ray and optical (spectra and PNe) masses, we could estimate the fraction of non-thermal pressure in the X-ray emitting gas to be typically 20-30% [8,19-21].

PN velocities are not only useful to trace the velocity dispersion into the halo, but they also allowed us to detect kinematic substructure already in one of the halos (Fig. OP.37, [15]). This is a promising subject for the future; we have recently acquired several data sets with ~500 PNs (e.g. [16,22]) which we are currently analysing for signatures of halo substructure.

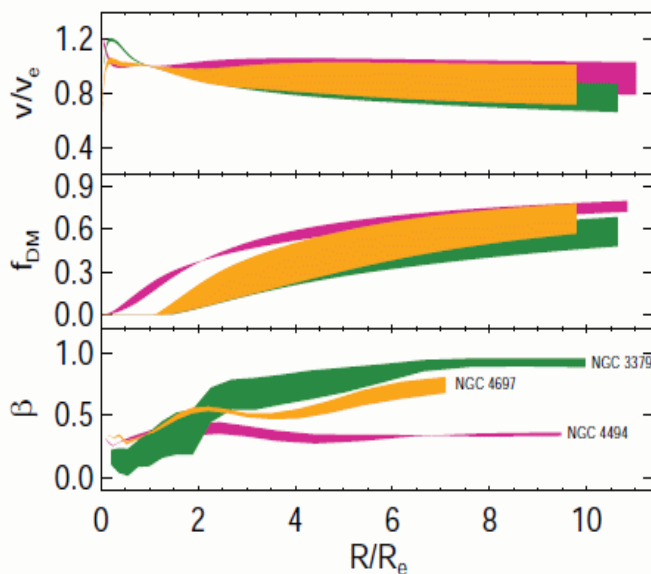


Fig. OP.36: Confidence regions for circular velocity, dark matter fraction, and anisotropy parameters for three quasi-Keplerian ellipticals, from [10].

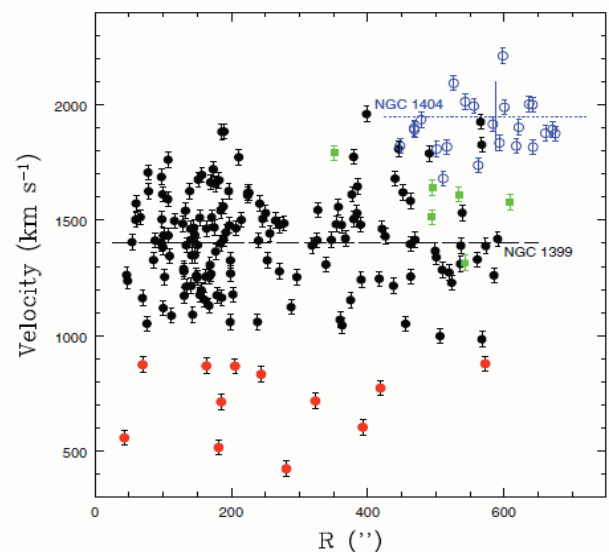


Fig. OP.37: PN phase-space in the Fornax cluster core, showing PNe from the central galaxy NGC 1399, its neighbour NGC 1404, and a diffuse low-velocity component [15].

3.9.4 Intracluster Light and Galaxy Accretion

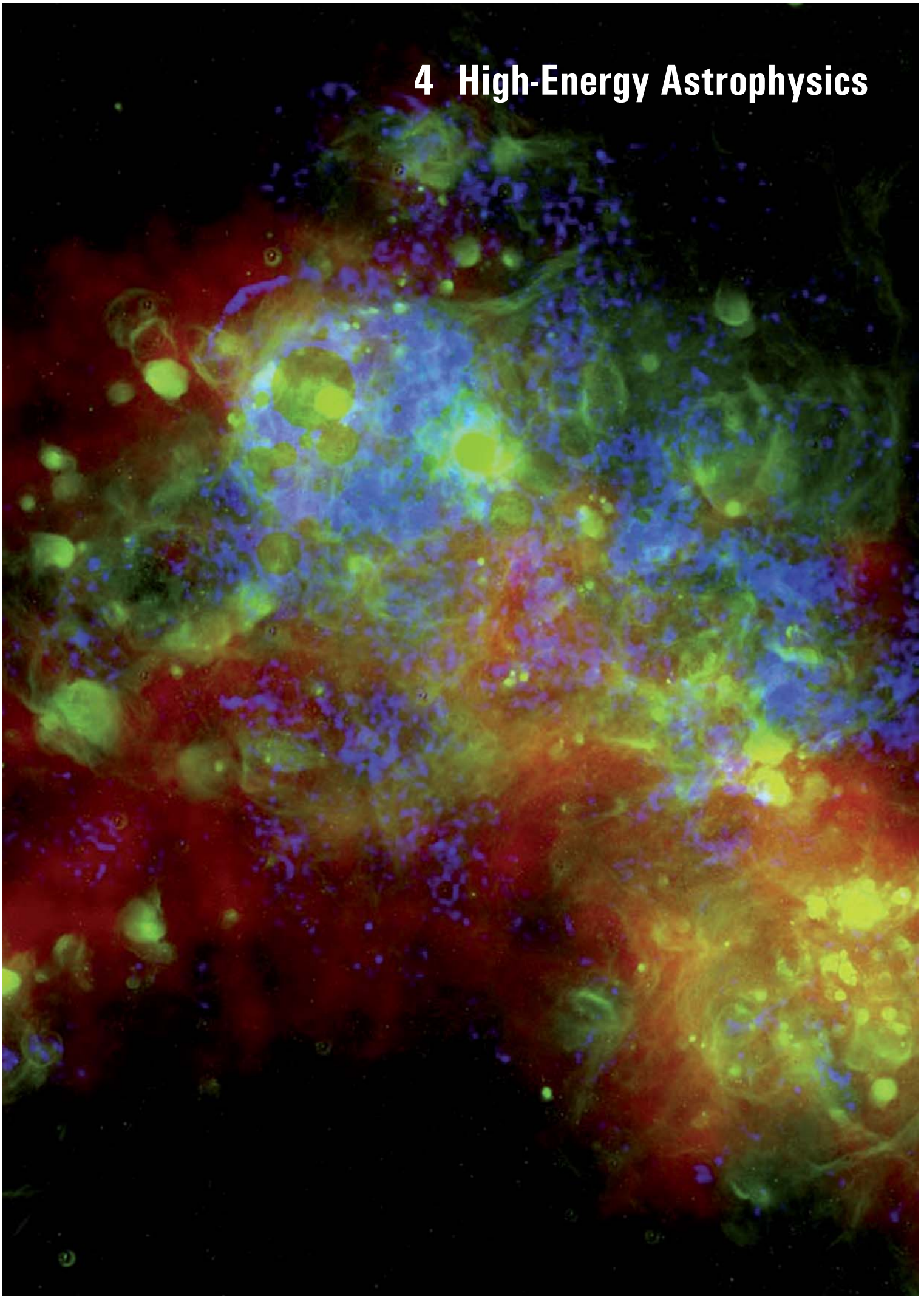
Diffuse intracluster light (ICL) has been observed in nearby and intermediate redshift galaxy clusters. Based on simulations and the available data, it is believed to consist of stars tidally disrupted from galaxies, and thus probes the evolution of galaxies in high-density environments. ICL is concentrated towards the cluster centre, it contains an average $\sim 10\%$ of the stellar mass of the cluster, but at very low surface brightness. With planetary nebulae as tracers, we have studied the kinematics of the ICL around the brightest cluster galaxies in the Coma and Hydra clusters. These data show that merger and disruption processes are transforming galaxies in both clusters. Thus, remarkably, cluster cores continue to evolve dynamically.

The densest of the nearby clusters is the Coma cluster, at ~ 100 Mpc distance. With multi-slit imaging spectroscopy, we detected and measured line-of-sight velocities for 37 PNe in the Bernstein field 150 kpc south of the main cD galaxy NGC 4874. Surprisingly, the main component of the line-of-sight velocity distribution is ~ 700 km/s off this galaxy's velocity; so these ICL stars cannot be bound to NGC 4874. Rather, their velocities are similar to that of the other cD galaxy in the Coma core, NGC 4889. Such a velocity inversion is typical for on-going mergers between giant elliptical galaxies, in which broad fans of halo stars are left behind both galaxies along their orbits. Thus the elongated distribution of ICL observed in the Coma cluster core can be explained as stars stripped from the halos of both cDs during their interaction [23]. Deep spectroscopy in the outer halo of NGC 4889 at 60 kpc showed that the outer halo stars have sub-solar metallicity and near-solar abundance ratio, i.e., an extended star formation history. By contrast, the inner half of the galaxy has high abundance ratio, consistent with rapid star formation at early times. The outer halo may have been accreted later as smaller galaxies. Now, this light is stripped again from the cD galaxy and incorporated into the ICL [24].

The Hydra cluster is known as X-ray quiet and dynamically relaxed. However, our PN LOSVD for the diffuse light within 100 kpc around the central galaxy NGC 3311 shows a multi-peaked structure, indicating diffuse light components from different galaxy groups falling through the cluster centre. In fact, a group of small galaxies with ~ 1000 km/s velocity relative to NGC 3311 is seen projected on the cluster core [25]. Deep photometry revealed evidence that one of these galaxies must be in the final stages of dissolution; its current luminosity and radius is $\sim 108 L_{\text{sun}}$ and ~ 2 kpc. A second galaxy, classified S0, is seen within a giant low-surface brightness tail of ~ 100 kpc length, and has already lost $\sim 50\%$ of its stars to the ICL [26]. The stars from the disrupted galaxies will not be bound to NGC 3311, but will spread out in the cluster core. Compared to the dark matter mass in the cluster core, the perturbation from this group of galaxies is relatively small; however, currently NGC 3311 is offset relative to its outermost halo. In fact, the most dramatic interaction, with the other giant galaxy in the cluster core, NGC 3309, is yet to come.

Apparently, even “relaxed” cluster cores are not quiet when looked at in depth but show signatures of merging and disruption. Much of the light from the disrupted galaxies builds up ICL, according to simulations. The halos of giant ellipticals are predicted to be built up by accretion of smaller objects in their earlier group environments. The Virgo cluster may be such an environment; it consists of several subgroups, and the density of ICL around the central galaxy M87 is low [27,28]. With a new large sample of PNe in the outermost halo of M87 [22] we are currently looking for signatures of this accretion process.

4 High-Energy Astrophysics



4. High-Energy Astrophysics

4.1 Introduction/Overview

The MPE High-Energy (HE) Group is one of the largest and most influential worldwide. Our success has been built and sustained by implementing a strategy of developing and providing instruments for major space projects, which we then exploit to our scientific advantage. The vast majority of operating high energy astrophysics space missions feature MPE HE contributions, including Chandra, XMM-Newton, Swift, INTEGRAL and Fermi. The group's core scientific interests currently focus on three areas: 1) Supermassive Black Hole Evolution 2) Clusters of Galaxies and Large Scale Structure and 3) Compact Object and Extreme Astrophysics. Our scientific portfolio is none the less rather broad, covering topics from the solar system to cosmology, with the binding thread being those astrophysical problems on which high energy observations, especially in the X-ray band, can shed new light.

Our current astrophysics research programs primarily involve the exploitation of data from the high energy space facilities mentioned above, with which we have developed great and often unique expertise. In this era of multi-wavelength astronomy, the high-energy spaced-based data are almost always augmented by ground-based observations. We use both common-user facilities (e.g. ESO) and our own ground-based instruments, notably GROND at the MPG 2.2m telescope in La Silla. Following this approach, the group has gone from strength to strength in terms of its scientific productivity. During the period relevant to this report (2007-2013) MPE HE group members authored approximately 1000 refereed publications, garnering over 30,000 citations.

Since 2007, there have been some significant changes in the HE group. Günther Hasinger departed in 2009, with Kirpal Nandra being appointed as Director starting in late 2010. The group's hardware activities have also been restructured. Our prior work in gamma-ray instrumentation has been discontinued in order to refocus and strengthen our efforts in X-ray astronomy instrumentation and optics. A new modus operandi for our X-ray instrumentation program has also been necessitated by the establishment earlier this year of the former MPE/MPP semiconductor laboratory (HLL) in Neuperlach as a central facility of the MPG. As the facilities and infrastructure of the HLL are no longer available to MPE staff for Silicon sensor development and fabrication, our strategy is to set up laboratories to relocate our instrumentation efforts back in Garching, to be completed by mid-2014. Our other major hardware activity is in X-ray optics testing, calibration and development, anchored by the world-leading PANTER facility. PANTER is currently extremely active, being heavily used for calibration of the eROSITA mirrors, but also in testing new lightweight optics technologies such as ESA's silicon pore optics, and slumped glass optics developments, including our own.

Our major current activity in terms of new hardware development is the eROSITA instrument, due for launch in late 2014 on the Russian/German Spektrum-Rentgen-Gamma mission. eROSITA will have a 7 year operational lifetime, performing an all-sky X-ray survey of unprecedented sensitivity in its first 4 years, with a pointed program thereafter. The main driving scientific goal is to perform cosmological investigations, including into the nature of dark energy, using galaxy clusters. As a by-product eROSITA will also yield vast samples of other cosmic X-ray sources, mostly active supermassive black holes in distant galaxies, but including Galactic sources such as active stars, X-ray binaries and many others. Even by MPE standards, eROSITA is an enormous project. Under the leadership of the eROSITA PI, Peter Predehl, the MPE HE group is responsible for the manufacture and integration of the telescope system and structure, the focal plane instrumentations, the ground segment and analysis software, and ultimately of course the scientific exploitation. Most of the group are currently involved in eROSITA-related work at some level, and many devote all their efforts to the project.

The scientific goals of eROSITA cannot be achieved using X-ray data alone, and another vitally important priority of the group has been to secure the necessary complementary and follow-up observations, particularly to determine the source redshifts. We have recently joined both the SDSS-III and SDSS-IV collaborations with a specific program in the latter for eROSITA follow-up called SPIDERS. We are also supporting and contributing actively to the recently-approved ESO 4MOST 4m-class multi-object spectroscopy instrument for the VISTA telescope, one of whose major science drivers is spectroscopic identification of eROSITA sources. We have also secured and/or are actively negotiating a number of collaborative programs across the wavebands to ensure the timely, efficient and comprehensive exploitation of the eROSITA data. Completing eROSITA, and enjoying its scientific returns will occupy the group for perhaps the next 10 years.

Beyond eROSITA, we are actively exploring a number of potential future space projects. Chief amongst these is Athena+, the next generation X-ray observatory, designed to trace the physics and evolution of the hot baryons in the Universe, and elucidate the role of black holes in shaping the properties of galaxies, groups and clusters of galaxies through cosmic time. Athena+ is a strong candidate for ESA's next large mission slot in the 2028 timeframe. MPE is among the leading institutes in the Athena+ collaboration and is expected to be the PI institute for the Athena+ wide field imager (WFI). The WFI is a novel, large format X-ray imager based on our own Silicon DePFET technology. The scientific drivers for the Athena+ WFI include performing a complete census of

accretion activity out into the deep universe ($z \sim 10$) and tracing virialised hot gas structures out to their formation epoch at $z=2-3$. A decision on Athena+ is expected in the 2013/2014 timeframe, and the future strategy of the group will be heavily dependent on that decision.

Other future space projects we are pursuing include the XTP mission, a large project of the Chinese Academy of Science, being conceived to perform broad-band spectroscopy and timing of compact sources, particularly black holes, to investigate strong gravitational effects and shed light on the physics of accretion. XTP is currently in a technology development phase, for a possible launch in the early 2020s, and we are in active discussion with our Chinese colleagues about possible MPE contributions to both the instrumentation and optics. On a smaller scale, we are also contributing to the instrumentation aboard the Franco-Chinese SVOM mission, the natural successor to Swift in pursuit of the mysteries of gamma-ray bursts. In collaboration with CEA Saclay, we are contributing the CCD detectors and ASIC for the MXT X-ray telescope for the mission.



Kirpal Nandra

4.2 Astrophysics Research

4.2.1 Supermassive Black Hole Evolution

In the past decade, studies of the local Universe have established the presence of supermassive black holes (SMBH) in the nuclei of virtually all galaxies with a bulge/spheroidal component, dramatically changing our perception of this class of objects, and implying a clear relationship between the growth of SMBH and that of the galaxy. Because the cosmological growth of SMBHs is mostly due to accretion of matter during active phases (Merloni & Heinz 2008), and the energy released in the process of accretion can be higher than the total binding energy of a massive galaxy, active galactic nuclei (AGN) can in principle have a profound effect on the galaxy formation and evolution processes. X-ray emission offers a unique signpost of accretion of matter onto the supermassive black holes in AGN, being able to penetrate through obscuring material and overcome light from stellar processes. Investigating whether and how nuclear black holes influence their host galaxies, and vice versa, has been a major focus in the activity of the MPE HE Group in the last six years. We have a leading role in X-ray (and multi-wavelength) survey design, as well as in data reduction, analysis and exploitation. AGN can also provide a unique view of the large-scale structure that “lights up” intermittently in X-rays in the regions where the most violent transformation occurs. The relationship between the three-dimensional structure of the cosmic web and black hole activity is a key issue for astrophysics and cosmology, which we are also exploring actively. The expertise accumulated in this area will allow us to fully exploit the rich scientific potential of the upcoming eROSITA telescope, that will reveal around 3 million AGN over the entire sky, and promises to bring evolutionary studies of AGN on robust statistical grounds comparable to that of current wide-area galaxy surveys.

From X-ray surveys to AGN demographics

It is well known that, for the study of AGN, X-rays have merits over other selection techniques, primarily a uniform and quantifiable selection function at all redshifts, relatively little attenuation by absorbing material along the line of sight, and minimal host galaxy light dilution (see e.g. Merloni & Heinz 2013, and references therein). For a complete AGN census, a combination of X-ray surveys (wide/shallow and narrow/deep) needs to be considered. The MPE HE group has a leading role in the science exploitation of almost all high-profile extragalactic surveys carried out by major high energy missions, including Chandra, XMM-Newton, Swift and Integral. In particular, members of our group held the leadership in the XMM-COSMOS survey (Hasinger et al. 2007; Cappelluti et al. 2009), the XMM deep Lockman Hole survey (Brunner et al. 2008), the Chandra AEGIS-wide (Laird et al. 2009) and AEGIS-deep surveys (Nandra et al., in prep), and the 60 months Swift/BAT survey (Ajello et al. 2008a). The group also has heavy involvements in the Chandra Deep Field South and Chandra COSMOS

surveys. We also use wide area serendipitous surveys such as XMM-SDSS (Georgakakis & Nandra 2011) and 2XMM (Watson et al. 2009), the latter via our involvement in the XMM Science Survey Centre (§ 4.4.3).

Currently, we are in the process of re-analysing in a homogenous manner the majority of the dedicated extragalactic X-ray surveys using custom pipelines. As a part of this effort we have been active in developing novel data analysis techniques, such as new X-ray source detection methods (Brunner et al. 2008; Guglielmetti et al. 2009; Laird et al. 2009), Bayesian-motivated approaches for the determination of source properties and X-ray sensitivity maps (e.g. Georgakakis et al. 2008b; Laird et al. 2009), likelihood-based codes for cross-associations (Brusa et al. 2007; Laird et al. 2009; Brusa et al. 2010). Our most recent work is in the development of Bayesian identification algorithms for matching X-ray source positions with multiple multi-wavelength catalogs (Salvato et al., in prep.).

Armed with secure source identifications, we can then proceed to determine the source redshifts, which are crucial for any evolutionary study; in fact, we participate actively in major spectroscopic campaigns of extragalactic populations. These include the zCOSMOS survey, and numerous additional observational programs that target X-ray sources in the COSMOS field (e.g. with Keck/DEIMOS, Subaru/FMOS), and the DEEP2, DEEP3 and MMT surveys in the AEGIS field. Besides their intrinsic scientific value, these spectroscopic data have been used to create an ad-hoc library of hybrid SED templates (combining normal galaxies and AGN) that have allowed us

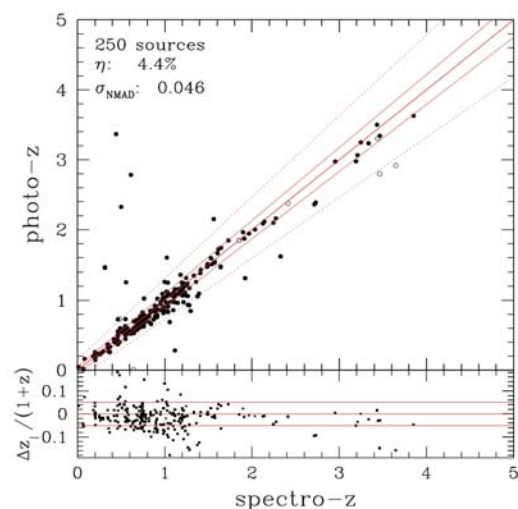


Fig. HE.1: Photometric vs spectroscopic redshift for the X-ray point sources in the AEGIS-X deep Chandra field, where accuracy and fraction of outliers are also indicated (Nandra et al., in prep). It is only recently that X-ray source detections, identifications and redshift determinations have become adequate for proper demographic studies, thanks in large part to efforts by members of our group.

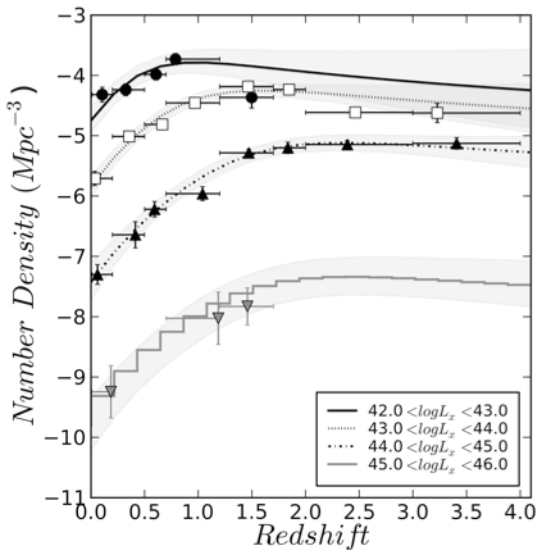


Fig. HE.2: The AGN number density as a function of redshift shows the growth of SMBH. It is well known that the accretion power in the Universe declines from $z=1-0$, but the exact behaviour at all redshifts depends on a precise understanding of the selection functions, redshift determinations and obscuration properties. From Fotopoulou et al. in prep.

to obtain photometric redshifts for faint and high-redshift AGN in the XMM- and Chandra-COSMOS fields with an accuracy never reached before at these regimes (Salvato et al. 2009, 2011). We are currently expanding the photometric redshift methodology to other fields, such as the (E)CDFs (Hsu et al., in prep.), Lockman Hole (Fotopoulou et al. 2012) and AEGIS-X surveys (Fig. HE.1; Nandra et al. in prep), providing an accuracy limited only by the number of bands available in a given field.

The methods described above that the MPE HE group is developing are the backbone for the scientific exploitation of high energy surveys. Only samples with a well-defined selection function, well-characterised X-ray source properties, secure identifications and accurate redshifts can be used for meaningful AGN demographic studies.

The accretion history of the Universe

Previous studies of the X-ray Luminosity Function (XLF) have revealed that AGN are a strongly evolving population, with the overall distribution shifting to lower luminosities between $z \sim 1$ and the present day (Hasinger et al. 2005; Silverman et al. 2008a). Such evolution is broadly characterized by a shift in the peak of the space density of AGN towards lower redshifts for objects of lower luminosities, but there are remaining uncertainties as to the exact form of the evolution, especially at high redshifts. In part, this is due to the difficulties of accurately measuring the faint end of the XLF, where incompleteness in X-ray detection and identification, and uncertain redshift information are all serious issues. To improve on this, we have recently compiled highly redshift-complete samples of AGN selected in the 2-10 keV (Aird et al. 2010) and 5-10 keV bands (Fotopoulou et al., in preparation). We have used Bayesian techniques to compute the best

fitting XLF, properly accounting for selection effects, thus providing a meaningful census of both (mildly) obscured and un-obscured AGN activity in the Universe out to $z \sim 4$ (see Fig. HE.2). The apparent anti-hierarchical behaviour seen in previous work still fits the data well, but appears to be much less pronounced when selection effects are properly considered. The accuracy of this work is still limited by small sample sizes and we expect major progress once the full suite of surveys is combined together.

A key additional uncertainty in determining the evolution of SMBH accretion is the effect of obscuration. In the search for a complete census of AGN, the missing population that systematically evades our accounting is the so-called Compton Thick (CT) AGN, i.e. those obscured by column densities so high to escape detection in the energy bands where X-ray imaging telescopes are most sensitive (up to ~ 10 keV). Until a few years ago, the only handle on such population came from the modelling of the cosmic X-ray background radiation (CXRB; Gilli et al. 2007). At MPE, we have used the Swift/BAT wide field imager to put new constraints on the CXRB at high energies using Earth occultation (Ajello et al. 2008b).

Harder X-rays (> 10 keV) also have more penetrating power, and we have used the Swift/BAT survey to perform a statistical analysis of a complete sample of local AGN selected in the very hard X-ray band (15-45 keV, Ajello et al. 2008a; Burlon et al. 2011). This latter work was used to constrain the intrinsic CT AGN fraction in the local Universe to about 20 per cent. X-ray spectroscopy below 10 keV offers an alternative approach to the identification of the most obscured AGN, which can be seen in scattered light with a characteristic spectrum. These X-ray techniques have been employed to determine the Compton thick fraction in bright, local IR-selected AGN, giving a remarkably similar fraction (Brightman & Nandra 2011).

At higher redshifts, characterisation of heavily obscured AGN is hampered by the lack of very high quality spectra. We have developed Monte-Carlo models for the spectral modelling of CT AGN (Brightman & Nandra 2011, 2012; see Fig. HE.3), and have applied them to search for obscured AGN in the CDFS (Brightman & Ueda 2012), and other fields. This approach has revealed relatively large samples of CT AGN for the first time, and indicates positive evolution of CT AGN fraction, which appears to increase up to $\sim 40\%$ in the broad redshift range $1 < z < 3$. Disentangling the effects of obscuration and its dependence on luminosity and redshift (e.g. Hasinger 2008) is the key towards providing a full understanding of the evolution of the accretion power in the Universe.

In the X-ray spectral domain we have also used survey data to characterise statistically the properties of prominent features, specifically the iron K α emission line. We found that the narrow iron K α emission line, the most prominent feature in AGN X-ray spectra, is clearly dependent on luminosity, but shows no sign of evolution in its equivalent width with redshift, at least up to $z \sim 1.2$ (Chaudhary et al. 2010). Because the narrow iron line

is produced by the same material on parsec scale responsible for the nuclear obscuration, this result argues against a strong evolution in the global properties of the obscuring medium in AGN. This provides an additional constraint on the evolution AGN obscuration in deep surveys. More work on larger complete samples, such as those provided by eROSITA will be very important to assess the amount of redshift evolution of AGN obscuration.

As far as the highest ($z>6$) QSOs are concerned, our current knowledge comes mainly from optical surveys, such as the SDSS and CFHT. However, these surveys only sample the high luminosity, un-obscured tail of the QSO population. X-ray selection is less sensitive to obscuration effects and is more efficient at picking up the bulk of QSO population at lower, more representative luminosities. While a full X-ray census is not yet available, the pioneering work from the MPE HE group in the COSMOS field (e.g. Brusa et al. 2009a; Civano et al. 2011) represents the current best constraint on the high-redshift ($3<z<5$) evolution of X-ray selected AGN, clearly showing a decline of AGN number density with increasing redshift. Still, the evolution of X-ray selected AGN at $z>6$ is today unconstrained, due mainly to the lack of area coverage at substantial depth, a situation that will change dramatically with eROSITA (§4.4.1), and later with Athena+ (§4.5.1).

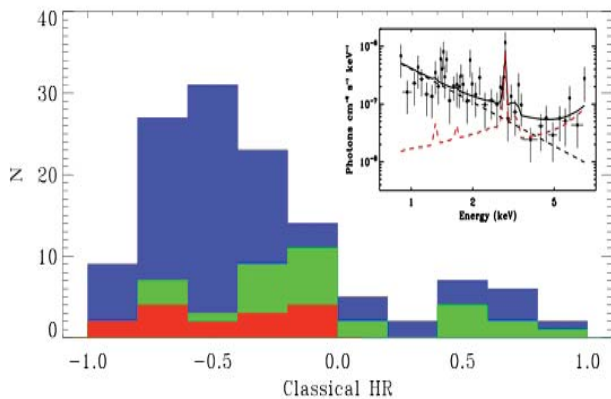


Fig. HE.3: Histogram of hardness ratios ($H-S/H+S$, where H is the flux in 2–10 keV band, and S is the flux in the 0.5–2 keV band) for a sample of local AGN from Brightman & Nandra (2011), with high quality XMM-Newton data. In blue are all AGN, in green sources with $NH>10^{23}$ cm $^{-2}$ and in red Compton Thick sources. All CT sources show soft hardness ratios due to scattered emission, and hence would be missed without more complex spectral fitting. Inset is an example spectrum of a Compton thick source in the AEGIS-XD survey identified through spectral fitting. With a hardness ratio of -0.05, it would have been missed using hardness ratios alone.

Co-evolution: the physical link between black holes and their host galaxies

The $M-\sigma$ relationship seen in the local Universe suggests a direct link between SMBH and their host galaxies. The demographics of AGN, which signpost accretion events onto SMBHs, is a powerful approach to shed light into

this relationship. Our group has performed much of the pioneering work in this area using data in the AEGIS and COSMOS fields, relating X-ray AGN activity to host colours (e.g. Nandra et al. 2007; Georgakakis et al. 2008a) morphology (Georgakakis et al. 2009) and environment (Georgakakis et al. 2007; Silverman et al. 2008b).

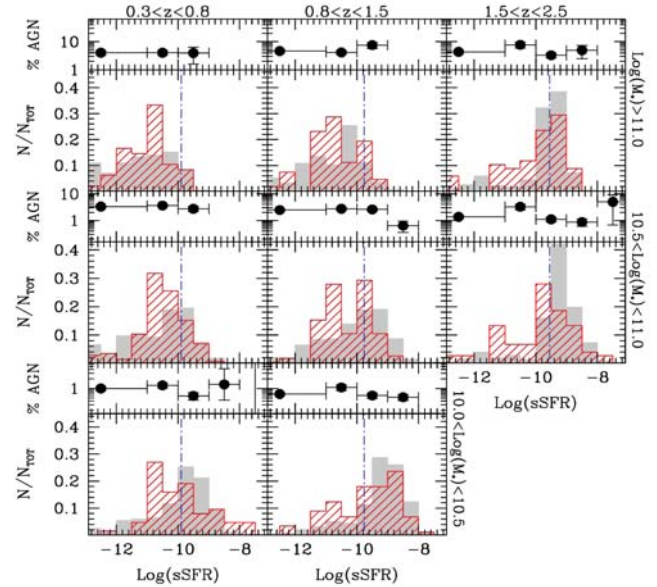


Fig. HE.4: The specific Star Formation Rate distributions divided into three redshift bins and three mass ranges for X-ray selected type 2 AGN host galaxies (red histogram) and normal galaxies (grey histogram) in COSMOS. The dot-dashed vertical blue lines are used to distinguish quiescent from star-forming galaxies. The upper panel of each histogram shows the observed AGN fractions. We do not see any clear difference in the SFR properties of AGN hosts and normal galaxies (Bongiorno et al. 2012)

A major observational challenge in any comprehensive study of AGN–galaxy co-evolution, however, is the accurate separation of the AGN and galaxy emission components at optical–IR wavelengths. Members of the MPE HE group have developed a two-component fitting procedure, in which the observed AGN SED is modelled with a large grid of templates based on a combination of intrinsic nuclear AGN (accretion disc plus torus, possibly absorbed) and host-galaxy models (synthetic spectra created from stellar population synthesis). Given wide multi-wavelength coverage, this technique allows us to derive robust measurements of the physical properties of the host galaxy (e.g. rest-frame colours, stellar mass, K-band luminosity and SFR). The method is applicable to all AGNs, obscured and un-obscured, independent of their luminosity. We have used this method in recent years to study: (i) the relation between host stellar masses and black hole masses in a sample of ~ 100 type 1 AGN at $1<z<2$ (Merloni et al. 2010); (ii) the AGN fraction as a function of host stellar mass in the CDFS (Brusa et al. 2009b); (iii) the stellar mass and star-formation rate properties of a complete sample of ~ 1500 X-ray selected AGN in COSMOS (Brusa et al. 2010; Bongiorno et al. 2012); (iv) the Herschel-based star-formation rate prop-

erties of the X-ray selected AGN in the CDFS (Rovilos et al. 2012). AGN hosts do follow quite closely the overall evolution of the stellar build-up of the parent galaxy population and populate both star-forming and more passive galaxies (see Fig. HE.4). However, it remains hard to find strong indications that AGNs play a direct role in shaping the global properties of their host galaxies, or their evolution.

Relating AGN to large-scale structure

The physical conditions under which AGN grow their mass, e.g. their fuelling modes and triggering mechanisms, imprint detectable signatures on the distribution of AGN in dark matter haloes. Therefore measurements of the clustering properties of active supermassive black holes provide important constraints on the processes that shape the accretion history of the Universe.

Researchers in the MPE HE group have been using the largest extragalactic survey programmes to weigh the dark matter haloes in which AGN live. Fig. HE.5 summarises the current state-of-the-art in measurements of the typical (average) dark matter halo mass of AGN, including data-points from MPE HE group-led studies (Cappelluti et al. 2010; Allevato et al. 2011; Mountrichas & Georgakakis 2012). It shows that X-ray AGN live in halos with average masses in the range $\log M = 12.5-13.5 M_{\odot}$, higher than the predictions of major-merger black hole formation scenarios ($\log M \sim 12 M_{\odot}$). This is interpreted as evidence against major galaxy mergers as the only trigger for growing black holes in the Universe.

A limitation of the measurements in Figure HE.5 is that they do not provide information about the distribution

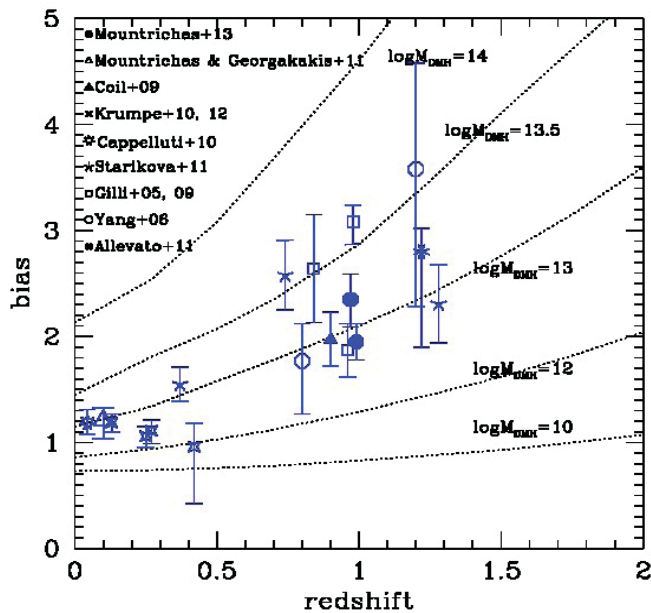


Fig. HE.5: Compilation of measurements of X-ray AGN bias – a proxy for dark matter halo mass - many of which originate from the MPE HE group or our collaborators. X-ray AGN tend to be associated with massive haloes, $\log M = 12.5-13.5 M_{\odot}$.

of AGN in dark matter haloes. We have recently made progress toward addressing this issue. A major research highlight of MPE HE group has been the first direct measurement of the dark matter Halo Occupation Distribution (HOD) of AGN (Fig. HE.6; Allevato et al. 2012). It is found AGN in satellites increases slower with halo mass than the HOD of galaxies. It is also found that massive structures ($\log M > 13 M_{\odot}$) within any survey bias the inferred clustering of AGN to large values that are unrepresentative of the entire population. Removing those structures yields lower halo masses, $\log M \sim 12.5$ (solar units) for the bulk of the X-ray AGN at $z \sim 1$ (Mountrichas et al. 2013). This range is consistent with the predictions of models in which cold-gas accretion dominates the growth of black holes.

Prospects for eROSITA

More than 20 years after the ROSAT (soft) X-ray all-sky survey, we are close to the next major revolution in the field with eROSITA. With on-axis spatial and spectral resolution similar to XMM-Newton, comparable effective area at low energies, and a wider field of view, eROSITA will be the most powerful X-ray survey instrument in history and furthermore a highly capable X-ray observatory for the next decade. Its X-ray mapping capabilities over the whole celestial sphere will likely be unmatched for decades to come. The scientific potential of eROSITA is discussed in Merloni et al. (2012).

The eROSITA sky will be numerically dominated by AGN, with about 3 Million accreting black holes expected at the end of the 4 year all-sky survey. This will be a uniquely powerful tool, not only for the study of AGN evolution,

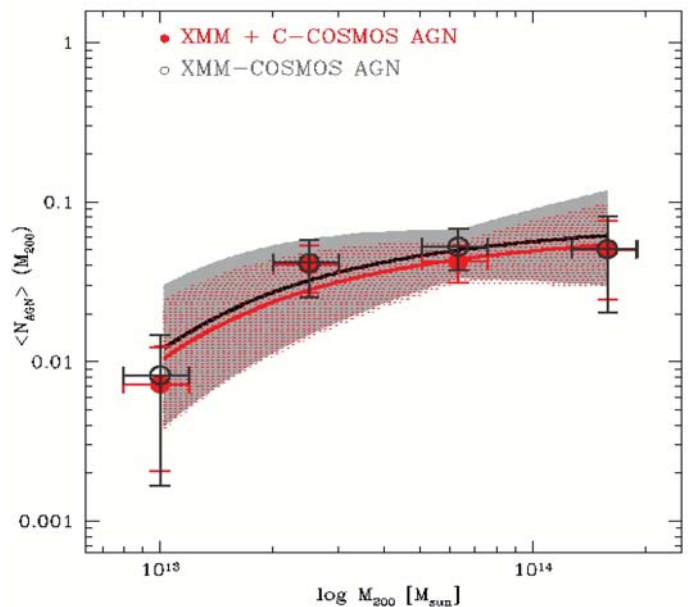


Fig. HE.6: Halo Occupation Distribution (HOD) of AGN in the XMM and Chandra survey of the X-ray COSMOS field. The curves correspond to fits by a rolling-off power-law dependence of the HOD. The shaded regions correspond to the 1σ confidence interval (Allevato et al. 2012).

but also in the search for rare objects (high-redshift QSOs, CT AGN), and the study of the SMBH-galaxy co-evolution. Today, small number statistics still hamper our ability to understand how the AGN-galaxy relationship evolves as a function of redshift, AGN luminosity, nuclear obscuration, host galaxy stellar mass, star-formation properties and environment. eROSITA will not just minimise Poisson noise and cosmic-variance errors but will also open a new parameter space for these investigations at the extremes of e.g. luminosities, Eddington ratios and host properties. To exploit the data properly, we require at minimum the redshifts of the sources, and the HE group is heavily involved in the planning of two wide-area spectroscopic surveys, SPIDERS and 4MOST specifically designed for this purpose (see § 4.5.4 and § 4.5.5). Photometric redshifts are none the less essential to exploit the full sky coverage and depth of eROSITA, and in addition to our leading work in assigning accurate photo-z to AGN discussed above, we are also developing techniques to apply these photo-z, incorporating the full uncertainties, to the determination e.g. of clustering and X-ray spectral properties.



Antonis Georgakakis, Andrea Merloni, Kirpal Nandra, Mara Salvato

(Other HE team members include Murray Brightman, Hermann Brunner, Johannes Buchner, Tom Dwelly, J. Greiner, Li-Ting Hsu, Marie-Luise Menzel, Gabriele Ponti, Arne Rau.

Former HE team members include M. Ajello, V. Allevato, A. Bongiorno, E. Bottacini, M. Brusa, D. Burlon, N. Cappelluti, P. Chaudhary, A. Finoguenov, S. Fotopoulou, G. Hasinger, S. Komossa, M. Rivilos, J. Silverman)

Selected References:

- Aird et al. 2010, *MNRAS*, 410, 2531
- Ajello et al., 2008a, *ApJ*, 678, 102
- Ajello et al., 2008b, *ApJ*, 689, 666
- Allevato et al. 2011
- Allevato et al. 2012, *ApJ*, 758, 47
- Bongiorno et al. 2010, *A&A*, 510, 56
- Bongiorno et al. 2012, *MNRAS*, 427, 3103
- Brightman & Nandra 2011, *MNRAS*, 414, 3084
- Brightman & Nandra 2012, *MNRAS*, 422, 1166
- Brightman & Ueda 2012, *MNRAS*, 423, 702
- Brunner et al., 2008, *A&A*, 479, 283
- Brusa et al. 2009a, *ApJ*, 693, 8
- Brusa et al. 2009b, *A&A*, 507, 1277
- Brusa et al. 2010, *ApJ*, 716, 348
- Burlon et al., 2011, *ApJ*, 728, 58
- Cappelluti et al. 2001, *A&A*, 496, 635
- Chaudhary et al. 2010, *A&A*, 518, 58
- Fotopoulou et al. 2012, *ApJS*, 198, 1
- Georgakakis & Nandra 2011, *MNRAS*, 414, 992
- Georgakakis et al. 2007, *ApJ*, 660, 15
- Georgakakis et al. 2008a, *MNRAS*, 385, 2049
- Georgakakis et al. 2008b, *MNRAS*, 388, 2205
- Georgakakis et al. 2009, *MNRAS*, 397, 623
- Gilli et al. 2007, *A&A*, 463, 79
- Guglielmetti et al. 2009, *MNRAS*, 396, 165
- Hasinger et al. 2007 *ApJS*, 172, 79
- Hasinger 2008, *A&A*, 490, 905
- Laird E.S., et al., 2009, *ApJS*, 180, 102
- Merloni & Heinz 2008, *MNRAS*, 388, 1011
- Merloni & Heinz 2013, to appear in "Planets, Stars and Stellar Systems", vol. 6, ed. W. Keel. [arXiv:1204.4265](https://arxiv.org/abs/1204.4265)
- Merloni et al. 2010, *ApJ*, 708, 137
- Merloni et al. 2012, [arXiv:1209.3114](https://arxiv.org/abs/1209.3114)
- Mountrichas & Georgakakis 2012, *MNRAS*, 420, 514
- Mountrichas et al. 2013, *MNRAS*, 430, 661
- Nandra et al. 2007, *ApJ*, 660, L11
- Salvato et al. 2009, *ApJ*, 690, 1250
- Salvato et al. 2011, *ApJ*, 742, 61
- Silverman et al. 2008a, *ApJ*, 679, 118
- Silverman et al. 2008b, *ApJ*, 675, 1025

4.2.2 Clusters and Groups of Galaxies

Investigations of clusters, groups of galaxies and large-scale structures in general, are among the prime areas of scientific interest for the HE group, also being the main driving science behind eROSITA. As the largest well defined objects in our Universe, clusters are ideal tracers to outline the large-scale structure and to test cosmological models. Our research in this area covers a broad scope, ranging from the nearby Universe to the most distant known systems, and from the most massive clusters to much lower mass groups of galaxies, the latter also out to high redshift. Our investigations range from surveys using both deep and wide fields, to detailed investigations of samples and individual objects. Systematic, deep X-ray studies of representative samples of galaxy clusters have given us a clear picture of their average structure as well as of the range of cluster morphologies. Adding also a detailed comparison of optical and X-ray properties we are in the position of predicting the range of many properties from just one observable. This knowledge is an important prerequisite for any cosmological modeling. We have also compiled large samples of distant clusters, among them, some of the highest redshift systems known. In addition, clusters and groups represent the highest density regions of the large-scale structure, so investigating the properties of galaxies in group and cluster environments as a function of redshift provides a unique probe of galaxy evolution.

Cosmological studies with galaxy clusters

The ROSAT All-Sky survey (RASS) remains an important basic resource for our cosmological studies with clusters. We have nearly completed two extended galaxy cluster redshift surveys in the northern (NORAS II Survey) and southern (REFLEX II Survey) part of the RASS for strictly flux-limited cluster samples comprising more than 1800 objects (Böhringer et al. 2013). Fig. HE.7 (top panel) provides a projected impression of the three-dimensional distribution of these galaxy cluster samples. The surveys are highly complete and have a very precisely determined selection function. The samples have the highest statistical quality of any cluster data set.

We apply these data to a large number of cosmological studies. One of the most immediate applications is the determination of the X-ray luminosity function of galaxy clusters, also shown in Fig. HE.7. This function is closely related to the mass function of galaxy clusters and can be predicted from cosmological models of structure formation. It is exponentially sensitive to cosmological parameters like the amplitude of cosmic density fluctuations, σ_8 and the matter density parameter, Ω_m . The right panel of Fig. HE.7 shows how the observed X-ray luminosity function can be turned into constraints of these two important cosmological parameters (Böhringer et al. 2013).

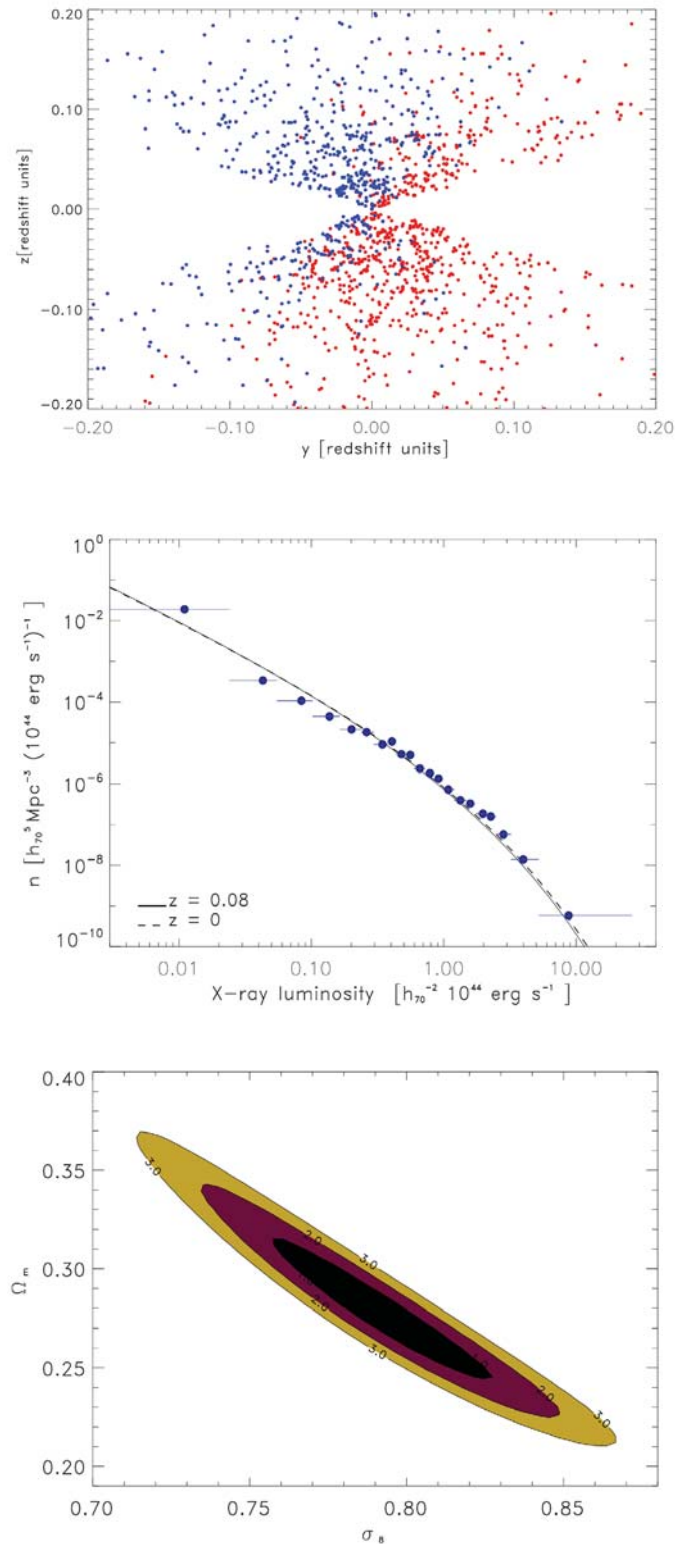


Fig. HE.7 Top: projected three-dimensional distribution of the galaxy clusters of the REFLEX II (red) and NORAS II Surveys (blue). The galactic plane is in the middle of the plot. Middle: X-ray luminosity function of the REFLEX II Survey. Bottom: Constraints on the cosmological parameters Ω_m and σ_8 from a comparison of theoretical predictions to the observed REFLEX X-ray luminosity function (Böhringer et al. 2013).

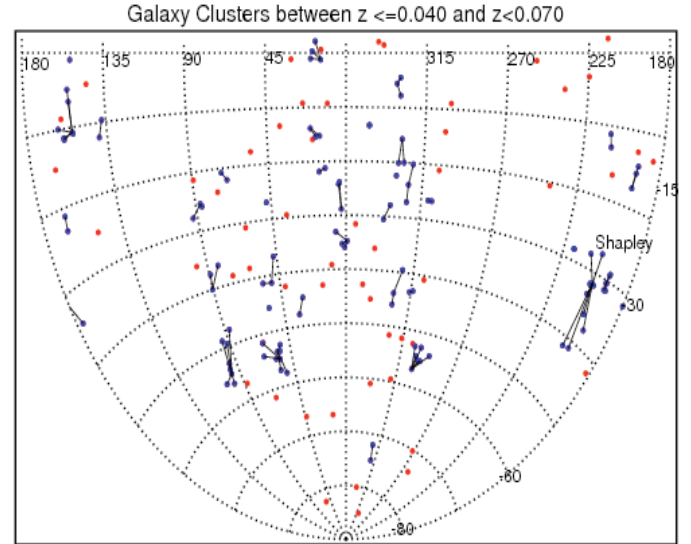
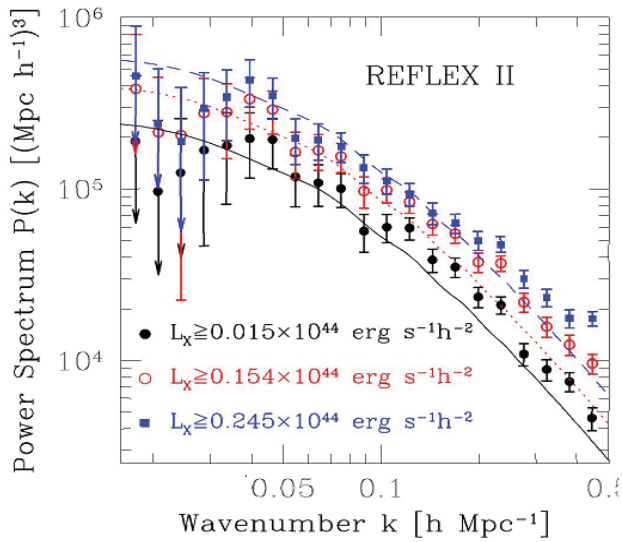


Fig. HE.8 Left: Power spectrum of the density distribution of the REFLEX II galaxy clusters. The amplitude of the power spectrum increases with increasing mean X-ray luminosity (mean mass) as predicted by theory (Balaguera-Antolinez et al. 2011). Right: Superclusters (marked in blue) found in the REFLEX II survey in the redshift range $0.04 < z < 0.07$ including the famous Shapley supercluster (Chon et al. 2013).

A widely used characteristic of the large-scale structure in the matter distribution in the Universe is the density fluctuation power spectrum. The corresponding power spectrum of the galaxy cluster density distribution follows that of the matter distribution in an amplified (biased) way. This biasing is theoretically calculable from first principles of structure formation theory. We have used the REFLEX II Survey to construct the cluster power spectrum and to test the biasing theory. Fig. HE.8 (left) shows the observed biasing effect in comparison to theory. The more massive and thus the more X-ray luminous the clusters in subsamples are, the larger the bias (amplification of the density fluctuations). Within the current uncertainties the observations follow the theory. We have now a confirmation that biasing is effective in nature and we are now no longer blindly trusting theory in this respect.

Galaxy clusters are not the largest structures we find in these surveys. We also find quite distinct groupings of clusters, or superclusters (Chon et al. 2013). Using REFLEX II we constructed a catalog of 164 superclusters, a subset of which is shown in Fig. HE.8 (right). Since these superclusters are constructed from a very well defined

nearly mass selected sample of clusters, we have now a supercluster catalog in hand which has much better statistical qualities than any previous supercluster sample. We can e.g. use our well defined selection function to construct similar supercluster samples from simulations and compare the properties of observed and simulated clusters in detail. We find that more than half of the clusters are located in superclusters that fill only 2% of the volume of the Universe.

Systematic study of the statistics of cluster structure

An important application of the RASS surveys is the selection of well-defined, representative samples of clusters for deeper studies. Our REXCESS study (Böhringer et al. 2007) of a strictly representative sample of 31 galaxy clusters with deep XMM-Newton observations (XMM-Newton Large Program, PI H. Böhringer) is a very important one of these. We use the sample to characterise the statistics of cluster structure, determining many average cluster properties and their dispersion. The results are widely used for comparison to simulations and for modelling of clusters, notably for clusters in the Planck Survey.

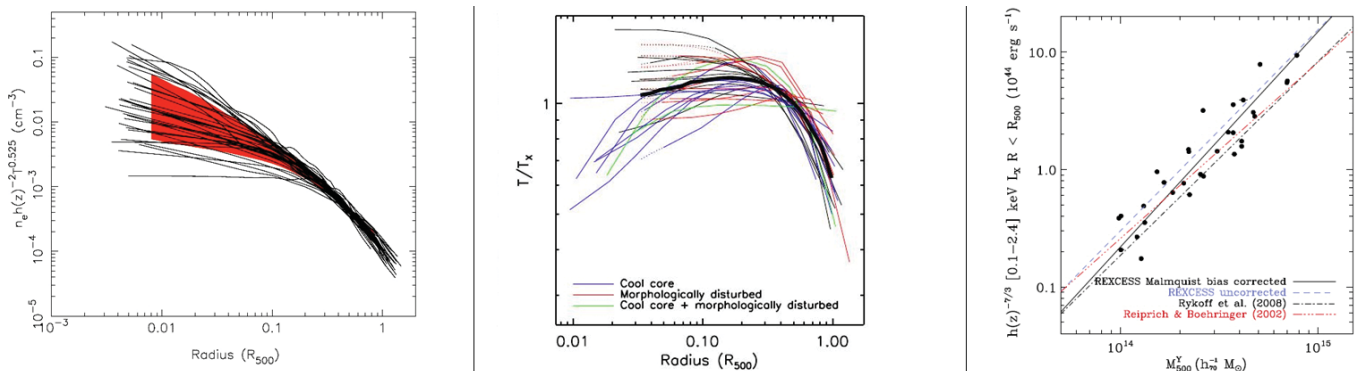


Fig. HE.9 Self similar shape of the gas density profiles (left) and temperature profiles (middle) for the REXCESS clusters. The right panel shows the relation of X-ray luminosity and cluster mass (Croston et al. 2008, Pratt et al. 2009).

While X-ray images of clusters seem to show a wide range of morphologies, detailed physical studies of the structure of clusters and their intracluster medium (ICM) reveal that they constitute a well defined family of closely self-similar objects. Fig. HE.9 shows the radial electron density profiles and temperature profiles of the ICM of the REXCESS clusters. Using the most appropriate scaling laws of cluster properties as a function of mass allows us to map the profiles very tightly on top of each other, as illustrated in the figure. The largest deviation appear in the center, where gas cooling and AGN feedback affects the ICM structure. Low scatter scaling relations as for example the X-ray luminosity – mass relation, shown in the right panel of Fig. HE.9 are the result of the self-similar behaviour of clusters. The relation shown lets us estimate the mass of galaxy clusters for given X-ray luminosity with an uncertainty of about 40%. Excising the central region with its large dispersion from the luminosity measurement tightens the relation to about 20%. A precise scaling relation between X-ray luminosity and cluster mass is absolutely crucial for the application of X-ray cluster surveys to cosmological tests. We also performed detailed studies of the dynamical state and substructure of galaxy clusters and find, for example, little change of the fraction of clusters with substructure as a function of cluster mass (Böhringer et al. 2011). Based on our detailed observational results, a survey of the literature and comparison to simulations we have constructed a scaling relation model that describes all current results, providing new insights in the redshift evolution of scaling relations pointing to an early energy input into the ICM by supernovae and/or AGN.

We are currently extending our cluster structure studies to the largest volume-limited X-ray galaxy cluster sample with deep XMM-Newton studies (2 Large Programs PI Böhringer). This will not only increase our statistics, but also avoid the sampling bias of flux-limited surveys. This offers an unbiased look at the cluster population, which shows, for example, less cool core clusters and more unrelaxed systems, compared to what was found in our previous surveys.

Distant galaxy clusters in the first half of cosmic time

In the past six years observational studies of distant galaxy clusters at $z > 0.8$ have seen tremendous progress. Within the XMM-Newton Distant Cluster Project (XDCP) we have been very successful in using deep XMM-Newton archival data to discover and characterize dozens of new distant X-ray luminous galaxy clusters based on their extended X-ray emission signature (Fassbender et al. 2011c, see left panel of Fig. HE.10). To date, the XDCP has compiled the largest sample of distant X-ray clusters with currently more than 40 spectroscopically confirmed systems in the redshift range $0.8 \leq z \leq 1.6$ as shown by the mass-redshift distribution in the central upper panel of Fig. HE.10. The availability of such a sample of distant X-ray clusters will enable numerous cluster evolution studies as a function of system mass and redshift up to lookback times of 9.5 Gyrs. The XDCP survey has also pushed the X-ray selection technique to systems in the previously unexplored cluster redshift desert at $z > 1.5$, for which detailed follow-up data have been recently obtained (see e.g. top right panel of Fig. HE.10).

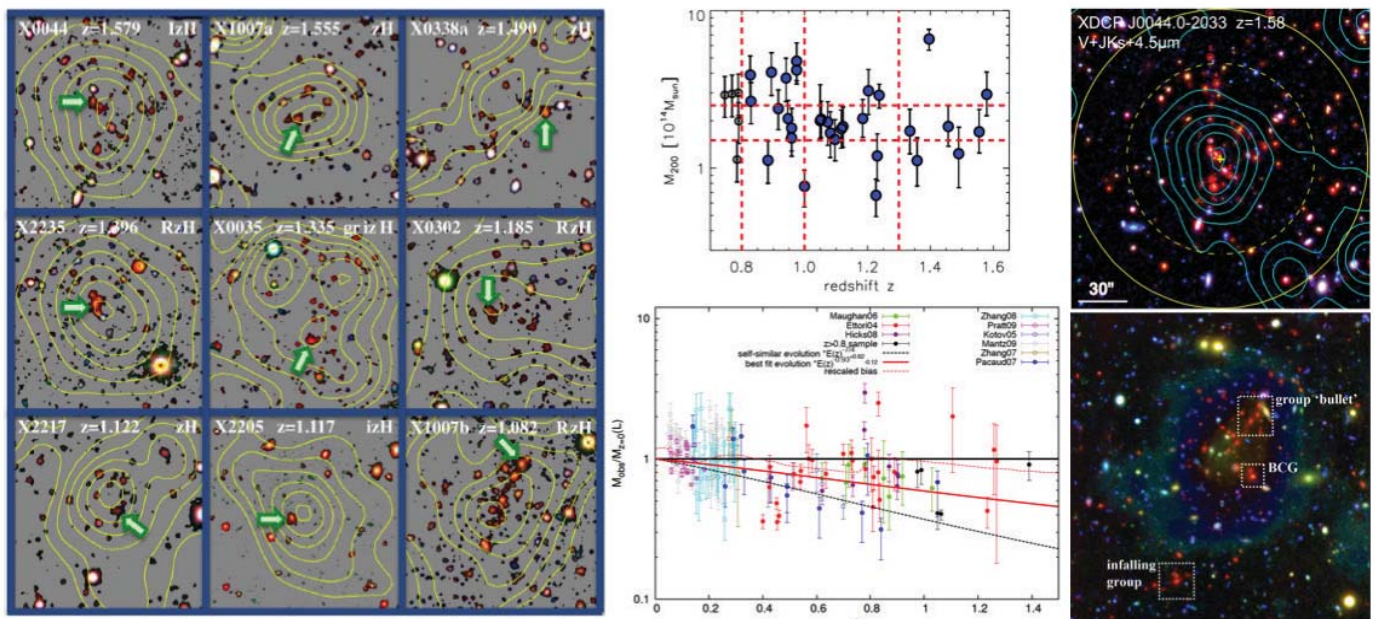


Fig. HE.10: Left: Gallery of selected $z > 1$ X-ray luminous galaxy clusters from the XDCP survey. XMM-Newton X-ray contours are overlaid on optical/NIR color images with a side length of 1.5 arcmin and a rescaled background for contrast enhancement. Green arrows mark the locations of the brightest cluster galaxies. Top center: Mass-redshift distribution of the current XDCP distant cluster sample. Bottom center: Empirical calibration of the redshift evolution of the mass-luminosity relation. The found evolution (red line) deviates significantly from self-similar evolution predictions (black dotted line). Right: Examples of two distant XDCP clusters at $z = 1.58$ (top) and $z = 0.98$ (bottom) with deep new multi-wavelength coverage that will allow a detailed physical characterization of the systems.

Many of the newly discovered galaxy clusters show interesting astrophysical processes at work that motivate in-depth follow-up studies such as ongoing cluster merging events (e.g. Fassbender et al. 2011a, bottom right panel of Fig. HE.10), high- z strong lensing features, or galaxy transformation processes at work. First sample studies based on high- z XDCP clusters have e.g. constrained the evolution of the important X-ray scaling relations out to $z \sim 1.5$ (lower central panel of Fig. HE.10) with significant deviations from self-similar evolution (Reichert et al. 2011); have studied the distribution of cluster-centric offsets and the luminosity gaps of the brightest cluster galaxies, and investigated the stacked radial distribution of X-ray AGN in the distant cluster environments.

Low mass clusters and groups in deep surveys

As in our work on SMBH evolution, we have systematically exploited the large number of available deep XMM-Newton and Chandra surveys to search for new clusters and groups. These deep surveys tend to yield lower mass system – poor clusters and groups of galaxies – than the much wider ROSAT and XMM archival surveys. Survey work lead by our group so far includes the exploitation of the CDFS, CNOC2, SXDF, COSMOS, AEGIS and DEEP2 fields (Finoguenov et al. 2007, 2009, 2010; Connelly et al. 2012; Erfanianfar et al. 2013). These have yielded deep catalogs of groups, reaching a flux level up to 10,000 fainter than that of the RASS. The exceptional multiwavelength data in these fields enables a unique set of investigations both of the groups and clusters themselves, and the galaxies that lie within these

large virialised structures. These multiwavelength studies have also offered extensive opportunities for collaboration within MPE in both the OPINAS and IR/submm groups, in which much knowledge can be added to the X-ray expertise in the HE group, for example for weak lensing calibration and star-formation properties.

Some of the fruits of this work include calibration of the scaling relations and clustering properties of groups using weak lensing data (Zhang et al. 2007, 2008; Leauthaud et al. 2010; Allevato et al. 2012) and the determination of the baryon budget in groups (Fig. HE.11 Giodini et al. 2009; Connelly et al. 2012). These surveys have also enabled a rich suite of studies of galaxy evolution within these dense environments. Our work has included the evolution of the star formation rate within groups (Fig. HE.12; Popesso et al. 2011; Ziparo et al. 2012), as well as the stellar mass function as a function of environment (Fig. HE.13 Giodini et al. 2012). The effects of feedback (Giodini et al. 2010) and the incidence of radio and X-ray AGN activity (Smolcic et al. 2010; Allevato et al. 2012) have also been investigated with these samples.

Detailed study of individual clusters

Among our detailed studies of nearby clusters including the Virgo cluster and Hydra A, we show here some recent results obtained from deep archival Chandra observations on Cygnus A in comparison to radio data (Chon et al. 2012). Studying the correlation of the structure of the radio lobes (observed with VLA and LOFAR) with the X-ray surface brightness we discovered a particular

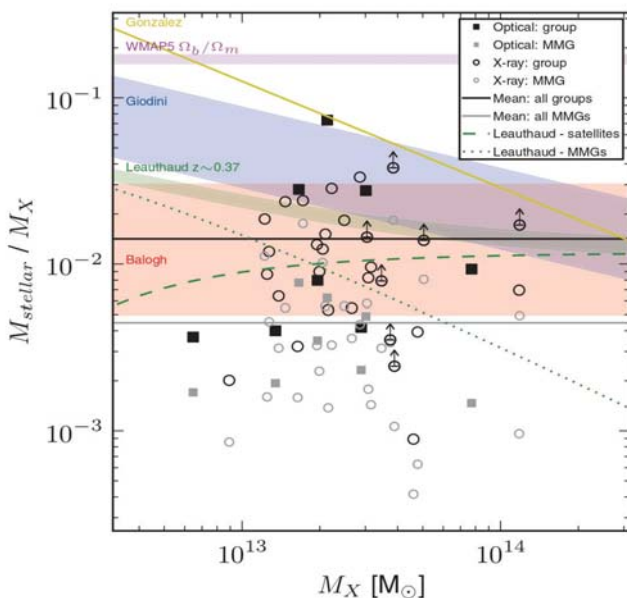


Fig. HE.11: The stellar mass fraction of galaxy groups from Connelly et al. (2012). A large variation in total stellar light and the contribution of most massive galaxy (MMG) is revealed. In order to be able to study the low mass groups, deep and highly complete spectroscopy programs with VLT and Magellan telescopes have been carried out.

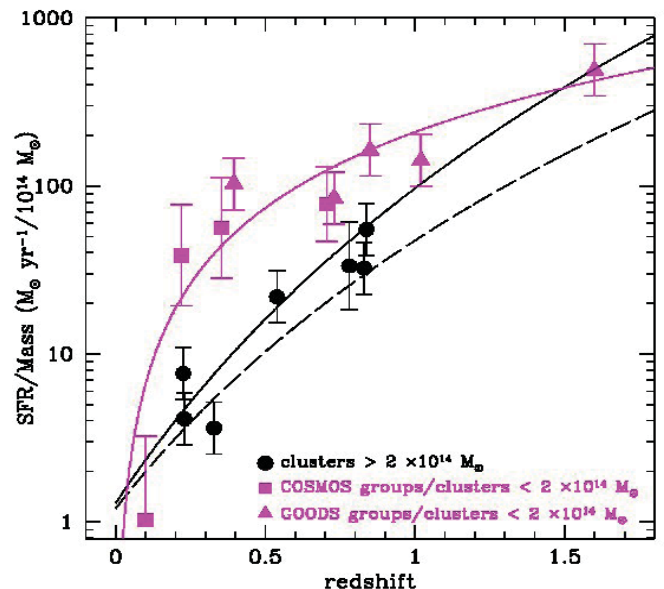
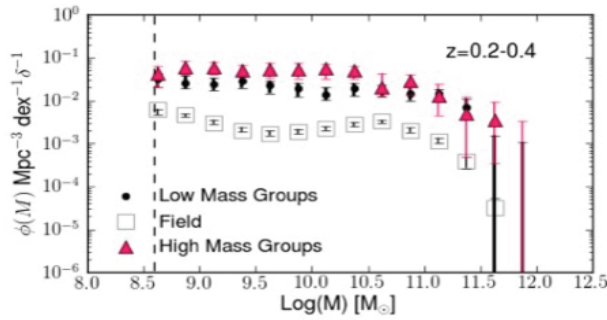


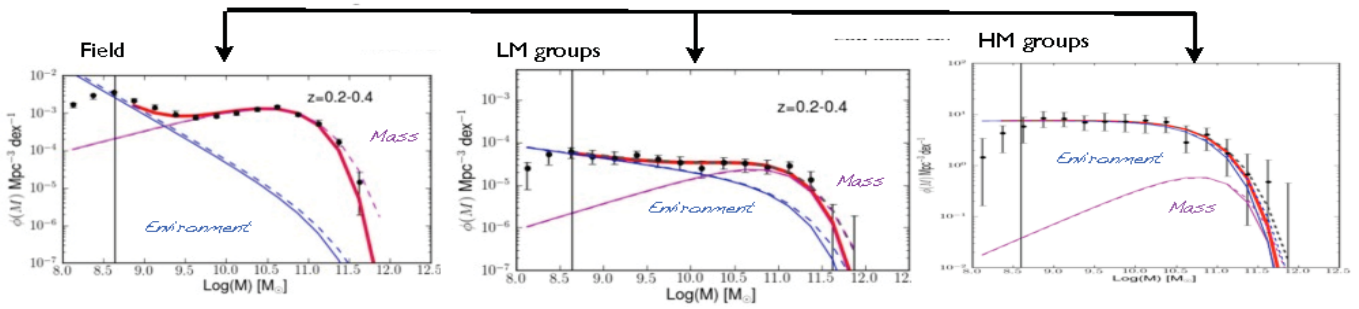
Fig. HE.12: The evolution of star-formation rate per halo mass. Herschel data have been used to estimate the star-formation rate in group member galaxies, which shows a much stronger evolution of star-formation with redshift compared to the field and a much higher level of star-formation overall compared to clusters (Popesso et al. 2012, Ziparo et al. 2013).

Passive Galaxies



Distributions are more complicated than for star forming galaxies: parametrized with double Schechter function.

The galaxy stellar mass distributions are different at $\text{Log}(M/M_{\text{sun}}) < 10.5$!



- Growing influence of environment
- Field forms first the very low mass part (steep slope at low mass!), while the intermediate part is in delay. (see also Tanaka+2005)
- Groups of high and low mass quench efficiently galaxies $\text{Log}M < 10^{11} M_{\text{sun}}$.
- M^* in groups larger than in the field: compatible with little amount dry merging.
- Little evolution of the low mass up to $z=0.6$ then the low mass part is below completeness.

Fig. HE.13 Study of the differences in the passive galaxy mass function with environment. Differences in the roles of mass (or AGN) vs environment quenching are revealed. In low mass (LM) groups red galaxies were not quenched by the environment, but by AGN, while in high mass (HM) groups and clusters most of the galaxies are quenched by the environment (Giodini et al. 2012).

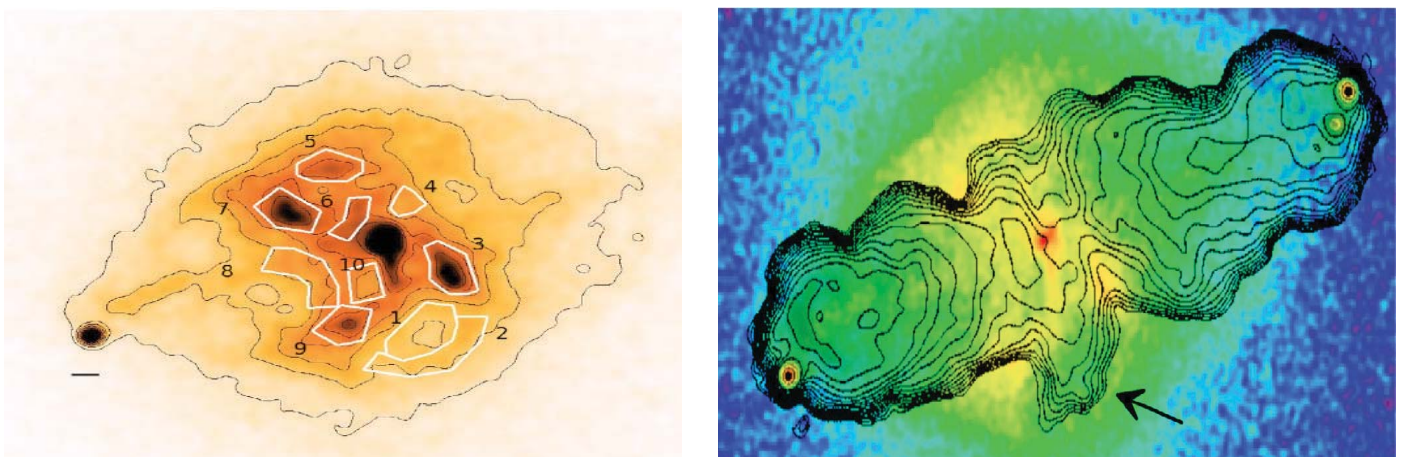


Fig. HE.14: Left: X-ray surface brightness map of the inner region of Cygnus A showing the cavity as a clear low surface brightness region labelled 1. Right: An overlay of the VLA radio map onto the X-ray image shows that the cavity region is filled with relativistic, synchrotron emitting plasma (Chon et al. 2012).

X-ray cavity filled with synchrotron plasma outside the main radio lobes of Cygnus A (Fig. HE.14). Based on analytical modeling and hydrodynamical simulations we interpret this X-ray cavity as a relic of a previous outburst of Cygnus A with a power which was about two orders of magnitude lower than the present very energetic outburst.

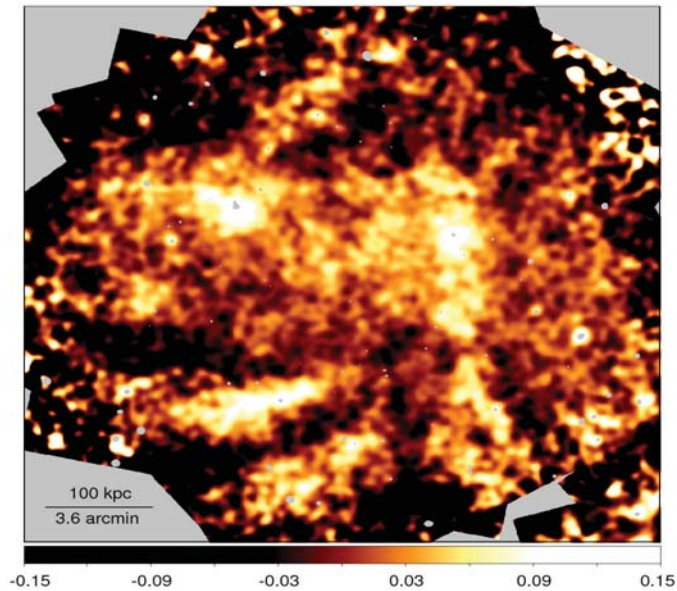


Fig. HE.15: Unsharp-masked Chandra X-ray image of the Coma galaxy cluster core, highlighting features on smaller scales and showing our newly-discovered linear structures. The colour bar shows the fractional surface-brightness deviation from larger-scale emission (Sanders et al. 2013).

Using deep Chandra observations, we have discovered that in the core of the nearby Coma cluster of galaxies there exist several 150-kpc-long linear structures in the intracluster medium (Fig. HE.15; Sanders et al. 2013). As some of these features are connected to much larger merger structures, they are likely the remnants of material which was stripped from a merging subcluster and are several hundred Myr old. These long-lasting filaments provide very valuable information on the nature of the intracluster medium, telling us about motions, turbulence and stripping in cluster cores.

Prospects for eROSITA

One of the main goals of the eROSITA Survey is the detection of the order of 100 000 galaxy clusters by their X-ray emission and the use of this cluster population to chart the large scale structure of the Universe and test cosmological models. The eROSITA survey will reach about 20 – 30 times deeper than the ROSAT All-Sky Survey for these studies. It will also allow the study of cluster properties and scaling relations to unprecedented precision and allow us to unveil what drives galaxy cluster evolution in great detail.

Fig. HE.16 shows the expected mass and redshift distribution of the galaxy clusters that will be detected in the 4 year eROSITA survey. While most of the groups and clusters of galaxies will be found at redshifts below $z = 0.35$, there will be hundreds of clusters detected between redshift $z = 1$ and $z = 1.5$ with the most distant clusters found in the ecliptic poles. Cluster evolution is exponentially sensitive to cosmological parameters and the number of clusters found above redshift 1 is quite dependent on the nature of dark energy; e.g. for a non-evolving equation of state parameter, w , a change of w by 10% would change the number density of clusters at $z > 1$ by $\sim 15\%$. Apart from studying the evolution of the cluster X-ray luminosity function, the spatial distribution of clusters as measured by the two-point correlation function or density fluctuation power spectrum are another important diagnostic of the growth of large-scale structure in the Universe providing good means to constrain cosmological parameters. Overall, constraints of $\Delta w = 0.06$, $\Delta \sigma_8 = 0.007$, $\Delta \Omega_m = 0.003$ are possible by combining eROSITA results with those of PLANCK.

For about 5000 – 10000 groups and clusters of galaxies we expect to obtain enough photons for the temperature determination. This will provide by far the best statistics for a precise correlation of X-ray luminosity and temperature which is an important ingredient for the cosmological modelling. For a number of nearby clusters we will be able to perform a very detailed analysis of the cluster structure with an unlimited field of view. The combination of X-ray and optical data from various sky surveys notably SDSS, DES and PanSTARRS will not only be important in an early step for the cluster identification, but will also provide unprecedentedly detailed insight into the correlation of the properties of the galaxy populations, the cluster structure, and the intracluster medium.

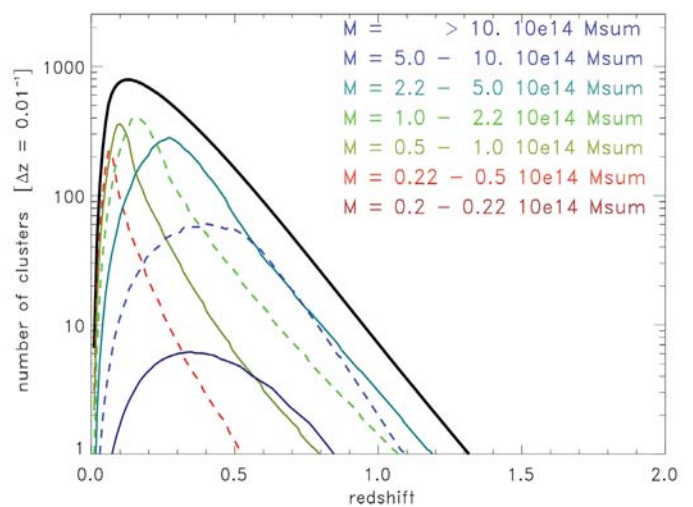
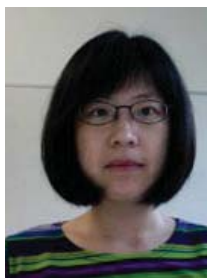


Fig. HE.16: Redshift distribution of the galaxy clusters to be detected in the 4 year eROSITA survey separated into different cluster mass classes. The most distant clusters to be detected will have typical a few 10^{14} solar masses. From Merloni et al. 2012.



Hans Böhringer, Gayoung Chon, Rene Fassbender, Alexis Finoguenov, Kirpal Nandra, Mara Salvato, Jeremy Sanders

(Other HE team members include Nicolas Clerc, Ghazaleh Erfanianfar, Florian Hofmann, Jochen Greiner, John Holland, Fabrizia Guglielmetti, Mohammad Mirkazemi, Alexandra Weissman,

Former HE team members include M. Ajello, V. Allevato, V. Biffi, F. Braglia, N. Cappelluti, J. Connelly, R. Fassbender, S. Giodini, M. Lerchster, Adina Mois, M. Mühlegger, A. Nastasi, N. Ota, D. Pierini, G. Pratt, A. Reichert, J. Santos, A. Simionescu, R. Suhada, M. Verdugo

Selected References:

- Ajello et al. 2009, *ApJ*, 690, 367
- Allevato et al. 2012, *ApJ*, 758, 47
- Böhringer et al. 2007, *A&A*, 469, 363
- Böhringer et al. 2010, 514, 32
- Böhringer 2011, *AIPC*, 1381, 137
- Böhringer et al. 2012, *A&A*, 539, 120
- Böhringer et al. 2013, *A&A*, in press
- Chon et al. 2012, *A&A*, 545, 3
- Chon et al. 2013, *MNRAS*, 429, 3272
- Connelly et al. 2012, *ApJ*, 756, 139
- Chen et al., 2007, *A&A*, 466, 805
- Croston, J. H. et al. 2008, *A&A* 487, 431
- Erfanianfar et al. 2013, *ApJ*, 765, 117
- Fassbender et al. 2008, *A&A*, 481, L73
- Fassbender et al. 2011, *A&A*, 527, A78
- Fassbender et al. 2011, *A&A*, 527, L10
- Fassbender et al. 2011, *New Journal of Physics*, 13, 125014
- Fassbender et al. 2012, *Adv. in Astronomy*, 2012
- Finoguenov et al. 2007, *ApJS*, 172, 182
- Finoguenov et al. 2009, *ApJ*, 704, 564
- Finoguenov et al. 2010, *ApJ*, 715, 1143
- Giodini et al. 2009, *ApJ*, 703, 982
- Giodini et al. 2010, *ApJ*, 714, 218
- Giodini et al. 2012, *A&A*, 538, 104
- Nastasi et al. 2013, *A&A*, 550, A9
- Nastasi et al. 2011, *A&A*, 532, L6
- Pierini et al. 2012, *A&A*, 540, A45
- Pratt, G.W. et al., 2009, *A&A*, 498, 361
- Pratt et al. 2010, *A&A*, 511, 85
- Reichert et al. 2011, *A&A*, 535, A4
- Sanders et al., *Science*, submitted
- Santos et al. 2009, *A&A*, 501, 49
- Smolcic et al. 2010, *ApJ*, 708, 909
- Šuhada et al. 2011, *A&A*, 530, A110
- Zhang et al., 2007, *A&A*, 467, 437
- Zhang et al. 2008, *A&A*, 482, 451
- Ziparo et al 2013, *MNRAS*, submitted

4.2.3 Compact Objects and Accretion Physics

The late and final stages of stellar evolution lead to violent processes that manifest themselves as highly energetic transients, such as novae, supernovae and gamma-ray bursts. They leave behind compact remnants such as white dwarfs, neutron stars, and black holes. Even if these objects can only rarely be seen directly, the characteristic radiation that emerges from supernova remnants, accretion processes or rotational-energy conversion allows us to study their nature and the extreme physical processes taking place in their immediate vicinity. In most cases, high-energy radiation is the key to unveil the nature of the compact objects. Indeed, X-ray binaries were the first discrete extra-solar X-ray sources discovered, and it soon became clear that they are powered by the accretion of matter onto a stellar mass compact object provided by a companion star. The High Energy Group was involved in the study of these objects starting with balloon experiments, and today the highly sensitive instruments on board of XMM-Newton and Chandra allow to study individual X-ray binaries in our own galaxy and nearby galaxies, and AGN, probing the inner accretion flows and environment of the compact object. In the HE group various aspects of the physics of accretion onto compact objects (from XRB to AGN) are investigated. As the X-ray radiation originate very close to the black holes, it allows for probing the dynamics of matter and the interactions between matter and radiation in the strong gravity limit. Both X-ray spectra and the time variability of the X-ray emission can thus be used to obtain key information on the properties of black holes and of the accretion flows surrounding them. Some highlights from the study of compact objects and accretion physics obtained by the High Energy Group are presented below.

Strong gravitational effects and accretion physics in black hole systems

X-ray emission provides a unique probe of the black hole environment and the matter flows (inwards and outwards) around them. An important diagnostic of the very innermost regions, close to the event horizon, is the iron $K\alpha$ emission line, which is often seen to be broadened and skewed by strong gravitational effects. The first systematic study of these phenomena in a sizeable sample of AGN has been performed with XMM-Newton (Nandra et al. 2007). A narrow 'core' at 6.4 keV is seen almost universally in the spectra, probably associated with distant, optically thick material such as the molecular torus. Approximately two-thirds of the sample shows evidence for further, broadened emission in the iron K band, but 30 per cent of the sample observations can be explained solely with narrow-line components, with no evidence for broadened emission at all. While these observations show robustly that the broad, relativistic features are present in some cases, the frequent lack of such signatures is puzzling. One possibility is that very strong relativistic effects, induced by the spin of the black hole, render the

features difficult to detect against the underlying continuum (Fig. HE.17; Bhayani & Nandra 2011). The key to further progress is likely to be the recently-discovered reverberation time lags in several AGN, work in which several current HE group members have been involved and which we are pursuing actively.

Broad Iron lines can also be observed in galactic objects, where they provide key diagnostics of the inner accretion flow dynamics. More than two decades ago we had found evidence for relativistic Fe line emission in the accreting X-ray binary LMC X-4, in data taken with the ESA satellite EXOSAT. The observational presence of relativistic velocities could now be confirmed with Chandra (Neilsen et al. 2009).

Studying the global properties of the AGN population (see §4.2.1) suggests that black holes accumulated most of their mass in highly luminous, short phases. The most extreme nearby AGN, the so-called Narrow-Line Seyfert 1 galaxies, have peculiar spectral and variability characteristics that may be explained with a combination of inhomogeneous accretion flows and/or strong relativistic effects. Detailed time-resolved spectroscopy of the brightest objects, may represent the best way to unveil the properties of accretion close to the Eddington limit. Comptonization of the UV seed photons in an extremely low temperature plasma cloud, and huge outflows due to Super-Eddington accretion explains the extreme UV and X-ray properties of active galaxies with steep α_{ox} values. One of the most extreme examples, studied with XMM-Newton, Swift and archival ROSAT observations, is the Narrow-Line Quasar LBQS 0102-2713 (Fig. HE.18, Boller et al. 2011). The soft X-ray spectrum is extremely steep and the source unusually X-ray faint. The source appears to be accreting above the Eddington rate.

The physics of accretion close to the Eddington limit is probably strongly influenced by the mass lost in winds and outflows. A highly ionised wind (traced by FeXXV and FeXXVI absorption lines) is present in many Galactic Black hole systems (Ponti et al. 2013). These winds have an equatorial geometry, with opening angles of a few tens of degrees, and so are only observed in sources in which the disc is inclined at large angles to the line of sight. These accretion disc winds are observed to be present in softer X-ray states only, when the radio jet (that we observe ubiquitously in XRB at low accretion rates) is quenched. Interestingly, the mass outflow rate is estimated to be of the order of the inner accretion rate or higher. Although the physical interaction between the wind, accretion flow and jet in the various accretion state of stellar mass black holes is still not fully understood, the mass flux and power of these winds and their presence ubiquitously during the soft X-ray states suggest they are fundamental components of the accretion phenomenon.

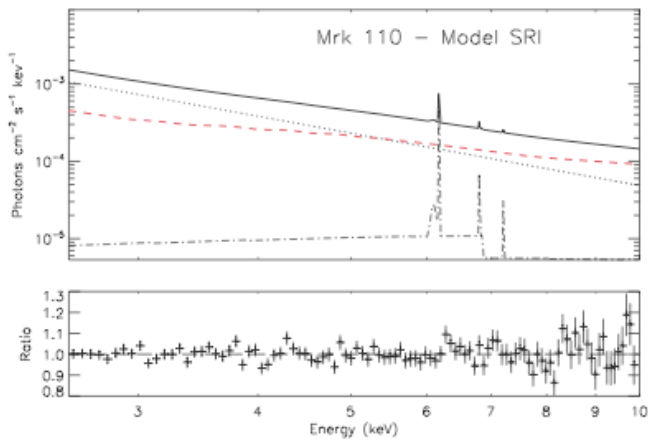


Fig. HE.17: XMM-Newton spectrum of Mrk 110 originally published by Boller et al. (2007). The red dashed line shows a relativistically blurred component, which has no obvious features and manifests itself as a relatively subtle curvature in the continuum. This could explain why not all accreting black hole systems show a prominent broad iron K α line (Bhayani & Nandra 2011).

Understanding the mode of accretion of black holes at lower accretion rates is also a key open issue in high-energy astrophysics, with a potential impact on a wide range of topics. Observationally, we have learned from systematic studies of LMXBs in the low/hard state, that black holes accretion at low rates is almost invariably associated to the acceleration of (low-power) relativistic jets. In the case of AGN, the best studied systems are nearby low-luminosity AGN within groups and clusters of galaxies, where the effect of the interaction of the relativistic jets with the environment could be observed in greater detail, thus providing 'calorimetric' measures of the output power. Merloni & Heinz (2007) showed that the output of low-luminosity AGN is truly dominated by kinetic energy rather than by radiation, and have allowed estimates of the kinetic luminosity function of AGN based on the observed radio emission of their jets (Merloni & Heinz 2008). In this work, tantalizing evidence was found for the kinetic power output from low-luminosity AGN dominating the overall AGN feedback energetics at low redshift, at least in the most massive structures in the Universe.

Black holes, Neutron Stars and White Dwarfs in nearby galaxies

Our XMM-Newton and Chandra monitoring of the central region of the Andromeda galaxy M 31 between 2006 and 2012 has shown that classical novae represent the major class of supersoft X-ray sources (SSSs) in our neighbour galaxy (Pietsch et al. 2007; Henze et al. 2009). Based on these studies we compiled a catalogue of all novae with SSS counterparts in M 31 known so far. The catalogue contains 78 objects, which allow statistical studies of their properties. We found correlations between X-ray and optical nova parameters like SSS turn-on time, turn-off time, blackbody temperature (from X-rays), decay time, and expansion velocity of the ejected envelope (from optical data). The catalogue includes estimates for

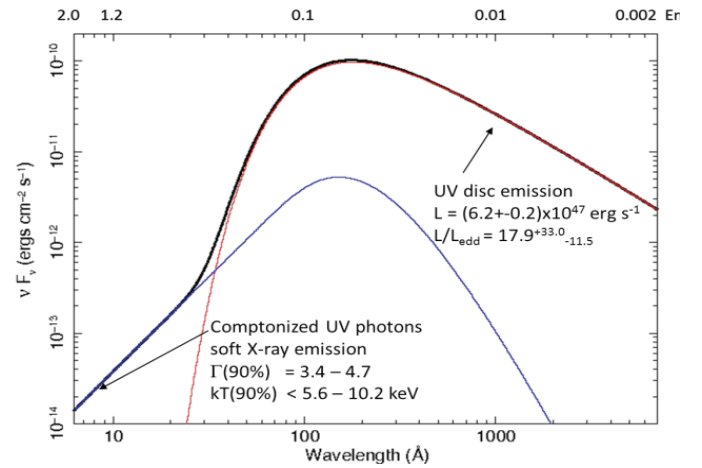


Fig. HE.18: Left: UV and X-ray emission from LBQS 0102-2713. Super-Eddington accretion and the strong UV radiation field cools down the Comptonizing material and produces steep X-ray spectra resulting into steep α_{ox} values (Boller et al 2011).

the white dwarf masses and the ejected mass during the explosion, yielding valuable insight into the physics of the nova process. This can provide important clues on whether the white dwarf in a classical nova can accumulate matter over time to become a potential progenitor for a type Ia supernova.

The Small Magellanic Cloud (SMC) hosts an exceptionally large number of Be/X-ray binaries (BeXRBs). BeXRBs are a subclass of massive binary systems with, in most cases, a neutron star orbiting an early type Be star. From more than 100 known systems the neutron star spin period has now been determined for about 60, allowing statistical studies of their properties. Many XMM-Newton observations of the SMC conducted by members of the High-Energy group have contributed with discoveries of new BeXRBs, with sometimes unique properties (e.g. the first robust association of a BeXRB with a supernova remnant surrounding it; Haberl et al. 2012a; b; Sturm et al. 2012). The neutron star can only accrete matter from the circum-stellar disk of the Be star when the gravitational forces overcome the centrifugal barrier caused by the rapidly rotating magnetosphere of the neutron star. This propeller effect slows down the rotation of the neutron star until an equilibrium period is reached which depends on mass accretion rate, magnetic moment and mass of the neutron star. In this simple stationary model a relation between spin and orbital period for BeXRBs is expected. Today, large samples of BeXRB pulsars with known orbital period exist only from the Milky Way and the SMC. Both samples show a similar, but loose correlation between spin and orbital period (see Fig. HE.19 for the case of the SMC). The large scatter is likely caused by the large variations in accretion rate which BeXRBs often show on orbital and longer (evolutionary) time scales.

BeXRBs are often X-ray transients and the eROSITA survey will have a large potential for the discovery of new systems in the SMC. Due to the vicinity to the south

ecliptic pole where the survey scans cross, this will be even more so for the Large Magellanic Cloud.

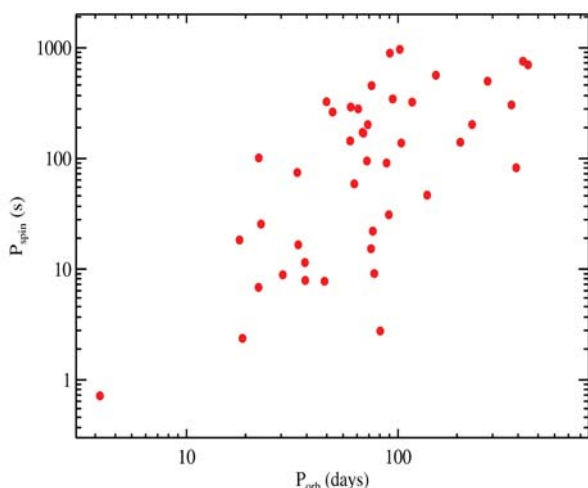


Fig. HE.19: Spin period vs. orbital period for high mass X-ray binaries in the SMC. With the exception of the supergiant system SMC X-1 (lower left data point) all other pulsars are most likely members of BeXRB systems.

Galactic Neutron Stars and Supernova Remnants

Neutron star and pulsar research has a long history at MPE. For more than 40 years we have studied these sources in order to investigate the physical properties of matter at densities above what can be reached in laboratories, and to explore the physical mechanism that leads to their beamed electro-magnetic radiation. Results from this basic research, especially on the pulsars' emission properties, find now its application in pulsar-based spacecraft navigation. Below, we enumerate a few highlights in the field from recent works carried out in the HE group.

The ROSAT all-sky survey revealed seven isolated neutron stars with predominantly thermal X-ray emission, which are often called the "Magnificent Seven" (M7). Despite extensive searches only few much fainter candidates were found since then. Over the last years the outstanding capabilities of the X-ray observatories XMM-Newton and Chandra with respect to sensitivity and spectral resolution increased our knowledge about the M7 considerably. For all seven, X-ray pulsations have been found in the range 3 to 12 s. Measurements of their spin down rates and kinematic estimates for their ages suggest that the M7 are of the order of a few 100 thousand to one million years old. Thermal emission with temperatures of about 0.3-1 million K dominates the X-ray spectra of the M7 and no non-thermal activity is seen. This offers the unique opportunity to investigate their relatively undisturbed thermal emission in X-rays, which has provided crucial insights on their surface temperature and magnetic field distributions. The results are essential to derive important information on the structure and chemical composition of the neutron star surface layers (Haberl 2007).

Highly luminous rapid flares are characteristic of processes around compact objects like white dwarfs, neutron stars and black holes. In the high-energy regime of X-rays and gamma-rays, outbursts with variability on timescales of seconds or less are routinely observed, for example in gamma-ray bursts or soft gamma-ray repeaters. At optical wavelengths, flaring activity on such timescales has not been observed, other than from the prompt phase of one exceptional gamma-ray burst. This is mostly due to the fact that outbursts with strong, fast flaring are usually discovered in the high-energy regime; most optical follow-up observations of such transients use instruments with integration times exceeding tens of seconds, which are therefore unable to resolve fast variability. With OPTIMA members of the High Energy Group discovered for the first time extremely bright and rapid optical flaring in a Galactic transient, SWIFT J195509.6/+261406 (Stefanescu et al. 2008). Our optical light curves are phenomenologically similar to high-energy light curves of soft gamma-ray repeaters and anomalous X-ray pulsars, which are thought to be neutron stars with extremely high magnetic fields (magnetars). This suggests that similar processes are in operation, but with strong emission in the optical, unlike in the case of other known magnetars.

Whether anomalous X-ray pulsars and soft gamma-ray emitters are powered by the decay of their super-strong magnetic field or by accretion is a question discussed since their discovery. A work performed by members of the High Energy Group recently included the proposal that the quiescent emission of anomalous X-ray pulsars/soft gamma-ray repeaters (AXPs/SGRs) is powered by accretion from a fallback disk (Trümper et al. 2010; 2013). Although this model describes the quiescent emission from anomalous X-ray pulsars and soft gamma-ray repeaters very well, it does not explain the high-luminosity bursts observed from these sources. They may be produced by the classical magnetar mechanism operating in super-strong multipole fields.

Using the High Resolution Camera (HRC) aboard the Chandra X-ray Observatory, we have re-examined the proper motion of the central compact object (CCO) RX J0822-4300 in the supernova remnant Puppis A (Becker et al. 2012). New data from 2010 August, combined with three archival data sets from as early as 1999 December, provide a baseline of 3886 days (more than 10 1/2 years) to perform the measurement. Correlating the four positions of RX J0822-4300 measured in each data set implies a projected proper motion of $\mu = 71 \pm 12$ mas/yr. For a distance of 2 kpc this proper motion is equivalent to a recoil velocity of 672 ± 115 km/s. The position angle is found to be 244 ± 11 degrees. Both the magnitude and direction of the proper motion are in agreement with RX J0822-4300 originating near the optical expansion center of the supernova remnant. For a displacement of 371 ± 8 arcsec between its birth place and today's position we deduce an age of 5.2 ± 1.8 kyrs for RX J0822-4300. The age inferred from the neutron star proper motion and filament motions can be considered as two independent

measurements of the same quantity. They average to 4450 ± 750 yrs for the age of the supernova remnant Puppis A.

An external reference system suitable for autonomous spacecraft navigation can be defined by pulsars. Their beamed periodic signals have timing stabilities comparable to atomic clocks and provide characteristic temporal signatures that can be used as natural navigation beacons, quite similar to the use of GPS satellites for navigation on Earth. By comparing pulse arrival times measured on-board a spacecraft with predicted pulse arrivals at a reference location, the spacecraft position can be determined autonomously and with high accuracy everywhere in the solar system and beyond. In the High Energy Group we work on a high-level pulsar-based navigator design (Becker et al. 2013). The recent developments of low-mass X-ray mirrors and active-pixel detectors make it very appealing to use the X-ray band for pulsar-based navigation. The unique properties of pulsars make clear already today that such a navigation system will have its application in future astronautics.

Prospects for eROSITA

Only a small fraction of individual AGN in the eROSITA sky will be detected with enough X-ray counts to ensure accurate spectral analysis. Nonetheless, the sheer number of objects means that the survey is endowed with tremendous potential for the study of the physical conditions of the accreting gas nearby SMBH. This can be harnessed provided sufficiently complete and extensive follow-up campaigns allow at least a photometric redshift determination for the detected sources (see §4.2.1), by stacking the observed spectra (and grouping sources) in

different bins in the luminosity-redshift plane. This will allow statistical analysis of major AGN properties, such as: (i) Principal Component Analysis of the X-ray parameter space, e.g. the soft and hard photon indices, luminosity, optical and UV parameters lines, the line strength of the forbidden lines in the NLR and the UV strength; (ii) relating the black hole growth with AGN outflows and Comptonization; and (iii) studying extreme X-ray variability and nonlinear X-ray variability.

A unique probe of accretion in Galactic nuclei is provided by interactions of dormant SMBH with stars in their vicinity – tidal disruption events (TDEs). The eROSITA survey strategy, with repeated scans of the whole sky over a period of 48 months, is ideally suited for blind searches of TDE, and thousands of events are expected up to $z \sim 0.5$, bringing to a new dimension the pioneering work first enabled by the ROSAT all-sky survey (see e.g. Komossa et al 2004, Komossa & Merritt 2008).

In our own galaxy, eROSITA will discover and study several 10,000 compact objects of all kinds. Using this unique dataset we will (i) measure the space density, galactic scale height and luminosity function of the various kinds of white dwarf accretors (cataclysmic variables, double degenerates, Super-soft sources, Recurrent Novae, and symbiotic binaries); (ii) determine the X-ray luminosity function of X-ray binaries (neutron star accretors) in the Milky Way; (iii) determine the contribution of high- and low-luminosity objects to the Galactic Ridge X-ray emission and ultimately determine the composition of its resolved phase; (iv) uncover the population of isolated neutron stars, within 2 kpc and constrain the evolutionary links between various known sub-classes of the neutron stars family.

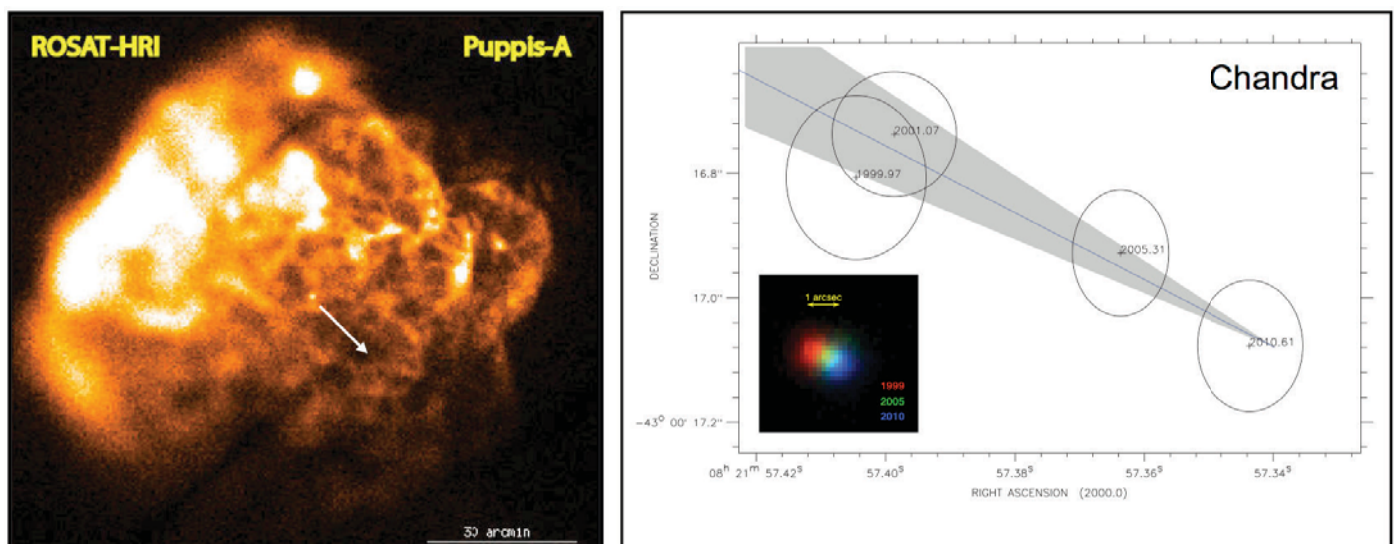


Fig. HE.20: Left: X-ray image of the supernova remnant Puppis-A as seen by the ROSAT HRI. The central point source RX J0822-4300 (seen only in X-rays) is the compact remnant that was formed in the supernova event. The arrow indicates its proper motion direction. Right: Four positions of RX J0822-4300 as measured over a baseline of 3886 days. The circles indicate the position uncertainty. Observation dates are labeled. The gray shaded bar depicts the direction to the remnant's optical expansion center, i.e. to the birthplace of the RX J0822-4300. The straight blue line indicates the CCO's proper motion path as fitted from the four positions. The inset is a color representation of actual Chandra data for the CCO, after registration onto a common coordinate system; the proper motion to the SSW is evident.



W. Becker, Th. Boller, F. Haberl, A. Merloni, K. Nandra

(Other HE team members include Mike Bernhard, Vadim Burwitz, Barbara De Marco, Konrad Dennerl, Jochen Greiner, Florian Hofmann, Pierre Maggi, Giulia Mantovani, B. Menz, Gabriele Ponti, Tobias Prinz, Arne Rau, Richard Sturm, Joachim Trümper, Georgios Vasilopoulos, Andreas von Kienlin)

Former HE team members include J. Brunschweiler, M. Henze, G. Kanbach, S. Komossa, W. Pietsch, G. Sala, H. Stiele)

Selected References:

- *Becker 2009, in Astrophysics and Space Science Library, Vol. 357*
- *Becker et al. 2012, ApJ, 755, 141*
- *Becker et al. 2013, in Acta Futura*
- *Bhayani & Nandra 2011, MNRAS, 416, 629*
- *Boller 2012, International Journal of Modern Physics*
- *Boller et al. 2007, A&A, 456, 87*
- *Boller et al. 2011, ApJ, 731, 16*
- *Boller & Müller 2013, Exciting Interdisciplinary Physics, 293-312*
- *Brunschweiler et al. 2009, A&A, 496, 121*
- *Haberl 2007, Ap&SS 308, 181*
- *Haberl et al. 2012, A&A 545A, 128*
- *Haberl et al. 2012, A&A 537, L1*
- *Henze et al. 2009, A&A 500, 769*
- *Kaur et al. 2012, A&A 538A, 49*
- *Komossa et al. 2004, ApJL, 603, 17*
- *Komossa & Merritt, 2008, ApJL, 683, 21*
- *Komossa et al. 2008, ApJ, 678, 81*
- *Merloni & Heinz 2007, MNRAS, 381, 589*
- *Merloni & Heinz 2008, MNRAS, 388, 1011*
- *Nandra et al. 2007, MNRAS, 382, 194*
- *Neilsen et al. 2009, ApJ, 696, 182*
- *Pietsch et al. 2007, A&A 465, 375*
- *Rau et al. 2010, ApJ, 708, 456*
- *Stefanescu et al. 2008, Nature 455, 503*
- *Sturm et al. 2012, A&A 537A, 76*
- *Trümper et al. 2013, ApJ 764, 49*
- *Trümper et al. 2010, A&A 518A, 46*

4.2.4 Gamma-Ray Bursts

Gamma-Ray Burst (GRB) studies at MPE are of a multi-wavelength nature at its best, exploiting the involvement of the HE group in Fermi-GBM, INTEGRAL-SPI/ACS and Swift-XRT, combined with the PI-instrument GROND at the 2.2m MPG/ESO telescope. This is complemented by a variety of successful observing proposals in the optical, near-infrared, sub-millimeter and radio regimes. The scientific emphasis, described below in some detail, is on afterglow properties and using GRBs as a tool for the study of their host galaxies as well as the high-redshift Universe.

GBM-studies of prompt Gamma-Rays

The GBM-team at MPE is actively participating in the daily analysis of GRBs via the “Burst-Advocate” shift system. The 4-yr GBM-GRB catalog as well as the 4-yr spectroscopic catalog are nearing completion, both with MPE lead authors. GBM members have been coordinating authors for a number of Fermi-LAT led papers. In particular, the quest for additional spectral components and thermal emission components has been analysed, both with GBM/BGO (Bissaldi et al. 2011) as well as LAT data (McGlynn et al. 2012). Besides a number of GBM-only papers on individual GRBs, MPE has also proved vital in providing expertise for the cross-calibration with INTEGRAL and Swift.

Combining prompt gamma-ray and ground-based afterglow data

Our photometric redshift for the bright LAT-detected GRB 080916C implied a very large bulk Lorentz factor of $\Gamma > 1090$ (Greiner et al. 2009), and the first of a later series of more and more stringent limits on the quantum gravity mass scale (Abdo et al. 2009, Sci. 323 1688). Second, a compilation of afterglow properties of the first 2-yr LAT-detected GRB sample, most notably jet opening angles as measured with GROND, demonstrated that the LAT-detected GRBs stand out from the total GRB sample as being particularly energetic (McBreen et al. 2010). Third, a first statistical analysis of rest-frame properties was performed using Fermi-GBM detected GRBs for which simultaneous Swift-BAT triggers allowed successful afterglow detection and redshift determination (Gruber et al. 2011) And last but not least, optical/NIR emission detected with GROND for GRB 091024 (Gruber et al. 2011) and GRB 121217 (Elliott et al. 2013, in prep) are placing interesting constraints on the burst emission mechanism, since the spectral energy distributions (SEDs) measured with GROND add the extra dimension of a spectral slope, also removing any ambiguity wrt. extinction.

Afterglow properties

Since the start of the GROND operation in 2007, the systematic availability of SEDs covering the optical/NIR range has helped substantially to solve several ques-

tions in the GRB field. In general, many of the variations in the afterglow light turned out to be chromatic, not only between the X-ray and optical regimes, but also within the optical through near-infrared GROND bandpass. This strengthened earlier evidence, that jet breaks are rarely seen, and is consistent with more recent relativistic hydrodynamic simulations according to which jet breaks should occur much later (of order 100 days after the GRB) than previously (0.5-2 days) thought.

The most surprising result of the systematic GROND observations of Swift-detected GRBs is the overwhelming breadth of short-term variability where straight power law declines were expected. Based on the combined optical/NIR and X-ray properties, several different phenomena can be distinguished: (1) Simultaneous GROND-measurements of the optical/NIR SED during minute-duration X-ray flares shortly after the prompt GRB have revealed clear evidence of spectral evolution with time, suggestive of a decrease of the peak energy from X-rays into the optical. This is similar to the frequently observed hard-to-soft evolution during the prompt emission, and points towards X-ray flares being late central engine activity of decreasing energetics (Krühler et al. 2009). (2) Extremely rapid intensity jumps (formal fits imply $f(t) \sim t^{10...12}$) by up to a factor of 5 have been seen with GROND at several hours after the prompt GRB, with no obvious changes in the simultaneous X-ray emission. Originally also interpreted as extreme cases of late central engine activity (Greiner 2011), more recent investigations suggest late collisions of low-contrast shocks (see Fig. HE.21; Greiner et al. 2013). If this interpretation proves to be correct, it would open up the possibility of independent and relatively simple measurements of the Lorentz factor, the half-opening angle of the jet and the off-axis angle of the observer relative to the jet axis. (3) Late-time bumps at 1-2 weeks after the GRB are generally associated to the supernova light from the explosion of the progenitor. Surprisingly, in a few GRBs, GROND has observed a late-time bump at 3-5 days after the prompt emission, in some cases even in concert with an X-ray brightening. These bumps are clearly not related to the supernovae. The flux amplitudes and SEDs also argue strongly against environmental effects like a strong density enhancement. The interpretation has not yet converged on these events, but in any case it challenges our conception of the central engine as a single-bang event.

Seriously complicated by the occurrence of the above described short-term variability, the prediction of the standard fireball scenario with respect to cooling break frequency changes have been difficult to extract. The first accurate and contemporaneous measurements of both the sharpness of the cooling break and its time evolution was achieved for GRB 091127. Detailed fitting of the time-resolved SED shows that the break is very smooth, and evolves towards lower frequencies

as a power-law with index 1.23 ± 0.06 , inconsistent with the predicted index of 0.5. A possible explanation for the observed behaviour is a time dependence of the micro-physical parameters, in particular the fraction of the total energy in the magnetic field (Filgas et al. 2011). Such non-standard interpretations can only be tested with coverage of an even wider wavelength band than we obtain so far with GROND and Swift. We have therefore embarked on a dedicated program which includes coordinated sub-millimeter (with APEX) and radio (with ATCA) observations. First results are promising (Greiner et al. 2013), though the sensitivity of these instruments makes such studies only viable for a very small fraction of GRB afterglows (not necessarily the brightest).

GRB afterglows as a tool

The GRB afterglow brightness at early times and its simple spectrum make for an ideal tool to probe the interstellar medium of high redshift and/or highly extinguished galaxies to very large redshifts where such galaxies normally are undetectable, as well as important probes of the intergalactic matter.

An ongoing conundrum in the absorption studies of GRB afterglows is the origin of a considerable discrepancy between the amount of total gas absorption along the line-of-sight inferred from X-ray, and from optical spectral data. The former is estimated to be typically an order of magnitude higher than the one measured from optical spectra (Schady et al. 2011), suggesting that the X-ray afterglow is absorbed by an additional and significant component of ionised gas that does not affect the UV and optical afterglow. Detailed analysis carried out at MPE suggests that the X-ray excess could originate from ultra-highly-ionised, dense gas in the GRB vicinity (Schady et al. 2011). Alternatively, it may be due to material external to the host galaxy, within a 'warm-hot'

intergalactic medium, or WHIM. or due to absorption by a large quantity of He. All these possible scenarios have important consequences for the interpretation of observations of distant galaxies and star-formation.

High quality GRB afterglow observations also enable the host dust abundance and extinction properties to be explored through dust depletion patterns (Savaglio 2006), and from the analysis of broadband IR through UV SEDs (e.g. Schady et al., 2007; Schady et al., 2010; Greiner et al., 2011). From accurate GROND-Swift SEDs, our group frequently measures the wavelength dependence of the host galaxy interstellar dust along GRB lines-of-sight, or dust extinction curve, which contains information on the extinguishing dust grain size distribution and composition. Work led at MPE has already revealed tentative evidence of a link between the abundance of dust and the prominence of the Milky Way-like dust attenuation feature at 2175 \AA (e.g. Krühler et al., 2011; Schady et al., 2012), the origins of which are currently unknown.

Already within the first three years of GROND operations, our systematic dust measurements from a 92% redshift-complete sample has settled the issue of dark bursts, (i.e. the missing optical afterglows when X-ray afterglow emission was readily detected). This optical darkness is due to substantial dust reddening in GRBs at intermediate redshifts where the redshift effect amplifies the dust extinction (Greiner et al., 2011).

High-resolution spectroscopy also allows us to study the metallicity of the host galaxy along the line of sight. This is of interest for our understanding of the chemical evolution in the early Universe as probed by star forming galaxies. Two particular noteworthy results have been obtained by our group, based on VLT-FORS follow-up spectroscopy of GROND-detected bright afterglows.

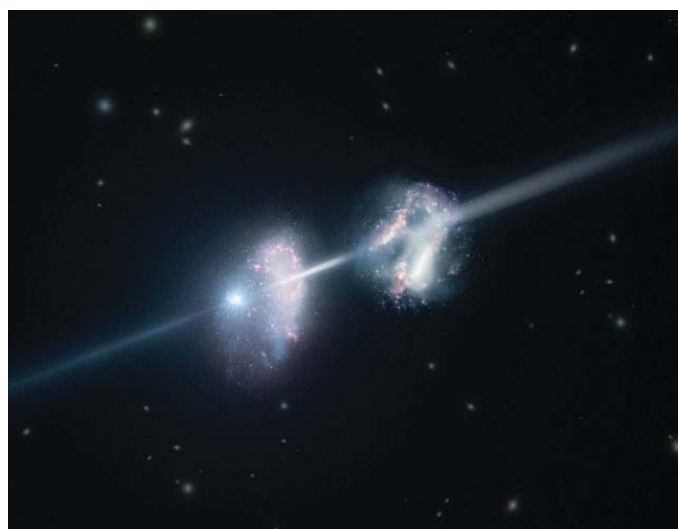
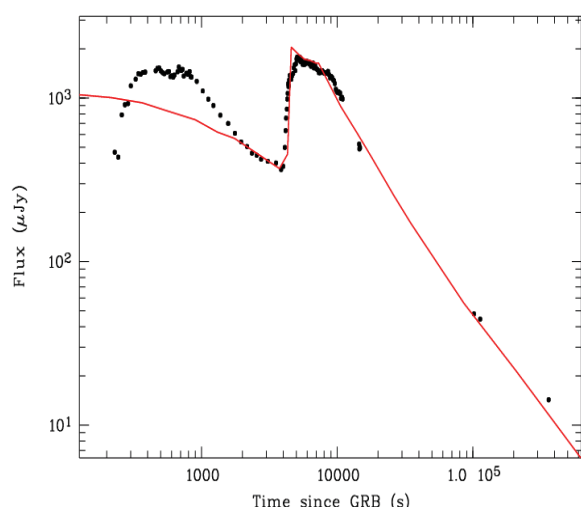


Fig. HE.21: Left: Model of the collision of two shocks (red) overplotted on the J-band Data of GRB 100621A as obtained with GROND. Apart from the early rise which is not part of the model, the intensity jump at 4000 s is surprisingly well described in both, steepness and amplitude, as is the short plateau phase at the maximum. (From Greiner et al. 2013). Right: Artist impression of GRB 090323 (bright stellar-like spot) shining through two galaxies before reaching the observer (to the right of the picture). Both galaxies are surprisingly rich in heavy chemical elements. (From Savaglio et al. 2012: ESO PR#11/43, www.eso.org/public/news/eso1143).

First, supersolar metal abundances were found at $z \sim 3.6$ in the galaxy (or galaxies) hosting GRB 090323 (see Fig. HE.21; Savaglio et al. 2012). These are the highest metallicities ever measured at $z > 3$. Second, and in stark contrast to this, a metal-poor ($\log(Z/Z_{\text{Sun}}) = -1.9$) damped Lyman- α (DLA) system was found in the afterglow spectrum of GRB 090926A at later times ($z=2.1$), one of the lowest values ever found in a GRB DLA system (Rau et al. 2010, ApJ 720 862). These two GRBs exemplify the recently mounting evidence, that the spread of metallicity in GRB-DLAs is at least two orders of magnitude. While this does not require a similar range in abundances of the GRB progenitors, the substantial dispersion in the chemical enrichment of the Universe at high redshift is intriguing.

The quest for the highest-redshift GRBs arose pretty quickly after the discovery of their cosmological origin in 1997. However, the progress was slow, with only 4 GRBs identified above redshift of 5 by mid-2007. Our systematic NIR-observations of GRB afterglows with GROND have changed this pace. Since the temporary redshift-record of GRB 080913 ($z=6.7$; Greiner et al. 2009b), GROND has been involved in every consequent redshift-record (meaning that there are no confirmed high- z GRBs at Decl $> +30^\circ$!), though 8-10 m class telescopes dominate the scientific progress obtained from these events. Within the last 5 years, another 8 GRBs at $z > 5$ have been found.

GRB host galaxies

We have investigated in detail the (at the time) largest sample of galaxies hosting GRBs (Savaglio et al. 2009), 46 objects in the redshift interval $0 < z < 6.3$ (89% of the hosts are at $z \leq 1.6$). The derived median stellar masses, star formation rates (SFRs), dust extinction in the optical, and metallicities are $M^* \sim 10^{9.3} M_{\text{Sun}}$, $Z/Z_{\text{Sun}} \sim 1/6$, $\text{SFR} = 2.5 M_{\text{Sun}} \text{ yr}^{-1}$, $A_V = 0.44$ mag. The low-redshift population is a star-forming small galaxy, which is representative of the population of galaxies where the formation of massive short-lived stars are expected to be. At intermediate redshift $2 < z < 4$, the GRB host galaxy population is found to be contaminated by a more massive, dust-extinguished and star-forming population (Krühler et al. 2011) which suggests a change in the GRB host population.

A sample 3 times larger than our initial sample is under investigation. A preliminary analysis of the stellar mass function at $z < 1.6$, done for the first time for GRB hosts, shows that this is not very different from that obtained for the population of star-forming galaxies (Savaglio et al., in prep.).

We maintain the largest public database dedicated to GRB hosts, called GRB Host Studies (GHostS, <http://www.grbhosts.org>, Savaglio). Since 2007, GHostS has been used for the publication of 21 peer-reviewed papers.



Jochen Greiner, Sandra Savaglio, Patricia Schady, Arne Rau

(Other HE team members include Jonny Elliott, Jochen Greiner, David Gruber, Arne Rau, Sandra Savaglio, Patricia Schady, Vladimir Sudilovsky, Mohit Tanga, Karla Varela, Andreas von Kienlin, David Yu

Former HE team members include P. Afonso, E. Bissaldi, C. Clemens, R. Filgas, S. Foley, F. Knust, T. Krühler, A. Küpcü-Yoldas, G. Lichti, S. Loew, S. McBreen, S. McGlynn, M. Nardini, F. Olivares, A. Stefanescu, G. Szokoly, A. Yoldas)

Selected References:

- Bissaldi et al. 2011, ApJ 733, 97
- Filgas et al. 2011, A&A 535, A57
- Greiner et al. 2008, PASP 120, 405
- Greiner et al. 2009a, A&A 498, 89
- Greiner et al. 2009b, ApJ 693, 1610
- Greiner et al. 2011, A&A 526, A30
- Greiner et al. 2013, A&A (in press; arXiv:1304.5852)
- Gruber et al. 2011a, A&A 531, 20
- Gruber et al. 2011b, A&A 528, 15
- Krühler et al. 2009, ApJ 697, 758
- Krühler et al. 2011, A&A 534, A108
- McBreen et al. 2010, 516, 71
- McGlynn et al. 2012, Proc. Munich GRB Conf.;
- Rau et al. 2010, ApJ 720, 862
- Savaglio 2006, New J Phys 8, 195
- Savaglio et al. 2009, ApJ 691, 182
- Savaglio et al. 2012, MN 420, 627
- Schady et al. 2007, MN 377, 273
- Schady et al. 2010, MN 401, 2773
- Schady et al. 2011, A&A 525, 113
- Schady et al. 2012, A&A 537, A15

4.2.5 Galactic Structure and the ISM

The interstellar medium with its structure and dynamics plays a key role in galactic evolution, being the birthplace of stars. At MPE star formation and its interstellar conditions and signatures are studied by our colleagues in the infrared group, while the high-energy group studies the terminal stages of stellar evolution and their impacts on the hot, dynamic, and relativistic phases of the interstellar medium. Stellar outputs, their wind and explosion energies and their ejecta lead to bubbles and superbubbles up to 1 kpc in size, they thus shape the state and dynamics of interstellar gas. Magnetic field configurations follow from this and determine observable radiation such as, e.g., synchrotron emission. High energy astronomy provides more observational tools through emission from relativistic particles in the ISM, and from interstellar radioactivities, in addition to the thermal emission which still can be traced up to X-ray energies. Lessons from specific emission processes, and from source regions and its objects, are transferred to populations of sources or entire galaxies. This connects these nearby universe studies to surveys of the more distant universe and to models of stellar and galaxy evolution. The interstellar medium in our and nearby galaxies can be studied at greater precision in a variety of tracers at different wavelengths, thus allowing in-depth studies of stellar feedback and evolutionary properties. XMM-Newton and Chandra observations show thermal X-ray emission from the hot ISM as it reflects shocks from explosions expanding into the ambient medium, and also hot interiors of superbubbles heated by the same. Radioactive decays from nucleosynthesis trace stellar outputs independent of gas density or thermodynamic state, and can be observed in gamma-rays, long-lived isotopes ^{26}Al and ^{60}Fe and positrons shining in INTEGRAL's energy window. In nearby galaxies such as in the Magellanic Clouds and M31 we can compose an outside view on a galaxy in sufficient detail to map both the interstellar gas and the various source populations influencing its state. Here we report about the interstellar medium in its hot and non-thermal phases, which are the objective of high-energy astrophysics studies hereto.

The hot interstellar medium.

The hot ISM can be best studied in the soft X-ray band (0.2 – 2 keV) in nearby galaxies where survey observations can cover the total galaxy while resolving structures down to parsec scales. Diffuse X-ray emission in the Magellanic Clouds has

been detected already by the Einstein Observatory and was further investigated by us using ROSAT. Between May 2009 and March 2010, we carried out an XMM-Newton survey of the Small Magellanic Cloud (SMC), which, together with archival observations, completely covered the bar and wing of the galaxy. Owing to the high sensitivity of the EPIC instruments the images which we obtained reveal the morphology of the diffuse X-ray emission in unprecedented detail. From a spatially resolved spectral analysis of the diffuse X-ray emission we obtained typical plasma temperatures of 0.2 keV (~ 2 Million Kelvin). The absorption by cold neutral gas along our line of sight strongly varies in the different regions of the SMC with a maximum in the south-west part of the galaxy. This is consistent with what we see from HI radio maps which indicate large amounts of neutral hydrogen in that region. The high X-ray absorption indicates that here the hot ISM is covered by neutral hydrogen in front of it. In contrast the diffuse X-ray emission from the north-east part of the SMC bar shows lower absorption, allowing a more direct view to it. This is nicely seen when comparing the emission from the hot ISM (soft X-rays) and from cooler gas (HI) as shown in Fig. HE.22. While in large parts of the SMC the hot ISM is still buried under cooler material, it shows features indicating outflows in other parts. Such outflows have been seen in soft X-rays from more distant galaxies with strong star forming activity like M82 and NGC 253. The latter was investigated by us with ROSAT and XMM-Newton.

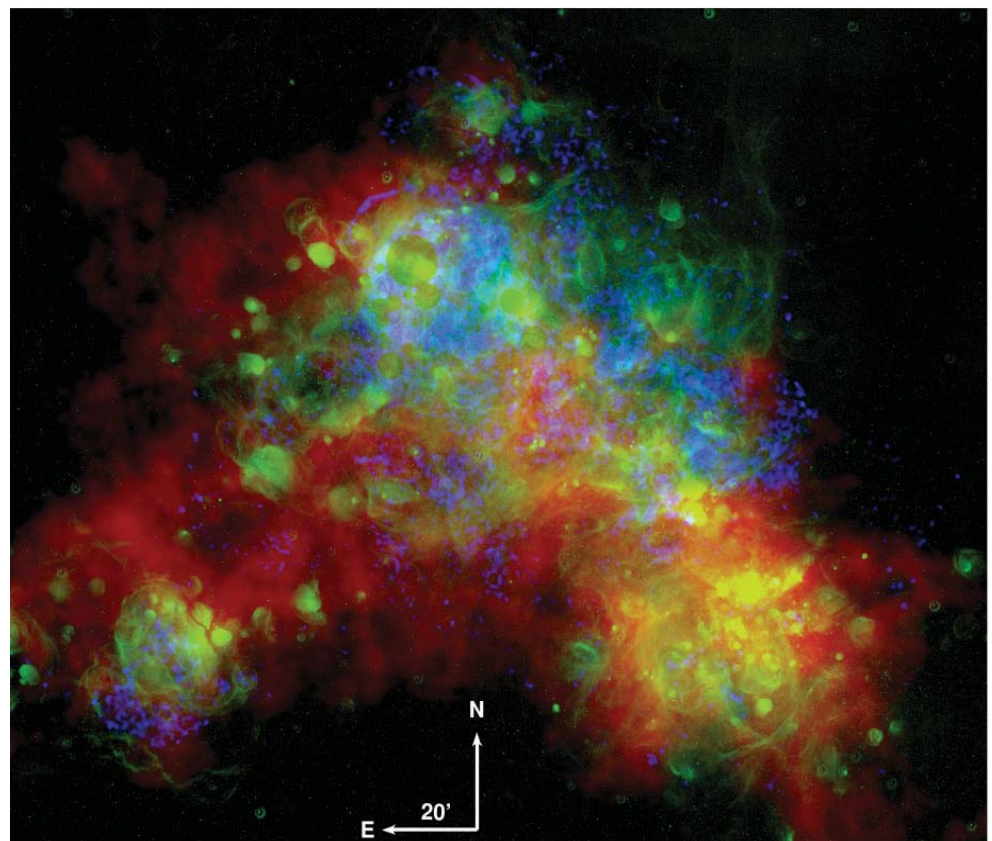


Fig. HE.22: The different phases of the ISM in the Small Magellanic Cloud. Blue: 0.2–1.0 keV emission from hot (~ 0.2 keV) gas as obtained from the XMM-Newton survey, green: H α and red: HI emission.

The relativistic interstellar medium. The astrophysics of relativistic-particle processes in the interstellar medium has been pursued in the HE group over the past years, building on missions CGRO, INTEGRAL and Fermi-LAT, now reaching a wider significance for high-energy astrophysics. Our GALPROP project numerically models cosmic-ray propagation in the Galaxy and makes predictions of the electromagnetic radiation including hard X-rays, gamma rays and synchrotron radiation, as well as the cosmic-ray direct measurements. This includes realistic gas distributions from radio surveys, and interstellar radiation fields from a detailed radiation transfer code, using all available observables and theory to provide the best constraints on the properties of high-energy particles in the Galaxy. GALPROP involves MPE, Stanford, SLAC and other institutes, and has a wide user community, e.g. being the Fermi-LAT standard for Galactic diffuse emission and associated topics such as Fermi Bubbles. Highlights of this work from the past 6 years include: a unified model of the non-thermal emission from hard X-rays through gamma rays, as measured by INTEGRAL, CGRO-COMPTEL and Fermi-LAT. In particular the 100 keV X-rays were shown to be of inverse Compton origin from cosmic-ray electrons; the spectral energy distribution of the Galaxy as seen from an external observer, from radio to gamma rays (possible only with such a model), important for comparison with external galaxies; Fermi-LAT Galactic diffuse emission results; study of synchrotron emission related to cosmic-ray electrons and magnetic fields, including WMAP polarization and Planck survey data (see Strong et al. 2007).

The radioactive interstellar medium. Nucleosynthesis processes and their implications on the interstellar medium have been studied in the HE group of MPE, building on experience with the gamma-ray mission CGRO and now using measurements with SPI on INTEGRAL. These studies expanded towards a wider astrophysical scope through more interpretational and modeling stud-

ies and international collaborations with nucleosynthesis source experts (a.o. in the framework of the ESF's Euro-Genesis program), and theorists simulating the interstellar medium (also in DFG's priority program on the ISM).

The superb spectral resolution of SPI (see Fig. HE.23) has now allowed to trace large-scale Galactic rotation throughout the inner Galaxy, refining and deepening earlier hints. Surprisingly, the ^{26}Al -carrying interstellar medium appears to be moving at much larger velocities than what we know from cold interstellar gas as seen in CO. The excess velocities of $\sim 100 \text{ km s}^{-1}$ have been modelled to be best explained if ^{26}Al -ejecting massive-star groups are located on the leading edges of spiral arms, and thus blow-out of nucleosynthesis ejecta by winds and supernovae occurs with a preferred directionality between arms, so that an additional velocity component arises (Kretschmer et al., in prep.). This has interesting implications for angular-momentum transport between the Galaxy's spiral-arm regions and the halo, and contributes to feed the Galaxy's central regions. In localized groups of massive stars, only the Cygnus region is a bright ^{26}Al source, and is being studied in terms of how its massive-star groups shape cavities and possibly chimneys as winds and supernovae stir the interstellar medium (Voss et al. 2009...2012, Martin et al. 2009, 2010). The discrimination of ^{26}Al emission in the foreground from the nearby Scorpius-Centaurus groups (Diehl et al. 2010) is now used to study propagating star formation evidence among those groups, combining infrared, radio, and gamma-ray data with the stellar census. Similarly, the nearby Orion region is a target of deep INTEGRAL observations, in an attempt to measure ejecta blowout into the Eridanus cavity, which extends from the Orion OB1 association towards the Sun (Voss et al. 2010; Fierlinger et al. 2012). A study of diffuse X-ray emission with XMM-Newton from the interior of the Eridanus cavity (Lubos 2012) could not improve upon earlier ROSAT findings, and dedicated observing strategies will be proposed to generate a suitable survey with XMM-Newton, for de-

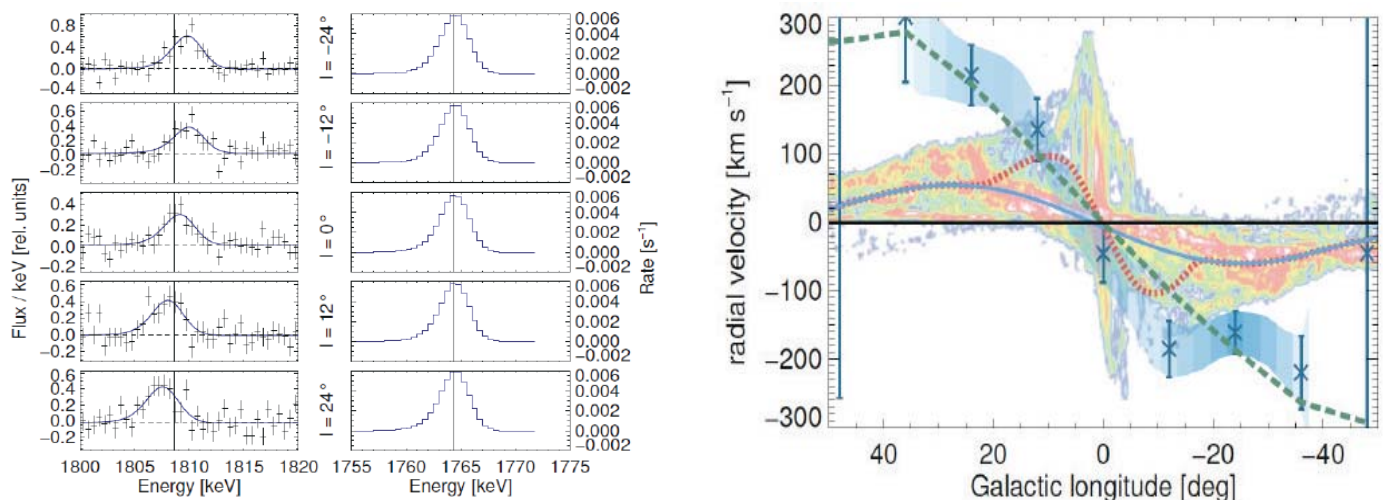


Fig. HE.23: Left: The Doppler shift of the gamma-ray line from decay of radioactive ^{26}Al in the interstellar medium varies along the plane of the Galaxy (left), tracing large-scale rotation. The righthand set of plots shows a nearby instrumental line, which is stable and provides the instrumental response. Right: The velocities of hot and tenuous ^{26}Al -carrying gas (datapoints) exceed velocities of cold interstellar gas (CO, color) along the ridge of the inner Galaxy by $\sim 100 \text{ km s}^{-1}$.

termination of hot-ISM temperature and homogeneity herein. Our simulations of massive-star feedback have shown us the importance of individual star and supernova cavities merging into superbubbles, and the significance of instabilities as the ejected gas cools. We found first evidence of the Vishniac instability in our 3D hydrodynamical simulations of the dynamic ISM. This instability gives, e.g., the Crab nebula its spectacular clumpy morphology in optical emission. This work has led us to a new model for the evolution of globular clusters, between the first-generation stars and gas losses towards their abnormal second-generation stellar population (Krause et al. 2013).

The measurements of positron annihilation gamma-rays with INTEGRAL have presented us with a puzzle of astrophysics related to relativistic particles, radioactivities, and the propagation of cosmic rays in the interstellar medium (see Weidenspointner et al. 2008): In annihilation gamma-rays, the inner Galaxy reveals a dominating extended source that cannot directly be related to any plausible source of positrons, while those sources are expected to be distributed throughout the Galaxy's disk. Thus, either positrons find a way to propagate from their source regions through the halo towards the Galaxy's bulge, or another, hitherto unknown source of positrons exists in this bulge (see review Prantzos et al. 2011). Our group has been studying nucleosynthesis positrons and their propagation, e.g. with GALPROP (Martin et al. 2010, 2012), and now started a new approach towards refined imaging of annihilation gamma-rays using information field theory, for best exploitation of the growing INTEGRAL survey database towards this puzzle.

Roland Diehl, Frank Haberl



(Other HE team members include M. Ghaempanah, G. Khachatryan, M. Krause, P. Maggi, G. Skinner, R. Sturm, T. Siebert, A. Strong, G. Vasilopoulos.

Former HE team members include F. Alexander, K. Kretschmer, M. Lang, P. Martin, H. Ohlendorf, G. Saez-Cano, W. Pietsch, E. Orlando, H. Stiele, R. Voss, W. Wang)

Selected References:

Ackermann et al. (Strong) 2012, ApJ 750, 1, 3;
Diehl 2013, Rep.Progr.Phys. 76b, 6301;
Diehl et al 2011, Springer Lect.Not.Phys 812;
Diehl et al. 2010, A&A 522, 51;
Haberl et al. 2012, A&A, 545A, 128;
Krause et al. 2013, A&A 550, 49;
Krause et al. 2012, A&A 546, 5;
Martin et al. 2012, A&A 543, 3;
Martin et al. 2010, 511, 86;
Prantzos et al. (Diehl) 2011, Rev.Mod.Phys. 83, 1001;
Strong et al. 2011, A&A 534, A54;
Strong et al. 2010 ApJ 722 L58;
Strong et al. 2007, Ann.Rev. Nucl Part. Sci. 57, 285;
Voss et al. 2012, 539, 66;
Voss et al. 2010, A&A 520, 51;
Voss et al. 2009, A&A 504, 531;
Wang et al. 2009, A&A 496, 713;
Wang et al. 2007, A&A 469, 1005;
Weidenspointner et al. 2008, Nature 451, 159

4.2.6 Planets and Solar System

The perception that our Solar System is a unique location for detailed, fundamental studies of high energy phenomena has emerged only over the last two decades. The High-Energy Group at MPE has considerably contributed to this new insight, mainly with the unexpected discovery of cometary X-ray emission with ROSAT. This finding has revealed the general importance of a process for the generation of X-rays which was overlooked before: charge exchange reactions between highly charged ions and neutral gas, a process which is now getting increased attention in various areas of astrophysical research (see the reviews by Dennerl 2010 and Dennerl et al. 2012).

Comets represent by far the best case to study the physics of charge exchange induced X-ray emission: the Sun is a copious source of heavy ions, which are emitted in the solar wind with varying composition, ionisation state, density, and velocity. When these ions encounter the huge neutral gas cloud around a cometary nucleus, they recombine and release a major fraction of their energy in the form of characteristic X-ray line emission, which can be studied in detail by utilizing the spatial, spectral, and temporal resolution of the current generation of X-ray satellites, providing a lot of diagnostic information about the underlying process (Fig. HE.24, left). Thus, comets can be utilized as natural space probes for sampling the heavy ion content of the solar wind at various phases

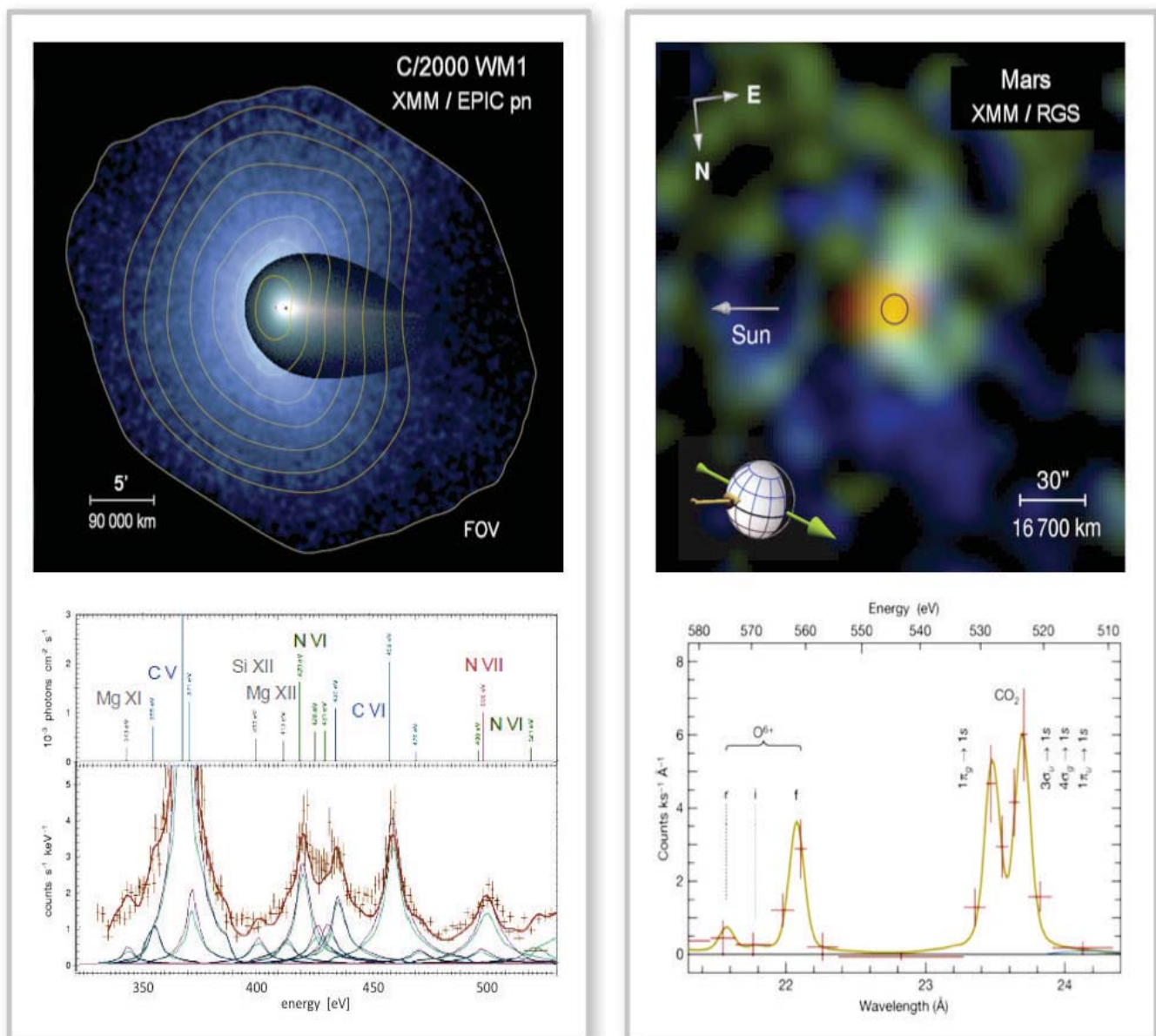


Fig. HE.24: XMM-Newton X-ray images (top) and X-ray spectra (bottom) of a comet (left) and of Mars (right), demonstrating the high efficiency of solar wind charge exchange for revealing the presence of tenuous amounts of gas in a cometary coma or in a planetary exosphere, and the high diagnostic value of the spectral information.

of the solar cycle. As their orbits are not confined to the ecliptic plane, this can also be done at high heliographic latitudes. A very interesting case will be comet C/2011 L4 (Pan-STARRS), which we observe in April and May 2013, i.e., right at solar maximum, at unprecedentedly high heliographic latitudes of 73–83 deg, with Chandra and XMM-Newton.

The fact that the cross sections for charge exchange are extraordinarily large ($\sim 10^{-15}$ cm²) makes this process an excellent tracer of tenuous amounts of gas, opening a new window for the study of planetary outgassing and the evolution of planetary atmospheres, thus linking X-ray astrophysics to astrobiology (Dennerl 2009). We have succeeded in obtaining an X-ray image of Mars which shows evidence for atmospheric loss during a period of extraordinarily high solar wind enhancement (Dennerl 2007, Fig. HE.24, right). By utilizing the high resolution X-ray spectroscopy of XMM-Newton/RGS we were able to prove that the extended bow shaped structure around the planet is caused by charge exchange and not by, e.g., fluorescence of solar X-rays, which we observe from the denser atmospheric regions closer to the planet. Here we see, probably for the first time in X-ray astrophysics, the oxygen fluorescence line to be split into two components, caused by the fact that the oxygen is embedded into a CO₂ molecule. We have also succeeded in identifying charge exchange induced X-rays from the exosphere of Venus, in addition to its X-ray fluorescence (Dennerl 2008).

In view of the currently anticipated future X-ray missions, the study of charge exchange, in particular from the Solar System, is likely to have a bright future: eROSITA, with its high sensitivity and spectral resolution at low energies and its large, essentially unlimited field of view during the all-sky surveys, will be well suited for investigating cometary X-rays, and its repetitive all-sky coverage will provide a unique opportunity for identifying charge exchange emission from the whole heliosphere. Another exciting prospect is the unprecedented non-dispersive spectral resolution of microcalorimeters, like on Athena+, which will be the perfect detectors for spatially resolved spectral studies of the extended X-ray emission of comets.

Gamma-rays from the Heliosphere

In 2008 we made a prediction that the Sun should be a strong source of gamma-rays via inverse Compton scattering by cosmic-ray electrons on the solar radiation field. This appears as a 'halo' of emission surrounding the Sun, on scales of degrees. Following this, we were able to discover the emission in the CGRO-EGRET data, for the first time, and found good agreement with the predictions. Now with Fermi-LAT, this emission can be measured in detail (published in 2011), and it probes cosmic-ray electrons in the inner heliosphere, which is not possible by other means. For Fermi-LAT this solar emission also provides an significant background over the sky which has to be accounted for in diffuse and point-source studies, and the model developed at MPE is the basis for such prediction.



Konrad Dennerl, Andy Strong

(Former HE group members include E. Orlando)

Selected References:

- Abdo et al. 2011, *ApJ*, 734, 116
- Dennerl 2007, in "The Mars Plasma Environment", ed C.T. Russell
- Dennerl 2008, *Planet. Space Sci.*, 56, 1414
- Dennerl 2009, *Adv. in Geosci.*, 15, 53
- Dennerl 2010, *Space Sci. Rev.*, 157, 57
- Dennerl et al. 2012, *AN*, 333, 324
- Orlando & Strong 2008, *A&A*, 480, 847

4.3 Hardware Development

4.3.1 X-Ray Detector development

A variety of detectors have been developed at MPE and the associated MPI semiconductor laboratory in recent years to fulfil the diverse specifications of projects for spectroscopy and imaging of X-ray photons. For the X-ray space telescope eROSITA, we developed PNCCD detectors which perform spectroscopy and imaging with high time resolution and excellent quantum efficiency. The MIXS instrument on ESA's mission BepiColombo requires fast and radiation-hard Macro-Pixel sensors of DePFET (Depleted PMOS Field Effect Transistor) type for analysing the element composition of Mercury's surface. Prototypes of DePFET sensors with even faster readout, homogeneity of response over large sensor area, and the avoidance of energy corruption for X-rays hitting the sensor during signal processing time are presently developed for the Athena project. Furthermore, there are ground-based projects which require X-ray photon counting over a large dynamic range and with high position resolution. Large-area PNCCD detectors have been developed and already applied at existing XFEL (X-ray free electron laser) facilities in Germany, USA and Japan. DePFET active pixel sensors, which are orders of magnitude faster, also permit much higher signal charge capacity. These are under development for the emerging European XFEL facility in Hamburg.

The main project of the High Energy Group at MPE is eROSITA. The focal plane of the eROSITA instrument is equipped with an array of seven identical PNCCD cameras. The PNCCD sensor wafers were designed and fabricated in the MPI semiconductor laboratory, until recently operated by MPE in partnership with the Max

Planck Institute for Physics (MPP). The detector concept is based on that of the XMM-Newton PNCCD, which has been in operation without significant degradation of performance since the launch of the ESA satellite in 1999. The CCD chip is tailored to the requirements of the project, e.g. the pixel size, the number of pixels, the on-chip optical blocking filter, and a frame store section. Tests of the advanced PNCCD detectors for eROSITA have verified the improvements over XMM-Newton: the excellent low-energy response permits spectroscopy even at photon energies of 200 eV (see Fig HE.25) and the low read noise of 2.5 electrons rms is important for accurate recombination of events with signal charge split over adjacent pixels. All eROSITA PNCCDs were tested at chip-level including spectroscopic performance by means of a unique so-called cold chuck probe station to select the seven best CCDs. The quantum efficiency and the detector response of these CCDs were measured at the synchrotron BESSY II in Berlin in the energy range from 1.9 eV to 11 keV. With a series of proton irradiation experiments at the TANDEM accelerator in Garching, we evaluated and verified the radiation hardness of the eROSITA detectors.

Before start of the assembly of the flight detectors, we measured and optimized the performance by testing of engineering models (see Fig. HE.25). The optimum operating conditions regarding supply voltages, timing sequences and temperature are already determined.

Apart from this space project, we have also developed X-ray CCD detectors for ground-based application at X-ray free electron lasers (XFELs). The detector plane

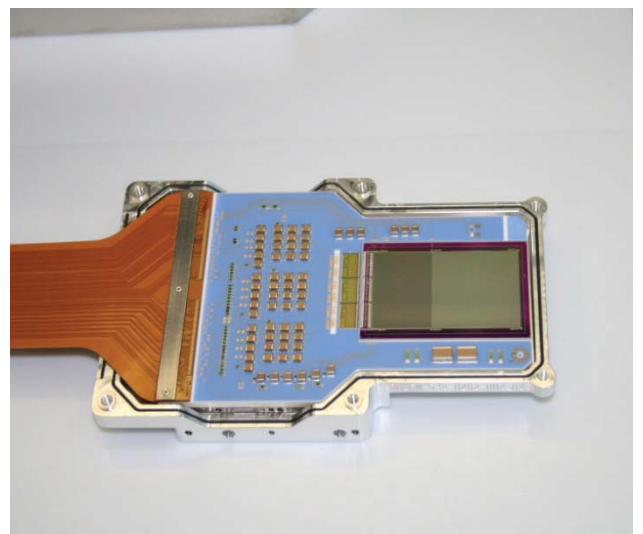
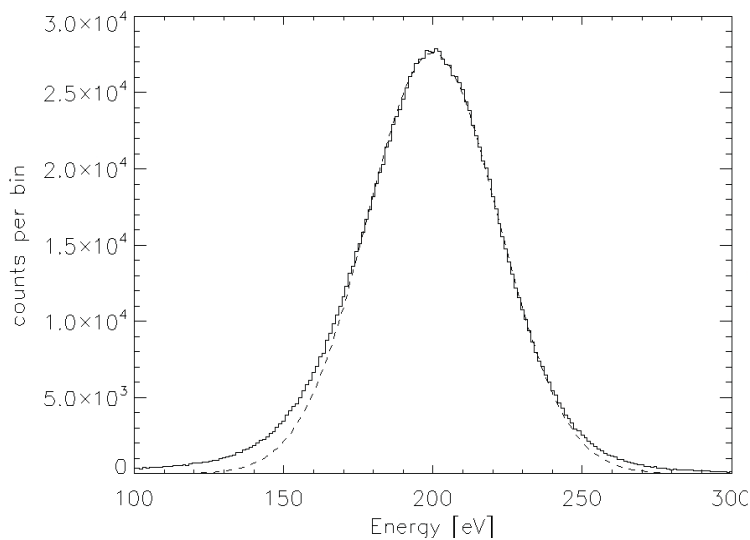


Fig. HE.25: Left: Spectrum of a 200 eV line measured with a prototype of the eROSITA PNCCD detector at BESSY II synchrotron. The FWHM of the line is 52 eV. The dashed line shows for comparison a Gaussian distribution which deviates only slightly from the measured peak. Right: eROSITA detector integrated in the housing. Mounted on the right-hand side of the blue detector board is the CCD chip (384 x 384 pixels with pixel size of 75 x 75 μm^2), while the electrical interface to the camera electronics is attached on the left-hand side.

consists of two CCD modules, with in total 1024×1024 pixels. The frame rate of 120 images/s was achieved for accurate and position dependent measurement of the number of diffracted X-ray photons in the keV energy range. By analysis of the diffraction pattern, the structure of the irradiated sample can be determined. These PNCCD detectors were recently successfully applied for experiments at the Stanford Linear Accelerator Center (SLAC) in USA and SACLA in Japan.

A second X-ray sensor type based on active pixels sensors (APS) with a depleted p-channel field effect transistor (DePFET) in each pixel has been developed for future challenging projects in space and on the ground. The first application of such a DePFET detector (see Fig. HE.26) will be the Mercury Imaging X-ray Spectrometer (MIXS) on board of the Mercury Planetary Orbiter (MPO) of ESA's BepiColombo mission. For this purpose an array of 64×64 macropixels with pixel size of $300 \mu\text{m} \times 300 \mu\text{m}$ and time resolution of $165 \mu\text{s}$ was designed and produced at the MPI semiconductor laboratory. The flight detectors are meanwhile assembled, tested, calibrated at the BESSY II synchrotron, and ready for integration into the instrument. An important issue was the radiation hardness of the detector which was successfully tested at the TANDEM accelerator in Garching with protons.

The first studies of detectors for future X-ray astronomy space projects, like the proposed Athena+ wide field imager (WFI) instrument, have also been made. Prototype DePFET sensors were designed, based on promising device simulations, fabricated, and tested. The homogeneity of the pixel response is an issue and had to be studied because of the large format of the planned sensor with $83 \text{ mm} \times 83 \text{ mm}$ and 1024×1024 pixels which cover a complete silicon wafer with 150 mm diameter (see Fig. HE.26). The readout rate is planned by operation in rolling shutter mode in the order of ms per frame or $16 \mu\text{s}$ for a small window area containing the point spread function (PSF).

Furthermore, active pixel sensors with different DepFET layouts have been designed and produced to study the optimum pixel layout. An important feature is the possibility to gate them during signal processing. By this method, accidental false measurements of the photon energy can be avoided. First tests with prototypes were very successful.

While the existing sensors are blind, i.e. insensitive, during the gate time, optimized DepFET pixels have been designed and are in production which can be gated but are still sensitive at any time. This is accomplished by separation of signal collection and readout area. The collected signal charge is then either transferred to the DepFET for signal processing or - by implementation of a second DepFET in the pixel - is read out by one DepFET while the other one is integrating. By this method dead time is avoided and all X-ray photons will be detected with correct energy.

An approach to exploit the maximum frame rate of such an APS sensor is realized for the DSSC camera at the European XFEL in Hamburg. All pixels are read out simultaneously permitting readout times of 220 ns per image albeit at the price of high power consumption and heat dissipation (meaning that the scheme is not feasible for a space project). First prototypes have been tested and the large DSSC sensors are currently being produced. A very special characteristic is the high dynamic range of the sensor ($1:10,000$ photons/pixel). This is accomplished by a non-linear response to the generated signal charge.

The ASIC which performs the analog processing of the sensor signals is a key component of the detector, of comparable importance to the sensor chip itself. We develop these readout ASICs, i.e. their concept and layout, and combine them with the PNCCDs or DepFET active pixel sensors in the detector system. None of the ASICs is commercial off-the-shelf: they need to be tailored to the individual project specifications. For eROSITA we use the well-proven CAMEX. This is an improved version of

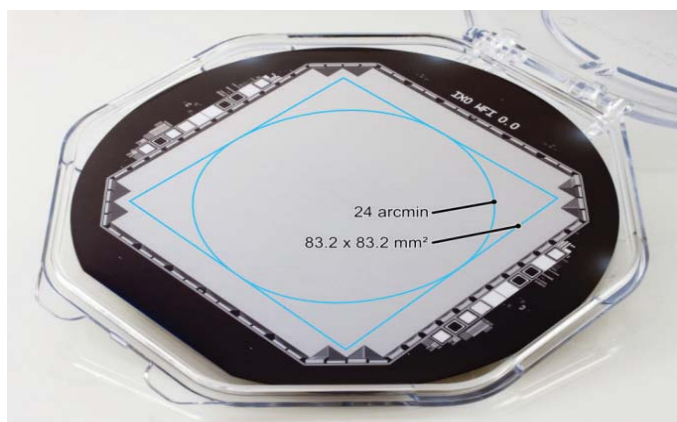
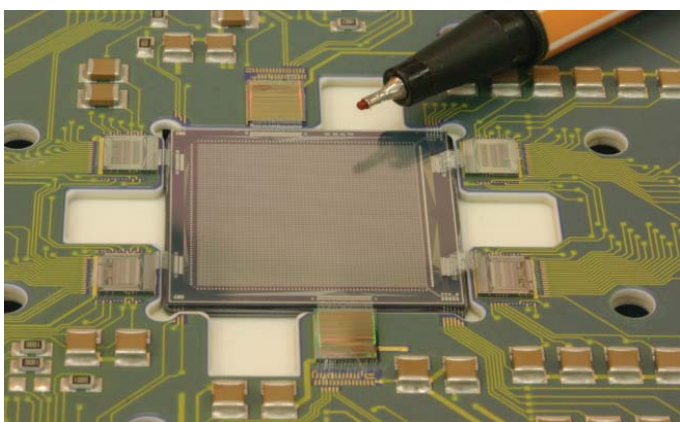


Fig. HE.26: Left: DePFET macropixel detector for the MIXS instrument on BepiColombo. Right: Demonstrator of DePFET APS sensor for the proposed Athena WFI instrument.

the ASIC used for the PNCCD camera on board of XMM-Newton and allows lower noise and faster readout. For the readout of the DepFET sensors of the BepiColombo mission, the ASTEROID ASIC has been developed. Future projects, like Athena+, will make use of the present ASIC development, called VERITAS, which can be applied for both sensor types, PNCCDs and DepFETs. It allows faster readout (e.g. because of smaller feature size) and higher dynamic signal range which permits applications with small signals (e.g. X-ray astronomy) or large signals (e.g. XFEL) without any change of the ASIC. The concept always provides the optimum weighting function independent of the timing by adjusting the gain. The VERITAS ASIC has been produced and is now under test.



Norbert Meidinger

(Other HE team members include R. Andritschke, F. Aschauer, A.Bähr, V. Emberger, L. Englert, T.Eraerds, B. Günther, G. Hauser, T. Lauf, N. Meidinger, D. Moch, M. Porro, S. Walther, G. Weidenspointner

Former HE team members include S. Granato, B. Huber, A. Mikova, G. Schmalzer, F. Schopper, A. Stefanescu, L. Strüder)

Selected References:

- Meidinger et al. 2010, *Nucl. Instr. & Meth. A*, 624, 321
- Meidinger et al., 2012, *Proc. SPIE*, 8453, 84530P
- Porro et al. 2010, *Nucl. Instr. & Meth. A*, 624, 509
- Strüder et al., 2010, *Proc. SPIE*, 7732, 77321I

4.3.2 X-Ray Optics Development

One of the most challenging tasks for future X-ray observatories is the enhancement of collecting area combined with very good angular resolution. Lightweight mirror materials, such as thin glass sheets, are needed to achieve these aims within the mass limits. We are developing a technology based on indirect hot slumping of thin glass segments. This technique enables us to produce the parabolic and hyperbolic part of the Wolter type I mirrors in one piece.

The current state of the art technologies for space borne X-ray telescope optics are solid zerodur mirrors (e.g. ROSAT, Chandra), replicated nickel shells (e.g. XMM-Newton, eROSITA), or segmented foils (e.g. Suzaku). Only the latter would be suitable for telescopes with a

collecting area of more than one square metre that are still light enough to be sent to space. However, the feasible angular resolution of foil telescopes does most likely not exceed 1 arc minute, while technologies that allow a better angular resolution limit the size of the telescope to not much more than XMM-Newton (0.465 square metre collecting area), due to the high mass per collecting area.

Next generation telescopes aiming for larger apertures create the need for mirrors made of lightweight materials. Large diameters (>1 meter) need to be manufactured as segments instead of closed monolithic shells. One new approach currently being studied by ESA is silicon pore optics (SPO). Our team is developing a possible alternative: thin glass sheets formed by thermal slumping. This technology offers several advantages: the material

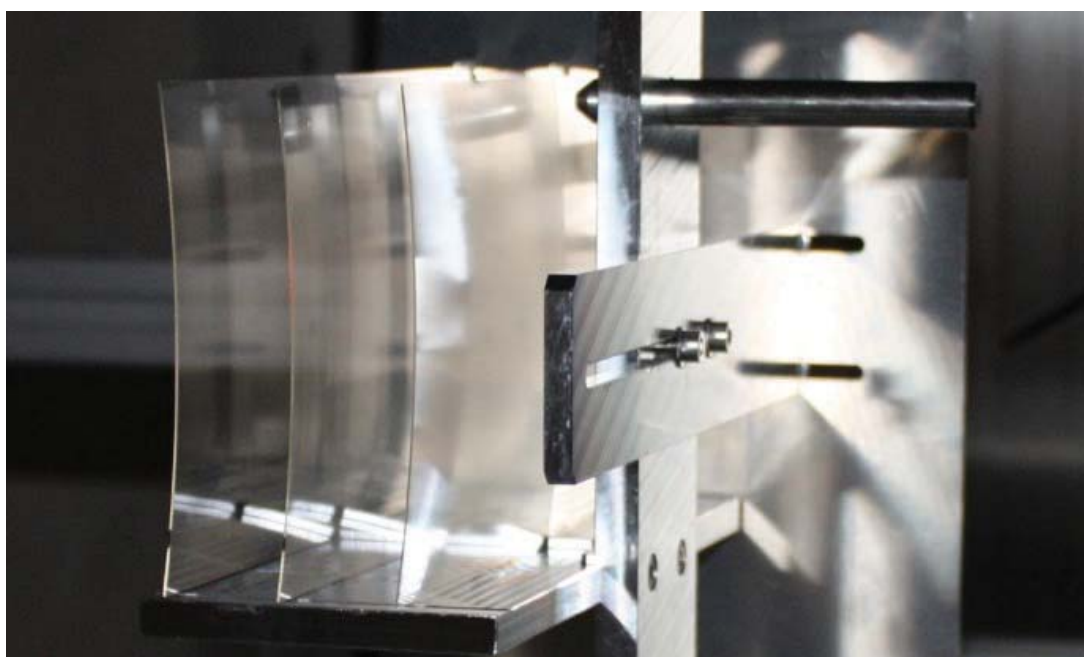
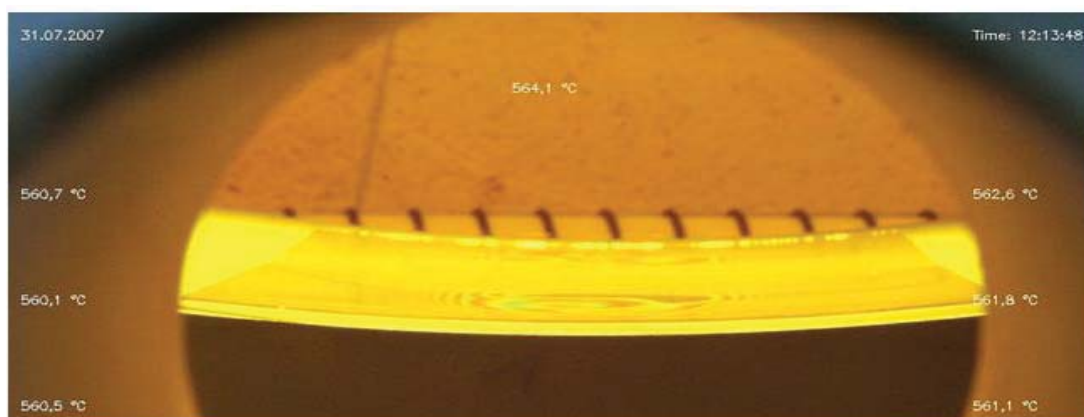


Fig. HE.27: Top: View through the observation window of the oven: the glass is just touching the mould indicated by fringes which will disappear later. Bottom: Three slumped glass segments in a simple mounting during an X-ray test.

is light, the glass sheets are thin yet very stable, and they can reproduce a true Wolter type I profile. Similar to SPO, slumped glass is not limited to specific sizes and shapes thus allowing a great variety of optical designs.

We have been studying the slumped glass technology at MPE since 2002, partly in collaboration with the Osservatorio Astronomico di Brera (OAB) and partners from industry. In a study with Zeiss (ended in 2007) we have learned how to make Wolter I mirror segments with parabola and hyperbola part in one piece, saving us the extensive adjustment of these two parts. Since then we have built up our own laboratory with a high temperature oven, cleaning equipment, and a high precision cross table plus optical sensors for metrology. We have studied in detail the optimum parameters of the slumping process (max. temperature, cooling rate etc.) for glass thicknesses below 0.5 mm. As we equipped our oven with an observation window we could monitor the slumping process for the first time ever (Fig. HE.27, top). In this way we were able to observe when, where and how the glass comes in contact with the mould and we could confirm that the glass comes fully in contact with the mould. We found that the most critical phase in the process is the cooling; it must be slow above the softening point and we have to avoid the slightest sticking to the mould during this phase. Therefore, the selection of the mould material is very important. In the last years we preferred a combination of a porous ceramic mould and a borosilicate glass (Schott D263) with a micro-roughness below 0.5 nm rms.

As opposed to other groups (e.g. at OAB and GSFC) our slumping process works with a concave shaped mould, meaning that the optical surface of the glass is the non-contact side ("indirect slumping"). This has the advantage that small-scale errors from the contact-side are damped. However, we need a process which makes the glass raw material constant in thickness; a polishing procedure for that has been successfully tested at Zeiss. We analyse the results of the slumping process by visual inspections and metrology. A surface scan with an optical sensor gives us the profile errors from which we can calculate the expected angular resolution for imaging. Finally, we have a set-up in which we can test the imaging performance of a few glass segments in MPE's X-ray test facility PANTER (Fig. HE.27, bottom): During the last years we have improved the angular resolution from ca. 2 arc minutes to ca. 1 arc minute HEW. An analysis of the error contributions reveals that still the profile errors of the mould (although significantly improved in 2012) contribute most. As the ceramic material is difficult to machine and we probably have reached its limits we are currently searching for alternatives.

Since 2012 we have also been focusing on the integration and alignment of glass segments into a mirror module. The two key issues of concern are the handling of a mirror segment during assembly, and the technology to structurally integrate the mirror segments with the supporting mirror module. Both steps can introduce significant shape errors to the mirror. Our approach (accompanied by FE analyses and experimental results) is based on the application of isostatic mounting principles and gravity compliance to minimize distortion effects.



Peter Friedrich

(Other HE team members include Elias Breunig, Vadim Burwitz, Peter Friedrich, Peter Predehl, Laura Proserpio, Anita Winter

Former HE team members include Renzo Capelli, Monika Vongehr)

Selected References:

Winter et al., 2012, Proc. SPIE, 8450, 84502E

4.3.3 PANTER X-Ray Test Facility

The PANTER X-ray test facility has been central to the development, testing and calibrations of mirrors and mirror technologies for almost all European X-ray astronomy experiments. PANTER is currently at a high level of activity related to the development of the eROSITA mirrors and for the calibration of the completed eROSITA flight mirror modules. PANTER has also been used to test the eROSITA camera cooling system and for outgassing the large telescope structure parts. The eROSITA end to end test will also take place in PANTER. Furthermore the X-ray test facility has been successfully upgraded (extended) to be able to make in focus measurements of X-ray optics modules such as Slumped Glass Optics

(SGO) and Silicon Pore Optics (SPO) for future ESA large observatory type missions such as Athena+. Many development tests of the SPO and the SGO modules have recently been performed using intra focal imaging. Last year for the first time ever, the combination of a JET-X mirror system and the X-ray polarization detector (GPD) were tested together at PANTER. Also promising are the results obtained from the tests of the Wide Field X-ray Telescope (WFXT) and the New Hard X-ray Mirror (NHXM) prototype shells. Also the low energy LE and medium ME energy detectors of the Chinese Hard X-ray Modulation Telescope (HXMT) are being tested at PANTER.



Fig. HE.28: An aerial view onto the PANTER X-ray test facility in Neuried, south west of Munich.

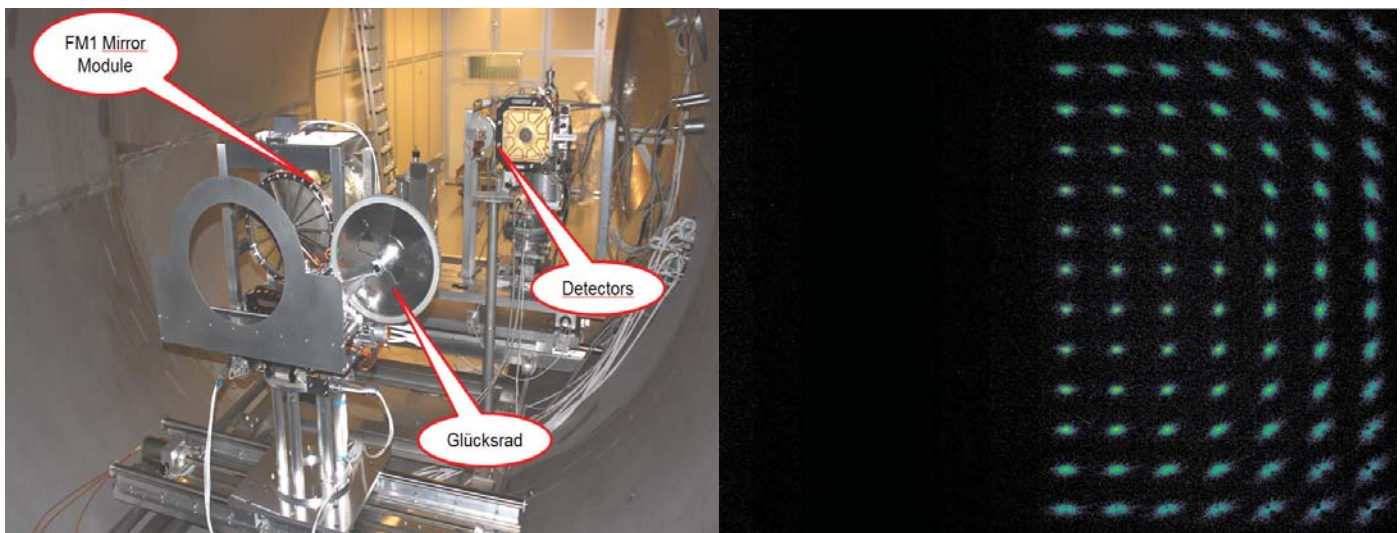


Fig. HE.29: Left: The eROSITA FM1 mirror module mounted in the PANTER vacuum chamber. Right: Map of the eROSITA PSF over a quarter of the focal plane in 5 arcmin steps obtained using PIXI, the on-axis PSF is at the bottom left.

The X-ray test facility was setup in the late 1970s and the PANTER configuration with the 130 m beamline was brought into service in 1980 to support the ROSAT mirror development and its calibration. Since then many upgrades and changes were performed to accommodate the new X-ray astronomy missions that were being developed and later calibrated before launch (EXOSAT, BeppoSAX, JET-X, Chandra (AXAF), XMM-Newton, ABRIXAS, Swift, and Suzaku). Now the PANTER test facility has been upgraded to accommodate the extensive eROSITA X-ray optical tests and also thermal control of the telescope components. To be ready for testing X-ray optics, with focal lengths $f > 10$ m optics and large mirror radii of up to 1 m, for future missions such as Athena+ a further extension of the beamline was successfully commissioned last year. During that campaign the first in-focus measurements of SPO and SGO modules with $f=20$ m were obtained. For the optics tests at PANTER the single photon counting detectors, the Position Sensitive gas Proportional Counter (PSPC) and the eROSITA prototype CCD camera TRoPIC have been joined by the recently commissioned Photon Integrating X-ray CCD Imager (PIXI).



Vadim Burwitz

(Other HE team members include Wolfgang Burkert, Michael Freyberg, Gisela Hartner, Benedikt Menz)

4.4 Current Projects

4.4.1 eROSITA Instrument

eROSITA is the main instrument aboard the Russian „Spektr-Rentgen-Gamma“ (SRG) mission, scheduled for launch in late 2014. The primary mission goal is to perform an X-ray all-sky survey lasting for 4 years. eROSITA consists of 7 identical telescopes, each equipped with nested Wolter-I mirror modules + pnCCD-cameras. The instrument design is driven by the goal of detecting 100.000 clusters of galaxies, to constrain cosmological parameters including Dark Energy. MPE is responsible for the design, development and integration of the entire instrument. The data analysis software development is also lead by MPE (§4.4.2).

X-ray telescopes

The telescope structure consists of the optical bench, the sunshield, the front cover including its release mechanism, and the hexapod, which is the interface between eROSITA and the spacecraft platform. The carbon fibre structure has been developed in house and was manufactured by Invent GmbH in Braunschweig. It was completed in early 2012.

The telescope structure supports the eROSITA mirror modules, each of which comprises 54 nested Wolter-I shells. The seven flight modules (plus one spare) are manufactured by Media Lario Technologies in Italy. Although we thought the mirrors were simply smaller versions of the XMM-Newton mirrors, the development turned out to be extremely challenging and required a tremendous effort here at MPE: For several years up to 8 FTEs were working on this until the performance goal of 15 arcsec angular resolution was reached. At the time of writing, four modules have already been delivered, with the remainder are expected to arrive by October 2013.

In front of each mirror module an X-ray baffle is mounted in order to suppress the unwanted single reflections from sources outside the field of view, thereby increasing the background. A baffle consists of 54 invar cylinders precisely matching the footprint of the mirror shells. These baffles have been developed and integrated entirely at MPE. Their X-ray performance is tested and close to the theoretical limit. Four baffles are completed, the rest is expected until the end of this year. Magnetic electron deflectors at the rear end of the mirrors should suppress the background due to low energy cosmic electrons. They have also been designed, fabricated and tested at MPE.

Focal plane instruments

Each eROSITA telescope focuses X-rays onto a CCD camera. The cameras are completely designed, developed, manufactured, and tested at MPE. The “heart” of each camera is a framestore-pnCCD (3×3cm²), devel-

oped in our semiconductor laboratory, which is surrounded by a massive copper shield to reduce potential radiation damage. When the Russian space agency Roskosmos decided to launch the mission into an L2-orbit, we were forced to redesign the existing camera electronics into a radiation hard version. The complete electronics comprises 7 camera boxes and two (redundant) interface & thermal control boxes with 54 PCBs altogether. The “heart” of each box is a Virtex-IV FPGA. The electronics are completely designed, developed, manufactured, and tested in house. They are currently in the engineering and testing phase. Each camera is equipped with a filter wheel in front having four positions (closed, open, filter, cal-source). The calibration source is a ⁵⁵Fe source which, together with an Al+Ti target, produces 3 spectral lines for gain calibration in orbit. The filter wheels are completely designed, developed and tested at MPE. The production of the flight-wheels is ongoing.

For optimal operation the CCD has to be cooled down to -95°C. The cameras are cooled passively by means of two large radiators and a cryogenic heat-distribution system comprising 4 “switchable Variable Conductance Heatpipes” (sVCHP), two ring-heatpipes and seven camera heatpipes. The switching of the VCHPs is needed to keep the cameras warm during the first weeks in orbit in order to allow outgassing. The complete heatpipe system including the novel sVCHP is an MPE development.

Tests and Qualification

Hundreds of individual tests (e.g. performance, vibration, acoustic noise, thermal-vacuum) were and still are needed for the development and qualification of components, subsystem and the complete instrument. This would not have been possible without MPE’s technical infrastructure, such as thermal vacuum chambers and our shaker. Particularly our long beam X-ray test facility PANTER is almost continuously occupied for tests and calibration of the mirror shells and modules. With a slight modification, this facility has also been used for thermal vacuum test of the entire instrument. The qualification tests of eROSITA were successfully performed at IABG between November 2012 and January 2013. These tests included acoustic noise, vibration, pyro shock, and space simulation.

For testing of all mechanical and electrical interfaces to the spacecraft, we have built a structural model and a “Technological Model”, both delivered to the Russian company Lavochkin Association.

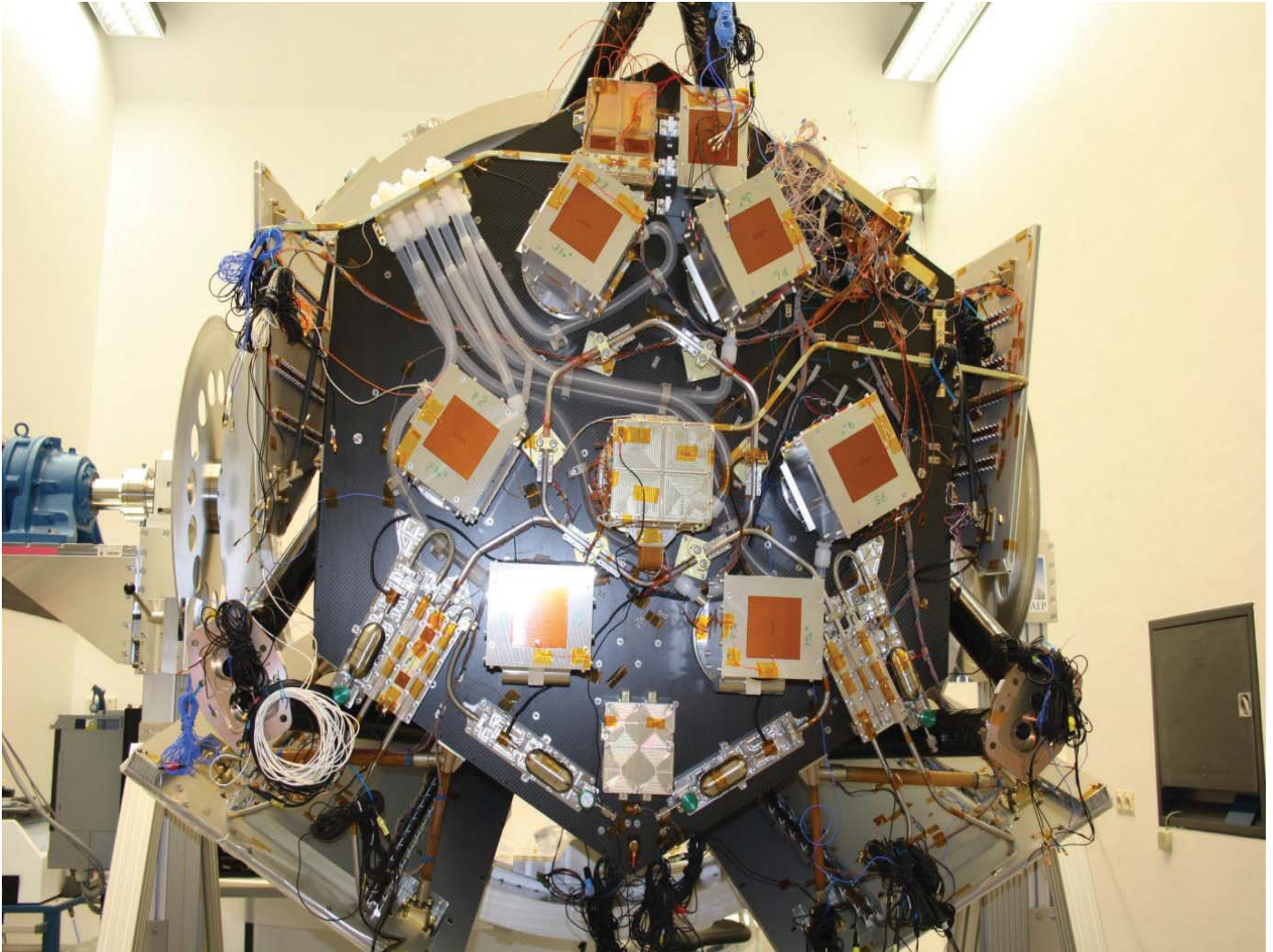


Fig. HE.30: For the qualification tests the camera platform was equipped with the central camera + 6 mass dummies. Also seen: the complete heatpipe system, the radiators, the test-harness, and the (grey) purging hoses (upper left) which are needed for cleanliness reasons during all ground operations prior to launch.



Peter Predehl

(Other HE team members include Robert Andritschke, Thomas Boller, Heinrich Bräuninger, Hermann Brunner, Wolfgang Burkert, Vadim Burwitz, Nicolas Clerc, Konrad Dennerl, Tom Dwelly, Josef Eder, Michael Freyberg, Peter Friedrich, Maria Fürmetz, Roland Gaida, Antonis Georgakakis, Fabrizia Guglielmetti, Frank Haberl, Gisela Hartner, Andreas v. Kienlin, Norbert Meidinger, Andrea Merloni, Kirpal Nandra, Elmar Pfeffermann,

Former HE team members include Marcella Brusa, Nico Cappelluti, Martin Mühlegger, Lothar Strüder, Monika Vongehr)

Selected References:

Predehl et al., 2010, "eROSITA on SRG", *Proc. of SPIE*, 7732, 10 (2010)

4.4.2 eROSITA – Ground Segment

Activities to set up a software system to support the operation of the eROSITA telescope were initiated immediately after the inception of the project. Drawing on the experience and huge code base of ROSAT, AbriXas, and XMM-Newton, an MPE-led team of up to 15 staff members, postdocs and PhD students at six eROSITA consortium and associated institutes developed a software system covering the areas pipeline data processing, calibrated data products and source catalogs, interactive data analysis, archiving and data access, instrument health monitoring, quick look science, and mission planning. Work on the software system is currently transitioning from code development to integration and testing. This is complemented by on-going activities to create simulated eROSITA data of increasing sophistication, supporting both software testing and science planning.

Pipeline data processing system

Inspired by the ROSAT pipeline processing software developed at MPE, four main functional units perform X-ray event calibration (TEL chain), creation of images and exposure maps (EXP chain), X-ray source detection and characterisation (DET chain), and creation of calibrated source level data products (SOU chain). This is complemented by software modules for pre-processing and packaging the incoming data and for conducting a near real-time analysis (NRTA), performing instrument health checks and quick-look science. At this stage, 12 FTE were expended on the eROSITA core data processing system, which is around 75% complete.

Calibrated data products and in-depth interactive analysis

Most programs comprising the eROSITA pipeline processing system also function as interactive data analysis tools, allowing the users to rerun and improve on the pipeline analysis. In addition, data products, such as calibrated event lists, images, exposure maps, and spectra, comply with established standards, permitting the use of well-known publicly available X-ray data analysis packages, which work seamlessly with the eROSITA data analysis tools. A general-purpose source catalog database system, developed at MPE, is currently adapted for eROSITA, providing a flexible interface for accessing and cross-matching eROSITA sources with existing catalogs.



Hermann Brunner

(Other HE team members include T. Boller, N. Clerc, K. Dennerl, T. Dwelly, M. Freyberg, P. Friedrich, A. Georgakakis, F. Guglielmetti)

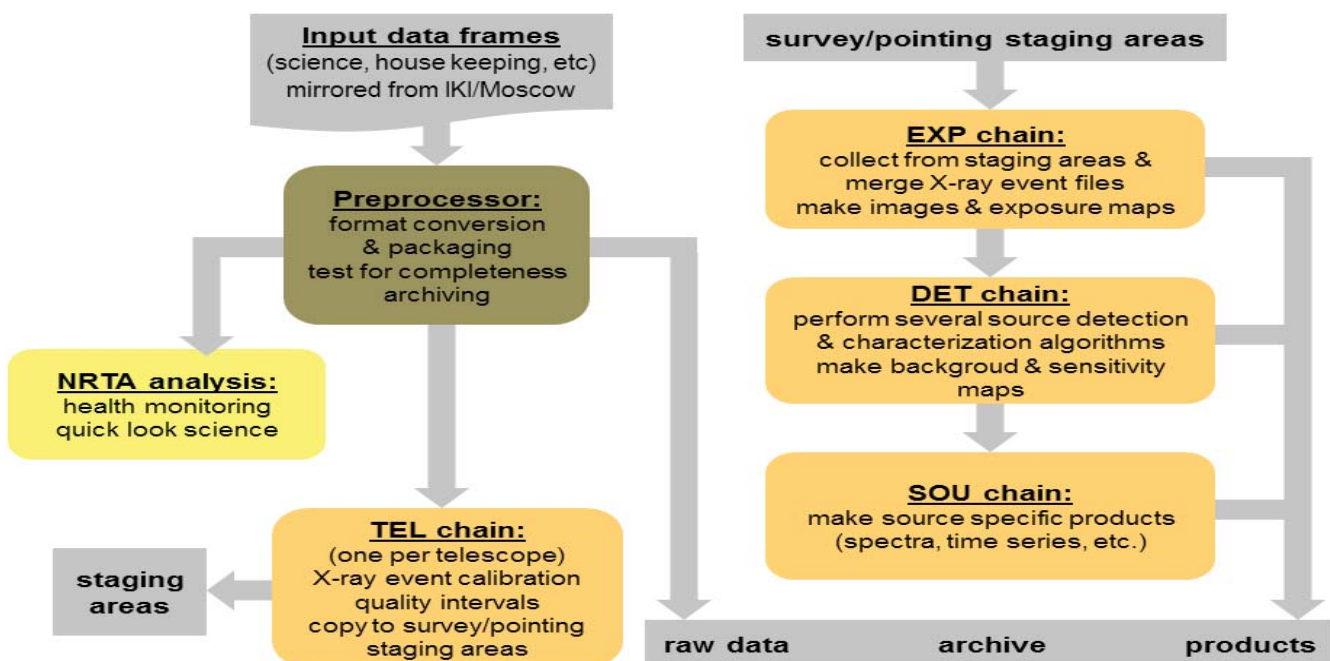


Fig. HE.31: eROSITA pipeline processing system

4.4.3 Operating Space Projects

MPE HE group has contributed hardware to a number of operating space missions. We are exploiting these for science, but also perform service and support activities related to these projects.

XMM-Newton

XMM-Newton, the major X-ray observatory of ESA currently in orbit continues to work perfectly. We are still strongly involved in the support of the mission with health monitoring and in-orbit calibration of the EPIC pn camera and contributions to the XMM-Newton Survey Science Center (SSC) collaboration. The EPIC pn camera onboard XMM-Newton is currently the most sensitive instrument in space for detecting low energy X-rays. In order to fully utilize this unique property, we have developed a method for suppressing a major noise component which is prominent at energies below 200 eV. We have also succeeded in improving the reconstruction of the absolute energy scale by correcting subtle shifts caused by the fact that some of the infrared radiation of the detector reaches its central area and reduces the charge transfer losses by partial saturation of traps (Fig. HE.32). These techniques have been included as specific 'tasks' into the XMM-Newton Science Analysis System (SAS) and are since 2012 generally available to XMM-Newton guest observers.

Within the SSC collaboration we maintained and extended EPIC and specifically EPIC pn tasks, contributed to the manual screening of the pipeline products, and we participated in the production of the second XMM-Newton serendipitous source catalogue 2XMM. The catalogue contains ~250.000 detections from 3500 public XMM-Newton observations, which relate to about 190.000 unique sources. The non-overlapping sky area is ~360 square degrees. The third version of the catalogue is in preparation.

INTEGRAL

ESA's INTErnational Gamma Ray Astrophysics Laboratory (INTEGRAL) was launched in 2002 for a nominal 3-year mission. It carries two major telescopes, an imager (IBIS) and a spectrometer (SPI). MPE is Co-PI institute of SPI, and contributed the anticoincidence detector system. All detector systems and the satellite have been performing fine, and could operate well beyond 2020, only limited by fuel and solar cell degradation. In 2-year intervals, the extension of the mission has been reviewed and approved by ESA, currently till 2014, with the next decision coming up in mid 2013.

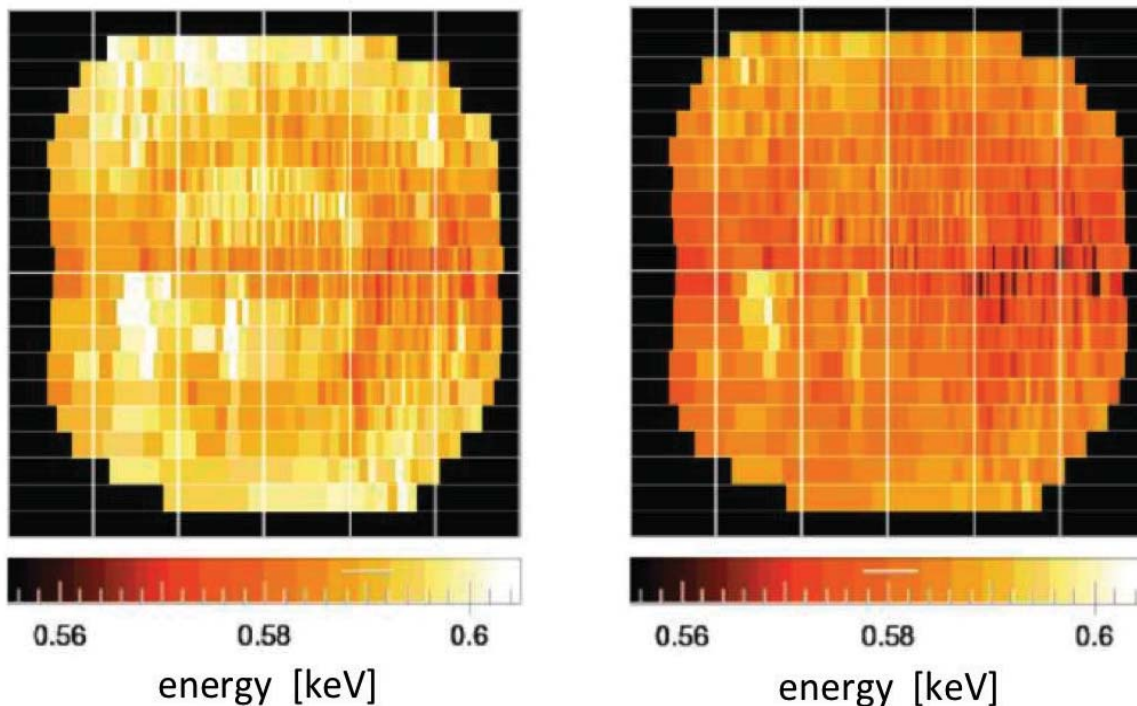


Fig. HE.32: Spatial distribution of the reconstructed energy of the O VII (0.57 keV) emission line from the Vela SNR over the EPIC pn CCDs before (left) and after (right) the correction with the task epspatialcti.

MPE processes all SPI data and performs routine response determination and science quality checks, maintaining a high-level data product database for spectroscopy at 0.5 keV resolution. MPE scientists have been studying gamma-ray bursts with SPI-ACS, and nucleosynthesis in the Galaxy as well as Galactic-diffuse emission from cosmic ray interactions and positron annihilation, and also studies of solar flares (in combination with GBM-Fermi). MPE-led papers are among INTEGRAL's most-cited papers, and several deep observing proposals have been successfully proposed by us in recent AOs. Year 2010 saw several highlighted journal papers on specific stellar groups in our Galaxy, and a review textbook on "Astronomy with Radioactivities". Breakthrough results were spatially-resolved spectroscopy of the ^{26}Al emission along the plane of the Galaxy, detection of ^{60}Fe from the Galaxy (2007), and mapping of positron annihilation emission in the inner Galaxy.

Fermi

After a decade of instrument development led by the HE group and in collaboration with German industry, the Gamma-Ray Burst Monitor GBM started operation after a successful launch onboard the Fermi spacecraft in June 2008. The instrument is working flawlessly, and by the end of 2012 has provided 2381 triggers, among those 1050 GRBs, 321 terrestrial gamma-ray flashes (TGF), as well as 91 autonomous repoint recommendations to the Fermi spacecraft. Due to the surprising results on TGFs, the flight software was changed in November 2012 to implement full-time continuous Time-Tagged Event (TTE) data production at 2 μs time-resolution. The dominant scientific emphasis is shared roughly equally between GRBs and TGFs, the remaining about 20% of papers covering a large range of topics from Soft Gamma Repeaters over monitoring of bright hard X-ray sources to pulsar research, and correlated source searches with LIGO (gravitational waves) and IceCube (neutrinos). GBM contributions are made to typically 30 conferences per year.

Chandra

The Low Energy Transmission grating (LETG) on Chandra was built by MPE in cooperation with SRON in Netherlands. The LETG is equipped with 540 individual grating elements which have been developed at MPE together with the company Heidenhain GmbH. Even after 14 years in orbit, the LETG works perfectly within its original specification. Our benefit is still a share of the Chandra guaranteed observing time allocation.



Roland Diehl, Jochen Greiner, Frank Haberl, Peter Predehl

4.4.4 Operating Ground-Based Projects

While the emphasis of the MPE HE group in terms of hardware is overwhelmingly on space projects and instrumentation, we are currently operating to ground-based PI instruments which are of interest for our scientific goals.

GROND

GROND is a 7-channel imager which was developed in the HE group in collaboration with the Thüringer Landessternwarte Tautenburg. It has started routine operations at the 2.2m MPG/ESO telescope in mid-2007. While originally developed as a dedicated instrument to observe GRB afterglows, GROND has become the workhorse instrument at its telescope. Meanwhile the observing time spent by non-MPE scientists on non-GRB targets has increased and even exceeds the time used for GRB afterglows.

GROND works very reliably (up-time about 99%). With few exceptions, every GRB detected by Swift at Declination south of +35 deg has been observed with GROND, obtaining more than 150 afterglow detections. Beyond contributing substantially to the race for the highest redshift objects, GROND also provides surprising constraints on the afterglow physics and GRB late-engine activity (see §4.2.4.). The GROND impact is exemplified via the number of publications since commissioning (Fig. HE.33), compared to the two other instruments on the same telescope, and HARPS@3.6m. Note that these numbers have not been normalised to the total telescope time used (see figure caption). The typically 50-60 GCN notices per year based on GROND observations are excluded.

OPTIMA

OPTIMA (The Optical TIMing Analyzer) is a sensitive, portable, stand-alone photo-polarimeter for observations of highly time-variable sources at optical wavelengths. It utilizes single photon avalanche diodes which are fed by a hexagonal field unit of fiber pick-ups in photometry mode, or alternatively by a Twin Wollaston prism that re-focuses the beam to four polarized images with different polarization angles. In the last six years, OPTIMA has been successfully operated on two telescopes; yearly for 4-6 weeks at the 1.3m telescope at Skinakas Observatory (Crete) and in 2009 for 3 nights at the Nordic Optical Telescope in La Palma (clouded out). Some scientific highlights are described in §4.2.3. Since 2011 OPTIMA is operated with new data acquisition electronics developed in part at MPE as well as completely new data acquisition software. These system improvements allow a significantly higher time resolution, and overall an increased observing efficiency.



Jochen Greiner, Gottfried Kanbach, Arne Rau

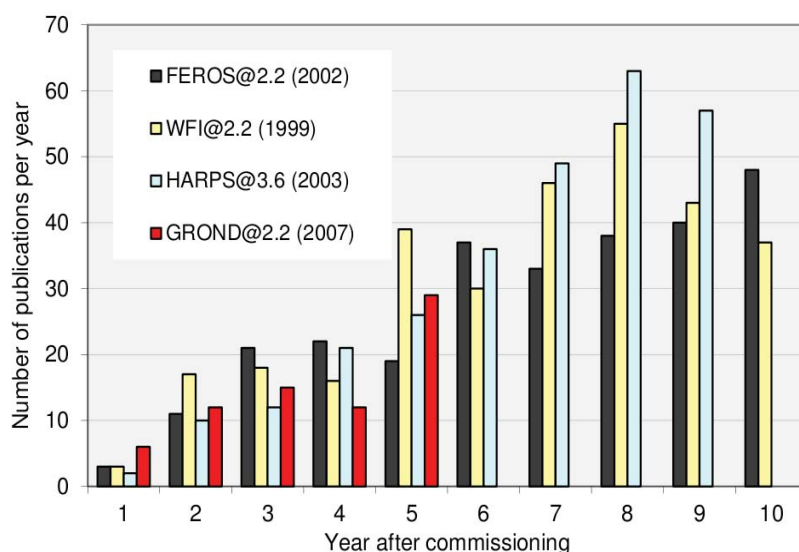


Fig. HE.33: Publications in the refereed literature until November 2012 of GROND and three selected other instruments in dependence of the time after commissioning (the corresponding year is given in the labels). These publications are based on different total observing times at the telescope: GROND (15%), WFI/ FEROS (45%), HARPS (85%).

4.5 Future Projects

While the group is heavily focussed on the completion of the hardware and ground segment for eROSITA, and the delivery of high quality X-ray data from the instrument when it flies, we are actively exploring future projects in two main areas. The first is in high energy space projects, particularly in X-ray astronomy, beyond the eROSITA timeframe. The largest of these is Athena+, which is currently entering into considering by ESA for a launch in 2028. The group's future strategy is heavily dependent on whether or not Athena+ is selected: if selected, it is likely to dominate our activities for the next

20 years. We are, however, also pursuing a number of smaller involvements in space projects which are interesting in their own right but also act as a contingency against the non-selection of Athena+ by ESA. Currently under consideration in this category are XTP-GRAVITAS and SVOM, both Chinese satellite projects. The other main area we are pursuing in terms of future projects is in ground-based instruments and facilities which are required for eROSITA followup. At present our main activities in this area are the SDSS-IV SPIDERS and 4MOST large-area multi-object spectroscopy projects.

4.5.1 Athena+

Athena+ (the Advanced Telescope for High Energy Astrophysics), is ESA's next-generation X-ray astronomy observatory. It has been conceived to address two key questions in modern astrophysics: 1) How does ordinary matter form the large-scale structures that we see today? 2) How do black holes grow and shape the Universe? Athena+ will provide a huge leap in observational capabilities compared to current X-ray astronomy facilities, providing factor ~ 10 improvements in imaging high resolution spectroscopy and wide field X-ray imaging. These advances are needed to determine the astrophysical processes responsible for the evolution of hot gas over cosmic time, the end point of which are clusters, groups and filaments which dominate the baryonic content of the Universe. Feedback from supermassive black holes apparently plays a major role in determining the evolution of these large baryonic structures, as well as that of galaxies. Athena+ will also perform a census of black hole activity stretching out to the highest redshifts ($z > 6$) and identifying even the most obscured systems

shrouded in dust and gas, possibly due to the feedback process itself. Spectroscopy and timing studies of nearby accreting black holes will shed light on the processes causing feedback – which ultimately originate close to the black hole event horizon – and the mechanisms by which the radiative and/or mechanical output of the black hole couples to larger scales, where it has such an apparently profound effect. Some of the scientific goals of Athena+ are illustrated in Fig. HE.34.

The heart of the Athena+ mission is the X-ray optics system, which uses the innovative silicon pore optics (SPO) technology pioneered in Europe by ESA. The Athena+ science goals require a 2m^2 effective collecting area with 5 arcsec angular resolution, achieved using a single 12m focal length telescope. The SPO provides this combination of very large area with good angular resolution with very low mass. The focal plane comprises two instruments which can be moved in and out of focus via an exchange mechanism. The X-ray Integral Field

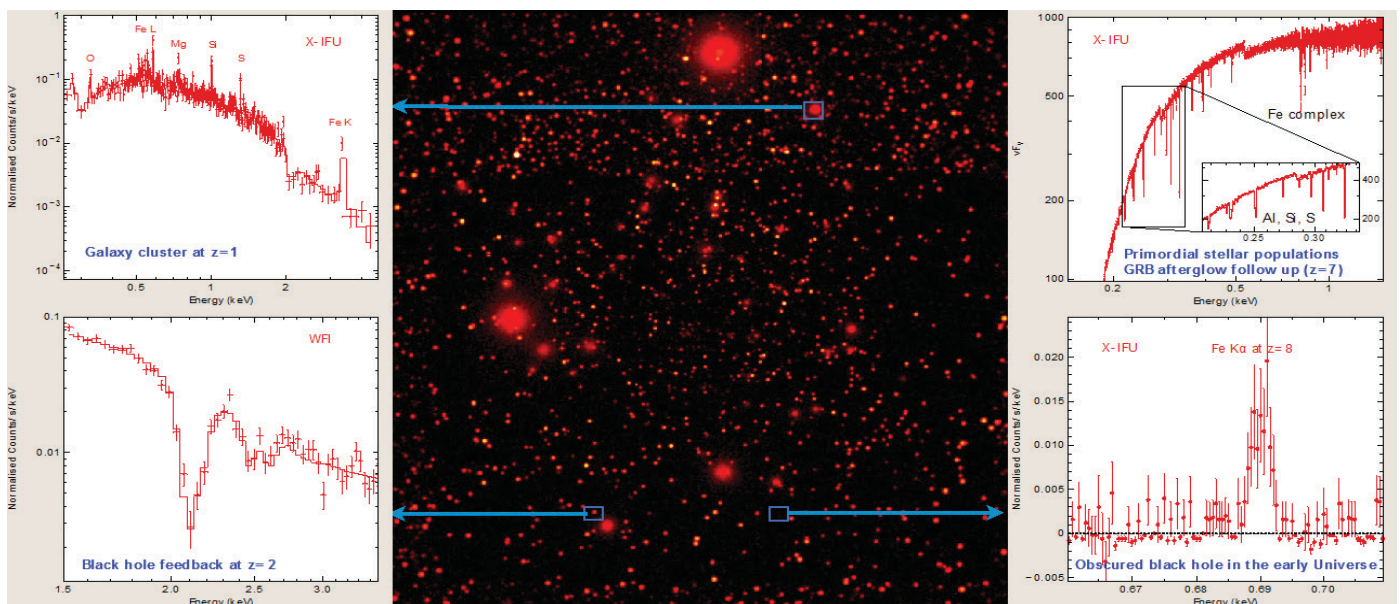


Fig. HE.34: Athena+ will provide revolutionary advances in our knowledge of the Hot and Energetic Universe. The central panel is a simulated deep WFI observation, while the four surrounding spectra illustrate advances in different science areas, none of which are possible with current facilities.

Unit (X-IFU) provides spatially resolved high resolution spectroscopy using TES calorimeters, cooled to 50mK. This provides 2.5 eV resolution ($E/DE=2500$ at 6 keV) over a field of view of $5^\circ \times 5^\circ$. The Wide Field Imager (WFI) consisting of an active pixel sensor camera based on Si DepFET technology, providing a $40^\circ \times 40^\circ$ field of view and $E/DE=50$, with high count rate capability and time resolution. Athena+ will be placed in orbit at L2 via an Ariane V launch, with a nominal 5-year mission lifetime, but with consumables for at least 10 years. In addition to enabling the core scientific goals, technological leap in capabilities provided by Athena+ will open up a vast discovery space leading to new areas of scientific investigation that we cannot currently envision. It will be operated as an observatory, with the scientific program predominantly determined by PI-driven proposals.

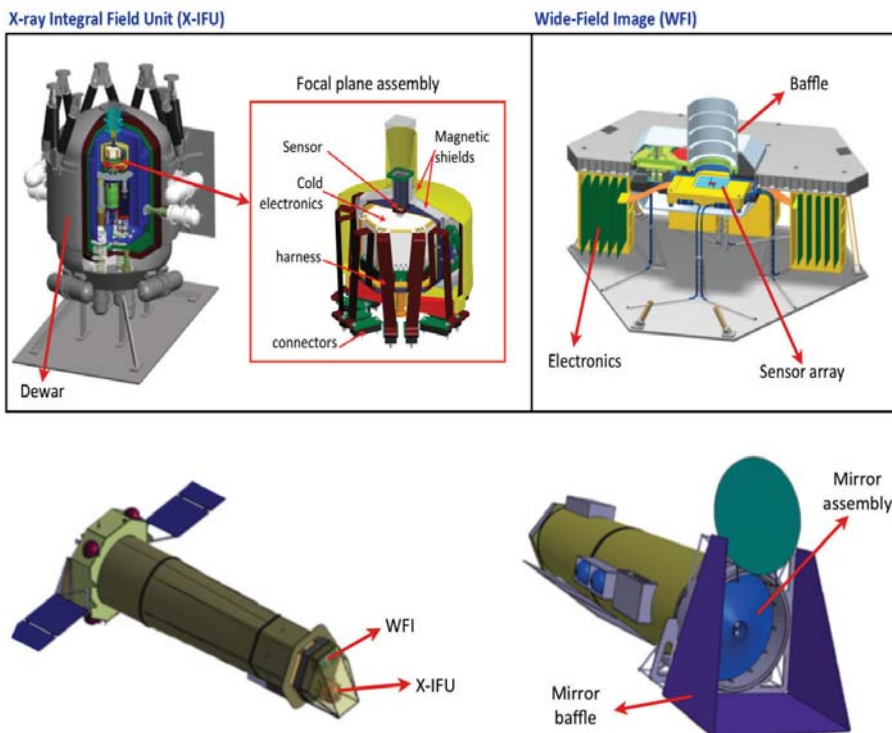
The major MPE contribution to Athena+ is expected to be the WFI instrument (see also §4.3.1), a novel detector concept based on Silicon DepFET technology developed by us, and already implemented via the MIXS instrument on BepiColombo. The DepFET-based instrument provides the possibility of large focal planes with near Fano-limited energy resolution, together with the potential for very fast readouts resulting in high time resolution and count rate capability. The WFI is being developed under the leadership of MPE with a German consortium including the Universities of Tübingen and Erlangen, and PNSensor GmbH, and an international consortium including the University of Leicester, UK and

IRAP, France. We are also participating substantially in the optics development program for Athena+, mostly via provision of the PANTER facility for testing (§4.3.3) and calibration of the SPO optics, but also in developing possible backup optics technologies for Athena based on slumped glass (§4.3.2). MPE also has a lead role in the science definition of the Athena+ mission, and is likely to make a substantial contribution to a community-based science data centre anticipated for the mission.

Athena+ is a leading candidate for the next ESA large mission launch slot in 2028, known as “L2”. The process of selecting scientific themes for L2 and the next large mission slot L3 in 2035 is just underway, with a decision expected later this year. This will be followed by a restricted call for the L2 mission in 2014. The future strategy of the MPE HE group will depend substantially on the out come of this selection process. If Athena+ is indeed chosen for the L2 slot in 2028, our post-eROSITA hardware developments will be dominated by work for Athena+ and particularly the development of the WFI.



Kirpal Nandra



(Other HE team members include Werner Becker, Thomas Boller, Murray Brightman, Johannes Buchner, Vadim Burwitz, Konrad Dennerl, Maria Führmetz, Antonis Georgakakis, Frank Haberl, Andreas von Kienlin, Norbert Meidinger, Andrea Merloni, Gabriele Ponti, Matteo Porro, Peter Predehl, Arne Rau, Mara Salvato, Jeremy Sanders)

Fig. HE.35: Top: design drawing of the Athena+ WFI, a revolutionary instrument for X-ray imaging, timing and spectroscopy being lead by MPE, based on our own Silicon DepFET technology. The WFI capitalises on the unprecedented effective area/angular resolution combination of the Athena+ X-ray telescope to provide unprecedented X-ray survey capabilities needed, for example, to perform a census of accreting black holes in the early Universe ($z>6$). Bottom: a concept for the Athena+ spacecraft, showing the location of the mirror assembly and the two interchangeable focal plane instruments.

4.5.2 XTP-GRAVITAS

The X-ray Timing and Polarimetry (XTP) satellite is a large-class astronomy facility currently under study by the Chinese Academy of Science (CAS) for a launch in the early 2020s. The main scientific driver is broad-band spectral-timing of observations of compact sources. Observations of the energy-depending variability patterns of both stellar and supermassive black holes are able to map out the strong gravity environment near the event horizon e.g. via reverberation signals where the telltale signatures of general relativity are revealed, including the spin of the black hole. These observations also offer the chance to map the inner accretion flow to understand how matter falls onto black holes under the effects of GR. Spectral and timing signatures can also be used to determine the mass and radius of neutron stars, and hence determine their equation of state with implications for theories of dense matter. These scientific drivers were also those behind the GRAVITAS concept (Nandra et al. 2012) submitted to ESA for consideration as a medium class mission, and this has naturally lead to a discussion about whether the concepts could be combined.

The payload and mission design of XTP is currently undergoing a preliminary design study by CAS. MPE scientists have been involved in the discussions about the de-

sign and the options for both optics and detectors for the mission, and both sides have expressed great interest in collaborating. The precise nature of MPE involvement is not yet defined but could include provision of hardware and/or technology for fast Silicon-based detectors (§4.3.1) and/or slumped glass optics (§4.3.2). The phase A study for XTP is expected to be completed in 2015 by which the payload needs to be defined and any MPE contribution elaborated.



Kirpal Nandra

(Other HE team members include Vadim Burwitz, Peter Friedrich, Maria Führmetz, Norbert Meidinger, Gabriele Ponti, Matteo Porro, Peter Predehl, Arne Rau, Anita Winter)

4.5.3 SVOM

SVOM, the Space Variable Objects Monitor, is a Chinese-French satellite project devoted to the detection and study of Gamma-Ray Bursts and other transient phenomena. The payload will contain four instruments: (1) the large field gamma-ray telescope ECLAIRs, which will detect GRBs, (2) the narrow-field telescope MXT which shall localize the X-ray afterglow of GRBs to much better accuracy, (3) the GBM gamma detector which shall extend ECLAIRs energy range up to 5 MeV, and (4) the narrow-field visible telescope which is dedicated to detect the optical afterglow emission. SVOM is presently scheduled for launch in 2017.

MPE is collaborating with CEA Saclay on the MXT instrument. We provide the PNCCD chip as well as the dedicated ASICs for readout of the analog sensor signals. This includes the circuit diagrams and detector operating parameters. A first prototype detector board has been developed at CEA. The back-illuminated CCD was originally produced in the MPI semiconductor laboratory for the DUO project proposal. It offers similarly advanced detector properties as the eROSITA detector, in particular with respect to the spectroscopic performance, e.g. $\text{FWHM}(5.9\text{keV}) = 130 \text{ eV}$. The main difference is the smaller image of 256×256 pixels which none the less is a good match to the MXT telescope parameters.

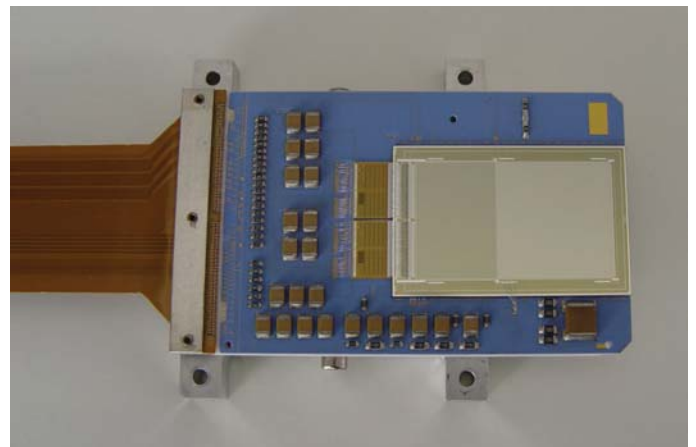


Fig. HE.36: PNCCD mounted on detector board with two readout ASICs of eROSITA type.



Jochen Greiner

(Other HE team members include Norbert Meidinger, Kirpal Nandra, Arne Rau)

4.5.4 SDSS-IV SPIDERS

SPIDERS (SPectroscopic Identification of EROSITA Sources, PIs: Merloni and Nandra) is a dedicated spectroscopic survey within the upcoming SDSS-IV program, planned for the period 2014-2020. The main goal of SPIDERS will be to carry out an efficient, complete, homogeneous and timely spectroscopic follow-up campaign to identify and characterize the sources detected by eROSITA in the first two years of operations. While the complete spectroscopic identification of faintest eROSITA sources will require a 4-meter class telescope (e.g. VISTA/4MOST), the sensitivity, field of view and throughput of the 2.5-meter SDSS telescope are very well matched to the expected optical magnitude distribution of the counterparts of X-ray sources detected by eROSITA half way through its all sky survey lifetime (see Merloni et al. 2012). SPIDERS will be executed as a subcomponent of the two main extra-galactic surveys of SDSS-IV: eBOSS (extended Baryon Oscillation Spectroscopic Survey, PI: Kneib) and MaNGA (Mapping Nearby Galaxies at APO, PI: Bundy), over $\sim 7500 \text{ deg}^2$ in the northern hemisphere.

The main astrophysical classes of objects targeted will be Active Galactic Nuclei (AGN/QSOs, $\sim 30\text{-}40 \text{ deg}^{-2}$) and clusters of galaxies ($\sim 1 \text{ deg}^{-2}$). In the case of AGN, the groundbreaking nature of SPIDERS is easily summarized. Selection criteria in the original SDSS-I/II survey were limited to two, mutually exclusive families: narrow emission line objects (mostly obscured AGN) extracted from the local galaxy sample with the help of line emission diagnostic diagrams and broad-line QSO at high redshift selected via a complex multi-color/morphological criteria. SPIDERS will be able to unify the two approaches under a well-defined, homogeneous sample of X-ray selected QSOs, bridging the gap both in the redshift distribution and in the physical characteristics (BH masses, accretion rates, dust-to-gas ratios, overall SED, etc.) of the AGN themselves, while still benefiting from the large number statistics provided by very wide field surveys at the expected depths. As far as clusters are concerned, the full exploitation of the eROSITA clusters for cosmological studies will require the synergy, over the entire sky, between eROSITA X-ray spectroscopy and optical follow-up necessary to determine distances and, when possible, complementary proxies for the mass. The SPIDERS survey, by construction limited in area covered and depth of the X-ray clusters catalog,

aims at providing a well defined, high-quality “calibration set” (for cluster mass measurements, photometric redshifts, etc.) for the final eROSITA survey, while allowing unique first cosmological tests of large scale structure via clustering and number density evolutionary studies with a sample of X-ray selected clusters about one order of magnitude larger than anything available now.

In order to assess the capability of a SDSS follow-up of X-ray sources, a pilot survey has been carried out with a BOSS ancillary program (PI: Merloni and Green). A full BOSS plate was used to target all bright X-ray sources in one of the few large enough ($> 7 \text{ deg}^2$) areas of the sky covered uniformly by XMM-Newton (the XMM-LSS survey). The high success rate of BOSS for all X-ray sources above the X-ray flux limit that will be adopted by SPIDERS is a good indication that most of the scientific goals of the survey (mainly a very high and uniform completeness level) can be met.



Andrea Merloni

(Other HE team members include H. Boehringer, G. Chon, N. Clerc, T. Dwelly, A. Georgakakis, K. Nandra, M. Salvato)

4.5.5 The 4MOST Spectroscopic Sky Survey

The high-capacity 4MOST Multi-Object Spectrograph proposed as an instrument for the ESO VISTA Telescope will enable us to obtain more than 25 Million object spectra in a 5 year survey. Among the core science programs of the 4MOST Survey is the massive spectroscopic follow-up of X-ray luminous galaxy clusters and AGN to be discovered in the eROSITA Survey. These survey data will provide important new insights into the evolution of black holes through cosmic history, the astrophysics of AGN, the large scale structure traced by AGN and galaxy clusters, and allow tests of cosmological model parameters with the eROSITA galaxy cluster population to much higher precision than without redshift data.



Hans Böhringer

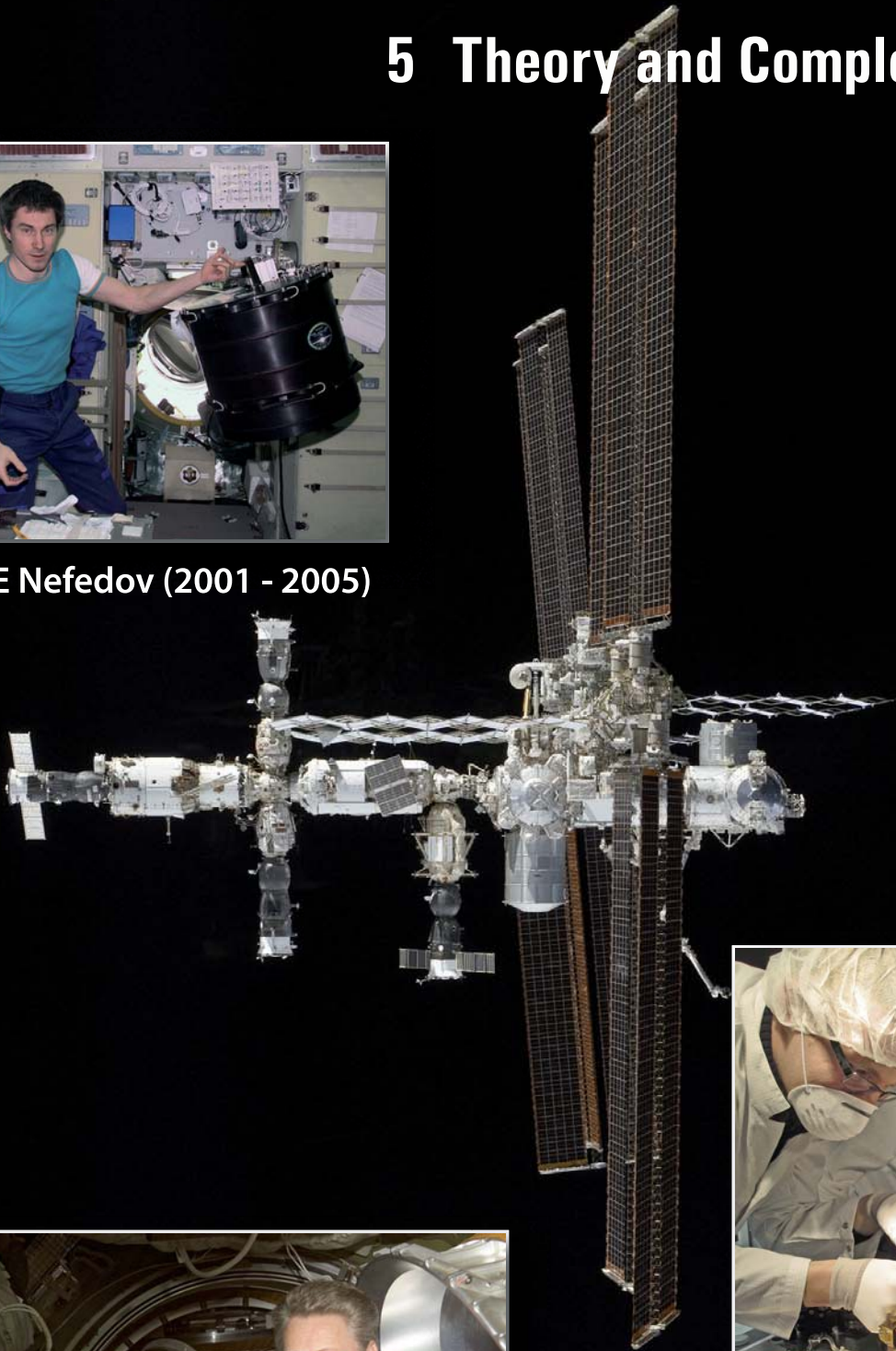
(Other HE team members include Thomas Boller, Gayoung Chon, Tom Dwelly, Andrea Merloni, Kirpal Nandra, Mara Salvato)

Following an ESO call for proposals a consortium lead by AIP Potsdam proposed the building of the 4MOST fibre spectrograph comprising 1600 low resolution and 800 high resolution fibres feeding 3 spectrograph units. The main consortium goal in the application of this instrument is spectroscopy of interesting targets from the GAIA and eROSITA sky surveys. The role of MPE within the consortium is the design of the survey operations concept and the construction of the survey operation software. For the preparation phase of the project a survey simulator software system has been built at MPE which performs the handling of prioritized target input catalogues from various science groups, allocates these targets to sky tiles and spectroscopic fibres in each tile, and evaluates the successful observations of the objects depending on instrument throughput and statistically simulated observing conditions. Mock catalogues of AGN and galaxy clusters (the latter drawn from a full analytical cosmological simulation) have been fed into the simulator together with catalogues from 5 other core science programs. It was shown that spectra of 1.4 Million galaxies in about 55 000 galaxy clusters and about 700,000 AGN can be harvested in a 5 year 4MOST survey. Overall it was shown that the operations software can handle the 7 core science projects in such a way that success of all projects can be achieved simultaneously. This successful multiplexing in the survey operation is a new achievement in the performance of such sky surveys.

5 Theory and Complex Plasmas



PKE Nefedov (2001 - 2005)



PK-3 Plus (2005 - 2013)



PK-4 (2014 - ...)



5. Theory and Complex Plasmas

5.1 Introduction and Overview

Introduction

Following the decision in the late 1980s to put a significant research effort into the study of a new research topic – “plasma crystals” – (the field is now usually referred to as “Complex Plasmas” in analogy to de Gennes’s characterisation of colloidal fluids as “complex fluids”) two major developments took place:

1) The “theory group” which up to this time had focused on theoretical (interpretative) plasma- and astrophysics, became an “experimental group”, with several laboratories in MPE and a continuous laboratory presence (since 2000) on the ISS for research under microgravity. This was made possible on the one hand by a tripling of my budget allocation plus access to technical workshops and engineering infrastructure by my colleagues (something I had no need of before – and for which I am very grateful) and on the other hand by special funding obtained from MPG. The “**Complex Plasma Group**” now includes about 35 members.

2) About 8 years ago it was realised that a “spin-off” from the plasma technology could be usefully employed in “**Plasma Hygiene and Medicine**”. The reason is that the plasmas required to produce colloidal (or microparticle) crystalline and liquid phases had to be “cold” (basically room temperature). For biomedical applications such “cold plasmas” produced at atmospheric pressure (preferably in air) are ideal. Accordingly, a new research field was opened, again supported internally and through a further generous grant from central MPG funds. This grant, designed to ease the way from basic research into applications, allowed us to equip a “plasma medicine laboratory” hire some scientists and engineers and organise a large interdisciplinary research network (including cell biology, microbiology, plasma physics, plasma chemistry and various branches of medicine) of about 10 institutes and 50 researchers (10 of which are in MPE). In this way the MPG funds were “multiplied” by about a factor 5 through partner contributions and in addition access to experts and specialised biological laboratories could be secured without own investments.

With these new research efforts, and with the arrival of Prof. Nandra, it was decided to transfer Hans Böhringer and his group (of about 10 researchers in “**Extragalactic Astrophysics**”, including students) to High Energy Astronomy. Previously, the “**Protostars and Planets**” group, headed by Dr. Neuhäuser, had moved to Jena when Dr. Neuhäuser was appointed Professor at the University.

Apart from the two big groups mentioned above, there is now only a small group involved in “**Information Extraction from Complex Data Sets**” – basically develop-

ing new theoretical information theory based techniques and algorithms to improve and extend knowledge retrieval quantitatively from complex and multivariate data sets. This includes astrophysical topics – eg. the characterisation of the cosmic microwave background and the homogeneity of the early universe.

Major Achievements

Here I will only give a “headline summary” – more details are given in the appendices.

1) Complex Plasmas

The main thrust of this research is the investigation of physical processes at the most elementary individual particle level, to study self-organisation at the kinetic level and to investigate the limits of cooperative phenomena that give rise to collective effects in matter. Special emphasis is placed on interdisciplinary research complementary to soft matter research. A small selection of topics (elaborated in the appendix) is:

- Dynamics of dislocations in plasma crystals
- Discovery of electrorheology in complex plasmas
- Phase separation in binary mixtures
- Fractal structures in 2D crystallisation
- Self-organisation in fluid flows
- Turbulence at the kinetic level
- Bubbles and drops at the smallness limit
- Heat conduction in 2D membranes
- First “extraterrestrial paper” – submitted from the ISS Heartbeat instability – a ten year riddle resolved?

2) Plasma Medicine and Hygiene

The main thrust of this research is the development and optimisation of cold atmospheric plasma sources with specific properties for hygiene (including food hygiene) and medicine, the physical, chemical and biological characterisation of these devices and finally their application for medical therapy. A small selection of topics (elaborated in the appendix) is:

- Development of plasma devices
- Bacteria inactivation
- Resistance build-up against plasma treatment
- Plasma chemistry control
- Plasma activation of water
- “ex vivo” study of plasma effects on human skin
- Control of secondary infection in chronic wounds
- Wound healing
- Alleviation of skin diseases
- Cell selectivity – cancer treatment
- Improving agricultural yield using plasma

3) Information extraction from complex data sets

The main thrust here is the quantitative characterisation of (for instance nonlinear) properties from complex, coupled and multivariate data sets using and developing information theory based specialised techniques that retain all (or most) of the information. An example from astrophysics is:

- Non Gaussianities in the WMAP data

The future

On July 31st 2013 I will retire from MPE after more than 28 years as a director. The research activities that I have built up (and that are still active at MPE at this time) will then be continued elsewhere by others – younger researchers that can then develop their own visions. This is how it should be.

The current status is as follows:

Of the roughly 55 members of my group, 10 have left to either academia or industry within the last year. About 30 scientists and engineers will move to DLR (Deutsches Zentrum für Luft- und Raumfahrt) at the end of 2013, with a chance to develop this research group into a new DLR Institute. The research topics of this new group are Complex Plasmas (with emphasis on research in space) and Plasma Medicine (with emphasis on Astronaut Health and Planetary Protection). These research topics were considered by DLR as well as the Federal and Bavarian Ministries for Economics as “strategically important” – and consequently these three organisations have agreed on co-funding this new group for a period of 5 years, after which the full integration into the DLR is planned, subject to an evaluation.

This does not cover all the members of my group – however, especially in Plasma Medicine there are a number of grant applications in preparation or already at the submission stage. It is hoped that some of these will be successful so that we can retain the specialist know-how. In addition, a small start-up company was founded in May 2011 and some members of the plasma medicine group may join this company. The small “Information Dynamics” group (3 scientists) has also founded a small consulting company and hopes to develop this into a viable business.

The bottom line – barring unforeseen last minute disasters – MPE will have the full resources of my group available by the end of 2013 for my successor. That includes all the institutional staff, scientist, finances, infrastructure etc.



Gregor Morfill

5.2 Complex Plasmas

„Complex Plasmas“ consist of electrons, ions, charged microparticles and some neutral gas component. The neutral gas temperature is normal room temperature and the ion temperature rapidly comes into thermal equilibrium with the neutrals by collisions. Plasma production is usually realized either by radio frequency excitation or by d.c. discharge. As a consequence, the electrons have thermal energies in the eV range – much hotter than the ions. Complex plasmas are “thermodynamically open” systems since energy has to constantly supplied to maintain the plasma against recombination.

When the microparticle number density is sufficiently high (comparable to the Debye length of the plasma) this component becomes energetically and dynamically dominant. Individual particles can interact electrostatically with their nearest neighbours. This can lead to collective and strong coupling effects, with liquid and crystalline states and self-organisation taking place. Also, the microparticles can be visualized individually – allowing analysis of many interesting processes at the hitherto barely accessible “atomistic” level. Add to this that the background medium (mainly the neutral gas) is not dynamically dominant – in comparison with “Complex Fluids” (microparticles embedded in a liquid background

medium) where the background medium only allows the study of overdamped systems or systems at equilibrium – and we have a situation where complex plasmas and complex fluids complement each other in their physics. Because of the comparatively large mass of the microparticles (billions times heavier than atoms) characteristic time scales are slowed down to around 0.01 sec (e.g. for the inverse Einstein frequencies). In “normal matter” the time scales are up to a million times faster – and not easily detectable.

Since the discovery of plasma crystals in 1994 (Thomas et al, PRL and I and Chu, PRL) over 5000 peer reviewed publications have appeared, addressing a multitude of topics – either investigations into this new form of matter itself or into generic physical processes found in other natural systems that so far could not be studied at the atomistic level. In recent years the interdisciplinary aspect, in particular the connection with soft matter, have gained increasing attention.

In the following, only a few of the many highlights of research in the last 6 years will be shown – a selection from over 100 peer reviewed publications:

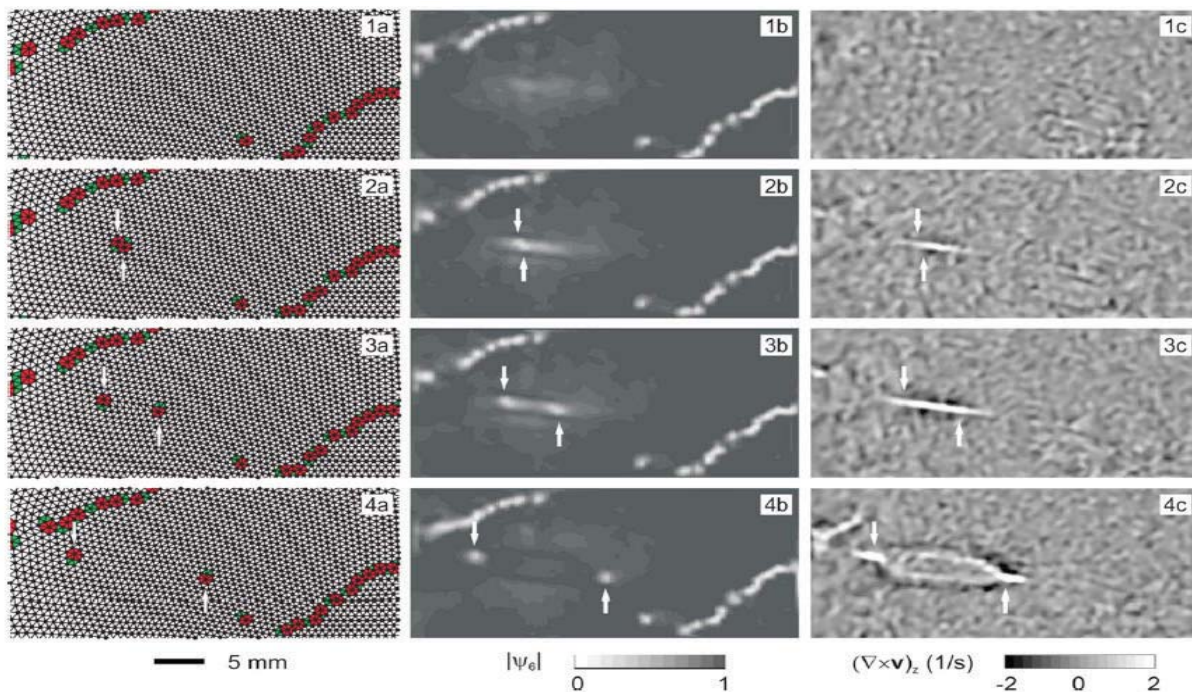


Fig. TH.1: The generation and motion of a defect (induced by shearing) is shown in a monolayer plasma crystal, an experiment performed on Earth. The panels on the left show four snapshots of the crystal, where the microparticle positions have been connected with lines to make the identification of the hexagonal lattice structure easier. Crystal defects (interconnected pentagons and septagons) are colour coded – they mark the crystal grain boundaries. The new defect occurs in the centre of the crystal grain and is marked by arrows. The middle panel shows the “bond orientational function, $|\psi_6|$ ”, a geometrical construction which equals 1 for the case of a perfect hexagon and which assumes lower values if the crystal structure is less perfect, all the way to zero if there is no hexagonal element. This representation is very useful for identifying crystal defects and areas where a defect may soon occur. The right panel shows “vorticity”, a dynamical measure of rotation. The random thermal fluctuations of the individual particles produce a “carpet” of randomly directed apparent rotations (positive or negative) leaving a background of lighter and darker patches. These are not relevant for present purposes (note that the grain boundaries hardly show up in this representation). However, the moving dislocations exhibit a clear signature, including a shock-like structure, as seen in Fig. 4c, which interconnects the two travelling dislocations. (From Nosenko et al., *Phys. Rev. Lett.* 99, 025002, 2007)

5.2.1 Dynamics of dislocations in plasma crystals

Dislocations are the most common form of crystal defects. When trying to grow pure crystals, these are the ones that usually limit the quality. Consequently a great deal of effort is invested to overcome such defects and different annealing technologies are employed. A fundamental study of such defects and their motion inside a crystal lattice is therefore a useful undertaking. Here we show for the first time how lattice defects move and reorganize inside a two-dimensional crystal – a membrane. The results are depicted in the Fig. and described in the Fig. caption.

5.2.2 Electrorheology in complex plasmas

Electrorheology is a process whereby a fluid (they are often referred to as “smart fluids”) are altered in their structure and properties by application of an external electric field. Colloidal (or complex) fluids belong to this class which exhibit electrorheological properties. The physical process is in principle easy to understand: the



above: without polarity switching
below: with polarity switching

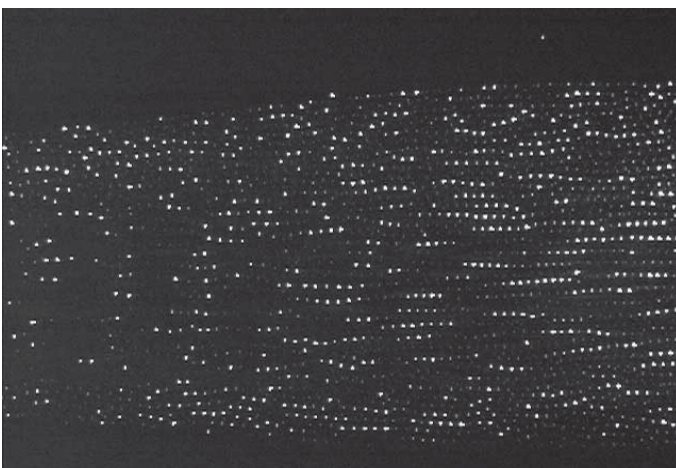


Fig. TH 2: Experiments performed with the PK-4 prototype during parabolic flight test. The experiment was intended to investigate Electrorheology. Without polarity switching the microparticles show an obvious disordered liquid state. When polarity switching is implemented, particle strings are formed. There is a transition from a regular disordered fluid to a “string fluid” – a typical signature of electrorheological behaviour. This will be one of the many fluid phenomena investigated when PK-4 is finally installed in Columbus on the ISS (Ilev et al. 2011)

electric field polarizes the microparticles embedded in the complex fluid. This leads to an internal structuring and rearrangement (the “rheology is altered”) such that the microparticles become preferentially aligned along the direction of the externally applied electric field. This changes the property, for instance, in smart self-adaptive shock absorbers in cars.

An interesting question is – if electrorheology (or something similar) might also be a process that exists in complex plasmas. Experiments to test this were performed on the ISS and in parabolic flights under microgravity conditions, since we were interested in bulk 3-dimensional properties.

5.2.3 Phase separation in binary mixtures

The oil-water problem. The questions – what is the thermodynamic process that leads to this form of self-organisation of two fluids? How small can the fluid drops be to still separate? Can we for the first time observe this at the “atomistic” level, with individual particles resolved in space and time?

No doubt there are many more questions – and probably the measurements will precipitate more still.



Fig. TH.3: Oil and water - From www.communifire.com (Tim Eisenhauer)

Then the issue is – is it possible to make two **plasma liquids** and to let them interact under microgravity conditions, of course? In theory this should be easy. Just use two different particle populations. They will have different interactions amongst themselves and crosswise. The experiment is then – one type of particles was injected into a pre-existing liquid cloud of the second type. The two particle clouds could easily have mixed completely, this did not happen. The two types of particles formed separate regions – each region devoid of the other particle type. This happened for droplets consisting of as little as 1000 particles! In atomic terms this would imply droplets of a size of around 1 nanometer!

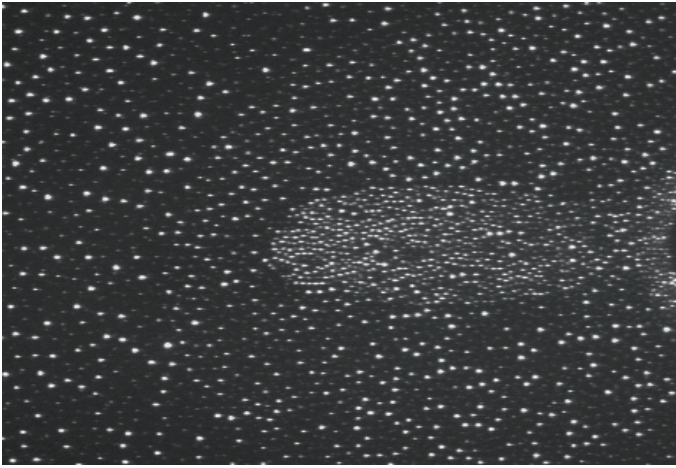


Fig. TH.4: Phase separation between two microparticle populations measured on board of the ISS with PK-3Plus. The small particle population forms a spheroidal droplet, in this image the vertical dimension corresponds to about 20 particle layers, the horizontal dimension to about 40 particle layers. Altogether this particular droplet contains about 5000 particles (Ivlev et al. *EPL*, 2009).

The picture shows a cut through a particle cloud (particle size 3.4 micrometer) embedded inside another cloud of larger particles (8.5 micrometer). The particles demixed into separate domains. The smaller particles form a droplet containing about 1000 particles. The larger par-

ticles have been ejected from the droplet. The analysis of the dynamics of this demixing for different drop sizes, the details of particle motions and the thermodynamics of this process – observed for the first time at the individual particle level – will take years of studies. But we now have an experimental system to study this with.

5.2.4 Fractal structures in 2D crystallization

In the Fig. below, a two-dimensional crystallisation experiment is shown in three representative stages.

Stage (a) shows a plasma crystal, almost perfect with just a few domain boundaries. This crystal was then “force melted” using an electrical impulse produced by a wire. After this the perturbed system was allowed to re-crystallise naturally at its own pace. As can be seen in stage (b), many small crystallites formed, each bounded by a string of paired dislocations (colour coded red and blue for 5 and 7-fold local lattice structures). As the evolution continued, the grainy structures became larger, the crystallites bigger. The grain boundaries merged as a consequence of stresses set up – all very similar to natural annealing – until there was not sufficient thermal energy in the system to continue this process spontaneously towards just a single perfect crystal.

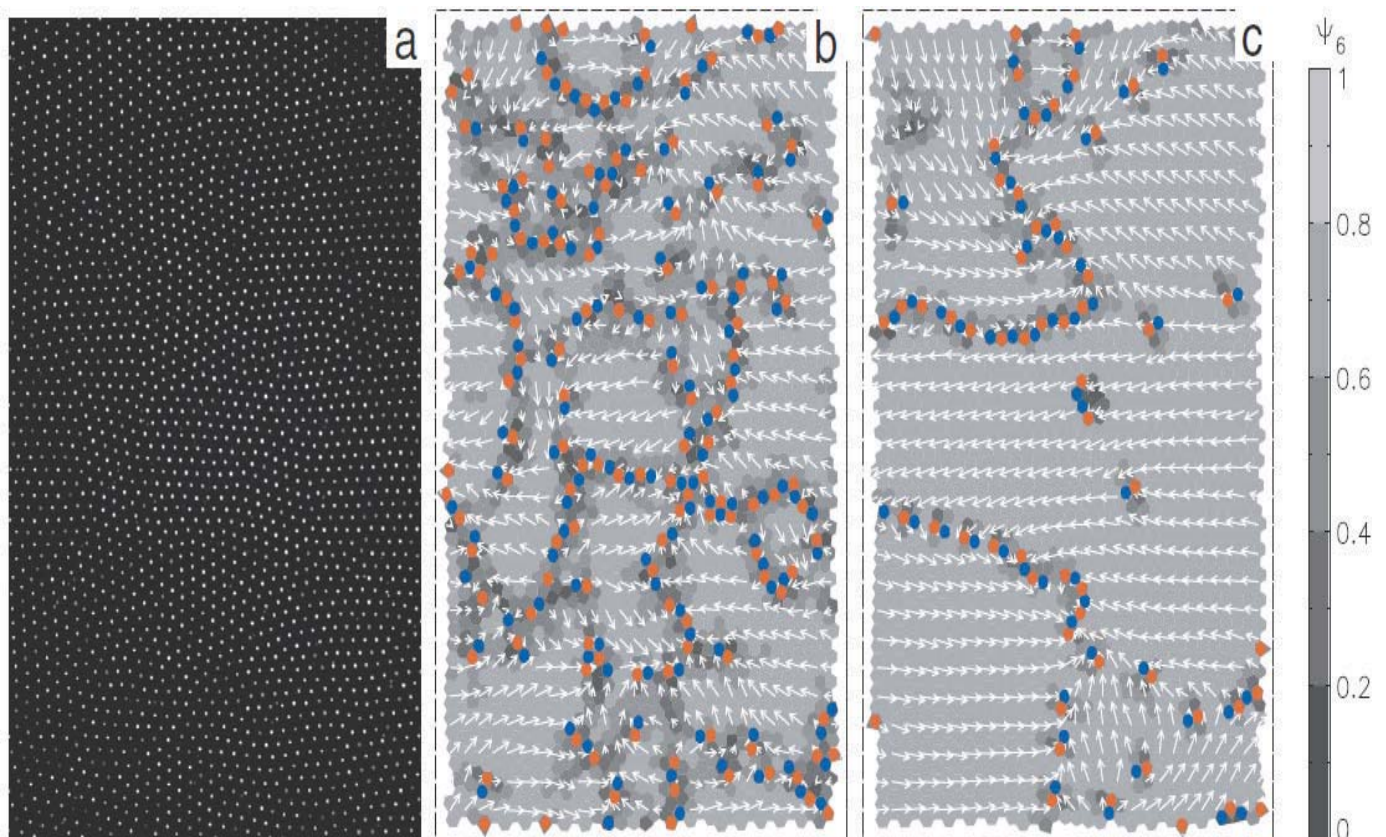


Fig. TH.5: Re-crystallisation of a two-dimensional (flat) complex plasma. The experiment was conducted in the laboratory on Earth. The left panel (a) shows the original plasma crystal, individual particles (size 9.19 micrometres) illuminated by a laser and recorded with a CCD camera. The middle panel (b) shows a snapshot after the crystal had been melted and started to recrystallise. The grey shading (see the scale on the left) gives the “bond orientational function”, $|\psi_6|$, a measure of the quality of the hexagonal structure, which is expected to evolve as the crystal becomes more perfect. The red and blue particle cells correspond to defects (5-fold and 7-fold respectively). One can see that the defects form lines, or domain boundaries, encircling tiny irregular crystallites. The arrows essentially denote the main orientation of the crystallites, illustrating that there really are quite different domains. (From Knapek et al. *Phys. Rev. Lett.* 98, 015004, 2007)

Whilst the development of crystallisation from disorder to order is no great surprise, there was nevertheless one puzzle in the data. This is summarised in the next figure. Now the figure itself does not look any different to many physical measurements – it has some data points and a line through them which more or less fits and guides the eye to appreciate a particular point that the researchers wish to make. What is plotted is the number of dislocations (5-fold and 7-fold), divided by (or normalised to) the total number of particles in the field of view, as function of the temperature of the monolayer complex plasma system. At an early stage after melting, when the kinetic temperature is still quite high (10's of eV, or 100,000's degrees) about 30% of the particles are in defects, suggesting that hexagonal lattice structures are more likely to be accidental rather than real – the system is well and truly perturbed and quite chaotic. As the system cools down, lattice defects disappear and as a consequence first small then larger crystallites evolve. This is what the previous picture showed – again no surprise.

The surprise is that the plot shows that there is a so-called “power law”. This was not expected from theories in existence at that time. A power law is something special. It occurs, for instance, when there is no scale in the system – a “scale-free” behaviour is indicated. But what could this be telling us?

The answer lies in the fractal structure of the domain boundaries. It can be shown that under the assumption (of a non-equilibrium state) that the entropy of the system is dominated by the particles in the domain boundaries that a fractal structure of these boundaries would lead to the observed power law as long as thermodynamic

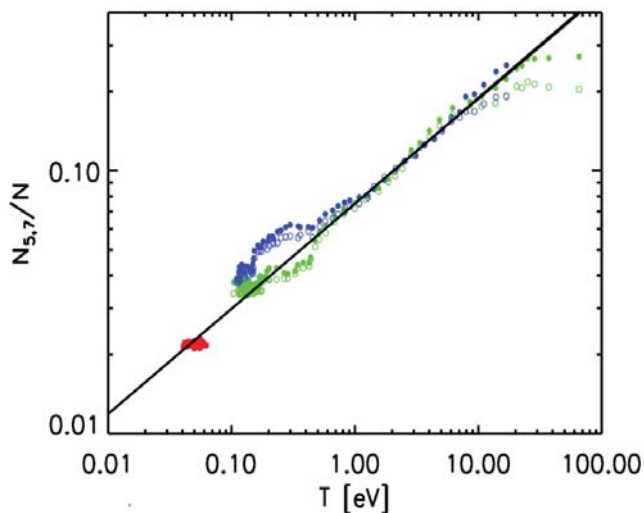


Fig. TH.6: Recrystallisation of a two-dimensional complex plasma. Plotted is the fraction of particles which are located in 5- or 7-fold defects as the complex plasma cools. Three different experiments (identified by the different colours) are shown. The lattice defects exhibit a power law dependence with temperature according to $N_{5,7} \sim T^{-0.4}$. This represents a classical scale-free behaviour of structure and temperature. (from Knapek et al. *Phys. Rev. Lett.* 98, 015004, 2007).

equilibrium has not been achieved. This has been investigated quantitatively (Knapek et al. *PRL*, 2012) and within the statistical uncertainty the theoretical model was shown to be in accord with the measurements. So here again we have evidence for a self-organisation process – during non-equilibrium crystallisation conditions – which results in a fractal (self-similar and scale free) structure, a generic phenomenon that has been inferred in other non-equilibrium situations, too. The big advance in the complex plasma observations is that this has been studied in a real system for the first time at the most fundamental individual particle level.

5.2.5 Self-organisation in fluid flows

With complex plasmas many other interesting experiments are possible. One of these concerns “nano-flows”, where again a monolayer is produced, this time a fluid monolayer of only a few particles in diameter, and where this fluid layer is confined to flow into a small funnel. What happens in such a situation is depicted in the figure below. In the upper panel (a) a snapshot of the microparticles (taken from above, as in the previous examples) is shown. During the exposure time the particles have moved somewhat from left to right, so that they appear as elongated rods. From the length of the trace and the known exposure time one can determine the particle speed. This is a widely employed technique. The particles, initially four (horizontal) layers deep, are confined to two layers as they flow towards the right side.

The first thing to notice – and this is shown schematically in the lower figure (b) is that in a given snapshot it is difficult to tell whether the system is at rest, practically in equilibrium, or whether the particles are moving (if it

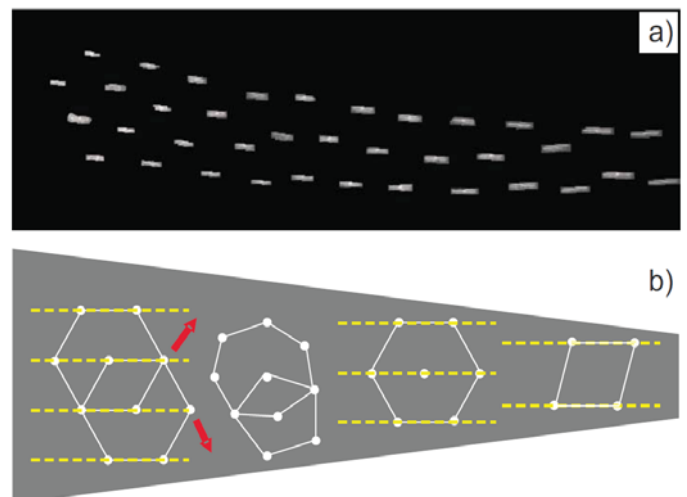


Fig. TH.7: Fluid structure and dynamical selection rules in a converging “microchannel flow” are investigated for a monolayer complex plasma. The interesting finding is that structurally (on an instantaneous snapshot) the system behaves like a solid in the most equilibrium-like state possible – hexagonal, whenever the number of stream lines allow this. In between the transition is achieved through the same structures that produce the most common crystal defects – interlocked pentagon and septagon pairs. (From M. Fink, private communication, PhD thesis, 2013)

were not for the elongated traces a snapshot would not give a unique answer to this question). This has some relevance for understanding the nature of the stability criteria for fluids.

When there are four “stream lines” of particles, the most common situation is that this looks like two interlocking hexagons. When the flow converges and four stream lines are no longer possible, the particles jostle for new positions and we obtain the next most common structure – the 5/7 dislocation, which was so dominant in the preceding examples. This allows a reduction of the system to three stream lines, which is then again a single hexagon. In most snapshots this is the structure that is found. When the flow converges further to only two stream lines then the usual instantaneous structure is that of a parallelogram.

5.2.6 Turbulence at the kinetic level

The Nobel Prize winner, Richard Feynman, described turbulence as “**the most important unsolved problem in classical physics**”. To obtain a new approach towards understanding the origin and development of turbulent flows, liquid complex plasmas can be studied under various conditions - starting with laminar flows and proceeding to controlled perturbed flows. The studies should involve both 2-dimensional and 3-dimensional systems (2-dimensional turbulence is, according to theory, very different from 3-dimensional turbulence). We expect the most interesting results to come from experiments to be performed by the next ISS laboratory, PK-4, which has been specially designed to investigate fluid complex plasmas. However, some interesting experiments can also be designed on Earth. One such experiment is shown in the picture below. The complex plasma is set

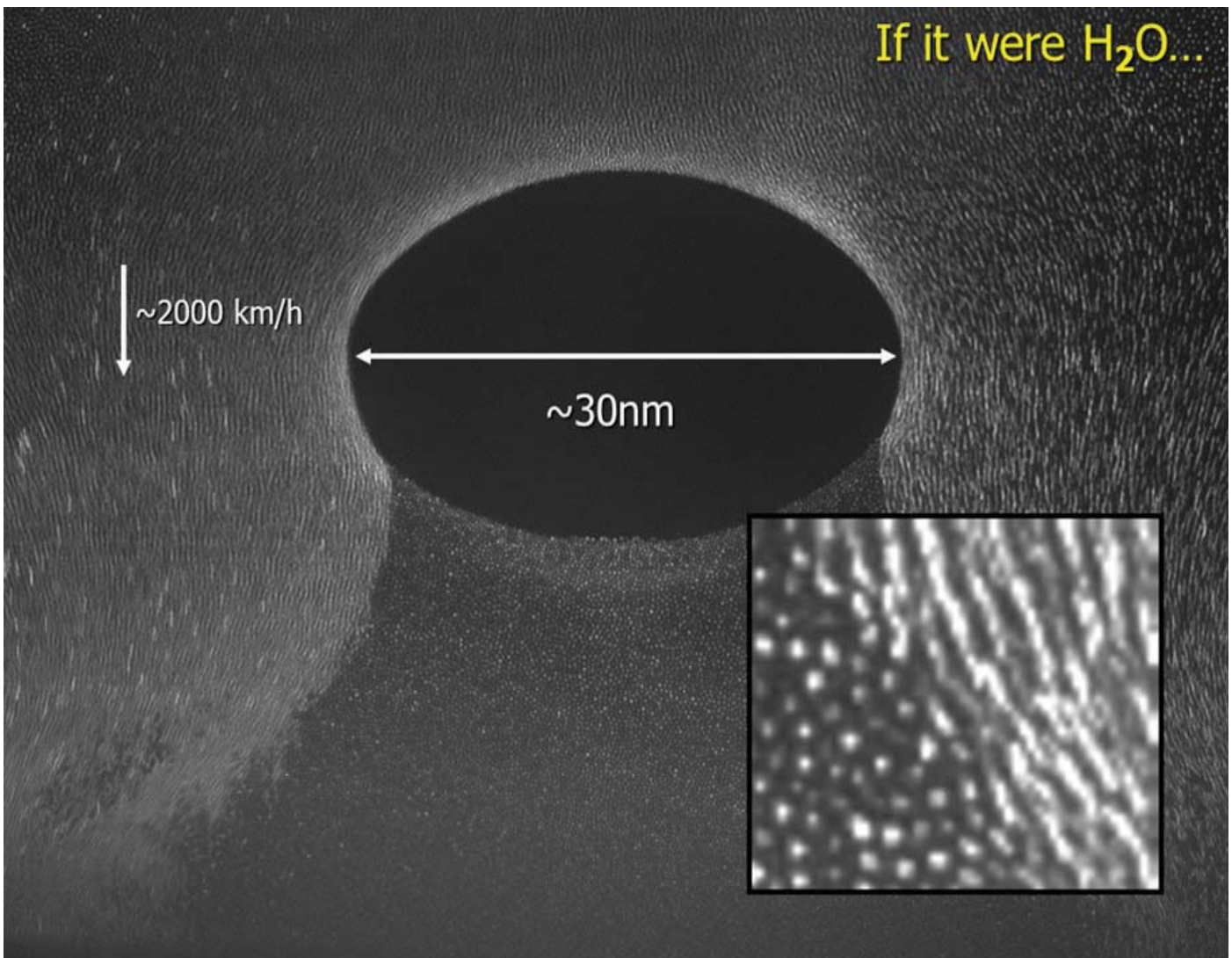


Fig. TH.8: Cross section through a cylindrical complex plasma flow. The microparticles are illuminated by a laser and recorded using CCD video cameras at 30Hz frequency. The microparticles flow in a very ordered laminar fashion around the obstacle (the black oval in the centre). Due to the exposure time of 1/30th of a second, the traces of the microparticles appear as short lines, which give a direct measure of the fluid flow. Behind the obstacle an almost stationary “wake” is formed (the microparticles are seen as little white dots – not lines). Around this wake the fast flowing microparticles first create a shear layer (seen to the left and right just below the obstacle), which further downstream breaks up into a disordered boundary layer pattern – possibly the first ever picture of the microscopic onset of turbulence. The insert shows a magnification of a small segment at the edge of the disordered boundary layer. The fast moving particles in the flow regime can easily be differentiated from the slow ones in the wake. The magnified image shows the disordered motion of some individual particles in the boundary layer. It should be mentioned that the laser light reflection makes the particles appear much bigger than they really are. In reality the separation between the particles is roughly 50 times larger than the particle size.

into a convective flow, which has cylindrical symmetry – directed upwards on the outside and downwards in the centre. It is forced to flow around a central obstacle, the void, which acts just like any other impenetrable body in ordinary fluid flow.

The figure also exhibits some numbers. These are derived from scaling properties to illustrate what the flow would be like if the system was water – not complex plasma. Then the size of the obstacle would be a mere 30 nanometers, the flow speed would be 2000 km/hour. Although it is not clear at present whether such scaling laws may be applied, it is nevertheless illustrative at what extreme levels complex plasmas can be employed to explore everyday processes like turbulence.

5.2.7 Bubbles and drops at the smallness limit

The important property of matter that leads to bubble or drop formation is “surface tension”. Surface tension is the feature that allows water skiing and enables water striders to “walk on water”. It is a cooperative effect of the interacting forces in fluids and the fact that there is a boundary.

Again, one of the major issues in physics is the question: Is there a limit how small drops and bubbles can be? Or specifically: What size drops can be sustained by the surface tension? Or on a more generic level: When does the cooperative process that governs the self-organisation of matter into drops and bubbles reach its limit? Exploring the limits of cooperative behavior is one of the key issues in contemporary physics – the applications are of great importance for our fundamental understanding of nano-phenomena. Complex plasmas would appear to be ideal candidates for such a fundamental study at the atomistic level – provided one finds a way to “make” little drops and bubbles.



Fig. TH.9: Common water strider (*tili remigis*). Photo from fcps.edu (copyright Charles Lewallen)

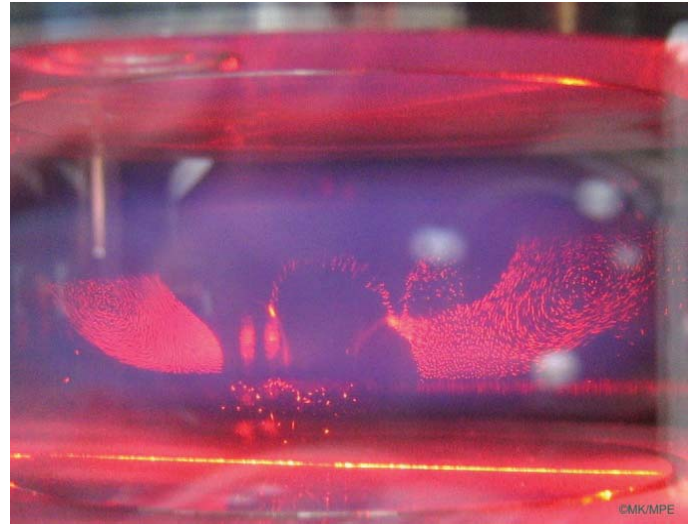


Fig. TH.10: Plasma bubble consisting of a monolayer surface (Photo: Mierk Schwabe, MPE)

Mierk Schwabe solved this problem and obtained remarkable results:

- **Monolayer bubbles**, consisting of only a few 100 particles, can be formed and exhibit properties (e.g. in their dynamical evolution) quite similar to larger soap bubbles. The discreteness of such small systems is apparently not yet significant enough to cause larger deviations from the classical continuous fluid picture.
- Even very **small drops**, consisting of less than 100 particles, basically still behave as if they were continuous fluids, i.e. they exhibit surface tension that keeps them together, they show evaporation effects, deformation during motion through the background (neutral gas) medium etc.

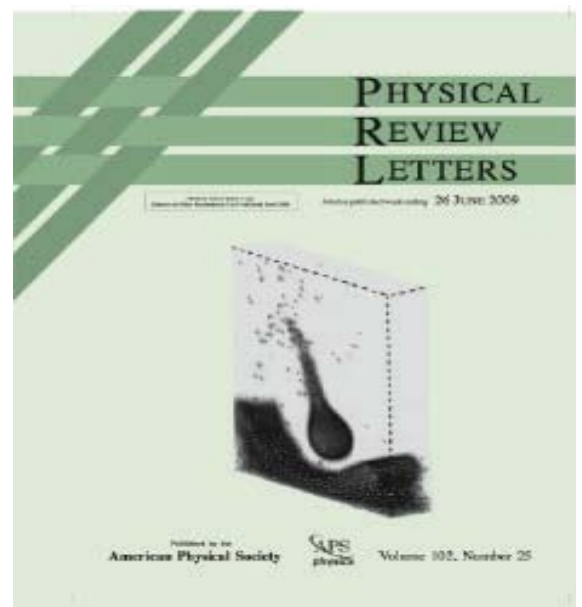


Fig. TH.11: A plasma bubble consisting of less than 1000 individual particles, taken from the cover of the Journal Physical Review Letters (Schwabe et al., PRL, 2009)

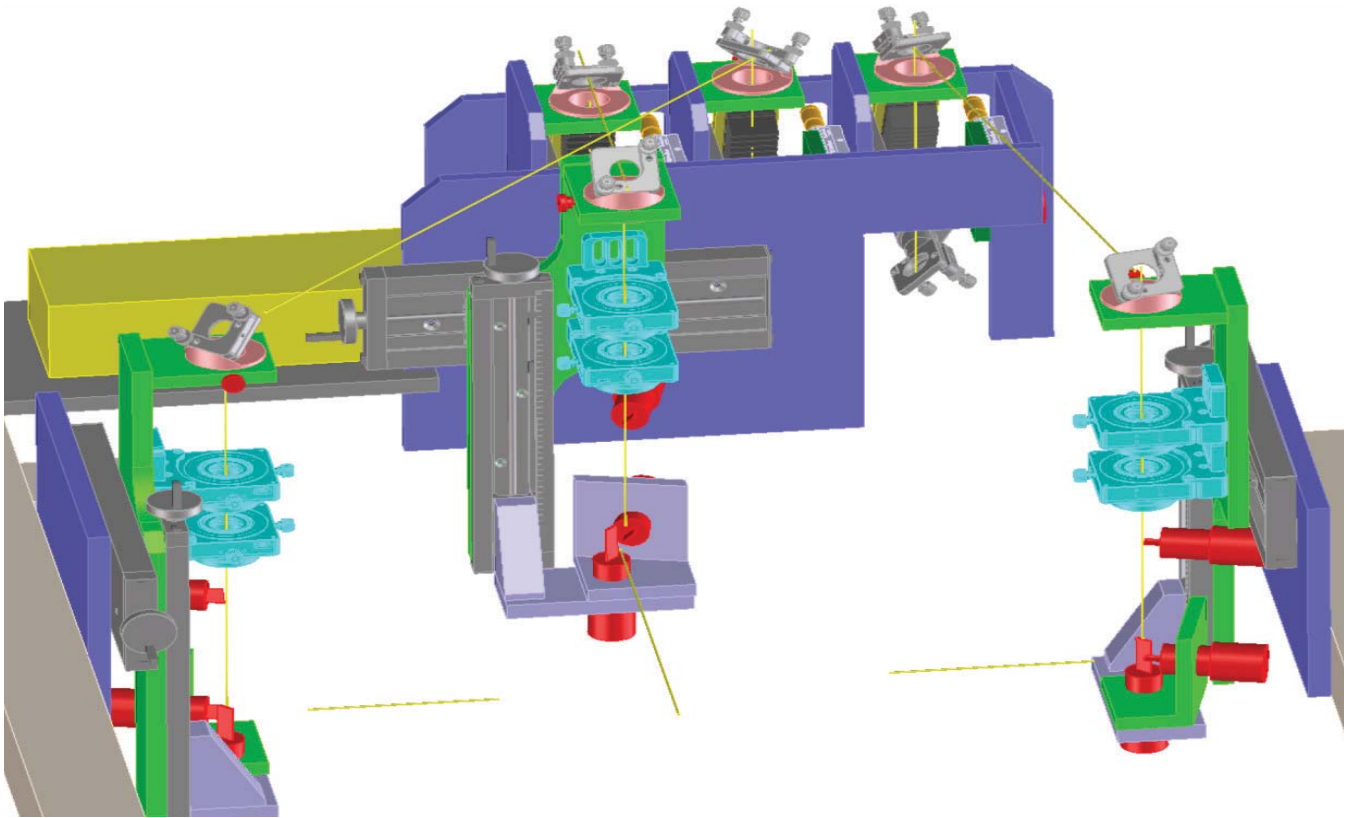


Fig. TH.12: Design drawing of the moving mirror system employed in these studies (G. Stadler)

5.2.8 Heat conduction in 2D membranes

Heat conduction in membranes is of considerable interest in the context of biology, thin film and nano-science. Also, the way in which thermal conduction functions at the particle level is of considerable interest and could not be explored experimentally before the advent of plasma crystals (or complex plasmas). Remember that the heat conduction equation is basically a diffusion-type equation assuming a continuous medium, where the heat transport is summarised and characterised by a parameter (or more generally a tensor), the coefficient of thermal conductivity.

The difficulty in measuring lies often in the control of reproducible conditions and in the measurement process itself, which must not disturb the system under study too much, so as not to interfere with the quantity to be measured.

One way to introduce controlled thermal noise into a monolayer plasma crystal, for instance, is to use laser light pressure applied to the microparticles in a random fashion with reflecting movable mirrors that can be computer controlled. In this way part of a plasma crystal can be artificially “heated” and the conduction of this heat into the colder regime can be studied at the individual particle level. The technique opens up many different opportunities for basic studies. The heat conduction can be investigated along different lattice directions (to see if there are anisotropies and if the heat conduction coefficient has to be written as a tensor), by using different mass microparticles the effect of damping (by the

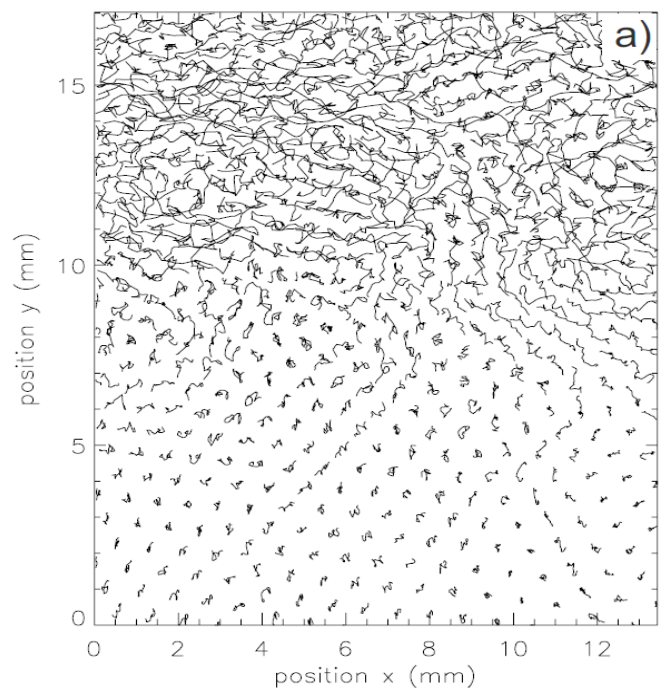


Fig. TH.13: Heat transport in a two-dimensional plasma crystal consisting of 8.09 micrometer diameter particles. The picture, part of a composite taken from Nosenko et al. (*Phys. Rev. Lett.* 2008), shows examples of particle trajectories taken over 1.7 seconds. **Laser heating was only applied in the region $y \geq 13.6$ mm.** As can be seen, heat conduction has taken place and the region below 13.6 mm down to about 6 mm is also “hot”, as witnessed by the much larger extent of the individual particle trajectories compared with those below about 5 mm – at the cooler end of the complex plasma monolayer. (Nosenko et al., *PRL* 2007)

neutral gas present) can be investigated, heating can be applied anisotropically, the effect of adding a second lattice plane of particles can be studied, the effects of local melting – the latent heat – can be investigated including the re-crystallisation front etc.

Here we just show in an example how such experiments look, what the basic information is that can be derived – but not how the measurements are used to develop models for two-dimensional heat conduction. The idea is to “give a flavour” of what is possible with plasma crystals.

5.2.9 First “extraterrestrial paper” - submitted from the ISS

Complex plasmas consist of micrometre-sized highly charged particles (“microparticles”) embedded in an ionized gas (“plasma”). The microparticle ensemble resembles a classical system of interacting atoms. This

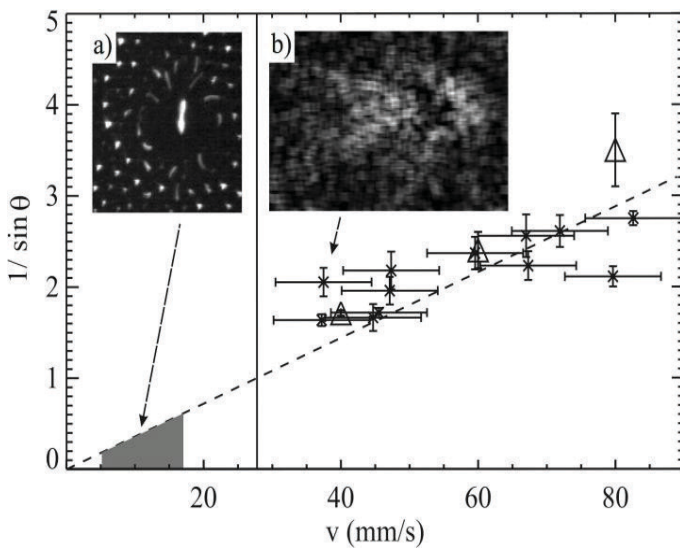


Fig. TH.14: Above: Mach cone relation linking the Mach cone angle θ with the probe particle speed v in experiments (crosses) and simulation (triangles). (a) Zoom showing the subsonic probe particle. (b) Smoothed difference between two successive frames, highlighting the Mach cone. Below: A manuscript of the paper free-flying onboard the ISS. (M. Schwabe, et al., EPL 96 55001, 2011)

system can form all of the classic phases, i.e., crystalline, liquid and gaseous. It can also support the propagation of sound waves, solitons and shock waves. In experiments carried out on Earth, gravity pulls the microparticles downwards resulting in two-dimensional structures. Under microgravity conditions it is possible to investigate big, three-dimensional systems. The PK-3 Plus laboratory provides ideal conditions for such experiments. It is installed in the Russian segment of the ISS and has been used repeatedly over the last 6 years. We performed experiments to measure the speed of sound during two missions with cosmonauts Volkov and Skvortsov. In Figs. (a) and (b) below we show how a bigger “probe” particle penetrated a cloud of smaller microparticles. At a speed several times faster than the speed of sound it excited a Mach cone. A double cone structure is discernible in this “atomistic” system. While moving through the cloud, the probe particle is decelerated to subsonic speeds. By measuring the Mach cone angle at several probe particle velocities, we determined the Mach relation. This allows us to directly measure the speed of sound and to infer the microparticle charge. In addition, the experimental results agree well with a 3D molecular-dynamics simulation, demonstrating in particular a double Mach cone structure.

The publication of this result was sent directly to EPL from the ISS – the first “extraterrestrial paper” submitted to any science journal.

5.2.10 Heartbeat instability – a 10 year riddle resolved?

The heart-beat instability was one of the first discoveries in complex plasma physics. Basically, under microgravity conditions the equilibrium microparticle cloud fills the whole plasma chamber – with the exception of a central “void”. Under certain conditions, the microparticle cloud becomes unstable – it contracts (closing the void) and then expands again (re-creating the void) – with a typical frequency around 1Hz. This rhythmic pulsation, including the frequency, is reminiscent of our heart beat – hence the name. In the figure, we show a snapshot taken from PKE-Nefedov on board the ISS. The lengths of the trajectories (seen as lines) suggest the motion of the particles in the cloud.

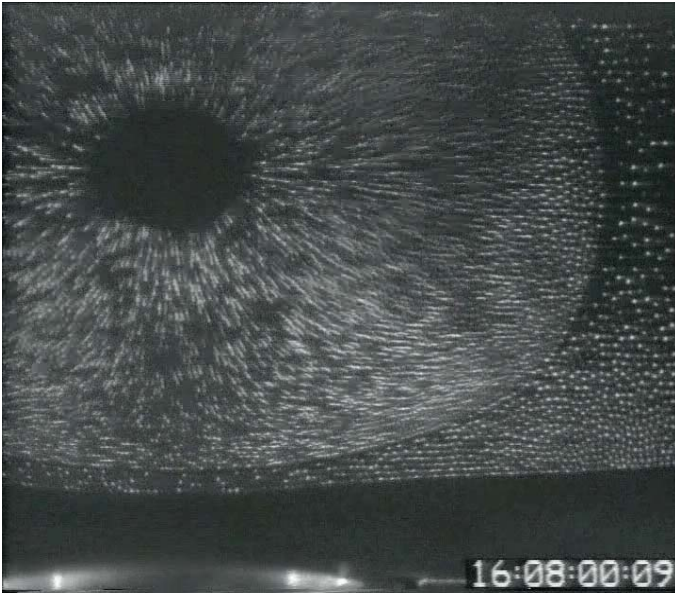


Fig. TH.15: Microparticle trajectories during the heartbeat instability (measurements performed on the ISS with PKE Nefedov by S. Krikalev, 2001)

A method of controlling the heartbeat instability in complex (dusty) plasma was developed. Close to the self-excitation threshold, it was possible to excite the heartbeat instability intentionally by a periodic illumination of the microparticle cloud (levitated by thermophoresis on the ground in the PK3+ chamber) by a beam of a tunable diode laser with the wavelength of 772.38 nm. This laser pumped the $1s_5$ metastable argon atoms to upper radiative $2p_7$ state. The pumping rate considerably exceeded the electron impact excitation rate to the $1s_5$ rate. Therefore, the laser was significantly reducing the number density of metastable states, leading to the modulation of the ionization rate with the depth of the order of 10^{-3} . The excitation had a resonance character (with the peak laser chopping frequency in the range of 40-60 Hz) and was proved to be the result of the parametric instability.

Three experimental facts substantiate the importance of the void boundary for the generation of the heartbeat instability: (i) the instability never occurs without the void, (ii) variations of the plasma emission intensity are opposite in phase inside and outside the void, (iii) laser excitation of the instability is only possible when the tunable laser beam hits the void. Therefore, a hypothesis was

suggested, that the heartbeat instability is the result of a periodically repeating critical phenomenon occurring on the void boundary. It was supposed, that this critical phenomenon is analogous to the formation of a sheath on the void boundary: when the plasma losses on the void boundary become so large, that ions have to be accelerated to the Bohm velocity, the sheath is formed. Electric field dramatically increased after this critical transformation pushes the dust particles on the void boundary towards the center of the void (attached figure).

No contradictions of the hypothesis with the known experimental facts were found. It was found to be consistent with the observed velocities of the dust particles and variations of plasma emission intensity in the contraction phase of the instability. It was also useful in understanding the dependence of the instability on the neutral gas pressure and discharge power.

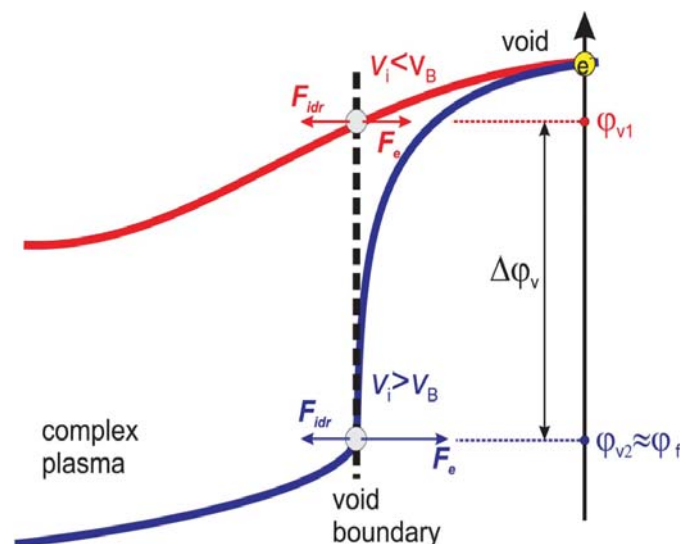


Fig. TH.16: Model of the potential at the complex plasma-void interface (from M. Poustilnik, 2012)



M. Fink, R. Heidemann, A. Ivlev, C. Knapek, V. Nosenko, M. Pustyl'nik, H. Thomas, M. Schwabe

(Other Theory team members include T. Antonova, P. Bandyopadhyay, P. Brandt, M. Chaudhuri, C.H. Du, H. Höfner, P. Huber, S. Khrapak, U. Konopka, M. Kretschmer, S. Mitic, G. Morfill, T. Nosenko, Th. Röcker, M. Rubin-Zuzic, S. Shimizu, R. Suetterlin, M. Thoma, L. Woerner, V. Yaroshenko, S. Zhdanov)

Selected References:

- V. Nosenko, S. Zhdanov and G.E. Morfill, *Physical Review Letters* (2007) 99: 025002
 C.A. Knapek, D. Samsonov, S. Zhdanov, U. Konopka and G.E. Morfill, *Physical Review Letters* (2007) 98: 015004
 A.V. Ivlev, G. E. Morfill, H. M. Thomas, C. R  th, G. Joyce, P. Huber, R. Kompaneets, V. E. Fortov, A. M. Lipaev, V. I. Molotkov, T. Reiter, M. Turin, and P. Vinogradov, *Physical Review Letters*, (2008) 100: 095003
 Schwabe M, Zhdanov S K, Thomas H M, Ivlev A V, Rubin-Zuzic M, Morfill G E, Molotkov V I, Lipaev A M, Fortov V E and Reiter T, *New J. Phys.*, (2008) 10: 033037
 Morfill, G.E. and H.M. Thomas, *Scientific American - Looking Up-Europe's Quiet Revolution in Microgravity Research* (2008) 82-90
 V. Nosenko, S. Zhdanov, A.V.Ivlev, G.E. Morfill, J. Goree and A. Piel, (2008) *Physical Review Letters* 100, 025003
 M.Schwabe, M. Rubin-Zuzic, S. Zhdanov, A.V. Ivlev, H.M. Thomas and G.E. Morfill, *Physical Review Letters* (2009) 102: 25505
 K. R. S  tterlin, A. Wysocki, A.V. Ivlev, C. R  th, H.M. Thomas, M. Rubin-Zuzic, W. J. Goedheer, V. E. Fortov, A. M. Lipaev, V. I. Molotkov, O. F. Petrov, G. E. Morfill, H. L  wen, *Phys. Rev. Lett.* (2009) 102, 085003
 K. Jiang, V. Nosenko, Y. F. Li, M. Schwabe, U. Konopka, A. V. Ivlev, V.

- E. Fortov, V. I. Molotkov, A. M. Lipaev, O. F. Petrov, M. V. Turin, H. M. Thomas and G. E. Morfill, *Europhysics Letters* (2009) 85, 45002
 A.V. Ivlev, S.K. Zhdanov, H.M. Thomas, and G.E. Morfill, *Europhysics Letters* (2009) 85, 4
 Philip C. Brandt, Alexei V. Ivlev, and Gregor E. Morfill, *The Journal of Chemical Physics* (2009) 130, 204513,
 Morfill, G.E.; Ivlev, A.V., *REVIEWS OF MODERN PHYSICS* (2009) 81 (4) Pages: 1353-1404,
 Schwabe, M., Rubin-Zuzic, M., Zhdanov, S., Ivlev, A.V., Thomas, H.M., Morfill, G.E., *Physical Review Letters* (2009) 102, 255005
 Wysocki, A.; R  th, C.; Ivlev, A.V.; S  tterlin, K.R.; Thomas, H.M.; Khrapak, S.; Zhdanov, S.; Fortov, V.E.; Lipaev, A.M.; Molotkov, V.I.; Petrov, O.F.; L  wen, H.; Morfill, G.E, *Physical Review Letters* (2010) 105 (4), 045001
 Jiang, K; Du, CR; S  tterlin, KR; Ivlev, AV; Morfill, GE, (2010) *Europhys. Lett.* 92, 65002,
 Khrapak, S.A.; Klumov, B.A.; Huber, P.; Molotkov, V.I.; Lipaev, A.M.; Naumkin, V.N.; Thomas, H.M.; Ivlev, A.V.; Morfill, G.E.; Petrov, O.F.; Fortov, V.E.; Malentschenko, Yu.; Volkov, S., *Physical Review Letters* (2011) 106, 205001,
 Heidemann, R.; Zhdanov, S.; Suetterlin, K. R.; Thomas, H. M.; Morfill, G. E, (2011) *Europhysics Lett.* 96, 15001,
 K. Jiang, L.-J. Hou, A. V. Ivlev, Y.-F. Li, C.-R. Du, H. M. Thomas, G. E. Morfill and K. R. S  tterlin, (2011) *Europhys. Lett.* 93, 55001
 R. J. Heidemann, L. Cou  del, S K Zhdanov, R. S  tterlin, M. Schwabe, H.M. Thomas, A.V. Ivlev, T. Hagl, G.E. Morfill, V.E. Fortov, V.I. Molotkov, O.F. Petrov, A.I. Lipaev, V. Tokarev, T. Reiter, and P. Vinogradov, (2011) *Phys. Plasmas* 18, 053701
 M. Schwabe, K. Jiang, S. Zhdanov, T. Hagl, P. Huber, A. V. Ivlev, A. M. Lipaev, V. I. Molotkov, V. N. Naumkin, K. R. S  tterlin, H. M. Thomas, V. E. Fortov, G. E. Morfill, A. Skvortsov and S. Volkov, (2011) *Europhys. Lett.* 96, 55001
 Morfill, Gregor E.; Ivlev, Alexei V.; Thomas, Hubertus M., (2012) *Physics of Plasmas* 19, 055402
 Du, C-R; S  tterlin, KR; Ivlev, AV; Thomas, HM; Morfill, GE, (2012) *Europhys. Lett.* 99, 45001
 M. Pustyl'nik, A. Ivlev , N. Sadeghi , R.J. Heidemann , S. Mitic , H.M.Thomas , G.E. Morfill, (2012) *Phys. of Plasmas*, 19, 103701
 S  tterlin, K.R.; Wysocki, A.; R  th, C.; Ivlev, A.V.; Thomas, H.M.; Khrapak, S.; Zhdanov, S.; Rubin-Zuzic, M.; Goedheer, W.J.; Fortov, V.E.; Lipaev, A.M.; Molotkov, V.I.; Petrov, O.F.; Morfill, G.E.; L  wen, H., (2010) *Plasma Physics and Controlled Fusion* 124042 (11 pp.)
 Morfill, G.E. and Thomas, H.M., (2012) *Public Service Review – European Science & Technology* 14, 90-93,
 Ivlev, A., Thoma, M., et al. (2011), *PRL* 106, 155001.

Book: Fortov, V. E. , A. G. Khrapak, V. I. Molotkov, G. E. Morfill, O. F. Petrov, H. M. Thomas, O. S. Vaulina and S. V. Vladimirov: *Types of experimental complex plasmas, Complex and Dusty Plasmas: From Laboratory to Space.* (Eds.) V. E. Fortov et al. CRC Press, London, 1-440 (2009).

Book: Ivlev, A., H. L  wen, G. Morfill and C.P. Royall, *Complex Plasmas and Colloidal dispersions: Particle-resolved Studies of Classical Liquids and Solids*, World Scientific, Series in Soft Condensed Matter, Vol. 5, ISSN 1793-737X (2012)

Book: Morfill, G.E., Baturin Yu., Fortov V.E., *Research at the Limit – from the International Space Station to Applications on Earth*, Imperial College Press (2013)

5.3 Plasma Medicine

Cold Atmospheric Plasmas (CAPs) are of considerable interest in medicine and hygiene due to:

- their ability to effectively inactivate pathogens without damaging healthy tissue/skin (see 5.3.1 below).
- recent experimental results which showed that no bacterial resistance against CAP was found (with an accuracy of approximately 1:1030 - see 5.3.2 below).
- their variability: CAPs and their produced chemistry can be specifically 'designed' for different therapeutic applications (see 5.3.3 below).
- the fact that plasma is a 100% sustained resource - it just requires electricity and air.
- the fact that no waste products accrue (like e.g. containers) - the plasma recombines back into the original atmospheric constituents after a short while.

Here is a selection (from around 50 peer reviewed publications) of the research performed in this new field in the last six years:

5.3.1 Plasma devices

Cold plasmas (at atmospheric temperature and pressures) can be produced in different ways. At MPE we have developed a number of different technologies:

• MicroPlaSter (Microwave Plasma Steriliser)

This is a device which uses Argon as a driver gas and a microwave power supply with matching network. It was designed and built in cooperation with Adtec Ltd.



Fig. TH.17: MicroPlaSter (top) and Plasma torch (bottom) courtesy of Adtec Ltd and B. Steffes (MPE) and Shimizu et al. (2008)

• SMD (Surface Micro Discharge)

This is a scalable flat device consisting of two electrodes separated (like a sandwich) by a dielectric, operating in air. One electrode is a continuous sheet-like conductor, the other electrode is structured (e.g. a wire mesh). On the side of the structured electrode many microdischarges are produced, each one lasting only a few nano – to microseconds and having a length of a few mm. Overall this produces a “plasma carpet” of a few mm thickness, which then interacts with air (in over 600 non-equilibrium chemical reactions) to produce Reactive Oxygen Species (ROS) and Reactive Nitrogen Species (RNS). These species are responsible for many of the bactericidal effects.

The SMD design has been incorporated in a rechargeable battery operated device, which has the size of a small torch, as well as in larger (100cm²) devices for biological experiments.

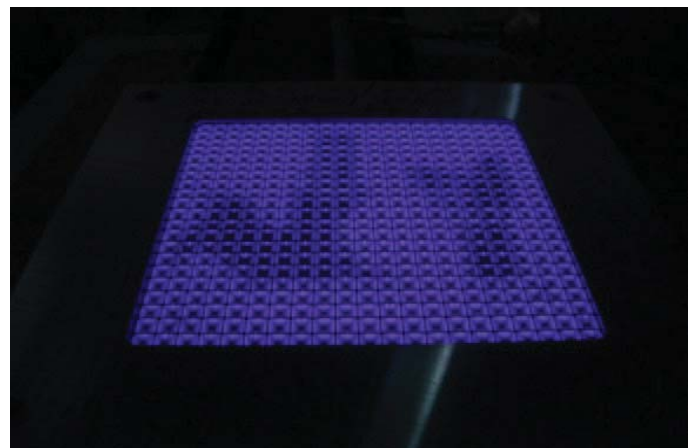
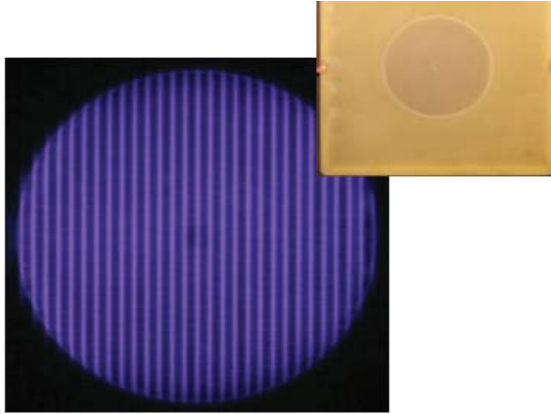


Fig. TH.18: Two examples of SMD devices (large area – top, small rechargeable – bottom) from T. Shimizu and Y.F. Li (MPE) and Morfill et al (2009)

• SSS (Self Sterilising Surface)

The structured electrode can be encapsulated in a hard dielectric (e.g. ceramic) – and becomes a working surface (e.g. for food preparation or biological experiments). When the plasma is turned on, the microdischarges occur on the surface of the hard dielectric and disinfect the hard surface within seconds. Hence SSS technology.



PCB+thick glass+thin board
2kHz, 22kVpp, sine wave
IMG_0519_c.jpg 20100408
see report 20100420

Fig. TH.19: Self sterilizing surface. The electrode is completely encapsulated in glass - nevertheless, plasma is produced on the glass surface.

• Venturi Device

It is notoriously difficult to ignite a plasma in air under high pressure and flow velocities. By making use of the Venturi principle, however, it is possible to ignite the plasma in a low pressure regime (about 0.2 to 0.5 Bar) produced by the high pressure flow. The plasma is then dragged out from the low pressure region and disinfests the whole pressure tube.

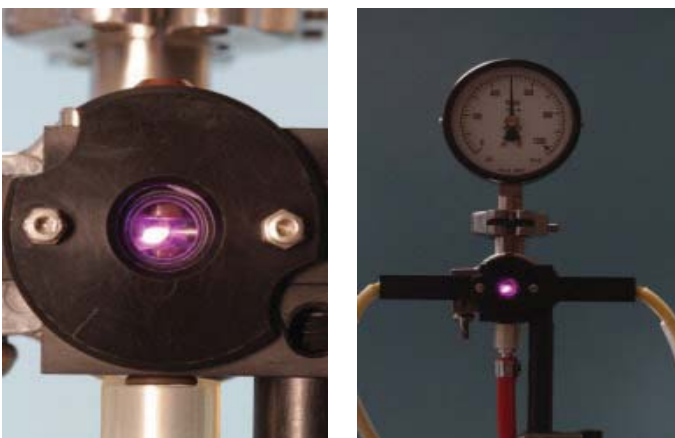


Fig. TH.20: Measurements showing plasma ignition in a Venturi device under 5 bar pressure air flow (B. Steffes, MPE)

• Energy Harvesting

It is possible to produce a plasma by mechanical action – using the piezo electrical effect. It turns out that the electric field produced by piezo action is of just the right magnitude (about 10 kV) to produce microdischarges in a SMD electrode. As a result, small easily transportable and self-sufficient devices have been produced that can disinfect small areas simply by activating a button.



Fig. TH.21: Piezo operated energy harvesting cold plasma source (Morfill et al. 2011)

5.3.2 Bacteria inactivation

The issues: Already in the US alone, there are 2 million hospital induced infections annually, resulting in 90.000 deaths. Of these, it is estimated that there are 100.000 new MRSA infections each year, accounting for 19.000 deaths. In other words, each patient that enters a hospital and is unlucky enough to become MRSA infected has a 19% chance of not surviving.

In Germany the figures are not much better. Hospital induced infections are estimated between 400.000 and 600.000 per year, resulting in 10.000 to 15.000 deaths.

Better hygiene is recognised to be a key issue for improving this situation. Any new fast and efficient technology is likely to be able to make a major impact. Plasmas could help.

The main areas under consideration for improving hospital hygiene are:

1. Plasma hand disinfection
2. Plasma sterilization of medical equipment
3. Plasma disinfection of work surfaces
4. Plasma wound field disinfection during surgery

There are some 21 Million surgical interventions every year worldwide. During this time and during intensive care and convalescence patients are at particular risk against infections, since they are weakened. This implies that any improvements in hygiene can save many lives and can prevent much illness.

Our plasma inactivation experiments revealed that CAPs produced with the SMD technology very efficiently inactivate Gram-positive and Gram-negative bacteria independent of the regarded species and their known antibiotic resistance level.

The table shows the current list of bacteria which were efficiently inactivated so far. This includes resistant bacteria (e.g. MRSA), mutations (e.g. EHEC) as well as the most radiation resistant *Deinococcus Radiodurans*.

Depending on the used power consumption of the plasma device and the distance between the electrode and the sample, a 6 log reduction of bacteria inoculated on agar plates could be achieved starting from 10 seconds of treatment time (Morfill et al. 2009, Li et al. 2012, Shimizu et al. 2012, Maisch et al. 2012, Zimmermann et al. 2012, Zimmermann et al. 2012, Klaempfl et al. 2012, Shimizu et al. 2011).

The two Figures below show the inactivation kinetics of Methicillin-resistant *Staphylococcus Aureus* (MRSA) treated with SMD plasma (with a power consumption of 0.5 W/cm^2). The data shows that a reduction of more than 5 log is achieved within 15s; more than 6 log is obtained for 30s of application (Zimmermann et al. 2012)

5.3.3 Resistance build-up against plasma treatment

To investigate possible resistance development against CAP, experimental studies and theoretical calculations were carried out with *Escherichia coli* and *Enterococcus mundtii*. The obtained results showed no primary resistance for both bacteria types and a lower limit to secondary resistance of 1 in 10^{30} , a limit which is equivalent to (at most) one bacterium out of the total biomass of bacteria on our planet possibly developing resistance. This indicates that the SMD technology is not constrained by bacterial resistance mechanisms (Zimmermann et al. 2012).

5.3.4 Plasma chemistry control

Gram-positive bacteria	Gram-negative bacteria
<i>Staphylococcus aureus</i>	<i>Escherichia coli</i> K12
Methicillin-resistant <i>Staphylococcus aureus</i>	<i>Escherichia coli</i>
<i>Deinococcus radiodurans</i>	<i>Enterohaemorrhagic Escherichia coli (EHEC)</i>
<i>Staphylococcus epidermidis</i>	<i>Burkholderia cepacia</i>
<i>Enterococcus faecalis</i>	<i>Pseudomonas aeruginosa</i>
Vancomycin-resistant <i>Enterococcus faecium</i>	
<i>Enterococcus faecium</i>	
<i>Enterococcus mundtii</i>	
<i>Bacillus cereus</i>	
<i>Bacillus pumilus</i>	
<i>Bacillus cepacia</i>	
<i>Clostridium difficile</i>	
Group A <i>Streptococcus pyogenes</i>	
<i>Corynebacterium jeikeium</i>	
<i>Pseudomonas aeruginosa</i>	
<i>Lactobacillus sakei</i>	
<i>Clostridium difficile</i>	

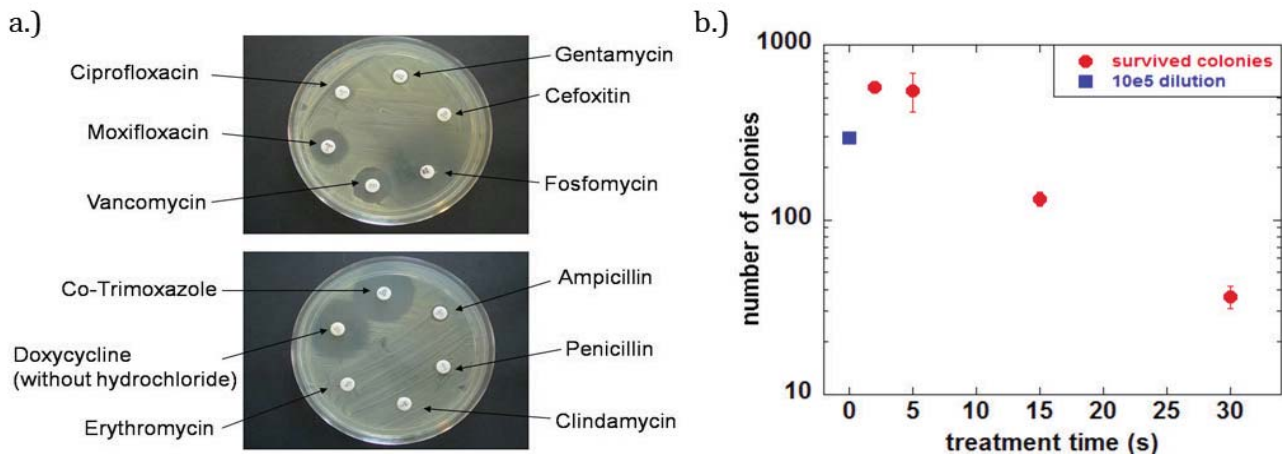


Fig. TH.22:

a.) Antibiotic resistance of the used Methicillin-resistant *Staphylococcus Aureus* (MRSA) strain. b.) Inactivation kinetics of this Methicillin-resistant *Staphylococcus Aureus* (MRSA) strain using SMD plasma. The blue data point represents the control – a 10^5 reduction of the original bacteria suspension (Zimmermann et al. 2012).

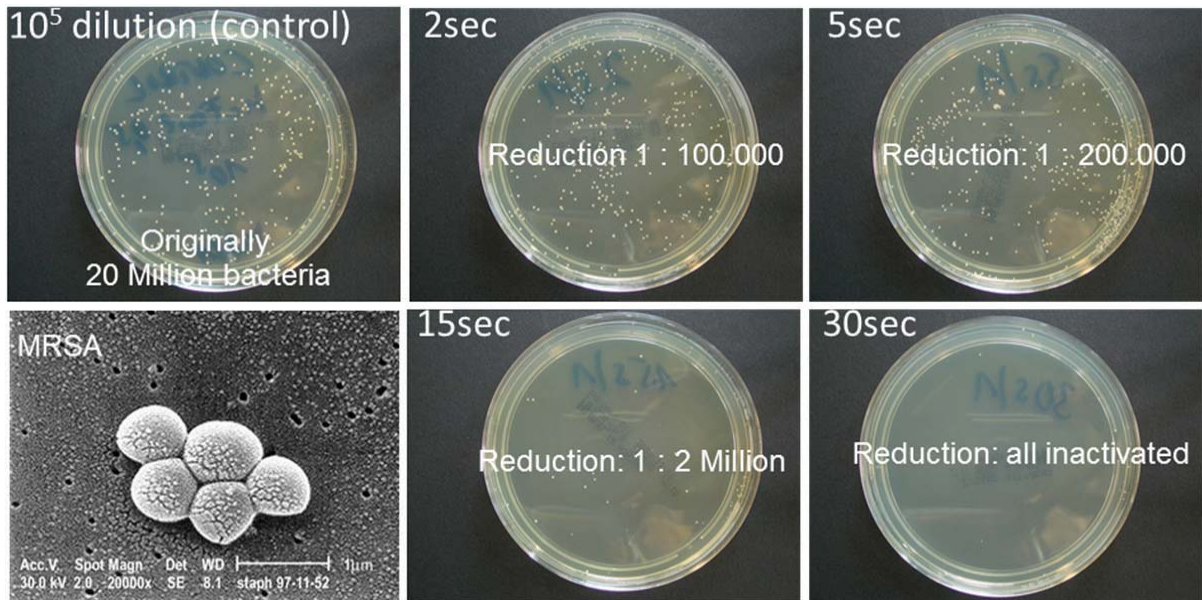


Fig. TH.23: Each white spot on the Petri dishes corresponds to a bacteria colony that has been grown from a single bacterium. On the top left a control sample is shown, not plasma treated, with the original bacterial load diluted by a factor 100,000. There were only about 200 bacteria left after the dilution. The other pictures show the bacteria colonies in the plasma treated samples. The plasma treatment time is given, as well as the bacteria reduction caused by the plasma (from Zimmermann et al. 2012). The bottom left panel shows an electron microscope picture of MRSA bacteria (Photo Credit: CDC/ Jim Biddle, Janice Haney Carr).

Recently we were able to show, that the plasma chemistry (produced by a SMD electrode) in a confined volume can be varied by changing the external parameters for plasma production [Shimizu et al. 2012]

The Figure shows the measured ozone density variations in SMD plasmas for different power input. For low power input (black curves with power consumptions ranging from $9.5 \cdot 10^{-4}$ W/cm² to 0.10 W/cm²) the ozone concentration increases monotonically (in some cases even up to several 1000 ppm) and finally saturates. For higher power input (green and red curves with power consumptions ranging from 0.25 W/cm² to 2.6 W/cm²) the ozone concentration first increases, but afterwards

decreases again quite quickly.

Chemical model calculations suggest that the ozone depletion at higher power densities is caused by quenching reactions with nitrogen oxides that are in turn created by vibrationally excited nitrogen molecules which react with O atoms. This observed 'mode transition' from a predominately oxygen (ROS) chemistry (generated at low power input) to a predominantly nitrogen (RNS) chemistry (produced at high power input) gives an example how SMD plasmas can be 'designed' by simply changing the external parameters.

5.3.5 Plasma activation of water

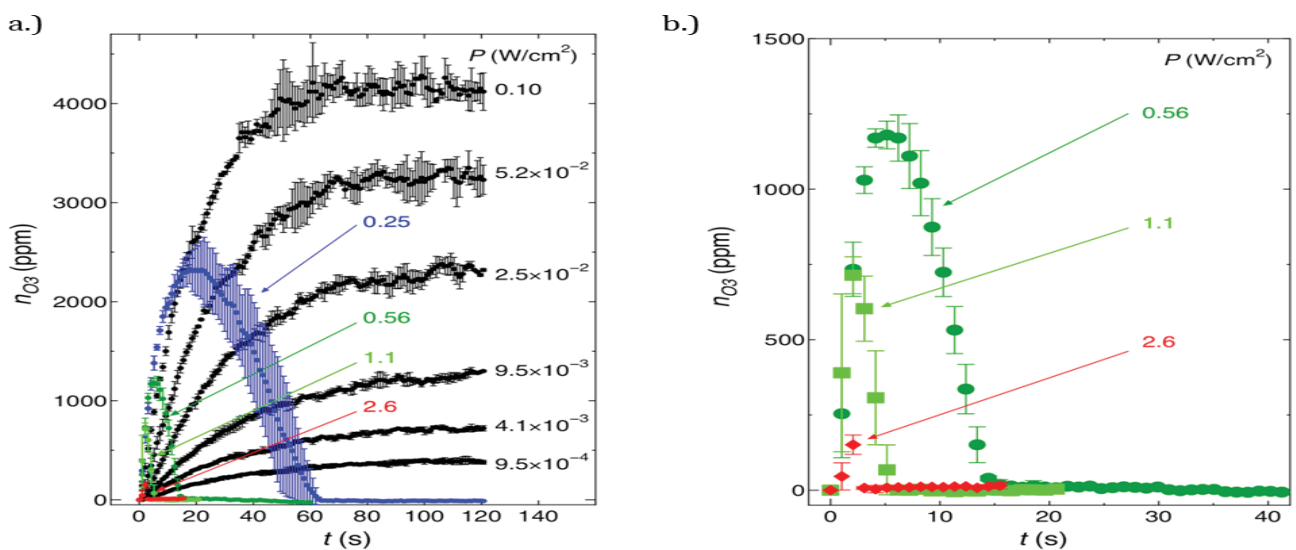


Fig. TH.24: a.) Time evolution of the ozone density (n_{O_3}) produced by a SMD electrode (in a confined volume of 5 cm³) for different power input measured with UV absorption spectroscopy at 254 nm. b.) Time evolution of the ozone density with power input of 0.56 W/cm² and higher. The applied voltage was 15 kV_{pp}. (Shimizu et al. 2012).

The annual beer consumption in 2010 in the US was 24 Billion liters, in China 44.7 Billion liters, in Germany 8.8 Billion liters and in Brazil 12.2 Billion liters – these four countries accounted for 47.5% of the world’s beer consumption in 2007 (CBC News, 20.8.2008). Mostly this beer is sold in half liter or 0.633 liter bottles. The requirement in terms of hygienically cleaned bottles for these countries alone is around 150 – 200 Billion bottles per year. Or in other words, during each working day roughly half a Billion bottles need to be cleaned and filled.
Or take drinking water – in the US alone 1500 plastic wa-

ter bottles are used - each second! Or 130 Million each day. 17 Million barrels of oil are needed each year to produce these water bottles (From: Petz Scholtus, www.treehugger.com/author/petz-scholtus/ October 15, 2009).

Current bottling plants manage approximately one Million bottles per day. This does not leave much time for disinfection. The amount of water needed per bottle during the cleaning, disinfection and rinsing process is 3 liters. And even then it cannot be guaranteed that the bottles are devoid of disinfectants before filling – and the disinfectant contaminated water has to be disposed of.

An interesting alternative could be “Plasma Activated Water” (PAW). Plasma interaction with water turns the water into a disinfectant. The effect only lasts for a few days (see figure below). Then the water reverts back to its original state.

5.3.6 “ex vivo” study of plasma effects on human skin

To investigate the safety of CAP on human tissue, “ex vivo” investigations are excellent models. Human skin, excised from around melanoma, can be used for this. The (healthy) skin is kept “alive” by placing it on a nutrient fluid and then the plasma treatment is applied. The skin sample is then tested for histological and other changes. Here are some examples:

5.3.7 Control of secondary infections in chronic

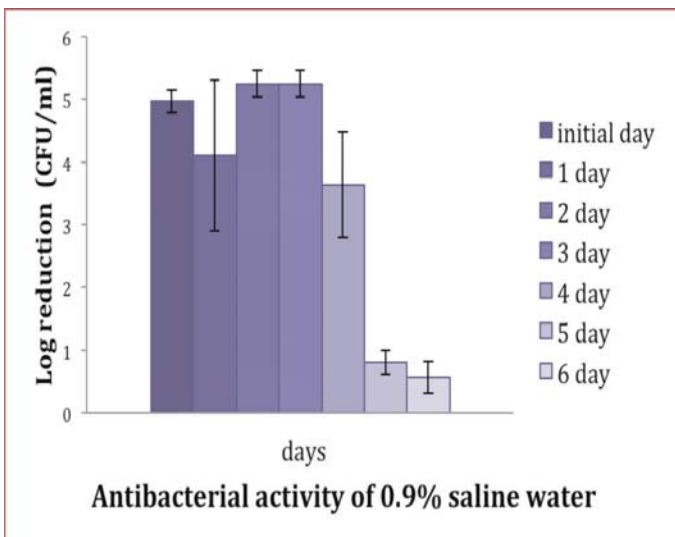


Fig. TH.25: Water exposed to plasma has antibacterial properties – the water can be used as a disinfectant. The effect lasts for a few days only, after that the water returns to its former state. This could be of interest when environmental issues prevail (Mitra et al, 2012).

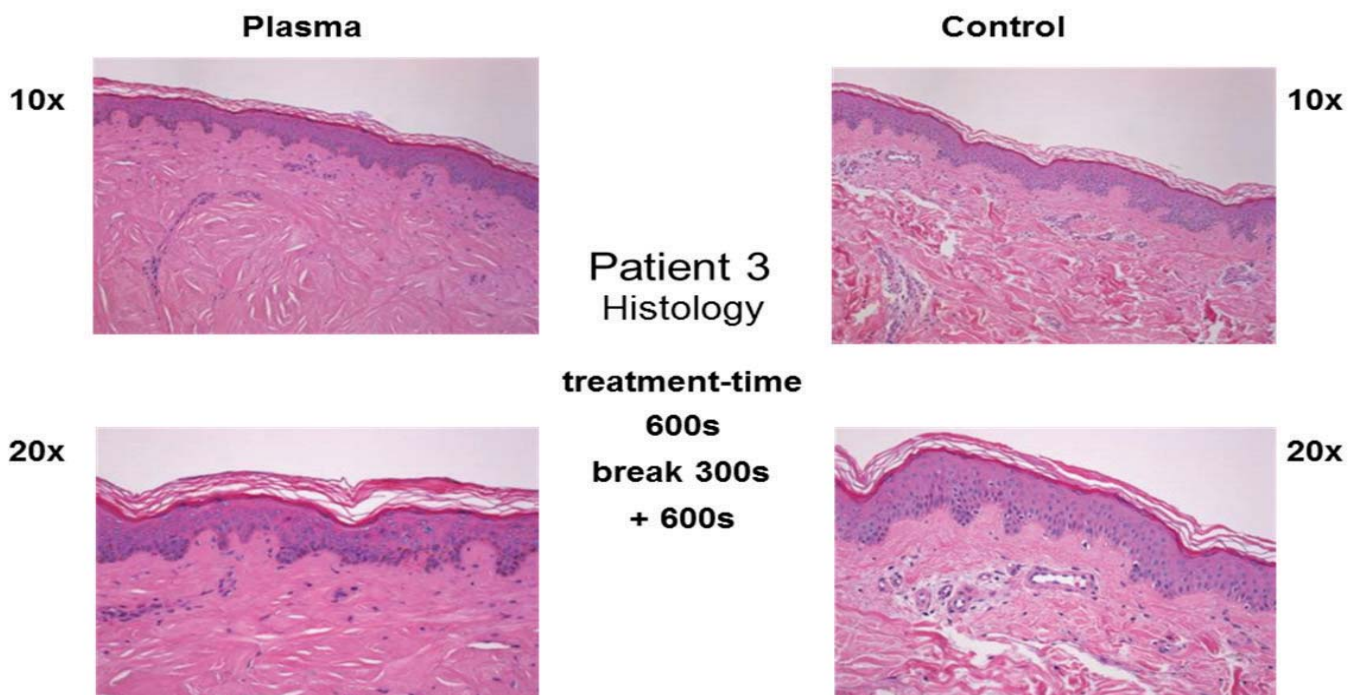


Fig. TH.26: Skin histology for plasma treated samples (left at two different magnifications) compared with control samples that were kept in the same way but without plasma treatment. There is no histological change in spite of the fact that the total plasma treatment of 1200 seconds is typically 100 times longer than that which was required to inactivate MRSA bacteria. This implies that there is a huge “therapeutic window” for e.g. hand disinfection or other hygiene applications on skin.

wounds

Chronic ulcers of the lower leg exhibit a prevalence of ~1% of the population of developed countries and are associated with considerable patient morbidity [Etufugh et al. 2007] and cost. Bacterial colonization of such chronic infected wounds is common and a well-recognized factor which contributes to impaired wound healing [Breidenbach et al. 1995, Robson 1997].

In a controlled clinical study over the last five years bac-



Fig. TH.27: The MicroPlaSter (Microwave Plasma Steriliser) developed by MPE and Adtec Plasma Technology Ltd. This is the plasma device used in all the clinical trials so far. By requirement of the Ethics Commission, clinical Argon had to be used as carrier gas for the plasma production for this worldwide first application of Cold Atmospheric Plasma in human clinical trials. The instrument was in addition installed with many operational safety features to ensure that no accidental use beyond that which was prescribed could occur.

terial infection of chronic wounds was treated by Cold Atmospheric Plasma in addition to the best available topical and systemic treatment. Over 3000 treatments were performed.

5.3.8 Wound healing

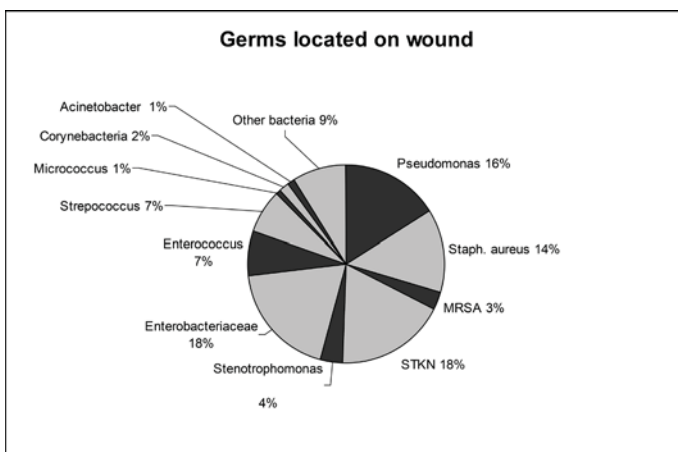


Fig. TH.28: Bacteria, which are typically found in chronic infected wounds (figure taken from Isbary et al. [Isbary et al. 2010]).

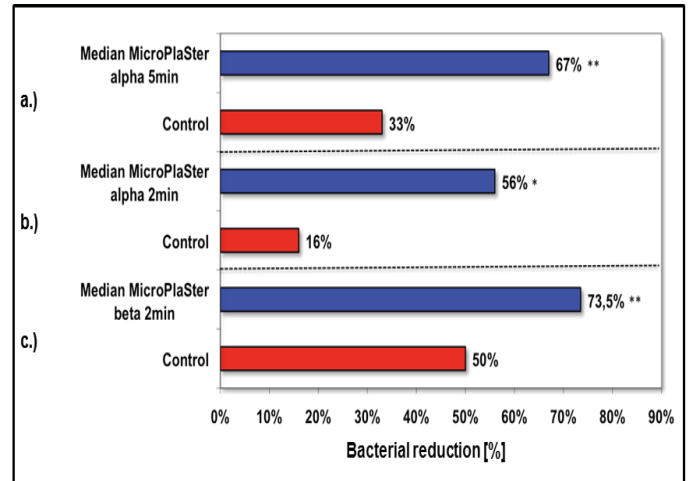


Fig. TH.29: Observation of bacterial reduction for: a.) 5 min CAP treatment with the MicroPlaSter alpha in comparison with the control b.) 2 min CAP treatment with the MicroPlaSter alpha in comparison with the control c.) 2 min CAP treatment with the MicroPlaSter beta in comparison with the control (Isbary et al. 2010, 2012)

To investigate the influence of CAP on the process of wound healing 40 patients with similar wounds, split-thickness grafts on the thigh, were treated with the MicroPlaSter. For the clinical study, the wound sites were divided into two equally sized areas and randomly assigned to two groups which were either treated with CAP or argon gas only (placebo mode) for 2 minutes daily.

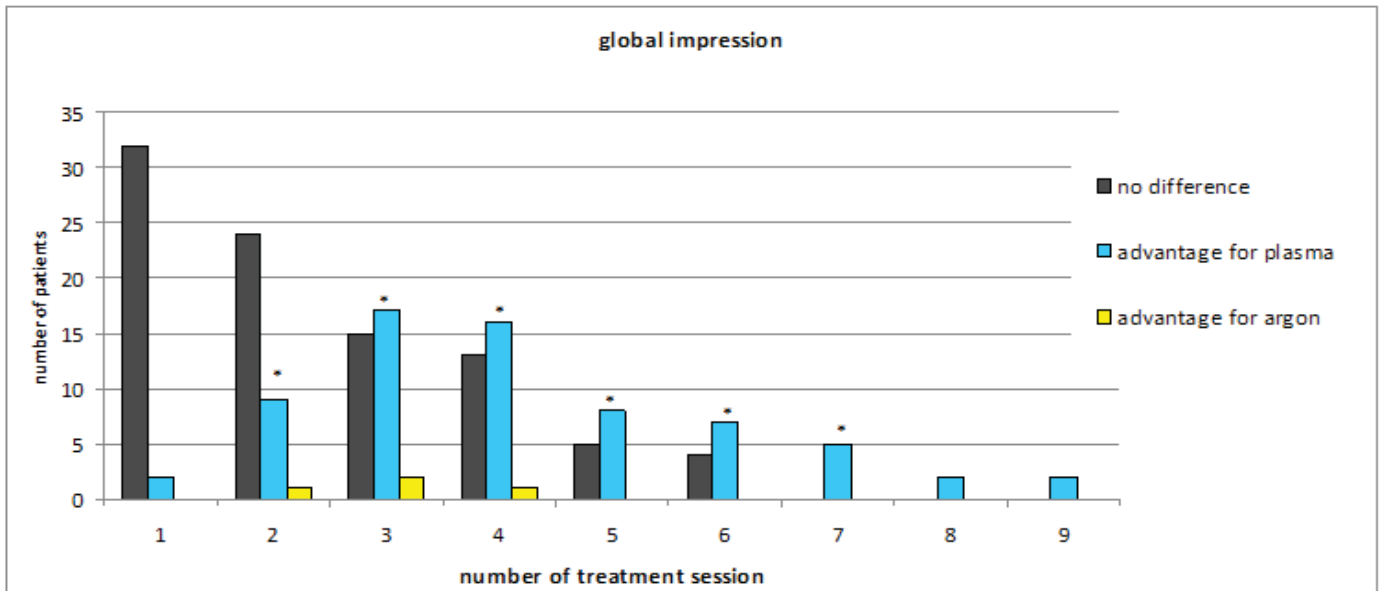
Wound healing was evaluated with regard to re-epithelialization, blood crust formation, fibrin layers and wound surroundings by two "blinded investigators" (who had no prior knowledge which part of the wounds received plasma, and which part placebo).

The results showed, that from the second treatment day onwards, wound areas treated with CAP (n=34) showed significantly more often improved overall impression of wound healing than the placebo-treated areas.

Results of the clinical study conducted on skin graft wounds: The global assessment shown above yields a significantly improved overall impression of wound healing for plasma treated wounds following treatment session two.

With regard to re-epithelialization significant results indicating superiority of CAP treated areas were found from the third treatment session onwards. Furthermore significantly fewer blood crusts were found in CAP treated skin graft wounds than in the placebo-treated wounds on days 3, 4 and 5. Fibrin layers were found in significantly fewer CAP treated areas than in the control areas (day 2-5). The wound surroundings were not influenced - neither by the CAP nor the placebo treatment (Heinlin et al.).

5.3.9 Alleviation of skin diseases



Treatment session	1	2	3	4	5	6	7	8	9
advantage for plasma	2	9	17	16	8	7	5	2	2
no difference	32	24	15	13	5	4	0	0	0
advantage for argon	0	1	2	1	0	0	0	0	0
p-value	0.25	0.011	<0.001	<0.001	0.004	0.008	0.031	0.25	0.25

Fig. TH.30: The figure shows the number of patients whose skin graft wounds were judged by medical experts. Black denotes no difference between plasma treated and untreated wound segments, blue denotes those cases where the experts found that the plasma treated segment was healing better, yellow where they concluded that the untreated segment was healing better. As expected, in the first two days (treatment sessions) the differences are not very great, but starting from day 3 they begin to be very significant, as seen quantitatively from the statistical p-value. (From Heinlin et al., 2012)

The Hailey-Hailey disease is an autosomal dominant condition resulting from mutations in the ATP2C1 gene and is particularly difficult to control during the hot summer months when sweat and friction aggravate the eruption. Additionally, the eroded lesions of the Hailey-Hailey disease often develop secondary infections. In a case study performed at the Dermatological Clinic in Schwabing, plasma in combination with standard topical treatment was employed for the first time (with the consent of the patient) who had been suffering for many years.

The addition of CAP (produced with the MicroPlaSter) to topical corticosteroids and local disinfectants resulted in a rapid improvement of the infected lesions in the axilla of the patient. The groin, which was only treated with topical corticosteroids and disinfectants, remained unchanged.

After application of CAP to the groin as well, a marked clinical improvement was observed. The observed beneficial effect of CAP was presumably in part due to its bactericidal and fungicidal properties but possibly also due to a positive influence on the oxidant-antioxidant system

in skin lesions of the Hailey-Hailey Disease. This was a very encouraging result. Nevertheless to confirm the usefulness of the CAP treatment for the Hailey-Hailey Disease a controlled clinical study is mandatory (Isbary et al. 2010).

5.3.10 Cell selectivity – cancer treatment

Cancer cells were treated “in vitro” with a standard Chemotherapy drug and with CAP. The cell lines used were glioblastoma cells (brain cancer). These are amongst the most aggressive cancers, the average life expectancy after diagnosis is only 14 months even with the best available treatment and after surgery.

One of the cell lines (LN18) is practically resistant against Chemotherapy (see the red curve in panel (a) of the figure). The other cell lines only show a mild reduction in cancer cell viability of less than 25% - in other words, 75% of the cells are still active even with a dose of 200 micromole TMZ.

In comparison, plasma treatment of the same cell lines is

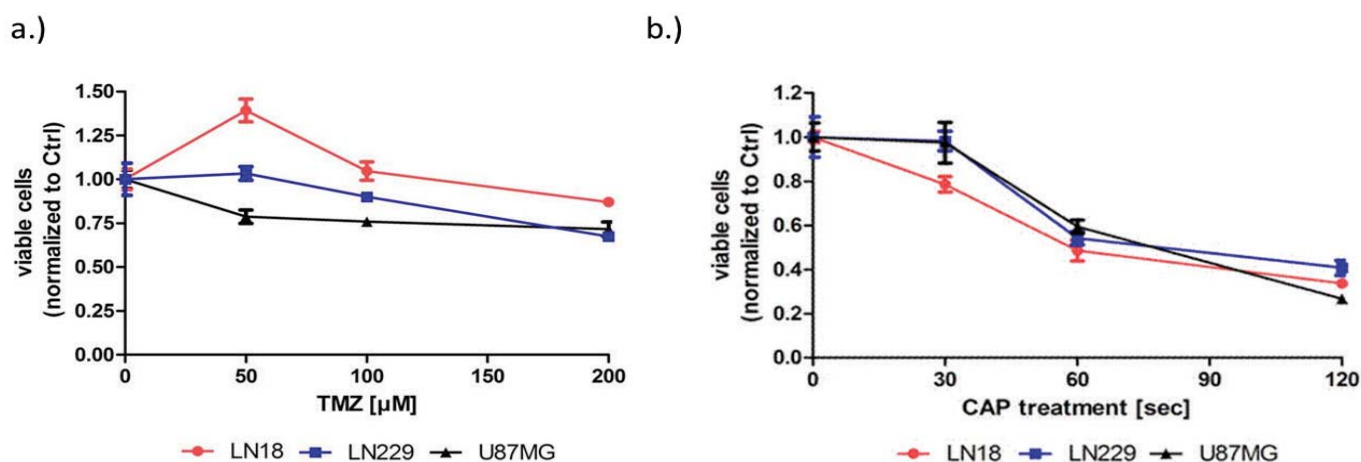


Fig. TH.31: a.) TMZ treatment of three glioma cell lines LN18 (resistant against TMZ), LN229 and U87MG. b.) CAP treatment of three glioma cell lines LN18 (resistant against TMZ), LN229 and U87MG (from Körtzer et al. 2013).

much more effective. For 2 minutes treatment only 40% of the cancer cells are still active. In addition, LN18 does not exhibit resistance against plasma.

In addition to the effect of plasma treatment alone, Körtzer et al. analyzed the effects of a combined therapy composed of CAP (produced with the SMD technology (power consumption: 0.02 W/cm^2)) and the chemotherapeutics TMZ on (TMZ-resistant and TMZ-sensitive) glioma cells. The combined treatment revealed synergistic effects and showed a more than fivefold higher inhibition of proliferation than the treatment with the same dose of TMZ alone. Furthermore, the experiments revealed that a pre-treatment with CAP restores the sensitivity of TMZ-resistant glioma cells towards the chemotherapy with TMZ (Körtzer et al. 2013).

5.3.11 Improving agricultural yield using plasma

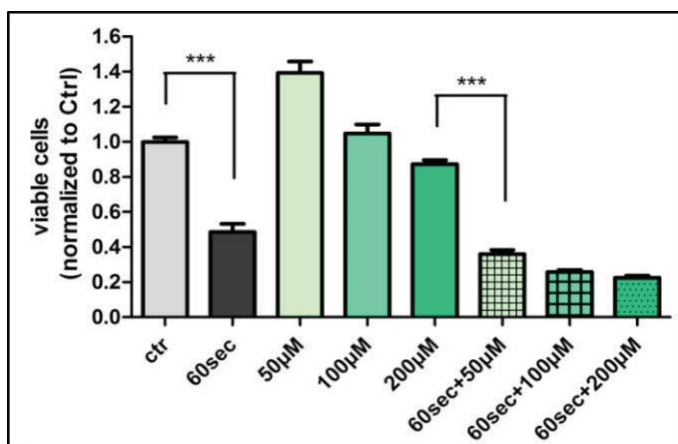


Fig. TH.32: Viable LN18 cells (cell line which is resistant against TMZ) for a CAP treatment of 60s, for a treatment with $50 \mu\text{M}/100 \mu\text{M}/200 \mu\text{M}$ TMZ and for the combined treatment 60s CAP + $50 \mu\text{M}/100 \mu\text{M}/200 \mu\text{M}$ TMZ. The data clearly shows, that the combined treatment revealed synergistic non-additive effects. (Körtzer et al. 2013)

The issues for employing plasma in agriculture are:

1. Hunger (how to increase the yield of crops, how to strengthen the young plants against parasites)
2. Pollution (how to decrease the pollution of the water reservoirs, in particular the ground water as a result of over fertilization).

At first sight it would appear possible to employ plasma in the former – protection against bacteria and fungi has after all been demonstrated in an impressive manner already. And the yield of seeds could perhaps be increased.

A recent investigation with chickpeas gives an interesting account of the potential. This was conducted by Anindita Mitra at the Max Planck Institute for extraterrestrial Physics in a very terrestrial application. She treated the seeds with plasma for different times and then sowed them and waited... (She did other research while waiting. Of course). There were two main results:

The first, partially expected, was that the yield increased. But the increase was large – up to 50%. This was an unexpectedly huge effect. Future work will show whether such increases, which could be the initial part of the story for combating the hunger problem, can be realized in other seeds and crops, too.

The second, totally unexpected, was that the growth rate of the plasma treated seedlings (measured by the average volume of the seedling) exceeded that of the untreated seedlings by up to a factor 6! Was this a cause for concern? Could there be some DNA modification – in which case the use of plasma would face a major problem? Well, so far there is no indication that the seeds (and the plants) are genetically modified. Instead, there is a much simpler explanation, which is being pursued (and which, though plausible, may not be correct). But the explanation is sufficiently elegant and compelling

that it can be explained:

The plasma reduces the bacteria and fungi on the seeds. The effect – between 90% and 99% depending on the plasma treatment time – is clearly sufficient to make the seeds more viable to germinate.

Next to bear in mind is the air chemistry initiated by the nonequilibrium reactions of the cold atmospheric plasma. These produce Nitrites and Nitrates (e.g. NO_3 or NH_3 , which plants can readily absorb), which are so-called “macronutrients” for plant growth. Macronutrients are labeled with an “NPK analysis”, where the letters correspond to the chemical signs of Nitrogen, Phosphorus, and Potassium (N-P-K). In the plasma treatment of the seeds there is therefore the additional effect that the seeds are coated with nitrites and nitrates.

Here is where the speculation starts. What is the plasma not only reduces the bacteria and fungi which inhibit germination, but also provide the seeds at the same time with their own “personalized” fertilizer? This would be an added bonus in many ways. The seedlings would grow faster and they would be stronger to ward off parasites during the formative period. Ground water pollution during this time would be entirely absent, since fertilization of the whole field would not be required. A fascinating speculation...

Plasma could in principle have a beneficial influence on the world hunger problem and at the same time protect the environment. The future will tell if this speculation has any substance or not.

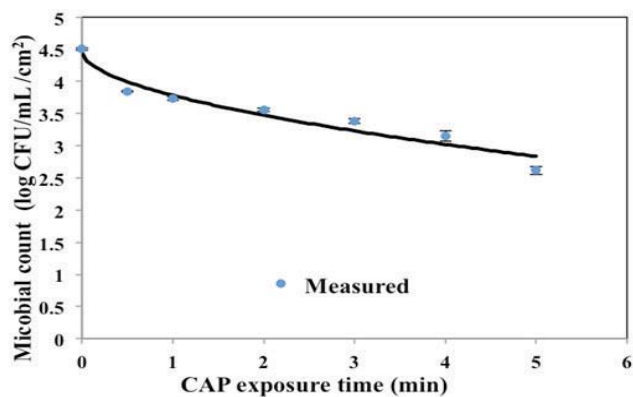


Fig. TH.33: Shown is the count of microbes on chickpeas as a function of plasma exposure. The microbial load decreases continuously, the longer the plasma is applied. The plasma source was a “standard” Cold Atmospheric SMD source applied in air. (Mitra et al. 2013)



J. Körtzner, A. Mitra, T. Shimizu, J. Zimmermann

(Other Theory team members include V. Boxhammer, J. Jeon T. Klaempfl, Y.-F. Li, G. Morfill, L. Taghizadeh)

Selected References:

- Y.-F. Li, T. Shimizu, J. L. Zimmermann and G. E. Morfill, *Plasma Process. Polym.* 9, 585–589 (2012)
- T. Shimizu, Y. Sakiyama, D. B. Graves, J. L. Zimmermann and G. E. Morfill, *New Journal of Physics* 14 103028 (2012)
- T. Shimizu, J. L. Zimmermann, and G. E. Morfill, *New Journal of Physics* 13 023026 (7pp) (2011)
- Y.-F. Li, J. L. Zimmermann and G. E. Morfill, *New Journal of Physics* 14 023058 (2012)
- T. Maisch, T. Shimizu, A. Mitra, J. Heinlin, S. Karrer, Y.-F. Li, G. E. Morfill and J. L. Zimmermann, *J Ind Microbiol Biotechnology* 39(9):1367-75 (2012)
- J. L. Zimmermann, T. Shimizu, H.-U. Schmidt, Y.-F. Li, G. E. Morfill and G. Isbary, *New Journal of Physics* 14 073037 (2012)
- J. L. Zimmermann, T. Shimizu, V. Boxhammer and G. E. Morfill, *Plasma Processes and Polymers* 9:8, 792-798 (2012)
- T. Maisch, T. Shimizu, Y.-F. Li, J. Heinlin, S. Karrer, G. Morfill and J. L. Zimmermann, *PLoS One* 7:4 e34610 (2012)
- V. Boxhammer, G. E. Morfill, J. R. Jokipii, T. Shimizu, T. Klämpfl, Y.-F. Li, J. Körtzner, J. Schlegel and J. L. Zimmermann, *New Journal of Physics* 14 113042 (2012)
- T. Maisch, T. Shimizu, G. Isbary, J. Heinlin, S. Karrer, Y.-F. Li, G. Morfill and J. L. Zimmermann, *Applied and Environmental Microbiology* 78(12):4242-7 (2012)
- J. L. Zimmermann, K. Dumler, T. Shimizu, G. E. Morfill, A. Wolf, V. Boxhammer, J. Schlegel, B. Gansbacher and M. Anton, *J. Phys. D: Appl. Phys.* 44 505201 (2011)
- T. Klämpfl, G. Isbary, T. Shimizu, J. L. Zimmermann, Y.-F. Li, W. Stolz, J. Schlegel, G. E. Morfill and H.-U. Schmidt, *Applied Environ Microbiology* 78(15):5077-82 (2012)
- G. Isbary and J. Koeritzer, A. Mitra, Y.-F. Li, T. Shimizu, J. Schroeder, W. Stolz, G. E. Morfill, J. Schegel, and J. L. Zimmermann, *Clinical Plasma Medicine Journal* online available under <http://dx.doi.org/10.1016/j.cpme.2012.10.001> (2012)
- V. Boxhammer, Y.-F. Li, J. Körtzner, T. Shimizu, T. Maisch, G. E. Morfill, J. Schlegel and J. L. Zimmermann
- C. Welz, S. Schwenk-Zieger, Y.-F. Li, J. Jeon, T. Shimizu, S. Becker, U. Harréus, G. E. Morfill and J. L. Zimmermann, *Journal of Physics D: Applied Physics* 46 045401 (9pp) (2013)
- S. Arndt, E. Wacker, S. Kaufmann, Y.-F. Li, T. Shimizu, H. M. Thomas, G. E. Morfill, S. Karrer, J. L. Zimmermann and A.-K. Bosserhoff, *Experimental Dermatology* 22(4): 284-9 (2013)
- J. Körtzner, V. Boxhammer, A. Schäfer, T. Shimizu, T. G. Klämpfl, Y.-F. Li, C. Welz, S. Schwenk-Zieger, G. E. Morfill, J. L. Zimmermann and J. Schlegel, accepted in *PLoS One*
- AG. Isbary, G. E. Morfill, H.-U. Schmidt, M. Georgi, K. Ramrath, J. Heinlin, S. Karrer, M. Landthaler, T. Shimizu, B. Steffes, W. Bunk, R. Monetti, J. L. Zimmermann, R. Pompl and W. Stolz, *Br J Dermatol.* (2010) 163(1):78-82
- G. Isbary, G. Morfill, J. L. Zimmermann, T. Shimizu and W. Stolz, *Archives of Dermatology* (2011) 147(4):388-390
- G. Isbary, J. Heinlin, T. Shimizu, J. L. Zimmermann, G. Morfill, H.-U. Schmidt, R. Monetti, B. Steffes, W. Bunk, Y. Li, T. Klaempfl, S. Karrer, M. Landthaler and W. Stolz, *Br J Dermatol.* (2012) doi: 10.1111/j.1365-2133.2012.10923.x
- J. Heinlin, J. L. Zimmermann, F. Zemanc, W. Bunk, G. Isbary, M. Landthaler, T. Maisch, R. Monetti, G. E. Morfill, T. Shimizu, J. Steinbauer, W. Stolz and S. Karrer, under revision in *Wound Repair and Regeneration*
- A. Mitra, Y.-F. Li, T. Klämpfl, T. Shimizu, J. Jeon, G. Morfill, J. Zimmermann, *Food Bioprocess Technol* (2013)

5.4 Information Extraction from Complex Data Sets

Non-Gaussianities in the WMAP data

Within the realm of investigating the statistics and isotropy of the CMB data we tested for phase correlations of the Fourier phases in the field of the temperature fluctuations. To this end we applied two key methods stemming from nonlinear data analysis, namely the method of surrogate data sets and estimators for (local) scaling properties of a point set. By generating surrogate maps possible phase correlations in the original map are wiped out by applying scale-dependent randomization procedures to the phases while exactly preserving the modulus of the complex spherical harmonic coefficients.

Comparing the foreground-cleaned CMB-data with the respective surrogate maps by means of scaling indices reveals consistent and highly significant signatures for intrinsic phase correlations at large scales- thus scale-dependent non-Gaussianities - and large deviations from isotropy - questioning the Copernican principle. In fact, the results represent the detection of the by far most significant, yet statistically robust, anomalies in the CMB.

Thorough checks on systematics revealed that the signature is intrinsic and insensitive to variations of the input map and possible small scale foreground remnants in the galactic plane. Furthermore, purely topological measures, namely the Minkowski functionals, led to the same results (see figure below).

As it was demonstrated before, a number of (linear) large scale anomalies, e.g. the power asymmetry, can be removed by subtracting a best fit Bianchi-template map from the CMB-data. Following this line we repeat the surrogate study for such maps and find that also the (non-Gaussian) signatures stemming from phase correlations nearly vanish, when Bianchi-corrected maps are used as input maps. Further similar studies may guide the way to physically well-motivated models explaining the origin of the detected phase-correlations.

On the other hand, a more detailed investigation of the presence and absence of phase correlations as identified in observational CMB data may shed more light on the meaning of Fourier phases for complex structures. First results suggest that it is possible to establish correlations between the information coded in the phases with higher order statistics as an extension of the well-known Wiener- Khintchin theorem. Those findings are of great interest in many (interdisciplinary) fields of research – namely whenever the Fourier representation of sufficiently complex data sets plays a crucial role in the representation and analysis of the data.

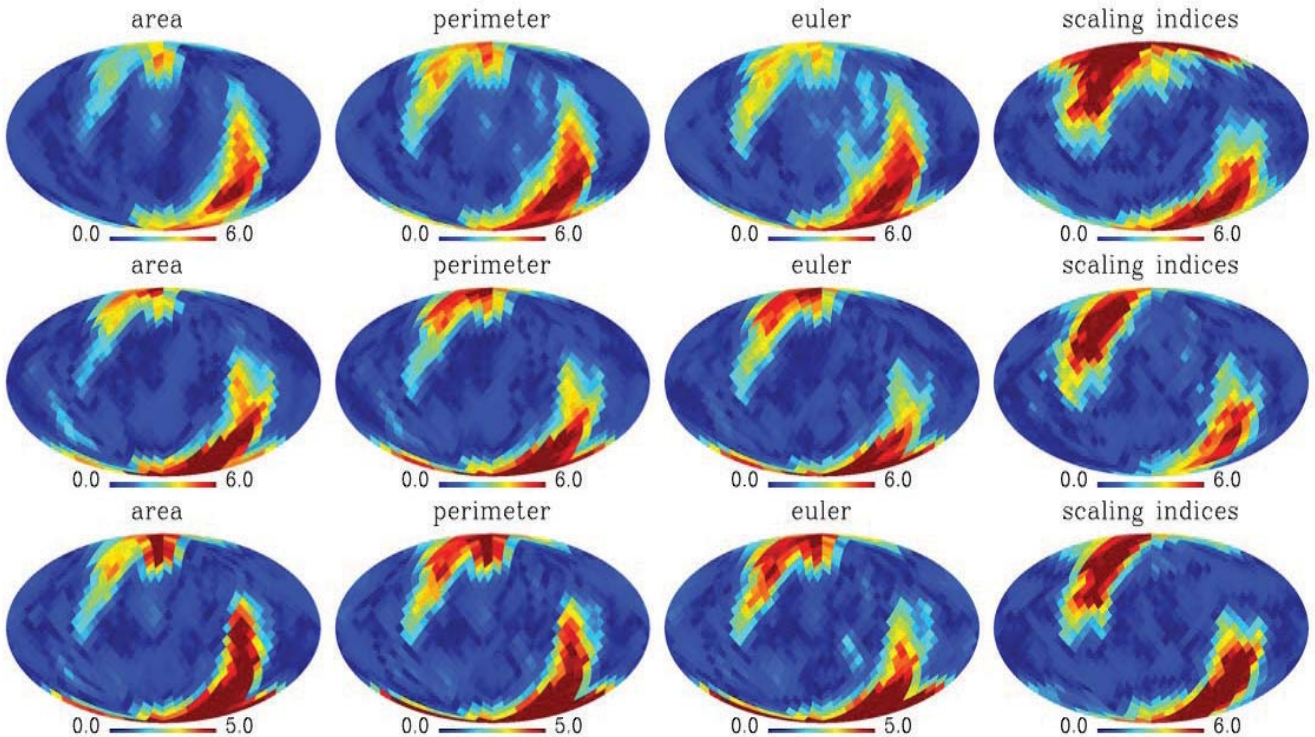


Fig. TH.34: Deviation $S(X^2)$ of Minkowski Functionals M_0 , M_1 and M_2 of the rotated hemisphere for the ILC7 (upper row, from left to right) and NILC7 map (middle row). In the lower row we show the results of the phase replacement method for NILC7. The l -range for the method of the surrogates is $\Delta l = [2, 20]$. The plots to their very right show the corresponding results $S(X^2)$ for the respective maps gained by the scaling index method.



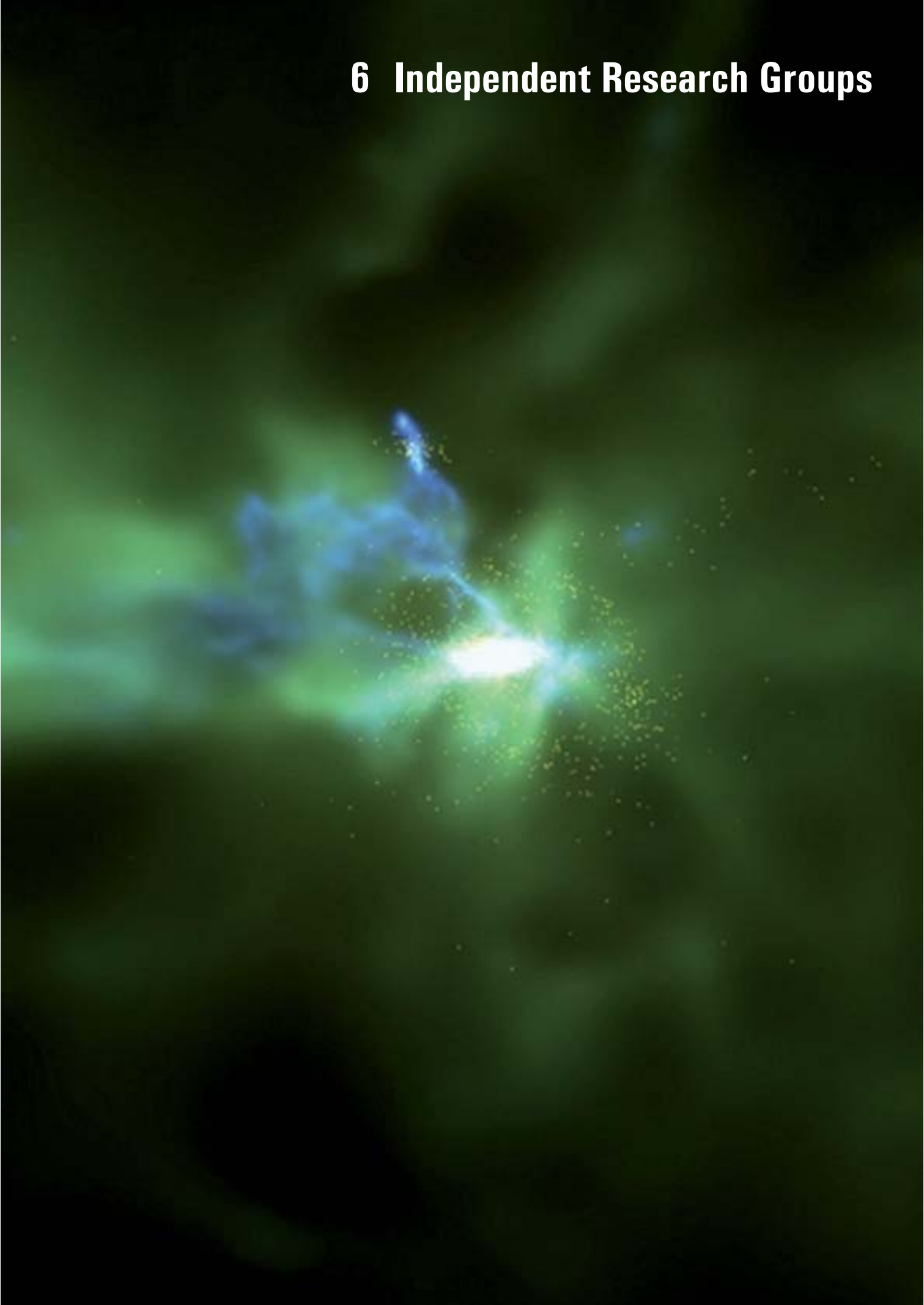
Christoph R ath

(Other Theory team members include T. Aschenbrenner, W. Bunk, S. Mihatsch, H. Modest, R. Monetti, G. Morfill, G. Rossmannith, H. Scheingraber)

Selected References:

- H. Modest, C. R ath, A. J. Banday, G. Rossmannith, R. S utterlin, S. Basak, J. Delabrouille, K.M. Gorski, G. E. Morfill, MNRAS, 428, 551-562, 2013*
- G. Rossmannith, C. R ath, A.J. Banday, K. Gorski, H. Modest, G. Morfill, Phys. Rev. D, 86, 083005, 2012*
- C. R ath, A. J. Banday, G. Rossmannith, H. Modest, R. S utterlin, K.M. Gorski, G. Morfill, MNRAS, 415, 2205 – 2214, 2011*
- G. Rossmannith, H. Modest, C. R ath, A. J. Banday, K. M. Gorski, G. Morfill, Advances in Astronomy, 2011, 174873, 2011*
- G. Rossmannith, C. R ath, A.J. Banday, G. Morfill, Month. Not. Roy. Astr. Soc. 99, 1921–1933, 2009*
- C. R ath, G.E. Morfill, G. Rossmannith, A.J. Banday, K.M. Gorski, Physical Review Letters, 102, 131301, 2009*

6 Independent Research Groups



6. Independent Research Groups

6.1 Research Group "Theoretical Modelling of Cosmical Structures" Sadegh Khochfar

The main research interest of the group is the modelling of structure formation with a focus on high redshift ($z > 2$) galaxy formation and early-type galaxies. To address these topics we conduct self-consistent cosmological hydrodynamics simulations, semi-analytic and analytic modelling of key physical processes in galaxy formation. Since 2010 Khochfar has published 45 peer-reviewed papers (including one Nature paper) receiving more than 1100 citations. In the following a few highlights of the research are presented.

6.1.1 Early-Type Galaxies

The ATLAS^{3D}-Survey—ATLAS^{3D} is a complete survey of 260 early-type galaxies within the local (42 Mpc) volume observed with the SAURON integral field unit on the WHT, and are complemented by observations with WRST, IRAM, CARMA and MegaCam for a subset of the sample. One of the main results of this survey is that early-type galaxies can be classified into fast and slow rotators based on their kinematics. Khochfar is one of the lead theoreticians within the ATLAS^{3D}-collaboration and was able to show for the first time within LCDM models that there is a close link between the presence of a stellar disc and fast rotators. On average fast rotators show disc fractions of more than 10% (Khochfar et al. 2011, Kranjovic et al. 2012). Slow rotators are the product of continued minor mergers contributing up to 80% of the stellar mass of massive early-type galaxies. Further notable results of the survey with involvement from Khochfar showed e.g. a possible variation of the stellar IMF in early-type galaxies (Cappellari et al. 2012).

AGN feedback in $z=2$ massive gas-rich progenitors of present-day early-type galaxies—In a series of papers (Gaibler, Khochfar et al. 2012; 2013) we studied the effect of jets on the inter-stellar medium (ISM) in affecting its ability to form stars. We used high-resolution 3D AMR simulations to show that jets in fact are able to initially trigger star formation in a ring around the central region that has been vacated by the jet. Once the jet-heads break out the disc the back flow is additionally able to trigger star formation over the whole galactic disc for a limited amount of time. Star formation is enhanced by up to a factor of two over tens of Myrs with respect to the same galaxies without a jet. These papers consist of a significant step forward in the understanding of jet-feedback and star formation in galaxies, as they are fully 3D and use realistic galaxy models at the peak epoch of star formation.

Mergers and the evolution of early-type galaxies—The role of mergers in the formation and evolution of early-type galaxies is of central importance. However, theoretically predictions seem to still diverge as to role

of minor vs major mergers. Khochfar joined a team of international researchers to produce the most complete and accurate evaluation of the merger rate over many different codes and modelling approaches (Hopkins et al. 2010a, 2010b). Minor mergers play an important role in terms of number as well as total mass contributed to massive early-type galaxies. We could show that the expectations for the size growth of early-type galaxies due to minor mergers is in agreement with observations, although there might be tension as to the size of the scatter in this relation between the models and observations (Shankar et al. 2010).

6.1.2 The First Billion Years of Galaxy Evolution

The first billion years of the Universe sees a period of rapid change, going from a mostly neutral state to one in which hydrogen is re-ionized, the first stars, black holes, and proto-galaxies form. It is then, when galaxies go through a growth spurt, doubling their stellar mass on average every 150 Myrs. The importance of this phase for present-day galaxies is highlighted in massive early-type galaxies, whose majority of stars were formed during the first few billion years of the Universe. Given the increasing sensitivity of observations that already reach galaxies of stellar mass $M_* \sim 10^9 M_\odot$ and luminosities $M_{100} \sim -17$ at $z \sim 6$, there is a strong motivation to resolve the formation path of such galaxies, which dominate in number the mass function of galaxies.

To bridge the gap between these two approaches, we have conducted in my group a set of smoothed particle hydrodynamics (SPH) cosmological simulations, the **First Billion Years Simulations (FiBY)**, of which the highest resolution simulation has a SPH particle mass of $\sim 1000 M_\odot$ throughout a volume of $(8 \text{ Mpc})^3$. The latter comprises one of the highest resolution hydrodynamical simulations to date of such a cosmological volume down to redshift $z = 6$. The simulation includes sub-grid physical models for population-III and population-II star formation, molecular networks and cooling, metal enrichment from stellar populations, metal line cooling from 11 elements, seeding mechanisms for black holes from population-III remnants and feedback from them, supernovae feedback, production of dust from stars and supernovae, and is coupled in post-processing to the radiative transfer routine SIMPLEX. These sub-grid models are prone to uncertainties in our understanding of physical processes, and one of the aims of this project is to advance our understanding and modelling of sub-grid physical processes.

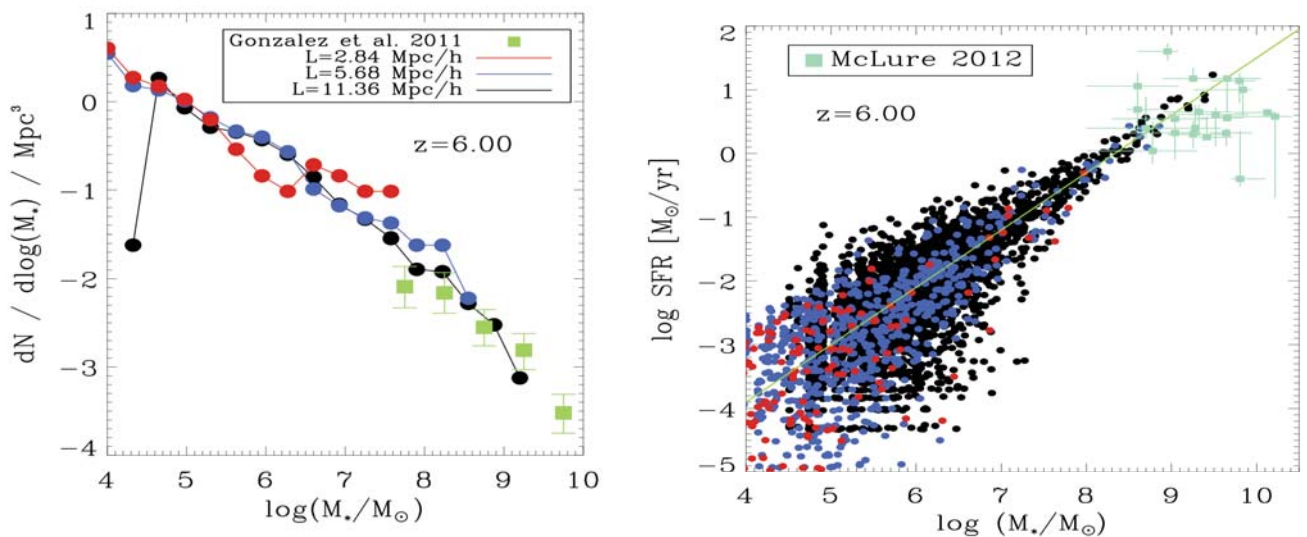


Fig. RG.1: The stellar mass function of galaxies in three different FiBY runs (left, solid lines). The relation between the star formation rate and stellar mass for the same runs (right) (Khochfar et al. 2013). The symbols with error bars show recent observational data.

The statistical properties of the galaxies in the FiBY agree well with those observed for the galaxy population at $z=6$ (Khochfar et al. 2013; see Fig. RG.1) making it an ideal testbed for investigating the formation of galaxies.

First results have e.g. shown:

Re-ionization of the Universe— Proto-galaxies with stellar masses of $M^* < 10^8 M_\odot$ can re-ionize the Universe at $z \sim 10$. The escape fraction of UV photons from low-mass galaxies is larger than from massive galaxies. This is mainly due to supernova feedback being very effective in blowing out gas and creating channels of low column density for photons to escape in low mass haloes. Our results are the first to calculate self-consistently the ionization fraction of hydrogen based on the escape fraction for thousands of galaxies, the clumping factor of the IGM, and the multi-frequency spectra of stars with different ages and metallicities from a cosmological hydrodynamical simulation (Paardekooper, Khochfar et al. 2013).

The impact of H_2 abundance on POPII and POPIII star formation— Lyman-Werner (LW) radiation with energies between 11.2 to 13.6 eV from population-III and population-II stars is able to photo-dissociate H_2 molecules in neighbouring primordial haloes, thereby suppressing the cooling of gas below $\sim 10^4 \text{ K}$ and population-III star formation in these haloes. The lack of associated feedback by pair-instability supernovae results in enhanced POPII star formation at later times. We find a factor two more in total stellar mass forms by $z=6$ allowing for LW feedback. Our results are the first to show the self-regulating nature of star formation due to a combination of radiative feedback in form of LW dissociation of molecules and mechanical feedback from supernovae feedback (Johnson, Dalla Vecchia & Khochfar 2013).

Formation of massive seed black holes— Gas in primordial haloes close to sites of star formation lack molecules due to Lyman-Werner radiation to cool down and

the Jeans mass of the gas reaches values large enough, which under certain physical conditions could lead to the formation of massive seed black holes via the direct collapse of gas (Agarwal, Khochfar et al. 2012; Johnson, Dalla Vecchia & Khochfar 2013). With initial seed masses of $10^{4.5} M_\odot$ and a predicted number density of 0.04 Mpc^{-3} at $z>6$ they are abundant enough to provide the seeds for super-massive black holes observed at $z=6$ (Agarwal et al. 2013). These studies are again among the first to take into account the spatial distribution of LW sources in a fully self-consistent cosmological setting.

Dark matter response to baryons— Facilitating the high resolution of the FiBY, we show that during the initial collapse of gas the adiabatic contraction model is a good approximation for the response of the halo (Davis, Khochfar et al. 2013). Once supernovae feedback kicks in dark matter haloes start expanding again due to the change of potential in the center. This abrupt change leads to the formation of a core in the dark matter halo profile similar to the ones observed in dwarf galaxies. Interestingly, we find haloes which host central galaxies that are off-center from the dark matter potential minimum, thereby heating the halo core via dynamical friction.

The transition from POPIII to POPII star formation— The critical metallicity at which POPIII star formation transitions to POPII star formation has only weak consequences on the overall topology of star formation in the cosmic web (Maio, Khochfar et al. 2011, 2013). Enrichment of the ISM takes place over time scales so short that in general one generation of stars is enough to elevate the metallicity above a wide range in critical values (Maio et al. 2010). Using the large volume of the FiBY we are able to investigate how efficient metal pollution of nearby haloes due to supernovae winds is. First results indicate a pollution by metals in the outer parts of nearby haloes, however, dense star formation sites within them are not significantly affected.

6.1.3 Development of new Methodologies

To achieve our research goals and overcome limits of present numerical approaches we are developing new methodologies beyond the state-of-the-art.

New SPH code including entropy mixing— We have employed a novel numerical implementation of smoothed particle hydrodynamics (SPH), including state of the art algorithms for force calculation and time dependent artificial viscosity, as well as a new algorithm for entropy/energy diffusion that we developed. Hydrodynamical instabilities and phase mixing are successfully reproduced in all numerical tests so far, and we expect this code to overcome failures of traditional SPH formulations and converges towards results from grid-based techniques, allowing to take full advantage of the SPH approach in modelling structure formation (Dalla Vecchia et al. 2013)

Radiative transfer code SIMPLEX— Within our group we have been continuing the development of SIMPLEX. It does now include H and He reionization, is able to follow multi-frequency radiation and has been coupled to hydro-codes to do radiative-hydrodynamics on the fly (Paardekooper et al. 2012, 2013)

Combining hydro simulations with semi-analytic models (SAM)— To be able to test results from high-resolution zoom simulations against large-scale surveys we have developed a tool to extract effective prescriptions for physical processes, and implement them into a SAM. We were able to succeed in this with very high accuracy (Neistein, Khochfar et al. 2012; Fig. 2). To our knowledge we are temporarily the only group that is able to do so, which is a crucial comparative advantage in studying galaxy formation given the need for simulations with pc resolution to e.g. accurately model feedback and star formation.

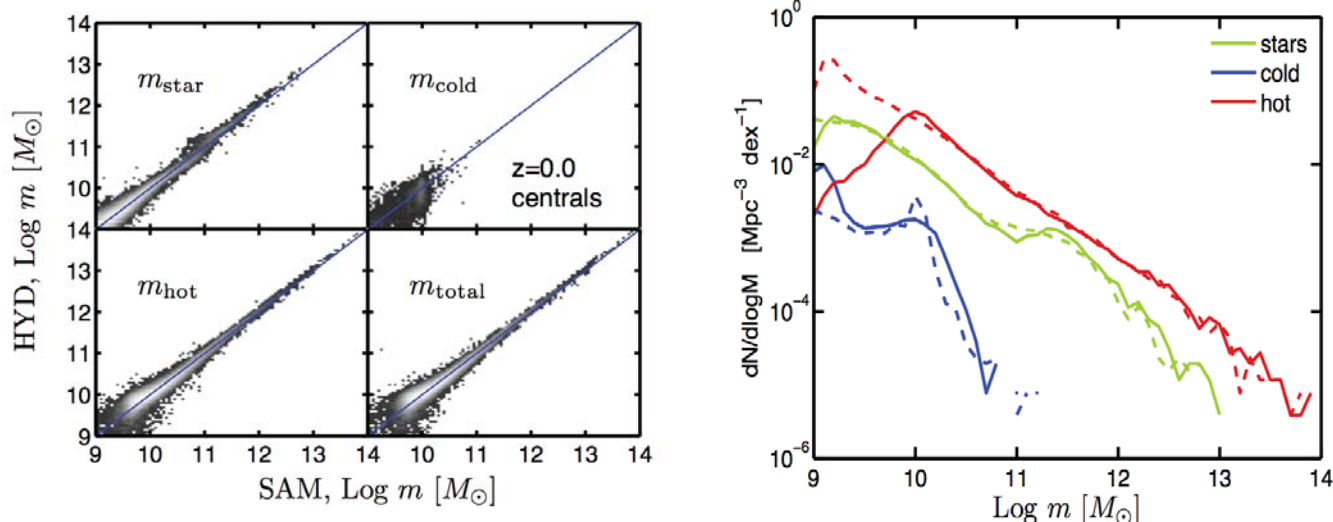


Fig. RG.2: Left: The relation between the stellar mass (top left), the star forming gas mass (top right), the hot gas mass (bottom left) and the total mass (bottom right) for individual galaxies in a hydrodynamical simulation and in our SAM using the effective models from the same simulation (Neistein et al. 2012). Right: The mass function for the same components in the SAM (dashed lines) and the hydro simulations (solid lines).



Sadegh Khochfar is a Max-Planck Research Group leader at the MPE since 2008. He will be taking up a faculty post at the Institute for Astronomy at the University of Edinburgh from Fall 2013. He has been leading simulation work on the formation of galaxies in the Universe, conducting the highest resolution simulation of the high-redshift universe in a cosmological volume to date. He is now leading an ambitious simulation project with international collaborators to resolve the formation of the first objects in a fully cosmological setting including radiative transfer and detailed chemistry.

(Other Research Group team members include Claudio Dalla Vecchia, Andrew Davis, Eyal Neistein, Jan-Pieter Paardekooper, Leila Powell, Bhaskar Agarwal

Former Research Group team members include Fabrice Durier, Volker Gaibler, Jarret Johnson, Umberto Maio)

References:

<http://mpe.iwww.mpg.de/339100/Publications>

6.2 Research Group "Gas Dynamics and Star Formation" Andreas Burkert

6.2.1 The Physics of Galactic Nuclei

In the first funding period of this Max-Planck-Fellowship group, we concentrated on the detailed understanding of the physics of (Active) Galactic Nuclei (AGN). Emphasis has been put on the puzzling mechanisms at work in the so-called molecular torus region as well as the Broad Line Region. In the second funding period, we are currently investigating the link between Galactic Nuclei and the larger scale environment. Additionally we continue working on successful projects concerning the distribution of gas and stars in the nucleus of the Milky Way. All of these projects are done in close collaboration with researchers from MPE.

During the first funding period of this group (2006-2011), the focus was on understanding the small scale physics of (active and inactive) Galactic Nuclei (GN). The various processes that fuel the supermassive black holes (SMBH) in AGN and that form the complex gaseous and stellar structures seen in the nuclei of nearby galaxies like the Milky Way have been explored. Special attention has been given to the puzzling broad-line regions in the vicinity of the SMBHs and the origin and nature of the gas tori and discs that are known to surround SMBHs and that provide the gas reservoir that fuels the central engine. On larger scales, the formation and physics of jets has been studied and the growth of SMBHs and their effect on galaxy morphology and evolution in galaxy mergers has been investigated. Finally, the anti-hierarchical cosmic evolution of the SMBH mass function has been studied.

During the first funding period, major progress has been made in the physics of AGN. It however has also become clear that GN do not evolve in isolation but are strongly linked to their galactic environment which provides the gas (fuel) to drive activities in the centre and feed the SMBH. The galactic environment, in turn, is strongly affected by energetic feedback from the nucleus. The next obvious step therefore is to couple the formation and evolution of galactic nuclei with cosmic galaxy evolution. This is the main task for the second funding period (2011-2016). The time seems ripe for such a project and the now well established and close collaboration between the MPE and the USM is ideally suited for this task.

The origin of GN and SMBHs is probably related to galaxy formation at high

cosmological redshifts. High-resolution spectroscopic observations of the MPE infrared group (lead by Prof. Reinhard Genzel) for the first time resolve the structure and kinematics of young, gas-rich clumpy disc galaxies at high cosmological redshifts of $z = 2$, corresponding to an epoch 2-3 Gyrs after the big bang (Genzel et al. 2011), revealing a small number of giant clumps ($\approx 10^9 M_{\odot}$, ≈ 1 kpc). This was also the most active period of cosmic star formation and morphological galaxy evolution (Genzel et al. 2008; Law et al. 2009). The high-redshift observations challenge our current understanding of galaxy formation. For example, it has been argued (Shapiro et al. 2010) that these giant clumps might represent the progenitors of globular clusters which are old stellar systems that formed during galaxy assembly and the seeds of the SMBHs, observed in the nuclei of present-day galaxies. A very interesting idea that has not been explored theoretically yet. The clumps with their SMBH seeds and stars might spiral into the central disc regions by dynamical friction, generating a bulge component and a young galactic nucleus, that later on continues to grow through recurrent Seyfert activities. In this sense, the clumps link galaxy evolution with the formation of galactic nuclei and might even provide hints for the formation of the seeds of SMBHs and galactic nuclei in the giant, gaseous clumps, detected in high-redshift disc galaxies. A PhD project (Manuel Behrendt) has been devoted to this

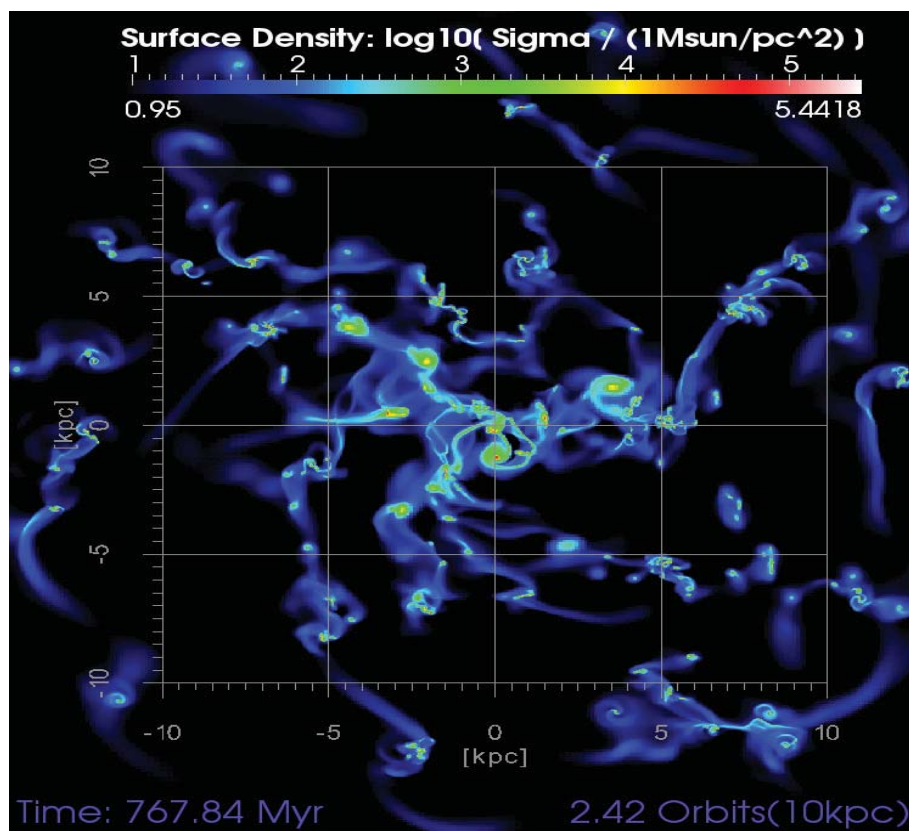


Fig. RG.3: Clump formation in simulations of disc instability in high redshift galaxies (Behrendt et al., in preparation).

idea, where we investigate in detail the formation of such clumps with the help of the RAMSES code (Teyssier et al. 2002). Their formation via “violent disc instability” and their evolution due to merging of clumps and dynamical interaction with the remaining galactic disc are studied in detail and compared to available observations in order to get insight into the physics at work in gas-rich disc galaxies (see Fig. RG.3).

In addition to this, the computational astrophysics group (CAST) at the USM has during the past years developed detailed models of the evolution of interstellar gas and star formation in different galactic environments, taking into account galactic dynamics, heating and cooling processes, gas phase transitions as well as star formation and stellar feedback. On cosmic scales, the CAST group is currently running one of the largest cosmological simulation that includes dark matter structure formation, gas dynamics, star formation, SMBH growth and feedback in order to study galaxy formation in a cosmological context (Dolag et al.). This expertise is crucial in order to understand the big picture of high- redshift galaxy formation and the physics of AGN, whereas the small scales are studied in high-resolution simulations, isolating the various processes (Fig. RG.3).

The research on the microphysics of galactic nuclei is also continued, where we focus especially on a self-consistent model of recurrent Seyfert activities in low- and high-redshift disc galaxies and their dependence on cosmic galaxy evolution. To this end, we currently focus on the detailed investigation of the nucleus of the Milky Way, which due to its vicinity and wealth of observational data is an excellent laboratory for the study of small-scale physical processes in GN. After having found a very promising scenario, which is for the first time able to describe the formation of the two inclined and counter-rotating discs of young stars, we will investigate this process with more detailed simulations. Fig. RG.4 shows a time series of such a simulation (done with the GADGET code, Springel et al., 2005): a molecular cloud as typically found in the nuclear environment interacts with the so-called circumnuclear disc.

This leads to multiple streams of gas pointing towards the SMBH in the centre. Depending on their mixture of co- and counter-rotating (disc or cloud) material and the (slight) offset from the disc plane, they enable the formation of stellar discs, which are in very good agreement with the observed characteristics of the two inclined and counter-rotating discs in the Milky Way’s GC. Furthermore, a tentative link to the origin of the mini-spiral in the GC has been found.

Recently, the discovery of a fast-moving, dusty and ionised gas cloud (named G2) by Gillessen et al. (2012, 2013) caught our attention. It was found to be on a highly eccentric orbit, reaching its closest approach of only 2200 Schwarzschild radii to the supermassive black hole (SMBH) in the GC in late 2013. This brings us in the unique situation of “watching” a gas cloud being disrupted by a SMBH and a huge dataset of observations is available and is planned for the course of this year. In order to test physical models of its origin and fate, we conduct detailed high-resolution hydrodynamical simulations. These will be discussed in detail in one of the following highlights from our group. In all of these projects, we strongly profit from the proximity of the observers and theorists at MPE which enables an inspiring and fruitful exchange of ideas and expertise.



Andreas Burkert

(Other Research Group team members include Ch. Alig, A. Ballone, M. Behrendt)

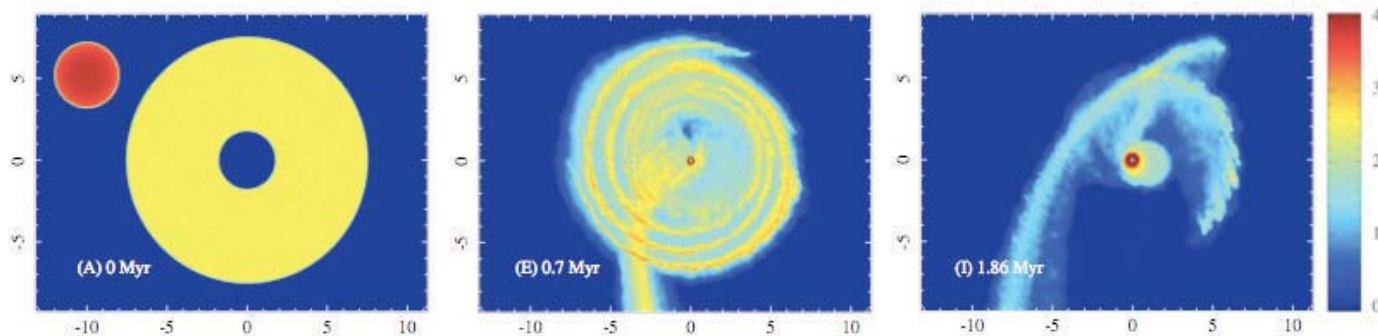


Fig. RG.4: Evolution of the encounter of a molecular cloud with the circum-nuclear disc as a promising scenario to form the observed counter-rotating stellar discs in the Galactic Centre. Shown is the surface density in units of M_{\odot}/pc^2 and length units are given in pc. The initial condition, as well as the state where two small-scale discs have formed are shown (0.7 Myr and 1.86 Myr).

6.2.2 The Physics of the Galactic Centre Cloud G2

We perform hydrodynamical simulations in order to understand the physics of the recently discovered gas cloud G2. To this end, we currently concentrate on two different scenarios, the so-called Compact Cloud scenario as well as the Compact Source scenario. The comparison of such simulations with observations enable us to get a detailed understanding of possible origin scenarios as well as to constrain wind parameters for the mass-losing compact source. We find that a diffuse cloud scenario necessitates a recent starting date, whereas a spherical shell is able to explain the observations of both components – G2 itself as well as the tail, following the gas cloud. Our best-fit Compact Source scenario has a wind mass loss rate of $9 \times 10^{-8} M_{\odot}/\text{yr}$ and a wind velocity of 50 km/s.

Recently, Gillessen et al. (2012, 2013) reported the detection of a fast moving dusty, ionized gas cloud in the central 0.04 pc of the GC, orbiting around Sgr A* on a highly eccentric ($e=0.966$) orbit. In this project we employ hydrodynamical simulations in order to investigate its physical origin and fate in the near future. Together with observational data, which will be obtained during this year, this has the unique prospect of probing the nuclear density distribution of the direct vicinity of Sgr A*. In order to get a basic understanding of the possible origins and the future evolution of the cloud, we started by investigating the evolution of Diffuse Clouds. In a second project, we concentrate on the possibility of a Compact Source of mass inside the cloud.

G2 modelled as a diffuse cloud

The so-called Compact Cloud was supposed to be able to describe the observations of G2 itself. It is a cloud with constant density and temperature (10.000K), which started its journey in 1995 on the orbit initially in pressure equilibrium. The so-called Spherical Shell was supposed to describe both components, G2 (head) and the tail. The most important ingredient – the gravitation of the SMBH ($4.3 \cdot 10^6 M_{\odot}$, Gillessen et al. 2009) – is modelled as a Newtonian point potential. The cloud is embedded into a hot and dense magnetised accretion flow, which we describe by an ADAF (Advection Dominated Accretion Flow) model of Yuan et al. (2003). With these

ingredients, we solve the Euler equations with the help of the PLUTO (Mignone et al. 2007, 2012) code in a 2D Cartesian coordinate system, using an isothermal equation of state for the cloud, dictated by ionising radiation of the young stars surrounding Sgr A*. Fig. RG.5 shows the time evolution of our Compact Cloud standard model. The white dotted line depicts the evolution of a test particle simulation, which indicates that the early evolution is dominated by tidal stretching due to the SMBH. Additionally the effect of the ram pressure of the ambient medium can be clearly seen, compressing the front part of the cloud, which is falling behind the ballistic orbits. Furthermore, it leads to a hydrodynamically stripped tail, which is dispersed by Kelvin-Helmholtz-instabilities. Close to peri-centre passage (panel f), the cloud has transformed into a long and thin filament, showing the effects of Kelvin-Helmholtz instability at its edges. The leading part of the cloud exchanges angular momentum with the dense ambient medium, which leads to accretion towards the centre in a nozzle-like feature. A total of 40% of the initial cloud mass is swallowed by the SMBH within the following 50 years. After peri-centre passage the cloud has increased in size dramatically, which leads to a significant interaction of the upstream part of the cloud with the ambient medium and cloud gas keeps being accreted towards the centre within the nozzle like feature. Concerning the Spherical Shell scenario, the basic behaviour is quite similar: It starts with constant density and temperature in spherical shape at its apocentre distance and soon develops the typical drop-like structure due to the tidal interaction with the central black hole. A tail of hydrodynamically stripped material is formed as well. As the time evolution from its apocentre is much longer, it develops the typical disturbances due to Kelvin-Helmholtz-instabilities invoked by the shear flow at the cloud's boundaries. Hence, parts of the cloud reach even closer to the centre, where density and ram pressure effects are higher. Therefore, this simulation leads to a rather filamentary disc-like configuration and much higher mass transfer rates towards the centre. The position-velocity diagram for our simulations is shown in Fig. RG.6a), where the observations are overlaid as contours. The Compact Cloud scenario describes the G2 component very well (first two panels) and the Spherical Shell scenario is able to account for the tail emission (panels three and four). Remarkably, the two models differ significantly in the near-future evolution: much higher line-of-sight velocities are reached for the case of the Spherical Shell

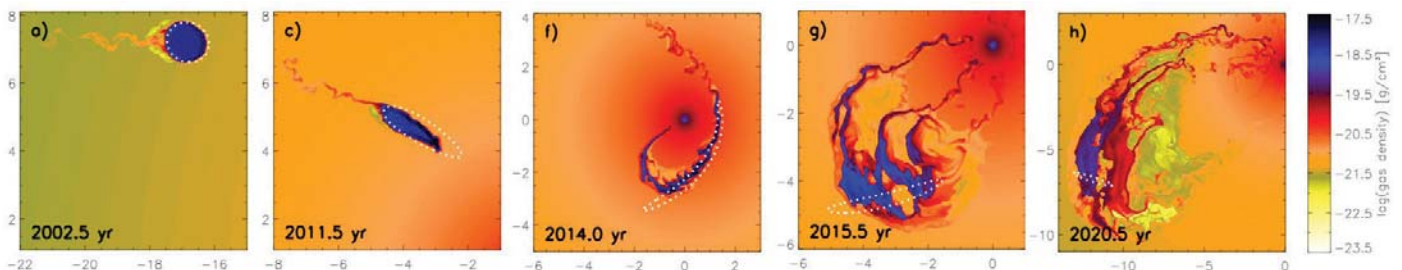


Fig. RG.5: Evolution of the density distribution in our Compact Cloud scenario. The white dotted line is the result of a test particle simulation.

model, which was indeed observed in the most recent observations. Another possibility to connect our simulations to observations is via estimating the change in the electromagnetic signal arising from the additional accretion of gas towards the SMBH. We only expect a significant boost of the X-ray and IR signal (compared to the quiescent value) from the Spherical Shell scenario.

G2 modelled as a compact source

The origin of such a low angular momentum cloud in the GC is still a debated puzzle and some authors have suggested and studied the possibility of G2 being the result of an outflow from a low luminosity star embedded in it (Gillessen et al. 2012; Burkert et al. 2012; Murray-Clay & Loeb 2012; Miralda-Escudé 2012; Meyer & Meyer-Hofmeister 2012).

We investigate this scenario by performing hydrodynamical simulations of outflows from a compact source with the Eulerian hydro-code PLUTO. As the evolution of G2 in the extreme GC environment is affected by many different physical processes as described above, detailed hydrodynamical simulations are necessary. Fig. RG.7 shows the density evolution for our standard model on a 2D cylindrical grid.

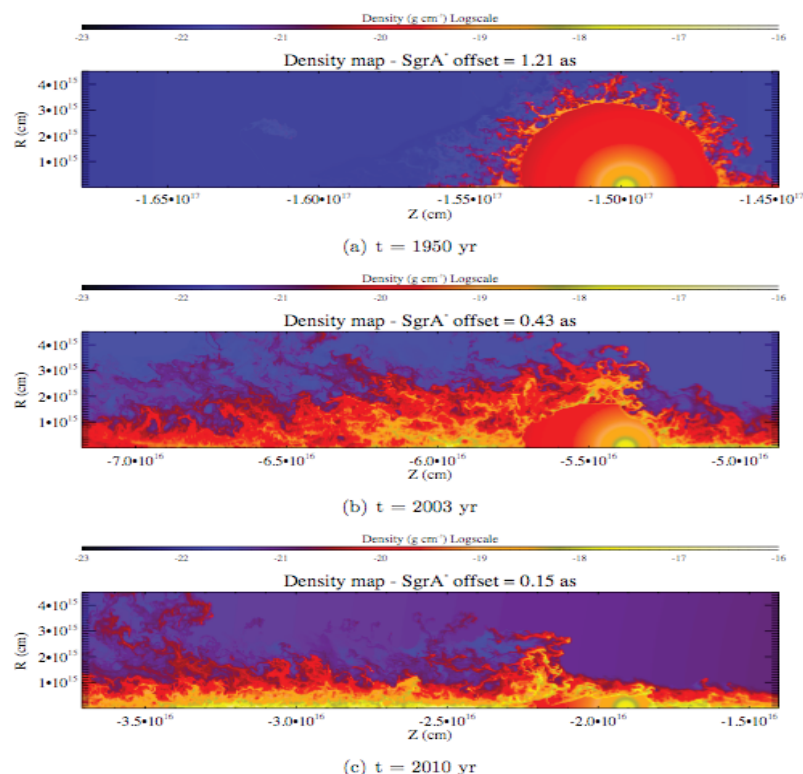


Fig. RG.7: Density evolution in the Compact Source scenario

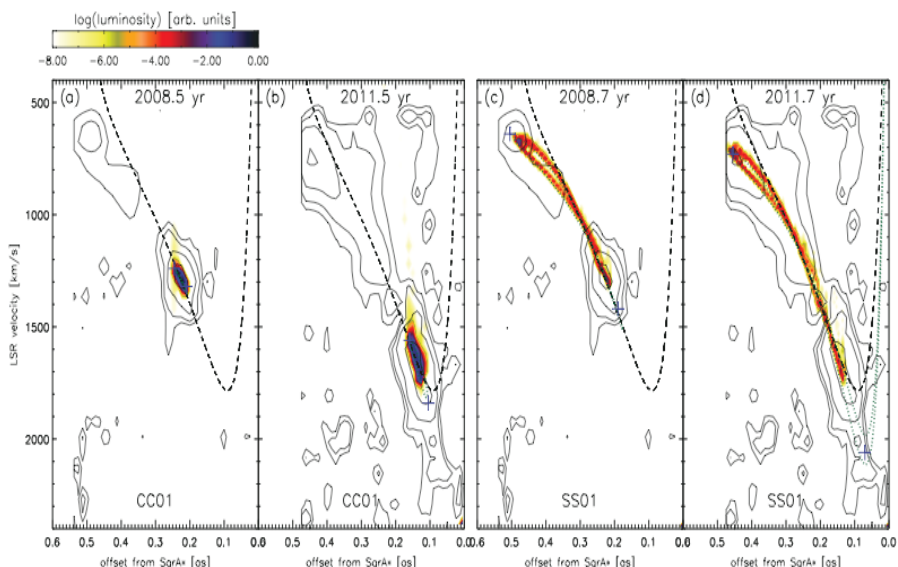


Fig. RG.6: Comparison of our simulations in a position-velocity diagram with observations (background contours) for the Compact Source and the Spherical Shell scenario.

The evolution can be roughly subdivided into three regimes: (i) Close to apo-centre, the wind expands roughly spherically symmetric until its ram pressure balances the thermal pressure of the surrounding atmosphere. (ii) After having significantly accelerated, the ram pressure due to the source’s motion becomes similar to the thermal pressure and the structure of the wind becomes anisotropic. (iii) In the final phase close to peri-centre, tidal forces dominate, which lead to the fast disruption of the cloud. The hydrodynamical interaction leads to stripping from the expanding shell and the formation of a long, turbulent tail. Interestingly, this model is roughly able to explain both, the observed luminosity evolution as well as the evolution in the position-velocity diagram



Marc Schartmann

(Other MPE team members include A. Ballone, A. Burkert, Ch. Alig, S. Gillessen, R. Genzel, T. Fritz, F. Eisenhauer)

6.2.3 Progress in Understanding Feedback in Galaxies

The stars in galaxies form from condensations in the interstellar gas. Without continuous energy input, the interstellar medium (ISM) would however form stars at much higher rates than observed. Massive stars feed back energy into the ISM which keeps it in a highly dynamic state, connects it with the gaseous halo of a galaxy and may even lead to large scale outflows. We study the effect of groups of massive stars in 3D-hydrodynamics simulations. Our results are consistent with an overall energy efficiency of about 10%. Massive star winds are important energetically, because the temporally extended energy injection has a more long-term effect on the ISM. Energy from supernovae (SNe) dissipates within about 10⁶ years, but this duration increases with the size of the superbubble, which the massive star winds and the preceding SNe have carved into the ISM. Massive star grouping, even on ≈ 10 pc scale enhances the effect of the massive stars, and in simulations of galactic outflows, we find higher outflow rates in simulations where the massive stars are more strongly clustered.

In any given galaxy, the baryons in stars make up for only a fraction of the baryons expected from the Cosmological ratio. The rate of star formation in galaxies is typically lower than expected from the gas mass (gas-rich galaxies, e.g. Milky Way) or accretion rate (large elliptical galaxies). Because the mass of the central supermassive black hole correlates with the bulge properties, but not with the stellar disc, one expects that star formation in disc galaxies is not very much affected by energetic outbursts of super-massive black holes, but instead controlled by the stellar feedback. Simulations of galaxy evolution reveal however a strong dependency of the galaxy properties on the parameterisation of the stellar feedback (e.g. Scannapieco et al. 2012, MNRAS, 423, 1726). Progress can therefore only be made by understanding the physics at play.

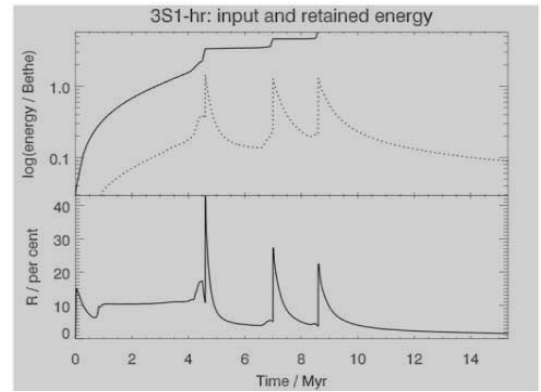
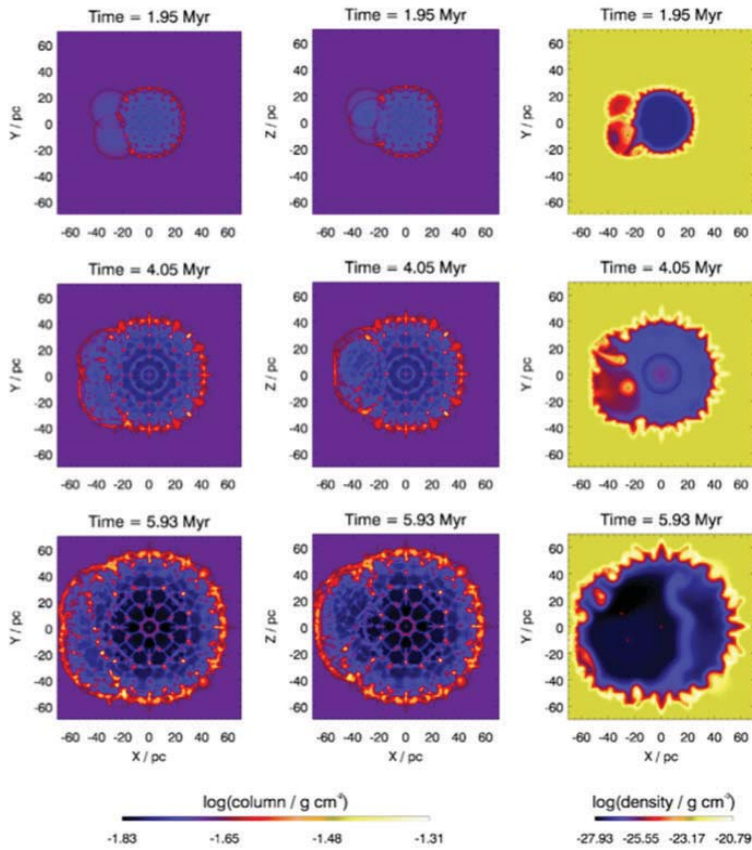
In order to address this problem, we combine observations of massive star regions from radio through gamma rays and interpret them in the context of our population synthesis model code and with hydrodynamics simulations of the interstellar medium. Optical and infrared observations constrain the stellar population in a given star-forming region. With our population synthesis code, we are able to infer statistically also the massive stars that have exploded already. Using stellar evolutionary tracks, we are able to derive the input from the massive stars into the ISM, which we feed into a numerical simulation with plausible assumptions about the gas distribution of the interstellar medium. From this, we derive morphologies, the efficiency of energy transfer to kinetic energy in the ISM and to radiative dissipation, mixing of hot ejecta with surrounding ISM, which determines the X-ray signal. In the Orion region, a first study of X-ray emission with XMM had been performed (Lubos, Diploma thesis, TUM 2012), and the expected distribution and kinematics of

long-lived radioactive trace elements (e.g. ²⁶Al) will be further pursued with a major observation program of INTEGRAL that was recently approved. The integrated gamma-ray line flux follows from the stellar evolutionary tracks alone and its observation provides a second constraint on the stellar population. Spatial and kinematic distributions of gamma-ray lines are inferred from hydrodynamic models (compare the pages of the INTEGRAL team for more on gamma-ray line measurements). For a comprehensive study of the Scorpius-Centaurus region, we have recently been awarded funding for a postdoc and 2 PhD projects from a DFG priority program, PIs Burkert, Diehl, and Preibisch/USM. Within this project, the USM team focuses on simulations of collective supernova shock impacts on molecular clouds, while the MPE team deepens the analysis and modelling of nucleosynthesis ejecta from the different Scorpius-Centaurus association subgroups (Diehl et al. 2010).

Here, we report 3D hydrodynamics simulations of the effect of massive stars on the ISM. We have studied the effect of clustering of massive stars by putting 3 stars at varying distances from each other. We use standard-ISM radiative cooling and heating due to the photoelectric effect on grains, which gives a temperature of 121 K for our uniform initial density of 10 cm⁻³. The wind bubbles expand and merge with filaments between bubbles being easily swept away due to the strong pressure differences in the individual bubbles (Fig. RG.8). Distances of about 50 pc are required to prevent the formation of a single superbubble before the first SN. We find that in the main-sequence wind phase about 10% of the injected energy remains in the ISM and 90% is dissipated by radiation (Fig. RG.9). SNe lead to short energy boosts, but the energy is also dissipated very quickly. Grouping the massive stars at distances of ≈ 30 pc or less enhances the feedback efficiency by a factor of at most a few.

Our results are consistent with the $\approx 10\%$ energy transfer derived in the Carina ISM by some of us (Voss et al. 2012, A&A 539, A66). We also infer that parent molecular clouds should be destroyed within a few 10⁶ years, strongly depending on the statistically varying occurrence of the most massive stars (Fierlinger et al. 2012, ASP 453). The richness of star clusters also makes a difference on galactic outflows: Varying the size of massive star groups systematically, we find in simulations including a galactic disc with its halo stronger outflows if the star clusters are bigger (von Glasow PHD 2012 & et al. submitted to MNRAS).

See also the ISM science report of MPE's high-energy group (HEG), and posters by Krause, by Diehl, and by Alexander.



↑ Fig. 8

← Fig. 9

Fig. 10

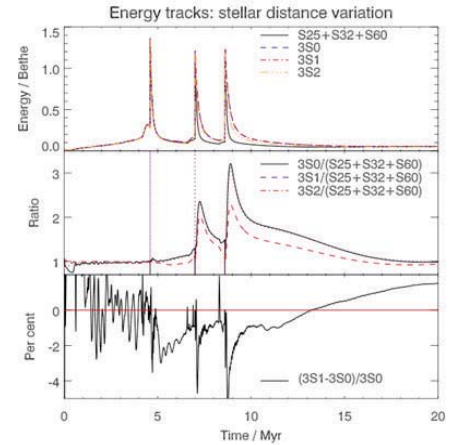


Fig. RG.8: 3D hydrodynamics simulation of the merging bubbles of three massive stars (25, 32 and 60 solar masses) at three snapshot times (top to bottom). The left and middle columns show column density for front view and top view. The right column shows a density slice through the midplane. The dense dots in column density are condensations due to a dynamical shell instability (Vishniac), most likely the sites of triggered star formation.

Fig.RG.9: Total energy in the simulation over time (top, input: solid, retained: dashed) and the ratio of the retained energy to the input energy (bottom, the rest is dissipated radiatively). The peaks correspond to the SNe of the three stars.

Fig. RG.10: Energetics of different 3-star simulations, varying the distances between the three massive stars. Top: total energy; middle: energy relative to the case when each massive star is in a separate simulation (infinite distances). For about 60 pc distances (red dashed line), we see an enhancement of up to a factor of about 2, the ≈ 30 pc and 0 pc cases reach up to a factor of 3. The bottom plot demonstrates that the difference between ≈ 30 pc and 0 pc distances is insignificant.



Martin Krause

(Other MPE team members include Andreas Burkert, Roland Diehl, Katharina Fierlinger, Wolfgang von Glasow)

7 The Institute



7. The Institute

7.1 Technical Services

It would be impossible to realise our scientific visions and ideas from the exploration of the Universe with satellites and earthbound instruments to fundamental research experiments during manned and unmanned spaceflights without the support of MPE's "central technical services". This division mainly consists of three different groups of specialists: the department of electrical engineering, the department of mechanical engineering, with their mechanical workshops each and the data processing group. They all work closely together with each other and the responsible project scientists.

Electrical Engineering

At the moment 30 staff members altogether (at the MPE and the Semiconductor Laboratory in Neuperlach) are working in the department of electrical engineering. Their tasks vary widely from the planning phase (drafting concepts), designing and manufacturing to commissioning of instrumentation for terrestrial and extraterrestrial observations and scientific experiment design for the International Space Station (ISS). The group technically supports ongoing missions and observations. Members of staff are expected to demonstrate substantial knowledge of electrical engineering, the confident and reliable handling of modern design and simulation tools and also to be well informed about electronic components. Experience in the field of vacuum-, cryo- and laser technique as well as other areas is required until our scientific visions finally take shape in an experiment. In order to keep their high standards these people cooperate internationally and interdisciplinary, continue professional training regularly, keep pace with the newest state-of-the-art techniques and are prepared to be away on business for several weeks at home and abroad.

Between 2010 and 2012 the department has contributed to the following instrumental projects of MPE: the X-ray mission eROSITA, the forthcoming instruments for complex plasma research PK-4 and PlasmaLaB, LUCI, the laser guide star for the LBT ARGOS, and the interferometer for the VLT GRAVITY.

In the year 2012 the first apprentice of the group successfully finished his training as "Elektroniker für Geräte und Systeme" (Electronic technician for devices and systems).

Mechanical Engineering

The department of mechanical engineering has 40 staff members altogether and 8 apprentices, working in the design office, the test facility for environmental tests, the plastic laboratory, mechanical workshops and the education workshop. It mainly develops and partly manufactures instruments for the experimental astrophysics mainly. For some of the projects the people of the mechanical engineering department also work closely with space industry.

The department deals with a wide spectrum of tasks reaching from optical precision Instrument engineering over special purpose machines to extreme lightweight construction. Also included are system engineering, product assurance and verification. Particular development problems result from mostly extreme requirements such as cleanliness, stress due to vibration loads during rocket launch or the operation of the instruments in vacuum and at deepest temperatures near absolute zero. For design and development, 2D/3D-CAD as well as

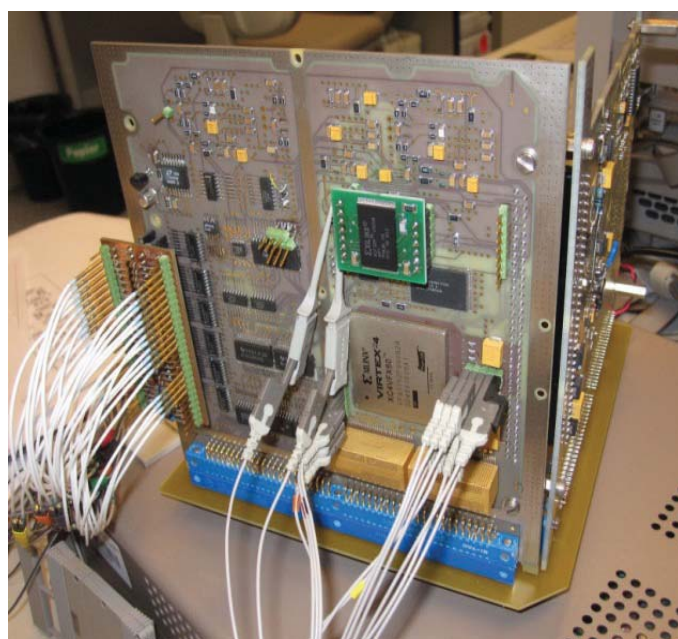
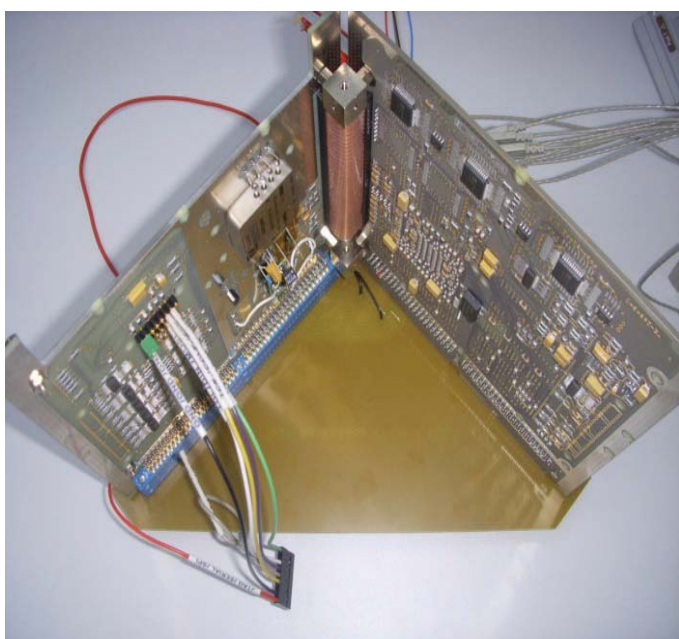


Fig. 1: The pictures show the engineering model of the eROSITA event analyser boards (designed by the electrical engineering group), while testing the performance. A Xilinx Virtex 4 FPGA with 2 PowerPC's on-chip is used to extract the photon events data out of the CCD image data frames in real-time.

FE-software are standard tools. For environmental tests e.g. a shaker and two thermal vacuum chambers can be utilized in the test facility.

In the years 2010 until 2013 the mechanical engineering group supported the following main MPE projects: the far-infrared instrument PACS on Herschel, the forthcoming X-ray mission eROSITA, the EUCLID satellite payload NIP, the complex plasma research instrument PK-4, the multiobject spectrograph LUCI, and GRAVITY, the interferometry instrument for the ESO-VLT and the adaptive optics system ARGOS for the Large Binocular Telescope (LBT).

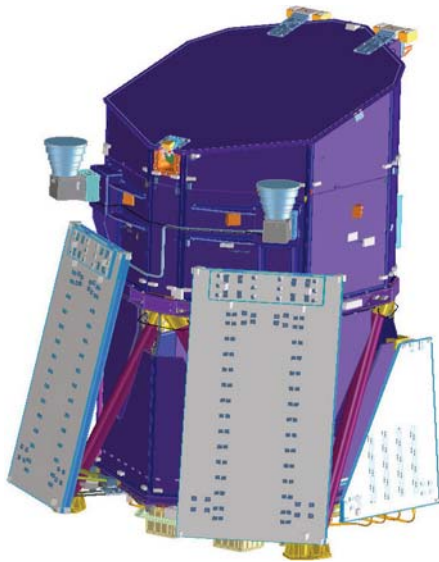


Fig. 2: 3D CAD (above and below), and FEM structural model (right) of the eROSITA telescope, designed by the mechanical engineering group. The main materials are CFRP (carbon fibre reinforces plastic and aluminium).



Fig. 3: Integration of the PK-4 engineering model IBP (integrated base plate) with its main components.

Data Management and Processing

Data management and processing is generally a collaborative task of the MPE computing support group and the individual research groups. The support people cover the central tasks and, in addition, support the science groups in their specific work with their IT-knowledge and manpower.

Computing and data processing activities are coordinated and handled by a committee with representatives from all working groups of the institute. A central group for system support and programming is assisting this committee whose main tasks are coordination and evaluation of new hardware as well as the software procurement, conception and control of central installations such as the local-area network, access to external networks and the public printers. In addition, the committee is coordinating the collaboration with the Garching Computer Centre (RZG) and takes care of the computer-related training of MPE members.

The members of the central computing support group maintain the central installations i.e. network, server workstations, printers, and the official WWW pages, with up-to-date information about the institute. They are also part-time involved in the data processing of and software development for our main science projects like XMM-Newton, eROSITA, Herschel/PACS, GRAVITY, KMOS, PanSTARRS and EUCLID. This guarantees the horizontal flow of information and experience.

7.2 General Services

The institute's **administration** plays a very distinct but equally essential role as the technical services mentioned above. It supports the managing directors of the Max Planck Institute for Astrophysics and the Max Planck Institute for Extraterrestrial Physics in carrying out their executive duties. These activities also extend to MPE's branches in Neuried (test facility) and in München-Neuperlach (semiconductor laboratory).

The administration's main areas of work involve the handling of personnel matters relating to its own staff as well as to junior researchers and foreign guest scientists, the procurement of scientific and other equipment, and the organization and maintenance of the institute's infrastructure.

Additional core tasks include the planning and administration of institutional and external funds, along with the due processing of receipts and expenditures, supplying proof of the correct usage of appropriated funds. The Administration is required to comply with the laws, statutory instruments, legal provisions and guidelines applicable to the Max Planck Society and its institutes. In addition, the Administration can advise and assist the directors on the implementation of these rules and guidelines.

In collaboration with the Administrative Headquarters of the Max Planck Society a new building was planned and finally built in the years 2011 to 2013. Attached to the building of the Max Planck Institute for Astrophysics, it is the workplace for most of MPE's administrative employees since April 2013.

Our **publication services** are also indispensable for the effectiveness of the institute's work flow. They are in the position to prepare all kinds of graphics and images for publications, brochures, and posters. We also have our own graphic group.

The **print shop** owns all the digital machinery necessary for the production of reports, brochures and preprints for both the MPE and the MPA. In addition, it produces business products such as stationary and envelopes and reproduces colour copies for both institutes.

The **Astrobibliothek** is the joint library for the Max Planck Institutes for Astrophysics and Extraterrestrial Physics. At present it holds a unique collection of about 45 000 books and journals and about 7200 reports and observatory publications, as well as print subscriptions for about 200 journals and manages online subscriptions for about 400 periodicals. In addition it maintains an archive of MPA and MPE publications, two slide collections (one for MPA and one for the MPE), a collection of approximately 400 CDs and videos, and store copies of the Palomar Observatory Sky Survey (on photographic prints) and of the ESO/SERC Sky Survey (on film). The library catalogue includes books, conference proceedings, periodicals, doctoral dissertations, and habilitation theses, reports (print and online).

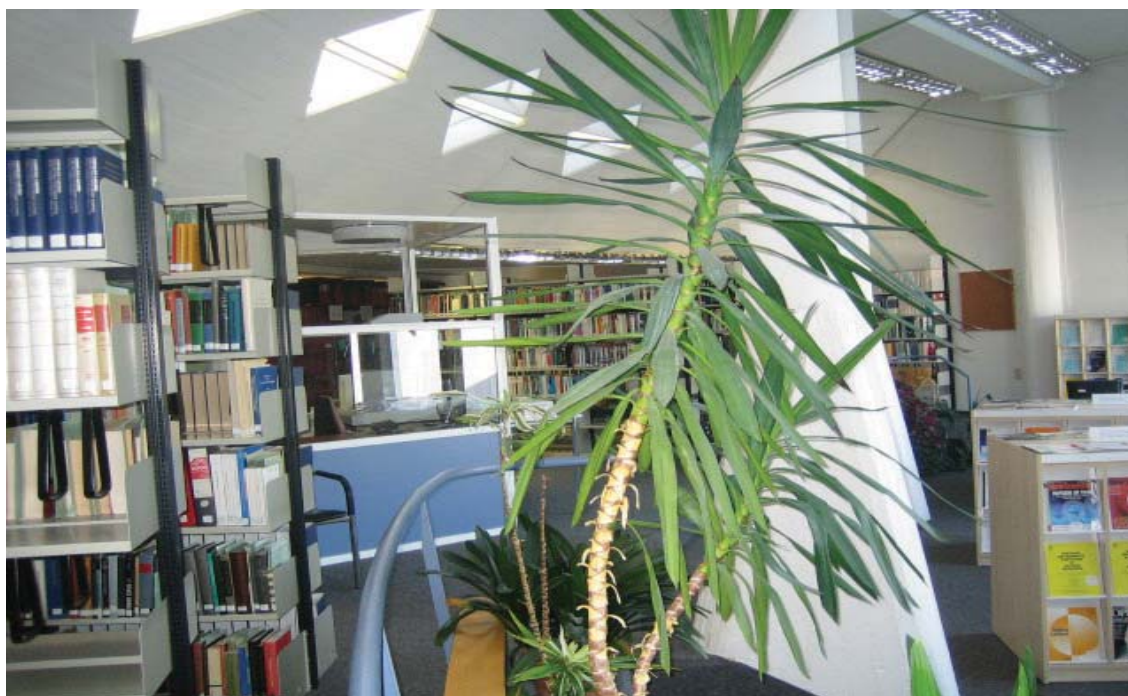


Fig. 4: The joint MPE/MPA Library

7.3 Vocational Training and Education

Our **education workshop for apprentices** in the mechanical area of MPE provides apprenticeship training positions. Eight trainees can be educated in a two or three years process for being an industrial mechanics. Occasionally students join the workshop for an internship, preparing for their professional career. Another important field of education, where we, together with four other renowned scientific institutions, all located in the Munich-Garching area, support young people to promote their knowledge and careers is:



Fig. 5: The workshop for the mechanical apprentices

The International Max-Planck Research School on Astrophysics (IMPRS).

IMPRS is a graduate school, offering a three years Ph.D. program in astrophysics and cosmology. Open for students from all countries world wide, the school intends to attract highly qualified and motivated young scientists heading for a graduate degree in Physics and Astronomy. Outstanding research facilities and training programs as well as Ph.D. fellowships available for students provide a unique environment for participants. The school can lay the foundation for long-term international cooperation and thus play a significant role for future science and research.

IMPRS was founded on the initiative of the Max-Planck Society in 2000. The four local institutes, all internationally renowned in astrophysics

research, MPE, the Max Planck Institute for Astrophysics (MPA), the European Southern Observatory (ESO) and the University Observatory of the Ludwigs-Maximilians-University of Munich form the school together. Access to their facilities will provide graduate students with a very wide range of possibilities for research. There are fewer than a handful of places world wide which can compete in breadth and level of research with the participating institutes. The large number of teaching scientists and advisors actively involved in research guarantee that the know-how available in the participating institutes is presented to the students by the experts themselves.

About 190 students applied for the IMPRS programme in 2013. Approximately 10 to 15% of them are accepted, based on their excellence as proven by their university record and by letters of recommendation. A committee composed of members from all participating institutes will review the applications and advise the potential supervisors about the candidates and their qualifications. Successful applicants with a degree equivalent to the Diploma or a German Masters degree can receive fellowships for a maximum period of three years if required.

In July 2012, IMPRS was successfully evaluated to further receive funding until August 2019.



Fig. 6: The IMPRS class of 2012

7.4 Public Outreach

Basic research is an important condition for the long-term survival of a modern, technological society. In a democracy however, this kind of research cannot exist without its acceptance in the public. Therefore it is absolutely necessary to communicate its activities and results to a broad public, which will then support it as an integrated and basic part of a vital and developing society.

MPE has formed a public outreach team, consisting primarily of its press officer and scientific secretary, which functions as a link between the institute and the public. This team, supported by many MPE members, organized a number of quite different activities in and outside MPE during the last years.

In 2011 MPE opened its doors for the public to contribute bi-annually to the campus-wide “**Open House**”, where the institute’s latest technological developments could be watched, and scientists offered public talks on interesting astrophysical topics, reaching from the solar system via Black Holes to the evolution of the Universe. These talks were supplemented by talks on our plasma physics research. The general program is complemented by a special children’s program, called “**Astronomy for Kids**“, where many MPE volunteers prepare attractions like rocket workshops, puzzle rallies etc. This children’s program attracted children of all age, even teachers with complete school classes participated. In total about 2500 people visited MPE, including roughly 600 juniors joining the children’s program.

Since 2008 we also take part in the nationwide “**Girls’ Day**”. Sponsored by the European Union, the Federal Ministry of Education and Research (BMBF) and the Federal Ministry for Families, Senior Citizen, Women and Young People (BMFSFJ) the yearly initiative „Girls’ Day“ has been established in Germany in 2001. Although on average girls do reach a higher level of education at school than their male peers, they still tend to choose traditional female fields of occupation. By providing girls, aged between 14 and 16 years with contact to professionals and an insight to modern working places in the area of technology, IT and natural sciences it is often possible to catch their interest and to encourage them to change their attitude. 50 girls each year visited MPE during the last 3 years, getting in touch with MPE and its science.

In 2011 the Max Planck Society celebrated the 100-year anniversary of its foundation. MPE participated in the nation-wide “**Max-Planck-Day**”, for which many Max Planck institutes opened their doors for high-school students. At MPE the more than 100 students from six schools spread throughout Bavaria learned about MPE’s astronomical research and work environment. Towards the end a panel of young scientists was prepared to be interviewed about their work experiences and every day work at an astronomical institute. In addition we supported the “**Science Tunnel 3.0**”, an exhibition of the Max Planck Society, by contributions from astronomy like exhibits and images.



Fig. 7 and 8: Impressions from the Open House 2011



Fig. 9: Impressions from Girls' Day 2012



Since end of 2010, the **MPE Brochure** is available describing the institute in general, its overall approach to research, its main scientific areas and some of the scientific results. The brochure, sized of 48 pages, is available in English and German. The **MPE Flyer** gives a short overview of the organisation of the MPE and the work of the individual groups.

Besides the organisation of these special events and the preparation of singular documents, there are also a number of regular tasks of the public outreach team. To groups the MPE offers **guided tours** through the institute on request. The tours are available in German and English. After a general introduction, scientists of the var-

ious groups of the institute will guide the visitors through their departments. This service has always been requested quite frequently (about 25 to 30 groups per year) and it can be really challenging to meet the requirements of the different visitors as the groups can be as diverse as e.g. high school and university students, senior citizens, interested hobby astronomers or even colleagues from other scientific institutions. We also support guided tours in the cosmology exhibition "Evolution of the Universe" in the "Deutsches Museum" in downtown Munich. This exhibition was built for the International Year of Astronomy in 2009 by five astronomical institutes of the Munich area, among them MPE, and – apart being open for the public - is now regularly used for lectures and guided tours.

MPE has revised its main web page in 2012, making it more attractive for public access to information about all aspects of the institute. Regularly issued **research news** are in the focus now. Each year about 20 to 30 new science results of MPE scientists are presented in a popular manner. Visitors are informed by a roughly one-page note about the new scientific achievements. On high-impact science results, **press releases** are issued, either by MPE itself or in cooperation with other scientific institutions. For such occasions journalists are often coming to MPE.

Together with four other astronomical institutes, MPE organises the monthly **Cafe & Cosmos** series of discussions. In a restaurant a scientist is briefly introducing a topic from the cosmos and then takes questions from the audience and discusses the cosmos issue.

On a regular basis MPE scientists give **public talks/lectures** for a scientifically interested audience. The scientists are invited to e.g. planetariums, schools, or special events to provide their expertise. About 30 such talks/

lectures are delivered every year.

Finally, MPE offers the possibility for doing **internships** at the institute, both for high school and university students. Every year about 10 to 15 high school students (1 to 2 weeks) and 5 to 10 university students (4 to 8 weeks) gain a more detailed inside-look by participating under supervision of a scientist with a small project in MPE's research.

7.5 Social Events

Knowing colleagues not only from a common working place but also from spending some time together with joint social activities can help to form a positive atmosphere in the institute. These activities cannot only help to link people from normally quite separated areas but also to integrate new MPE-members. Our social activities range from small group-internal celebrations (e.g. the success of a certain scientific project or a PhD defence, special birthdays etc.) to MPE-wide celebrations like the Christmas party and the three well-established annual trips: the skiing excursion, the summer works outing, and the visit to the Munich Oktoberfest in autumn.

For the summer outing in 2012, we went to Kochel am See, a prominent holiday destination in Bavaria at the rim of the Alps. The location offers, in addition to museums and the "Kochelsee", a great scenery and numerous of hiking-trails, from short walks to full-day tours. The day was free for individual activities. While some people just enjoyed the scenery of the Alps' panorama from a restaurant or went swimming in the lake, most went on a hiking tour, a more or less challenging one depending on individual fitness. As usual the outing ended with a common dinner in the late afternoon before the buses started back to Garching.

As every year, also in 2012 a large MPE crowd spent a pleasant afternoon - and most also the evening – together at the famous Munich Oktoberfest, enjoying Bavarian sociability. Many colleagues have dressed up for this occasion in traditional Bavarian costumes. The unique



Fig 10: MPE members taking a break on a hiking-trail during the work outing 2012.

atmosphere of eating, drinking and celebrating together is very favourable for making new and deepening existing connections between MPE staff members, students and guests.



Fig 11: Visit to the Oktoberfest

Max-Planck-Institut für extraterrestrische Physik

Giessenbachstraße
85748 Garching, Germany
Phone: (0 89) 30000-0
Telefax: (0 89) 30000-3569
email: mpe@mpe.mpg.de
<http://www.mpe.mpg.de>

All rights reserved:
Dokumentationsstelle of the MPE
ISSN 0947-8787
July 2013

